



Torben Seifert, Dipl.-Ing.

Investigations on a multi-component heating element based on (Ba,Ca)TiO₃ barium titanate ceramics

DISSERTATION

zur Erlangung des akademischen Grades

Doktor der technischen Wissenschaften

eingereicht an der

Technischen Universität Graz

Betreuer

Ao.Univ.-Prof. Dipl.-Ing. Dr.techn. Klaus Reichmann

Institut für Chemische Technologie von Materialien

Ao.Univ.-Prof. Dipl.-Ing. Dr.techn. Karl Gatterer
Institut für Physikalische und Theoretische Chemie

EIDESSTATTLICHE ERKLÄRUNG

Ich erkläre an Eides statt, dass ich die vorliegende Arbeit selbstständig verfasst, andere als die angegebenen Quellen/Hilfsmittel nicht benutzt, und die den benutzten Quellen wörtlich und inhaltlich entnommenen Stellen als solche kenntlich gemacht habe. Das in TUGRAZonline hochgeladene Textdokument ist mit der vorliegenden Dissertation identisch.

Datum

Unterschrift

Abstract

There is a great potential for efficiency enhancement of ceramic heating elements based on PTCR thermistors (Positive Temperature Coefficient Resistor) respective current consumption and heat extraction. Simulations from the University of Leoben revealed that the PTCR ceramic should not exceed 100 μm in thickness for an optimum in heat extraction. For this purpose we have proposed a multilayer assembly based on a structural ceramic and donor doped barium titanate as PTCR ceramic. A sufficient mechanical stability shall be achieved by the structural ceramic hence allowing a reduction in thickness of the functional ceramic. Both ceramics shall pass through thermal processes simultaneously. The mechanical and chemical interactions during production were investigated using analytical methods such as optical microscopy, SEM including EDX analysis as well as X-ray diffraction. Interdiffusions of barium, titanium, zirconium and yttrium ions have been identified and their chemical reactions have been determined. Proposals for a reduction of the chemical interactions have been developed. Furthermore the thermal and electrical properties of developed prototypes were measured.

Kurzbeschreibung

Bei keramischen Heizelementen auf der Basis von Kaltleitern besteht ein hohes Optimierungspotential bezüglich Stromaufnahme und Wärmeauskopplung. Simulationen am Institut für Struktur und Funktionskeramik der Montanuniversität Leoben ergaben, dass die Schichtdicke der Kaltleiterkeramik für eine optimale Wärmeauskopplung 100µm nicht überschreiten sollte. Hierfür haben wir einen Mehrlagenaufbau aus einer Strukturkeramik und donordotiertem Bariumtitanat als Kaltleiterkeramik vorgeschlagen. Die ausreichende mechanische Festigkeit des Bauelements soll durch die Strukturkeramik gewährleistet werden und somit die Dickenreduktion der Funktionskeramik ermöglicht werden. Beide Keramiken sollen gemeinsam im Verbund die thermischen Prozesse durchlaufen. Die mechanischen und chemischen Wechselwirkungen während des Herstellungsprozesses wurden mittels analytischer Methoden, wie optischer Mikroskopie, REM mit EDX Analyse sowie Röntgendiffraktometrie untersucht. Die Interdiffusion von Barium-, Titan-, Zirkonium- und Yttriumionen wurde identifiziert und deren chemischen Reaktionen wurden bestimmt. Vorschläge für eine Reduzierung der chemischen Interaktionen wurden entwickelt. Weiterhin wurden thermische und elektrische Eigenschaften an entwickelten Prototypen gemessen.

Preamble

This doctoral thesis originates in the department of development for PTC thermistors at EPCOS OHG in Deutschlandsberg.

I especially thank Prof. Dr. Klaus Reichmann from Graz University of Technology for his mentoring during my PHD study.

At this point, I would like to thank for the kind support during my doctoral thesis. The willingness for help and discussion of all employees, which has been shown to me, offered a very unique and very comfortable working atmosphere for writing this thesis.

I kindly thank Dr. Steinberger for the dedicated mentoring, the helpful discussions and suggestions and the kind co-operation.

As last I thank my family, my former host family and my partner Liane Peschel for all the support and helpful suggestions.

Table of contents

1	Motivation	9
2	Fundamentals of the material combination	10
2.1	Positive Temperature Coefficient Ceramics	10
2.1.1	Barium titanate	10
2.1.2	PTCR effect.....	15
2.1.3	Characterisation of PTC thermistors.....	16
2.1.4	Influences on the PTC behaviour	18
2.1.5	Applications	18
2.2	Zirconia.....	19
2.2.1	Production of zirconia	20
2.2.2	Properties of zirconia.....	20
2.2.3	Applications	21
2.3	Alumina.....	21
2.3.1	Alumina Production	21
2.3.2	Properties of aluminiumoxide	22
2.3.3	Applications	23
2.4	Material properties and interactions within a ceramic composite.....	23
2.4.1	Thermal expansion	23
2.4.2	Shrinkage	24
2.4.3	Diffusion within poly crystalline solids.....	25
2.5	Multi-component forming methods.....	29
2.5.1	Dry pressing	29
2.5.2	Tape casting.....	30
2.5.3	Debinding.....	32
2.5.4	Sintering	33

3	Material development	34
3.1	Material characterisation.....	34
3.1.1	PTC ceramics	34
3.1.2	Yttria stabilized zirconia (YSZ)	41
3.1.3	Alumina	50
3.1.4	Barium titanate	51
3.2	Tape development	52
3.3	Investigations of the chemical interactions based on pressed powder mixtures.....	55
3.3.1	Thermal analysis and density measurements	57
3.3.2	Electrical measurements	59
3.3.3	Mechanical measurements.....	62
3.3.4	Microstructure evolution	64
3.3.5	SEM analysis.....	66
3.3.6	X-ray diffraction analysis	71
4	Prototypes	78
4.1	Thin PTC heater bonded on alumina.....	78
4.1.1	Production and electrode development	78
4.1.2	Electrical results	80
4.1.3	Calorimetric results.....	81
4.2	Prototypes based on Yttria stabilized Zirconia	85
4.2.1	Production	85
4.2.2	Structural analysis	86
4.2.3	Mechanical strength	89
4.2.4	Electrical characteristics	91
4.3	Prototypes based on YSZ barium titanate and PTC	93
4.3.1	Production	93
4.3.2	Structural analysis	93

4.4	Prototypes based on alumina	103
4.4.1	Production	103
4.4.2	Structural analysis	105
4.5	Investigations on the sintering of the material composite	107
4.5.1	Heating microscope evaluation.....	107
4.5.2	High temperature x-ray diffraction analysis (HT-XRD).....	110
5	Discussion of results	115
5.1	Material development	115
5.2	Prototypes	117
6	Conclusion and prospect	119
7	Index	120
7.1	Index of sources	120
7.2	Index of figures	123
7.3	Index of tables.....	126
7.4	Index of equations	127
7.5	Index of appendix	129
A	Appendix	132
A.1	Material characterisation.....	132
A.2	Material development	150
A.3	Prototypes	154

1 Motivation

Ceramics of barium titanate show by suitable doping a very sharp rise in resistance within range of the Curie temperature. This special electrical behaviour offers a variety of applications for ceramic semiconductor based on BaTiO_3 , particularly to protect electronic parts from high voltages and temperatures, as switching and heating device and as temperature sensors.

Investigations and consumer requests have shown that there is a need for Positive Temperature Coefficient Ceramics that also show a high mechanical strength and a higher chemical resistance. Especially within automotive applications a higher resistance to mechanical stress will offer a variety of applications. First investigations have shown that a material combination of zirconia and barium titanate can achieve these positive characteristics.

The aim of this thesis is the development of a ceramic system based on a structural ceramic, with a high mechanical strength and a good chemical consistency, and an electro ceramic with a self-levelling of the electrical resistance. Thus the material combination of zirconia and barium titanate as well as alumina and barium titanate shall be further investigated. According to the required properties the materials have to be chosen and characterized. In order to realize a stable conjunction of both ceramics the thermal expansion coefficient and the mould shrinkage of the ceramics masses have to be adjusted. The adjustment has to be further done by developing intermediate layers between both ceramics. In order to make a concurrent sintering of both ceramic masses possible, the sintering temperature and dwell time have to be adjusted, too. Prototypes shall support these investigations. For this ceramic tapes shall be developed. Prototypes shall be produced by the use of dip casting technology and the developed ceramic tapes. All prototypes have to be characterized and analyzed. Especially electric, dilatometric and mechanical strength investigations shall be used. In order to show defects the microstructure has to be analyzed, too. All in all the investigations will show whether a material combination of zirconia and barium titanate can be reliably and repeatable produced and the desired properties can be achieved.

2 Fundamentals of the material combination

2.1 Positive Temperature Coefficient Ceramics

Positive Temperature Coefficient thermistors are ceramic components, whose electrical resistance sharply rises when exceeding a specific temperature. Due to this property there is a variety of applications in modern electronics. A PTC thermistor is a temperature-sensitive semi-conductor, whose resistance sharply rises when exceeding the reference temperature T_{Ref} . T_{Ref} is located near the Curie temperature and is experimentally determined. The high positive temperature coefficient above the reference temperature has given the PTC its name. Relevant standards for Positive Temperature Coefficient thermistors are EN 60738-1, IEC 60738-1, DIN 44081 and DIN 44082 [Epc09].

2.1.1 Barium titanate

Barium titanate is characterized in its pure and chemical modified form by extraordinary electro physical properties, such as ferro and piezo electricity. These Properties are determined to a great extent by the typical crystal structure of the $BaTiO_3$ [Gab01]. In the following the production, the structure and modification as well as important electrical properties $BaTiO_3$ shall be highlighted.

Phase diagram BaO-TiO₂:

Figure 1 shows the phase diagram of the BaO-TiO₂ system. There are five binary phases: Ba_2TiO_4 , $BaTiO_3$, $BaTi_2O_5$, $BaTi_3O_7$ und $BaTi_4O_9$. The lowest eutectic is at a temperature of 1317°C and a composition of 68 Mol-% TiO₂. Barium titanate, the key phase of this system, originates at a composition of 50 Mol-% TiO₂ and 50 Mol-% BaO and dissipates to liquid phase at 1618°C. [Haa60]

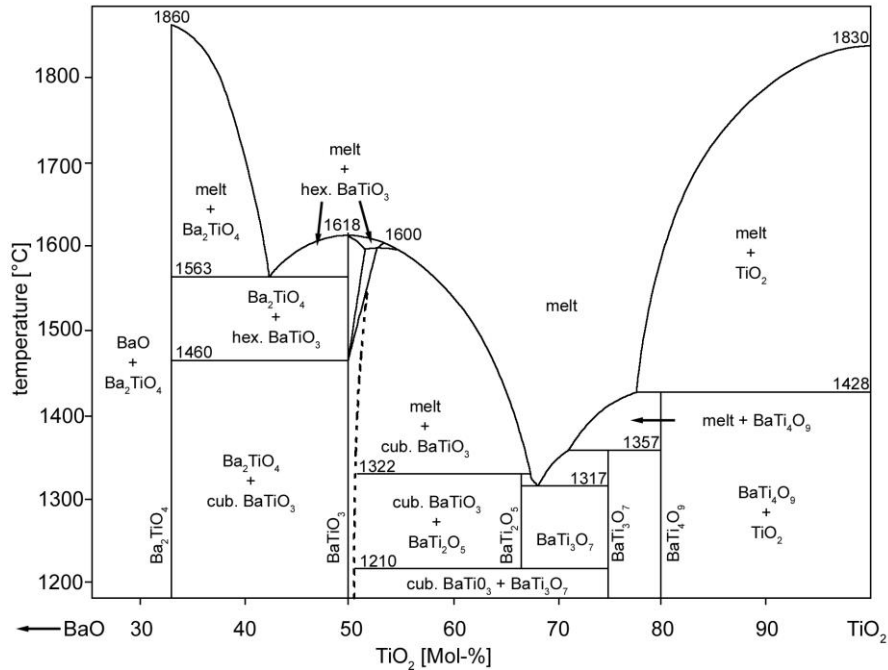


Figure 1: BaO-TiO₂ system according to Roy und Osborn [Haa60]

Production of barium titanate:

There are various preparation methods, to produce powder on basis of BaTiO₃. Primarily it is distinguished between the classic mix-oxide-method and wet chemical methods. Both methods have to be adapted to one's needs, since each have assets and drawbacks. Wet synthesis procedures like sol-gel, precipitation and hydrothermal techniques as well as complex precursors can produce a favourable quasi-atomic distribution of the barium and titanium ions, but are rather expensive. [Gab01] Thus the synthesis of barium titanate powder as preliminary stage for the production of PTC ceramics is carried out in large-industrial-scale according to the conventional mix-oxide-method. This method is also applied for the material used in this investigation. The individual process steps are shown in Figure 2.

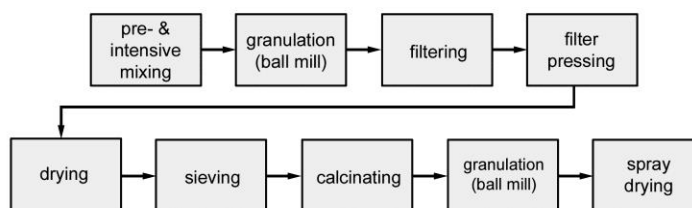
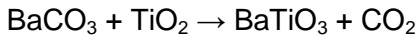


Figure 2: process map of the mix-oxide-method

The raw materials barium carbonate and titanium dioxide together with auxiliaries and dopants (see chapter 2.1.4) and water as suspension medium are intensively mixed and grinded to activate the mixture by surface enlargement. By filtering and filter pressing the moisture is reduced below 15%. After the filter cake is dried in the compartment dryer 3% moisture is left. After sieving, the prepared powder is calcinated. During calcination the barium carbonate decays by forming solid BaTiO₃ and gaseous carbon dioxide CO₂.



Equation 1: production of BaTiO₃

For complete conversion as shown in Equation 1 a calcination temperature of 1100-1200°C is needed. However, other phases such as BaTi₂O₅ or Ba₂TiO₄ are formed. Figure 3 shows the forming mechanism during calcination according to Niepce and Mutin [Gab01]. The produced BaTiO₃ powder consists of coarse grained particle agglomerates up to 100 µm large and is again grinded. After following spray drying the BaTiO₃ granulate can be used [Gab01, Epc09].

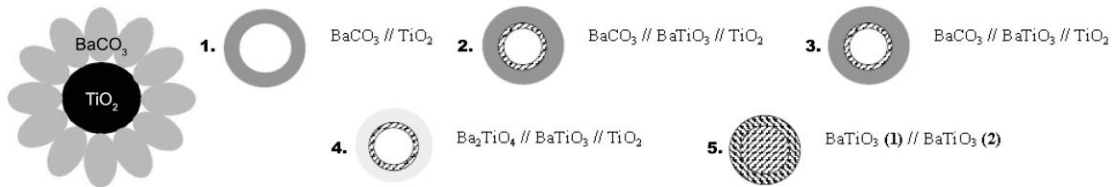


Figure 3: BaCO₃-TiO₂-system (left), BaTiO₃ genesis according to Niepce und Mutin (right)

Structure:

Barium titanate occurs in two polymorphic structures, the hexagonal type and the perovskite. Many different oxides of the form of ABO₃ show a perovskite structure. The sum of charge of the ions A and B for charge equalisation of these oxides is thus six. One of both cations has a size comparable to O²⁻ and the other cation is comparatively small. The ionic radii of the constituents of barium titanate have the following values: Ba²⁺: 134 pm (CN12), O²⁻: 140 pm and Ti⁴⁺: 68 pm (CN 6). Figure 4 displays the oblique projection of the perovskite structure. The titanium ions form a cube, at whose edges the oxygen ions and at whose centre the barium ion are arranged. Another structural model is a corner-linked TiO₆-octahedron, in which the barium atoms occupy the gaps, twelvefold coordinated by oxygen. Each oxygen ion is part of two octahedrons, so that a three-

dimensional network develops. The described perovskite structures can occur in four different modifications of barium titanate, which can be converted into one another by change of temperature. The exact changes in modification are represented in Figure 5. At a temperature of -90°C the perovskite changes from the rhombohedral modification into the orthorhombic modification. With 0°C this changes into the tetragonal structure. Reaching the Curie temperature, the perovskite changes back to the ideally cubic modification. For barium titanate the Curie temperature is about 130°C . This transformation plays an important role for the electrical characteristics [Gab01].

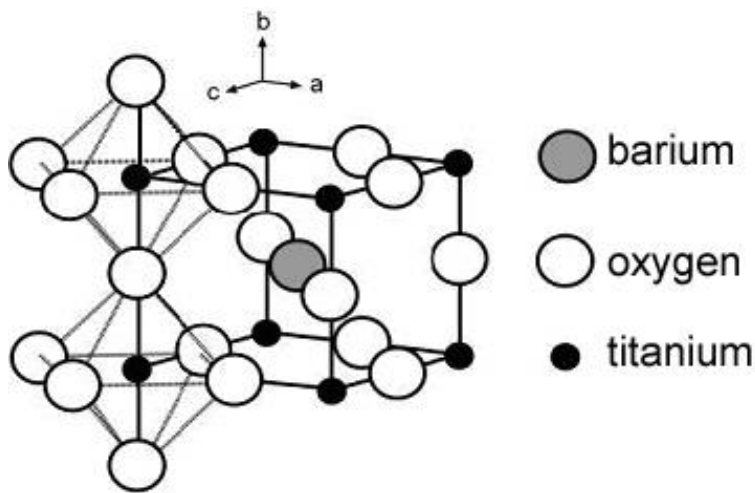


Figure 4: oblique projection of Barium titanate's perovskite structure [Gab01]

modification	rhomboedric	orthorombic	tetragonal	ideally cubic
design model				
transformation temperature	$\longleftrightarrow -90^{\circ}\text{C}$ $\longleftrightarrow 0^{\circ}\text{C}$ $\longleftrightarrow T_c = 130^{\circ}\text{C}$			
length of edge	$a=b=c=399,5 \text{ pm}$	$a=401,0 \text{ pm}$ $b=400,8 \text{ pm}$ $c=397,0 \text{ pm}$	$a=b=399,8 \text{ pm}$ $c=402 \text{ pm}$	$a=b=c=399,6 \text{ pm}$
planar angle	$\alpha=\beta=90^{\circ}\text{C}$ $\gamma < 120^{\circ}\text{C}$	$\alpha=\beta=\gamma=90^{\circ}\text{C}$	$\alpha=\beta=\gamma=90^{\circ}\text{C}$	$\alpha=\beta=\gamma=90^{\circ}\text{C}$

Figure 5: change in modification of barium titanate

Electrical properties:

By cooling below 130°C the cubic modification is converted into the tetragonal modification and at the same time a spontaneous polarisation occurs. The polarisation results from the fact that with distortion of the elementary cell two energetically more favourable positions (potential wells) for the Ti^{4+} -ion are offered. It comes thus to the displacement as represented in Figure 6.

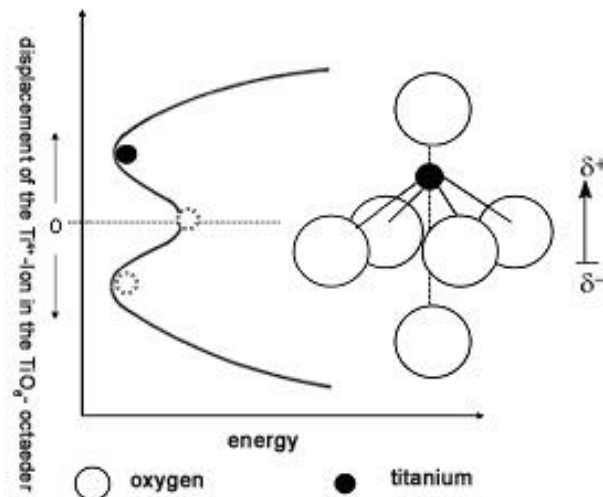


Figure 6: displacement of the Ti^{4+} -Ion in tetragonal modification [Gab01]

Two separated centres of charge are formed and a permanent electric dipole is created. The ideal cubic modification above 130°C has no displacement of the titanium ion and therefore there is neither a permanent dipole nor a spontaneous polarisation. The barium titanate becomes paraelectric above the Curie temperature. Below T_c a so called ferro-electric hysteresis occurs. By shortfall of an induced electric field a residual polarisation remains.

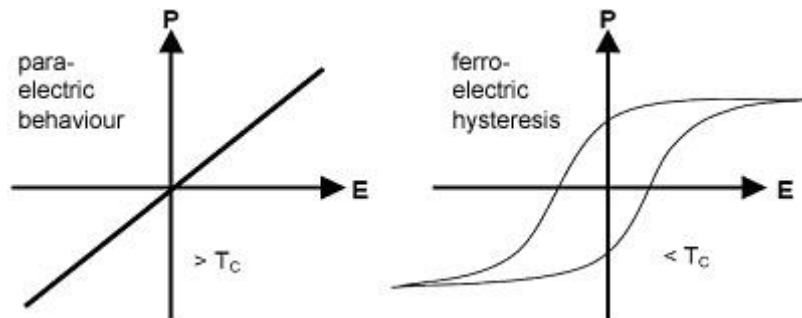


Figure 7: hysteresis of BaTiO_3 : above T_c (left) and below T_c (right)

In Figure 7 both phenomena are compared. On each axis the polarisation P [C/m²] and electric field strength E [V/m] is plotted. Above the Curie temperature the dielectric constant obeys the law of Curie-Weiss. The dielectric constant ϵ has a maximum and decreases with increasing temperatures. [Gau01].

$$\epsilon_r = \frac{C}{T - T_c}$$

Equation 2: Curie Weiss law

ϵ_r	dielectric constant	[F]
C	Curie constant	[FK]
T	working temperature	[°C]
T_c	Curie temperature	[°C]

2.1.2 PTCR effect

Positive temperature coefficient thermistors are made of a doped poly crystalline barium titanate ceramic. In general ceramics are known as good insulators with a high resistance. Semi-conducting properties and a low resistance are gained, when the ceramic is doped with elements of higher valences than the crystal lattice is built up of. A few of the barium and titanium ions are replaced with ions of higher valency in order to reach a certain amount of electrons to obtain a conductive ceramic. For this kind of donator doping cations of higher valences like La^{3+} , Y^{3+} , Sn^{3+} , Er^{3+} or Dy^{3+} replace Ba^{2+} and the Ti^{4+} -ion is replaced by Sb^{5+} , Nb^{5+} or Ta^{5+} . The net donator concentration is 0.1-0.4 mol-%. Net concentration means that only the portion of donators, needed for compensating the acceptors, is available. These acceptors can be impurities like aluminium and sodium [Sch94]. As shown in Figure 8 the structure consists of many single crystals.

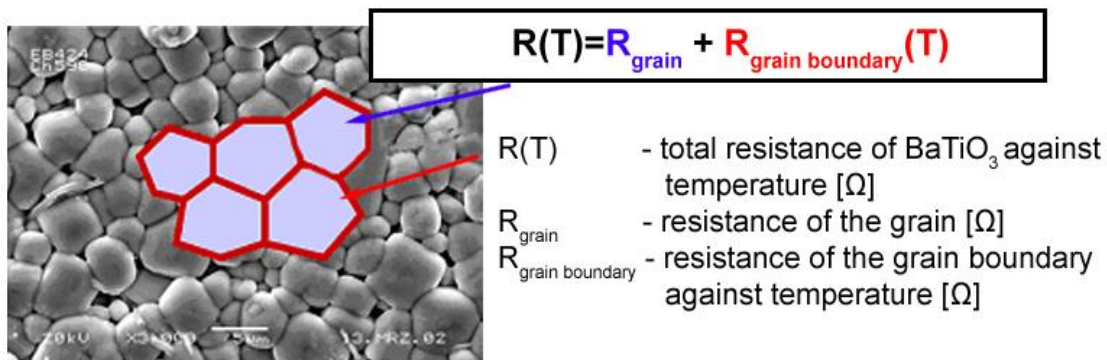


Figure 8: composition of the crystal's overall resistance

At the grain boundaries of the single crystals potential barriers are formed. They prevent free electrons from diffusion into adjacent areas. This results in a higher resistance of the grain boundaries. However, this effect is waived at low temperatures. A high dielectric constant and a sudden polarization of the grain boundaries prevent the formation of potential barriers at low temperatures and make thereby an unimpaired flowing of the electrons possible. Above the Curie temperature the dielectric constant and polarization are reduced so much that it comes to a strong rise of the potential barriers and thus the resistance. Within a certain temperature range above the Curie temperature the resistance rises exponentially. This effect is also known as positive temperature coefficient resistor effect (PTCR effect) [Epc09]. In the year 1955 researchers at Philips discovered this spectacular characteristic of barium titanate, which was new at that time. Up to this year the material had mainly been used due to its piezoelectric and dielectric characteristics [Dan79].

2.1.3 Characterisation of PTC thermistors

The key characteristic of a PTC thermistor is the resistance-temperature-curve displayed in Figure 9. The resistance has been plotted logarithmically and the following characteristics can be extracted:

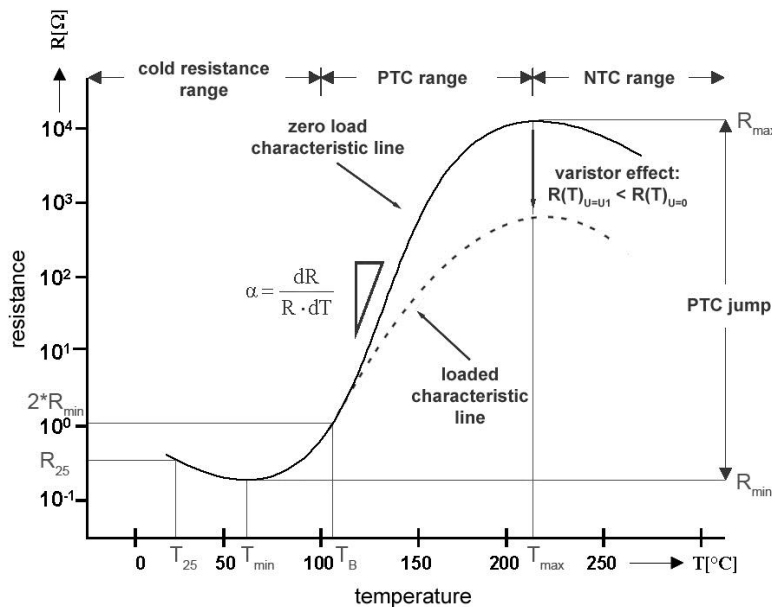


Figure 9: Resistance-temperature-curve of a PTC

R_{25} :	the resistance at a temperature of 25°C	[Ω]
R_{\min} :	the lowest value of resistance of the PTC	[Ω]
R_{\max} :	the highest value of resistance a PTC can reach	[Ω]
R_B :	reference resistance calculated according to Equation 3	[Ω]
T_B :	reference temperature when a PTC reaches R_B	[°C]
T_{\max} :	temperature at the highest resistance	[°C]
α :	temperature coefficient that reflects the slope of the R-T-curve above T_B	[1/K]
$R(T)_{U=U_1}$:	resistance against temperature with an applied voltage U_1	[Ω]
$R(T)_{U=0}$:	resistance against temperature without an applied voltage	[Ω]

At temperature below T_{\min} a PTC ceramic acts as a semiconductor, whose resistance drops with higher temperature. Reaching the reference temperature the resistance sharply rises. The negative temperature coefficient (NTC effect) comes in after exceeding the maximum value of resistance and lowers the electrical resistance with rising temperatures. In the following some characteristics of a PTC are further described.

Reference temperature:

The reference temperature T_B or T_{Ref} is located near the Curie temperature, but can be easier determined by experiments. It is defined as the temperature, where the PTC reaches the reference resistance R_B . R_B is calculated using Equation 3.

$$R_B = 2 \cdot R_{\min} \quad \text{Equation 3: calculation of reference resistance}$$

R_B :	reference resistance	[Ω]
R_{\min} :	lowest resistance	[Ω]

Temperature coefficient:

The temperature coefficient α equals the slope of the R-T-curve. Within the steep slope above the reference temperature α can be assumed as constant and can be determined according to Equation 4.

$$\alpha = \frac{1}{R} \cdot \frac{dR}{dT} \quad \text{Equation 4: calculation of the temperature coefficient } \alpha$$

α :	slope of the R-T-curve	[1/K]
------------	------------------------	-------

R: resistance [Ω]
 dR/dT: change in resistance with regard of a change in temperature [Ω/K]

2.1.4 Influences on the PTC behaviour

In order to adapt the characteristic properties of a PTC different possibilities are available. The stoichiometric composition for producing BaTiO₃ lies within a narrow range. The proportion is, as described on the phase diagram in Figure 1, 50 Mol-% BaO and 50 Mol-% TiO₂. With great deviations the resistance of the future part is changed and the amount of barium titanate gained is lowered. By isovalent substitution of e.g. strontium or lead for Barium targeted Curie temperatures can be installed. Figure 10 shows the change in reference temperatures [Sch94].

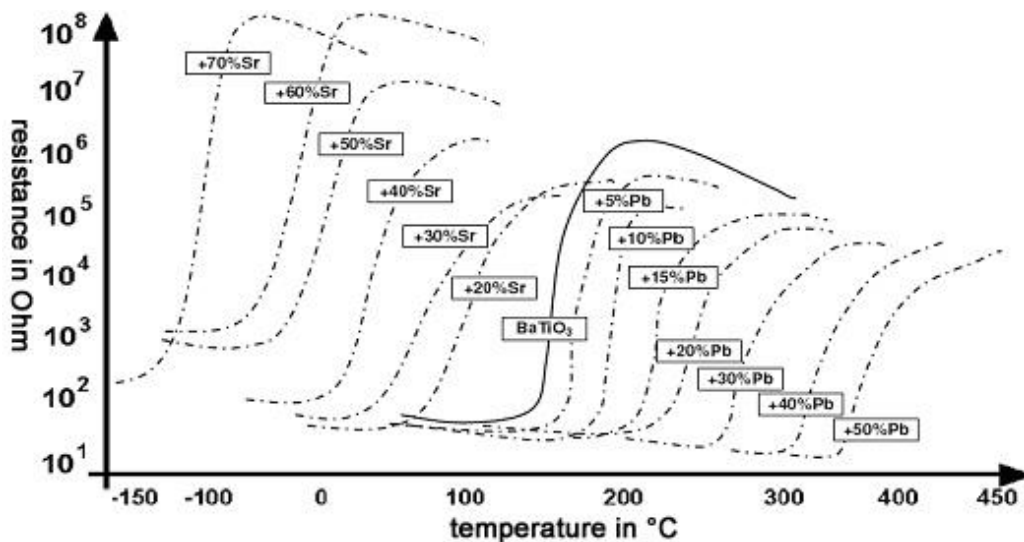


Figure 10: Adaption of reference temperature by doping with strontium or lead [Gau01]

2.1.5 Applications

Temperature dependent resistors based on semi-conductive barium titanate with a high positive temperature coefficient offer a variety of applications. Two application ranges, directly and indirectly heated PTCs, are differentiated. Indirectly heated PTCs are heated by the surrounding and are used as sensors. Directly heated PTCs convert an applied current into heat. Positive temperature coefficient thermistors are used for over current protection, degaussing devices,

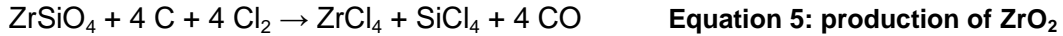
motor starters, heating devices and as temperature sensors. Since the material combination shall be used for heating applications this shall be investigated further. Because of its temperature dependent resistance, the PTC is favourable as heating device. Additional temperature control and protective devices are not needed. A good heating output is given by high heat dissipation from surface, being in contrast to the bad thermal conduction within ceramic and insulation materials. Thus metallic heating elements, which ensure a better heat dissipation, are attached to the PTC. Heating PTC resistors are available in different geometries and for application temperatures from -40 to 360°C. [Kai88, Epc09].

2.2 Zirconia

Pure zirconium dioxide can occur in three different modifications: monoclinic at room temperature, tetragonal at temperatures above 1170°C and cubic above 2370°C. During cooling the transformation from tetragonal to monoclinic modification can shift for 100 K to 1070°C, where a volume expansion of 3 to 5%, resulting in cracks and breaking, occurs [Kol04]. In 1929 examinations conducted by Ruff showed that by adding calcium oxide a stabilisation of the cubic modification can be achieved at room temperature [Ruf29]. Later on it has been shown that this polyphase material, partial stabilized zirconia (PSZ), can also be achieved by adding oxides like CaO, MgO, CeO₂ and Y₂O₃. The microstructure consists of the cubic modification with low chemical depositions of the monoclinic and tetragonal phase residing on its grain boundaries. A substantial improvement of the mechanical properties can be achieved with tetragonal zirconia polycrystals (TZP) that are doped with 2-3 mol-% yttrium oxide [Kol04]. One disadvantage of the TZP ceramic is the low temperature degradation within a temperature range of 200 to 300°C and particularly under steam atmosphere. The metastable tetragonal phase spontaneous transforms into the monoclinic phase and the ceramic loses mechanical strength [Kol04]. Fully stabilized zirconia can be achieved by further adding oxides like MgO, CaO and Y₂O₃; thus achieving a stable cubic zirconium oxide modification for a temperature range up to fusing temperature.

2.2.1 Production of zirconia

The most important zirconia minerals are Baddeleyit (ZrO_2) and Zircon ($ZrSiO_4$), which both include small amounts of hafnium compounds. Baddeleyit is only mined in South Africa and Russia. The rest of the world's production is based on the mineral zircon that contains 67.1 m-% zirconia and 32.9 m-% silica. In order to extract zirconia it has to react with chlorine gas as shown in Equation 5.



The resulting tetra chlorides can be separated by distillation. By hydrolysis $ZrCl_4$ transforms into $ZrOCl_2$ that reacts to ZrO_2 and HCl during calcination [Sal83].

2.2.2 Properties of zirconia

Zirconia offers particularly good thermal, mechanical and electrical properties.

Thermal properties:

The thermal expansion coefficient of completely stabilized zirconium dioxide has been determined to $10.8 \cdot 10^{-6} K^{-1}$ for temperatures of 25 to 1200°C [Stu75]. Partial stabilized zirconia shows a lower value and therefore has a better resistance to thermal shock. The thermal conductivity of stabilized zirconia is low ($2 W m^{-1} K^{-1}$) and is almost temperature-independent. [Sal83]

Mechanical Properties:

Partial stabilized zirconia offers excellent mechanical strength. This is based on the presence of tetragonal depositions within the cubic matrix. The energy absorption that is associated with the transformation from tetragonal to monoclinic modification leads to high fracture energies. The elastic modulus of zirconia is 200 GPa and the bending tensile strength varies from 60 to 1000 MPa. The hardness according to Vickers is 1300 N mm². [Sal83]

Electrical properties:

At high oxygen partial pressures pure ZrO_2 shows a hole-conductivity (p-conductivity). With decreasing partial pressure a certain amount of ionic conductivity is shown. At very low partial pressures and high temperatures n-conductivity appears. Measurements have shown that ZrO_2 is primarily an ionic

conductor below 700°C and is an electronic conductor between 700 to 1000°C. By doping with low-valency cations as done for stabilized ZrO₂ pure ionic conductance is achieved. [Sal83]

2.2.3 Applications

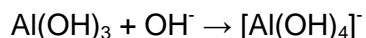
Due to its high mechanical and chemical strength zirconium dioxide is used for as wear protection in mechanical and chemical engineering, for sensors as well as the processing of raw minerals. ZrO₂ is for example used as yarn carrier, extruding die for metal production and because of its high oxygen ionic conductance for measuring the partial pressure of oxygen in kiln or exhausts of engines [Sal83]. Zirconia is also used as thermal insulation for stationary gas turbines and jet engines, for the solid oxide fuel cell (SOFC), as hip joint implants, as refractory lining and for synthetic jewellery. [Sal83]

2.3 Alumina

Aluminium oxide also known as alumina or clay is the most widely used oxide ceramic. Alumina materials are distinguished upon their alumina content: 80-90 wt.-% (KER 706), 90-99 wt.-% (KER 706) and over 99 wt.-% (KER 710). The raw materials with low Al₂O₃ contents contain high amounts of SiO₂, CaO and MgO in the form of silicates and spinels. [Sal83]

2.3.1 Alumina Production

The basis for the preparation of all technical aluminium raw materials are natural or synthetic alumina rich minerals. One of these natural oxide-hydroxide raw materials with the highest Al₂O₃ content are Bauxite. Bauxites are clay rich weathered materials consisting of aquoxides, aluminium oxides, iron and silica. The most important natural Bauxite deposits are in Guyana, Guinea, Italy, Greece, Southern France, Hungary, Australia, Jamaica and Russia. The best known alumina production process shown in Equation 6 is the Bayer process, which is based on the solubility of aluminium-aquoxides in strong acids. [Pet90]



Equation 6: Bayer process

After grinding to <1mm Bauxite is treated at temperatures of 250°C and a pressure of 40 bar with caustic soda, in which alumina hydrate dissolve. Iron hydroxides, silica and titania stay undissolved and are separated as red mud. The solution is seeded with finely dispersed alumina hydroxide so that $\text{Al}(\text{OH})_3$ (Hydragillit) exsolves. The filtered off alumina hydroxide is then calcined between 1200 to 1300°C in rotary or fluidised bed kilns where Al_2O_3 forms. [Sal83]

2.3.2 Properties of aluminium oxide

Aluminium oxide shows high thermal conductivity, low thermal expansion and high compressive strength which together leads to a good thermal shock resistance. Only a few chemicals react with aluminium oxide.

Thermal properties:

The thermal expansion coefficient of alumina increases almost linear with higher temperatures. The mean thermal expansion coefficient from 20 to 1000°C is $8.6 \cdot 10^{-6} \text{ K}^{-1}$. The thermal conductivity of alumina is 25 to 30 $\text{W m}^{-1} \text{ K}^{-1}$ and lowers to 4-5 $\text{W m}^{-1} \text{ K}^{-1}$ at 1200°C. The specific heat capacity at room temperature is 0.5 $\text{J g}^{-1} \text{ K}^{-1}$. [Pet90]

Mechanical properties:

The mechanical properties vary with the composition and the microstructure. Pure alumina exhibits a bending tensile strength of 400 MPa, an elastic modulus of 400 GPa and the hardness according to Vickers is $2.3 \cdot 10^4 \text{ N mm}^{-2}$. For a lower alumina content of 85 wt.-% the bending tensile strength is reduced to 250 MPa [Sal83]

Electrical properties:

Highly pure alumina has a very low electrical conductance of 10^{15} to $10^{16} \text{ } \Omega\text{cm}$. Technical alumina qualities with more than 99.5 wt.-% show up to 2 decades lower values. The dielectric strength is above 10 kV/mm. [Sal83]

2.3.3 Applications

Since Al_2O_3 can withstand temperatures of up to 1700°C it is used as refractory material particularly in blast furnaces as crucibles, pipes or as casing of thermo elements. Due its good electrical isolation, good resistance to wear and high hardness it is used for the mechanical, plant and electrical engineering. [Sal83]

2.4 Material properties and interactions within a ceramic composite

For a stable and firm material combination made of two different ceramics certain properties such as the thermal expansion and shrinkage have to be achieved or rather adjusted to one another. Furthermore interdiffusions and the creation of chemical compositions at the boundary layer between the individual materials have to be taken into account.

2.4.1 Thermal expansion

The thermal expansion is very important since a different expansion of the structural and functional layer can lead to cracks and thus destroy the material combination. In general all bodies expand with increasing temperature. This expansion is based on the increasing enharmonic oscillation of the atoms, leading to an increase of their distance within the solid body. The thermal expansion behaviour is characterized by the linear thermal expansion coefficient α that is defined by Equation 7. In analogy Equation 8 describes the volume expansion the volume expansion coefficient β .

$$\alpha = \frac{1}{l_0} \cdot \frac{dl}{dT}$$

Equation 7: calculation of the linear thermal expansion coefficient α

$$\beta = \frac{1}{V_0} \cdot \frac{dV}{dT}; \beta \approx 3 \cdot \alpha$$

Equation 8: calculation of the volume thermal expansion coefficient β

l_0 :	original length	[m]
dl/dT :	change in length with regard of a change in temperature	[m/K]
V_0 :	original volume	[m ³]
dV/dT :	change in volume with regard of a change in temperature	[m ³ /K]

The testing method for the determination of the linear thermal expansion coefficient is described in DIN 51045 [DIN76] and is experimentally measured with the dilatometer. According to [DIN76] accuracies of 0.2 % for the length l_0 , 0.004 % for the change in length and ± 5 K for the temperature measurement as well as the temperature constancy over the probe are required. It is important that for coarse-sized materials the diameter of the probe is at least three times the diameter of the largest grain. The presentation of the value is done in 10^{-6} K^{-1} . There are also other methods like an interferometer, where a better accuracy can be achieved. The thermal expansion coefficient itself is temperature-dependent: At 0 K it is zero, increases with higher temperatures and becomes constant at high temperatures. Besides the described mechanism, a reversible thermal expansion can also occur due to reversible phase transitions that for example quartz and not stabilized zirconia show. The thermal expansion of a material is exclusively dependent from its solid components. The size and amount of pores in the material has no influence on the thermal expansion [Kol04].

2.4.2 Shrinkage

Contrary to the reversible thermal expansion an undesired irreversible expansion, also known as after-contraction or after-expansion, has to be taken into account. After-contraction can result from high-sintering. After-expansion is mainly caused by irreversible phase transitions, mass exchanges, crystalline transformations, fusion phase transformation, and crystallisation [Sal83, Kol04]. A pre-treatment at higher temperatures than the operation temperatures can avoid this irreversible thermal expansion. [Kol04] Ceramic bonding during firing is always associated with a contraction. Haase [Haa60] described the shrinkage as outer characteristic of the sintering that has taken place and equals the reduction in length relating to the initial length of the part. Shrinkage behaviour is characterized by the linear shrinkage s_l , defined in Equation 9. In analogy Equation 10 describes the volume shrinkage s_v .

$$s_l = \frac{l_0 - l_1}{l_0}$$

Equation 9: calculation of the linear shrinkage

$$s_v = \frac{V_0 - V_1}{V_1} = \left(1 - \frac{l_1 \cdot b_1 \cdot h_1}{l_0 \cdot b_0 \cdot h_0} \right); s_v \approx 3 \cdot s_l$$

Equation 10: calculation of the volume shrinkage

l_1, b_1, h_1 length, width and height of the part after sintering [m]

l_0, b_0, h_0 length, width and height of the part before sintering [m]

s_l, s_v : linear and volume shrinkage

The testing method for the evaluation of after-contraction and –expansion is described in DIN 51045 [DIN76]. A probe is heated up at a given rate and dwells at the testing temperature for 12 hours. After cooling to room temperature the change in length of the probe is determined. There is a correlation between compaction, shrinkage and bulk density. Shrinkage increases with compaction, though the increase in shrinkage is lesser with higher compaction. The shrinkage and the increase in shrinkage are lower with higher bulk density.

2.4.3 Diffusion within poly crystalline solids

Diffusion is defined as characteristic property of kinetic processes and describes the redistribution of mass, energy (heat) or charge over macroscopic distances. Generally diffusion is relatively fast in gases, slow in liquids and very slow in solids. Rates of important chemical reactions are limited by how fast diffusion can bring reactants together. One of the major advances in the field of diffusion has been done by Adolf Fick (1829-1901). He first introduced the idea of a diffusion coefficient during his experimental studies of salt in water. [Meh07] He proposed two laws, known as Fick's laws, describing the diffusion of matter. His first law, shown in Equation 11, describes the flux of particles in media. Whereas the nabla operator denotes the three dimensional concentration gradient, J_x describes the particle flux in x-direction.

$$J = -D\nabla C; J_x = -D \frac{\partial C}{\partial x};$$

Equation 11: Fick's first law

J, J_x particle flux (in all directions, respectively x-direction)

D diffusivity, i.e. diffusion coefficient

$\nabla C, \frac{\partial C}{\partial x}$ concentration gradient (in all directions, respectively x-direction)

Whereas Fick's first law is governing a steady-state description of diffusion, Fick's second law takes further the continuity equation into account.

$$\frac{\partial C}{\partial t} = \nabla \cdot (D \nabla C) \quad \text{Equation 12: Fick's second law}$$

Diffusion in general and the random movement of particles is based on defects within a solid's structure. These defects can be 0-dimensional such as vacancies, interstitial atoms and foreign atoms, 1-dimensional like edge and screw dislocations or 3-dimensional like stacking faults and grain boundaries. [Meh07]

With increasing temperature the rate of diffusion also increases. One reason for this is that particles can leave their positions easier with higher thermal energy. The diffusion coefficient follows an Arrhenius relation as stated in Equation 13.

$$D = D_0 \exp\left(-\frac{Q}{k_B T}\right) \quad \text{Equation 13: Arrhenius relation of diffusion}$$

D_0	Diffusion	[m]
K_b	Boltzmann constant	[m]
Q	activation energy	[J]
T	absolute temperature	[K]

Kirkendall effect:

Ernest Kirkendall and his co-workers observed the inequality of copper and zinc diffusion during interdiffusion between copper and brass as the interphase between the two different phases moves. The movement of inert markers placed at the initial interphase of a diffusion couple is called Kirkendall effect. Furthermore the interactions accompanying the Kirkendall effect can, for example, induce stress and deformation on macroscopic scale. It can also cause migration of microscopic inclusions inside a reaction zone and diffusional porosity, also known as Kirkendall voids. Figure 11 pictures the Kirkendall displacement from the original to the resulting marker position. [Meh07]

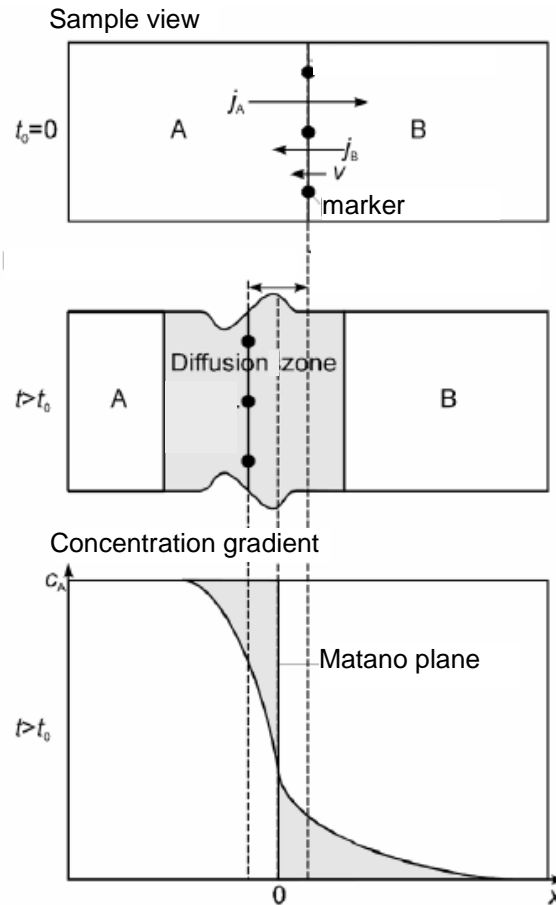


Figure 11: Kirkendall effect [Spr11]

Diffusion kinetics in polycrystals:

Grain boundary diffusion is a complex process which involves direct lattice diffusion from the source, diffusion along the grain boundary leakage of the diffusant from the grain boundary and subsequent lattice diffusion into fringes around the grain boundary. [Meh07]

The most widely used classification of the diffusion kinetics for polycrystals was first introduced by Harrison. [Har61] He distinguishes between three regimes A, B and C shown in Figure 12. Type A kinetics is observed after diffusion anneals at high temperatures or/and with long annealing times or/and in materials with small grain size. With the condition shown in Equation 14 the diffusion fringes around neighbouring grain boundaries overlap and a diffusing atom may visit many grains and grain boundaries during a diffusion experiment. This results in a planar diffusion front with a penetration depth proportional to \sqrt{t} . [Meh07]

Type B kinetics emerges after diffusion anneals at lower temperatures, or/and in materials with large grain size. Under these conditions the bulk diffusion \sqrt{Dt} can become much smaller than the spacing d between grain boundaries and the width of the grain-boundary fringes can be much larger than the grain-boundary width δ . These conditions are summarized in Equation 15. [Meh07]

Type C corresponds to conditions where lattice diffusion is practically ‘frozen in’ and thus diffusion takes place only along grain boundaries. This situation can be matched in diffusion anneals at sufficiently low temperatures and/or for very short diffusion times, where the condition shown in Equation 16 occurs. [Meh07]

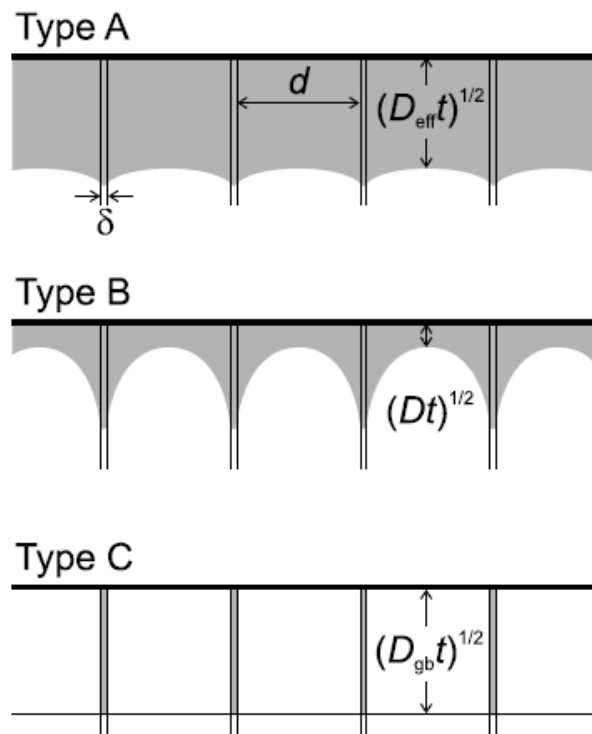


Figure 12: Harrison's type A, B and C diffusion regimes in a polycrystal [Meh07]

$$\sqrt{Dt} \geq d/0.8$$

Equation 14: conditions for type A kinetics

$$s\delta \ll \sqrt{Dt} \ll d$$

Equation 15: conditions for type B kinetics

$$\sqrt{Dt} \ll s\delta$$

Equation 16: conditions for type C kinetics

2.5 Multi-component forming methods

The developed material combination of barium titanate and zirconia requires a multi-component forming process. The part's shape can be achieved with the use of multi-component injection moulding, tape casting and multilayer dry pressing. Pressing is used for preliminary investigations and further on ceramic tapes shall be developed within this doctoral thesis. Multi-component injection moulding can also be applied but will not be discussed further. The main processes of pressing and tape casting and the most important parameters shall be investigated within this chapter.

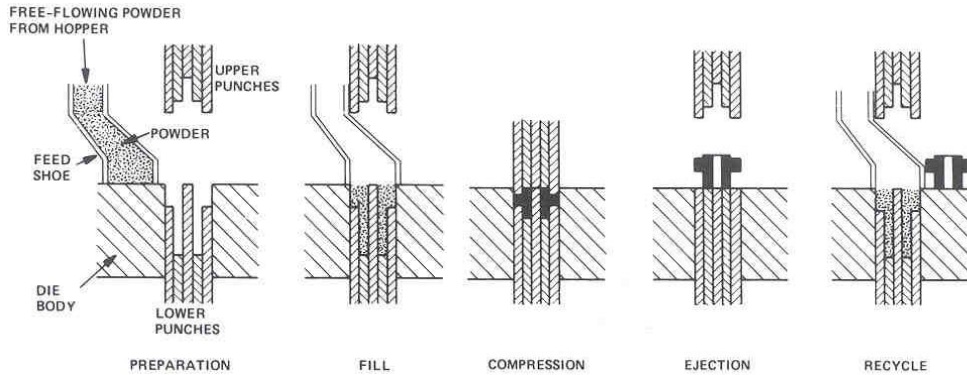
2.5.1 Dry pressing

Pressing is the most widely practiced forming process for reasons of productivity, high accuracy to size and essentially no drying shrinkage. Pressed products are a variety of magnetic and dielectric ceramics, fine-grained ceramics such as cutting tools, ceramic tiles and porcelain, and coarse-grained refractories, grinding wheels, and structural clay products. According to [Ree94] common disadvantages are the restrictive parts' geometry and gradients in density. Pressing is a shaping method, where a free-flowing to friable mass is compacted at high pressure. In dry pressing the humidity content can range from 4 to 8%. Since the shrinkage depends on the part's compaction, the same packing should be achieved, thus the pressure should be constant over the part, too. Because of the friction between mould and ceramic a pressure distribution is built up using unilateral pressing. This leads to different sintering shrinkages and a part's warp. Organic additives like oils and stearates can lower this effect. During pressing the common ceramic powders are compacted to 50% of their initial volume, thus the mould has to be twice as high to neutralize the compaction. The coherence of pressure, part's volume, density in raw state and porosity is crucial for pressing [Sal83]. According to Van der Zwan und Siskens [Van80] the pressing of spray-dried powder agglomerates can be classified into four steps:

1. compaction by more dense spherical packing of the grains
2. breaking up and plastic deformation of the grains

3. filling of cavities among the grain packing
4. breaking up and plastic deformation of the primary particles

As shown in Figure 13 the process steps of dry pressing are preparation, filling of the die, compaction as well as the ejection of the part. The free-flowing granules are fed to the die by means of a sliding feed shoe. Small ejected parts are commonly displaced to a conveyor by the leading edge of the feed shoe. [Ree94]



2.5.2 Tape casting

Tape casting is an industrial scale shaping method to produce large and thin ceramic products at low costs. Tape casting is extremely sensitive for process fluctuations, thus high yields can only be achieved by certain quality assurances over the whole process. The small process window can be attributed to the production of the slurry made of different components, the relatively small shaping forces during casting, the drying process and inhomogeneities in shrinkage. Tape casting is limited to the tape's thickness, which can be greatest 1.5 mm and has to be at least 10 μm thick. [Kol04] Tape casting requires homogenous castable ceramic slurry which is stretched out to a thin tape and dried afterwards. The great success of this method is based on the possibility to produce multilayer parts by punching, silk-screen printing and lamination. The ceramic tape casting process goes back to activities to produce thin ceramic parts for resistors during World War II in 1943. Typical products are substrates of Al_2O_3 , AlN or BeO for microelectronics. Furthermore low temperature co-fired ceramics (LTCC), condenser, inductivities, piezometer and gas sensors are produced by metallization of green tapes and laminating them to multi-layer

parts. Next to these functional ceramics applications also plane compound materials of oxide and non-oxide powder for optimization of mechanical properties have been produced, based on for example Al_2O_3 , ZrO_2 , or SiC and MoSi_2 [Kol04]. The main process steps of tape casting are:

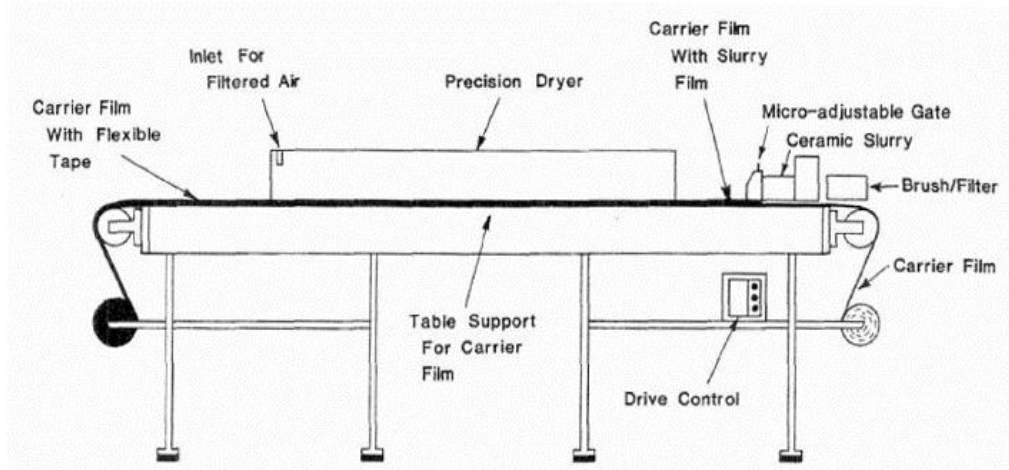
Slurry production:

For tape casting homogenous slurry with stability in time, a certain viscosity, pseudo plastic behaviour and a high solid content is needed. Ceramic slurries consist of a multi-component system, where all components are interacting with each other. The slurry mainly consists of an initial ceramic powder and various organic additives that controllable adjust the slurry's properties. Generally solvents, binder, dispersants and softeners are used. The slurry production is based on the processed powder, which shall adjust the desired properties of the final ceramic. Thus the ceramic powder has to be characterized at the beginning of the slurry production concerning purity, particle size distribution, humidity content and other parameters. The main objective is the homogenous mixing of the individual parts. The individual components are normally mechanically dispersed within a ball mill. After milling the slurry is screened to remove any coarse inhomogeneities, agglomerates and undissolved organic material must be much finer than the thickness of the tape for proper forming and for best thermal and mechanical properties. Sieves with an aperture as fine as $10\ \mu\text{m}$ are used. Dissolved gas in the slurry is commonly removed in a closed container under vacuum. Viscosity is monitored to assure that the solvent loss is controlled [Ree94]

Tape production:

The tape production can be done by casting or diving. Commonly used, also at EPCOS OHG, is the casting method or so called doctor-blade method, where the slurry is within a pan, whose blade can be adjusted in height. Below the pan a tape carrier made of metal or polymer moves and draws the slurry below the

blade opening of the pan as a thin tape [Kol04]. Such a tape casting line is shown in Figure 14.



Drying and further processing:

The ceramic slurry layer is dried on the carrier by counter flowing air in a drying chamber. Then it is separated from the carrier and is further processed by punching, metallization and lamination. Using silk-screen-printing electrical circuits, resistors, capacities and other functional structures can be printed on the green tapes with different pastes. The metallised and not metallised green tapes can be processed to multilayers. Therefore the tapes are stacked and laminated. At lamination the tapes are joined under pressure (10-30 MPa) and temperature (60-80°C) above the T_g temperature of the binder. During this so called thermo compression method the binder softens and the particles of neighbouring tapes are slid into each other. In order to make this possible the tapes have to meet certain requirements on porosity, binder and inorganic content. For production of not metallised products lamination can even be avoided with multi-tape casting. This is done by casting on a not totally dried tape [Wag00]. After all parts have been processed as desired debinding and sintering occurs.

2.5.3 Debinding

In debinding the binder is carefully removed from the parts. According to the binder system and its characteristics an aqueous, thermal or catalytic debinding can be accomplished. The aqueous debinding can also be

accomplished in other solvents, however, water showed up as particularly suitable due to its environmental compatibility [Qui98]. In a water quench, heated up to 60°C, the part can gradually release the water-soluble components. An additional thermal debinding is necessary to reduce the remaining binder. The thermal debinding must be sufficiently slowly, otherwise tears, blows and flame formation can occur. The temperatures are up to 400°C and the heating gradients are between 2 and 50 K/h [Ker06, Gau00].

2.5.4 Sintering

The actual material formation occurs during sintering. In a high-temperature kiln the parts are densified below melting point with an accompanying shrinkage of up to 30 vol.-% [Kol01]. According to the powders used the sintering temperature is between 1350 and 1750°C. Dwell times at 300 to 400°C should be applied to burn the binder left-over's. The main parameters are the maximum temperature, dwell times, heating gradients and the atmosphere. The sintering curve not only influences the ceramic but the electrical characteristics. Therefore the optimal sintering program for the ceramic mass has to be found [Gau00, Sch94].

3 Material development

This chapter is on the material development that has been conducted for this doctoral thesis. First the different ceramic masses had to be evaluated. A conducted process analysis has shown that the powder has to be characterized particularly with regard to grain size distribution and specific surface area. In order to prove a concurrent sinterability, the properties of the sintered ceramic masses had to be determined and the optimal sintering regime for the desired electrical and mechanical properties had to be revealed. This optimal sintering regime for the material combination has been investigated using statistical investigations. A stable material combination can only be achieved by adapting thermal expansion and shrinkage of the single materials. Corresponding dilatometry measurements have been carried out to characterize the linear shrinkage and linear thermal expansion coefficient of the ceramic masses. Based on the characterized ceramics, tapes have been developed and assessed. Prior to this ceramic slurries had to be produced and their rheological behaviour had to be characterized.

3.1 Material characterisation

3.1.1 PTC ceramics

For the investigations two PTC masses A and B have been used. Mass A is free from lead and strontium and has a reference temperature of 120°C and a nominal specific electrical resistance of 100 $\Omega \cdot \text{cm}$. Mass B on the other hand is lead, strontium and silicium rich, has a similar reference temperature of 123°C and a similar specific electrical resistance of 100 $\Omega \cdot \text{cm}$. Table 1 shows the molecular proportions of the cations of both PTC masses.

Table 1: molecular proportions of the cations of PTC masses

Analytic value (mol%) specifications								
Compositon	Ba ²⁺	Ca ²⁺	Sr ³⁺	Pb ³⁺	Ti ⁴⁺	Si ⁴⁺	Y ³⁺	Mn ²⁺
PTC mass A	84.508	15	0	0	101	0	0.41	0.082
PTC mass B	62.95	3.6	15.4	17.5	100.05	2.00	0.48	0.07

Powder characterisation

According to the results from the process analysis especially the grain size distribution had to be verified. With normal powder processing of the PTC mass A, used at Epcos, a medium grain size d_{50} of 2.5 μm is produced according the specification. The exact grain size distribution is shown in A. 1. The specific surface area has been determined to 3.48 m^2/g . In Figure 31 the powder is recorded with a scanning electron microscope.

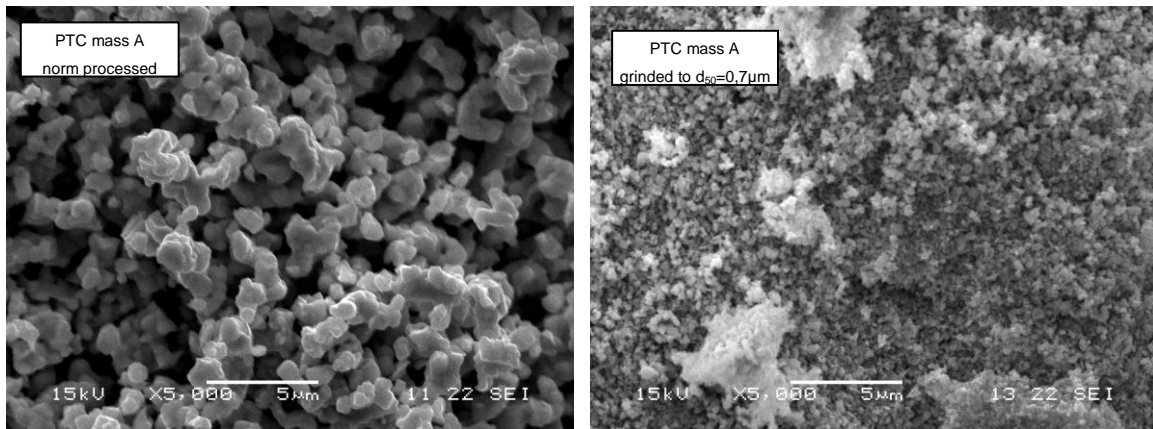


Figure 15: SEM analysis of PTC powder (left: norm processed, right: grinded)

Pre-investigations

Prior investigations have been carried out to reveal the temperature limits for the sintering of the barium titanate. First the PTC mass A powder has been charged with 4 wt.-% binder in order to achieve a free-flowing mass. Then discs with a diameter of 12 mm, a thickness of 2 mm and a green density of 3.19 g/cm^3 have been produced using a unilateral press. With these discs a series of sinterings have been carried out in a kiln from Linn High Therm GmbH. The kiln has heating elements on all four sites of the hearth and different gases can be passed through the kiln. An air flow of 25 l/min has been adjusted for all sinterings. As sintering curve the norm sintering regime shown in Table 2 has been used. The sintering temperature has been varied from 1300 to 1400°C. Respectively ten parts have been sintered in a rouleau on an alumina plate sprinkled with a thin zirconia layer to avoid reactions between parts and sintering aids.

3 Material development

Table 2: Norm sintering regime

gradient [K/min]	5	8	10	6	20
temperature [°C]	500	1000	Sintering temperature	900	0
dwel time [min]	0	0	30	0	

The sintered parts have been optically checked and measured with a micrometer gauge. After that the parts were metallised by sputtering within the pilot sputter station Leibold-Heraeus Z400. The exact procedure is cathode evaporation under argon atmosphere. A 1 µm layer composed of chrome, nickel and silver was applied on the parts. Base chrome realizes the degradation of the boundary layer. Nickel enables the solder ability and silver prevents the oxidation of the sputtered layer. After this sputtering process the specific electrical values have been determined. The Keithley 199 System DMM/Scanner was used to measure the electrical resistance R_{25} . The device has a clip on instrument for measuring the parts and was inside an air-conditioned room with the temperature of 25°C. The specific electrical resistance was calculated according to Equation 17.

$$\rho_{25} = \frac{R_{25} \cdot A}{d} \quad \text{Equation 17: calculation of the specific electrical resistance}$$

ρ_{25} :	specific electrical resistance at $25 \pm 1^\circ\text{C}$	[$\Omega \cdot \text{cm}$]
R_{25} :	resistance at $25 \pm 1^\circ\text{C}$	[Ω]
A	cross-section of the part	[cm^2]
d	thickness of the part	[cm]

The measured dimensions and electrical resistances are shown in A. 3 and A. 4. The results show that a sintering temperature higher than 1350°C is needed to achieve a completely sintered part with a reasonable specific electrical resistance. Figure 16 shows the specific electrical resistance in dependency of the sintering temperature. It can be seen that the specific resistance at room temperature R_{25} decreases with higher sintering temperatures. The standard deviation also decreases with higher sintering temperatures. This can be traced back to a more homogenous temperature distribution within the kiln.

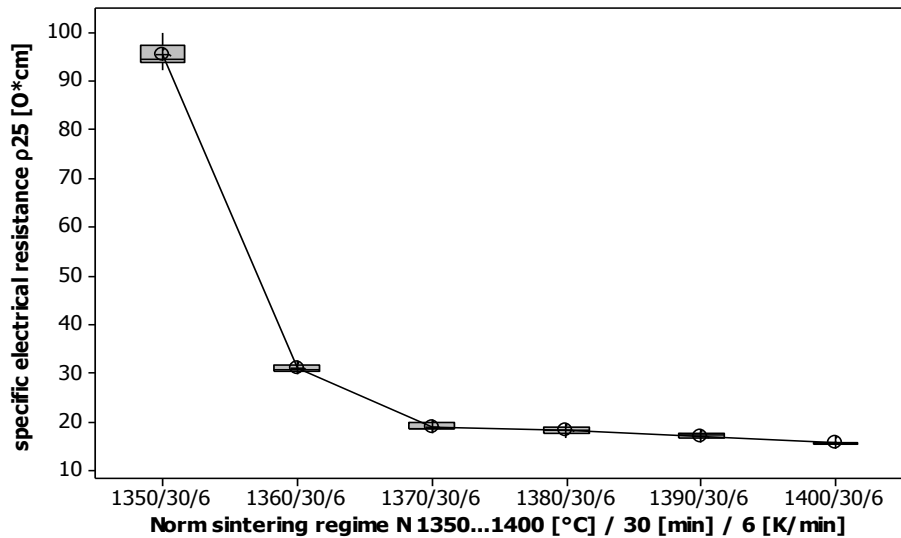


Figure 16: ρ_{25} of PTC mass A in dependency of different norm sintering regimes

Electrical characteristics

For a more detailed analysis of the electrical values next to the specific electrical resistance the reference temperature and the slope of the R-T-curve have been measured and evaluated with a regression analysis. According to the results of the pre-investigations the sintering temperature has been varied from 1360 to 1400°C and the dwell time has been varied from 20 to 80 minutes. The characteristic R-T-curve of the sample has been measured in an oil-filled temperature-controlled tank Proline RP 18409, by Lauda GmbH. The electrical resistance of the parts has been measured with the Keithley 2000 Multimeter at 18 temperatures between 20 and 180°C. The resistance has then been plotted in dependency of the temperature. Exemplary the R-T curve of a part sintered with the norm sintering regime 1400/50/6 is shown in Figure 17.

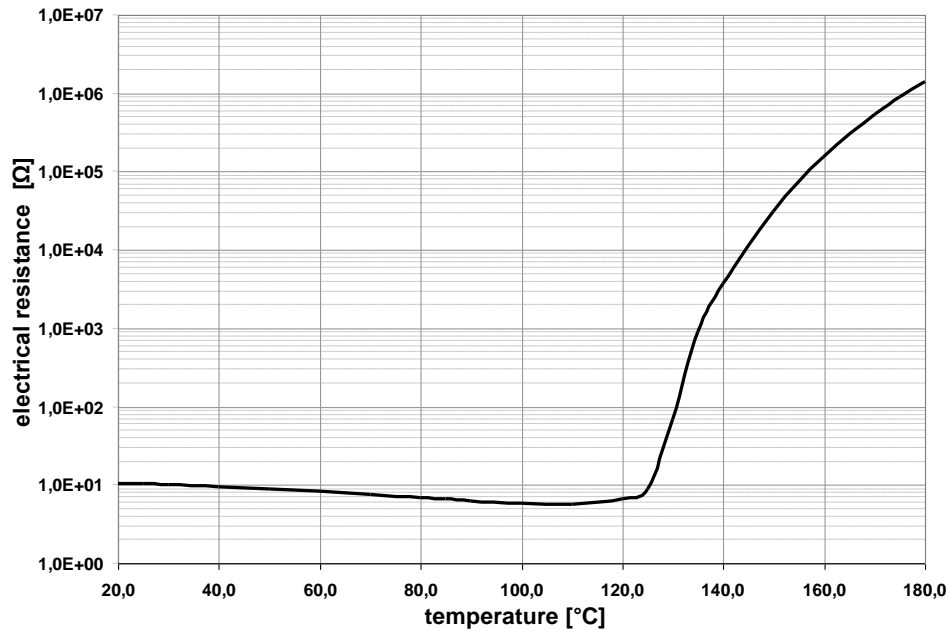


Figure 17: R-T-curve of PTC mass A sintered with N 1400/50/6

Based on the measurements the specific electrical resistance, the reference temperature and the slope of the R-T-curve have been calculated. The specific electrical resistance values are displayed in A. 5 to A. 7. The highest specific electrical resistance of 2200 $\Omega\cdot\text{cm}$ has been measured with a sintering temperature of 1360°C. With increasing sintering temperature as well as a short dwell time the specific electrical resistance can be lowered to 20 $\Omega\cdot\text{cm}$. The results of the regression analysis that has been carried out on the specific electrical resistance values are shown in Figure 18. For the determination of the significance a confidence interval of 95 % has been used. Thus if a calculated p-value is greater than 0.05, the null hypothesis, that no significant influence exists, has to be assumed. The regression is with a p-value of 0.00 significant. The influence values sintering temperature and dwell time possess both with p-values smaller than 0.05 a significant influence on the specific electrical resistance. According to the indicated coefficient of determination $R^2(\text{adj})$ 53.6% of all values are on the identified regression line shown in Equation 18. The reference temperature and the slope of the R-T-curve are displayed in A. 8 to A. 10. Within the investigated sintering interval the reference temperature is very stable at about 125°C and shifts only for 3 K to 122°C with the lowest sintering

temperature of 1360°C. The slope of the R-T-curve varies from 35.2 to a maximum of 75.4 %/K with longer dwell times. The conducted regression analysis on the temperature coefficient values is shown in Figure 19. Both, the dwell time and the sintering temperature have a significant influence on the temperature coefficient α . The regression has been proven to be significant and the R^2 adjusted value of 97.4 % is a sign for a very good regression. The determined regression equation for the slope of the R-T-curve is shown in Equation 19. All in all the investigations showed that the PTC mass A possesses a low specific electrical resistance and a suitable R-T-curve.

Predictor	Coef	SE Coef	T	P
Constant	68031	4873	13.96	0.000
temperature	-49.477	3.560	-13.90	0.000
dwell time	13.864	2.373	5.84	0.000

S = 505.855 R-Sq = 54.2% R-Sq(adj) = 53.6%

Analysis of Variance						
Source	DF	SS	MS	F	P	
Regression	2	50557967	25278983	98.79	0.000	
Residual Error	167	42733488	255889			
Total	169	93291454				

Source	DF	Seq SS
temperature	1	41826974
dwell time	1	8730992

Figure 18: regression analysis of the specific electrical resistance of PTC mass A

Predictor	Coef	SE Coef	T	P
Constant	1.1048	0.2083	5.31	0.000
temperature	-0.0007035	0.0001521	-4.62	0.000
dwell time	0.0078179	0.0001014	77.08	0.000

S = 0.0216183 R-Sq = 97.4% R-Sq(adj) = 97.4%

Analysis of Variance						
Source	DF	SS	MS	F	P	
Regression	2	2.9146	1.4573	3118.23	0.000	
Residual Error	167	0.0780	0.0005			
Total	169	2.9927				

Source	DF	Seq SS
temperature	1	0.1383
dwell time	1	2.7764

Figure 19: regression analysis of the slope of the R-T-curve of PTC mass A

$$\rho_{25} = 68031 - 49.5 \cdot T + 13.9 \cdot t$$

Equation 18: regression equation for the specific electrical resistance of PTC mass A

3 Material development

$$\alpha = 1.10 - 0.000704 \cdot T + 0.00782 \cdot t$$

**Equation 19: regression equation for the slope
of the R-T-curve of PTC mass A**

ρ_{25} :	specific electrical resistance	[$\Omega \cdot \text{cm}$]
α :	slope of the R-T-curve	[1/K]
T:	sintering temperature between 1360 and 1400	[$^{\circ}\text{C}$]
t:	dwel time between 20 and 80	[min]

Dilatometry measurements

The dilatometry measurements have been carried out with pressed parts with a size of 3 by 3 by 25 mm. For the shrinkage measurement green samples have repeatedly been measured in the dilatometer DIL 402CD together with a normal based on alumina. From the measured difference in length over temperature the shrinkage has then been calculated using Equation 9 (see chapter 2.4.2). The shrinkage curve of the PTC mass A is displayed in Figure 20. It shows that with heating up to 1200°C the ceramic mass compacts and shrinks by 2%.

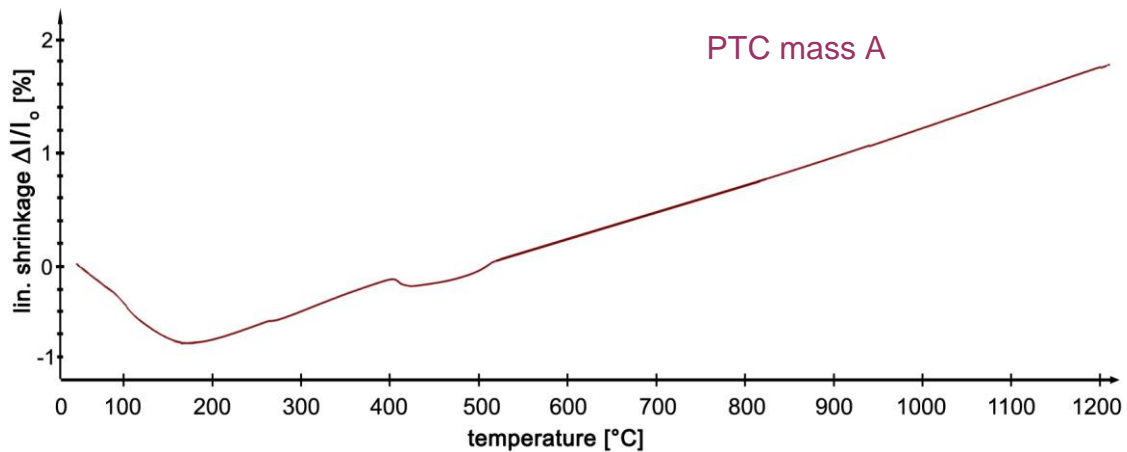


Figure 20: shrinkage measurement of PTC mass A

The thermal expansion has also been recorded in the dilatometer DIL 402CD using sintered samples with a length of 25 mm and an alumina normal. The linear thermal expansion coefficient has been calculated from the measured difference in length using Equation 7 (see chapter 2.4.1). The thermal expansion coefficient over time curve is shown in Figure 21. Eye catching is a change in the thermal expansion coefficient at about 130°C. This temperature equals the Curie

temperature. The PTC mass contracts until the Curie temperature is reached and then the crystal lattice transforms and a change in the thermal expansion coefficient occurs. Above T_C the linear thermal expansion coefficient is comparatively steady and can be determined to $7.70 \cdot 10^{-6} \text{ K}^{-1}$. Above 1200°C liquid phases are formed, thus it was not necessary to measure at higher temperatures.

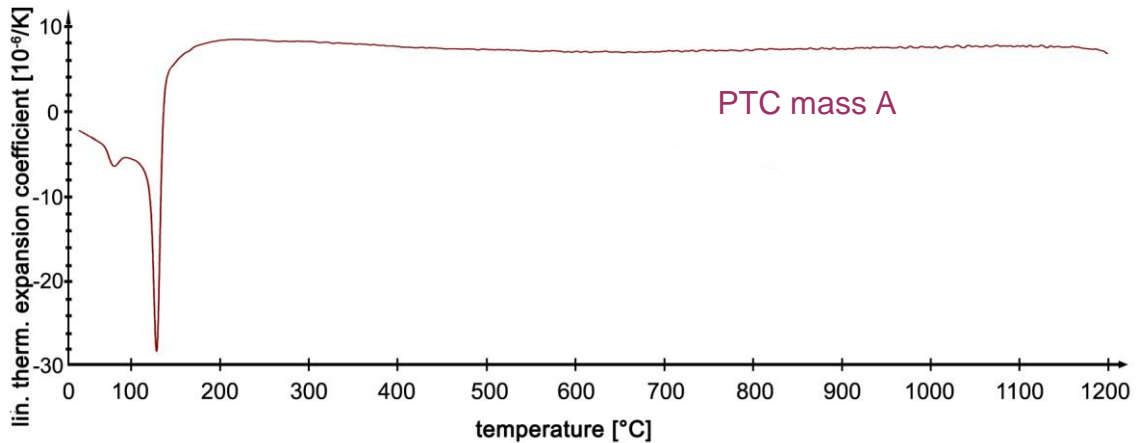


Figure 21: thermal expansion measurement of PTC mass A

3.1.2 Yttria stabilized zirconia (YSZ)

As stated in chapter 2.2 zirconia can be stabilized by adding different ions such as CaO, MgO, CeO₂ and Y₂O₃. Yttrium oxide is the most commonly used stabilisation agent. For the investigations an yttria stabilised zirconia (product name: Melox 3Y, supplier: MelChemicals, England) has been used. Table 3 shows the specified composition of this yttria stabilized zirconia. In order to avoid confusions and for convenience reasons it shall be further referred to as YSZ within this thesis.

Table 3: composition of yttria stabilized zirconia Melox3Y

Analytic value (max %) specifications					
ZrO ₂ + HfO ₂	SiO ₂	Fe ₂ O ₃	TiO ₂	Solid content (wt.-%)	Y ₂ O ₃
94	0.01	0.005	0.01	30	5.3

3 Material development

Powder characterisation

The yttria stabilized zirconia has a d_{50} of 0.7 μm . A. 11 displays the exact grain size distribution. The specific surface area has been determined to 16.3 m^2/g . Figure 22 shows the powder recorded with a scanning electron microscope.

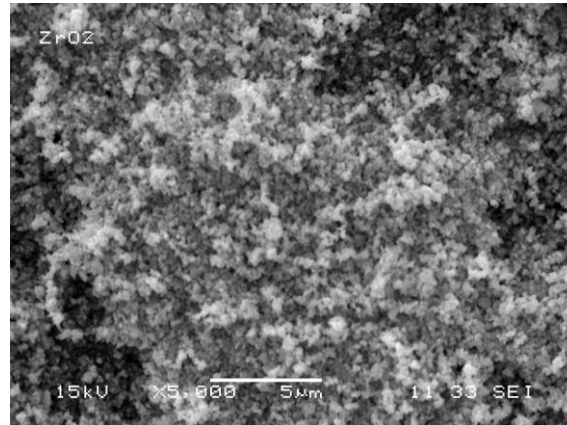


Figure 22: SEM analysis of zirconia powder

Pre-investigations

Prior investigations have been carried out to evaluate the zirconia's mechanical strength and bulk density. The YSZ powder has also been charged with 4 wt.-% binder and an additional 1 mol-% SiO_2 . This has been done due to first investigations of Steinberger [Ste09]. He found out that with adding the silicium dioxide higher mechanical strength values can be achieved. This is due to a more dense sintering of the mass and thus fewer defects are left. From the processed YSZ powder substrates with a thickness of 2 mm and a green density of 2.5 g/cm^3 have been pressed. The substrates have then been sintered in the already described kiln from Linn High Therm GmbH. The air flow has been set to 25 l/min. The norm sintering regime with varied sintering temperature from 1350 to 1400° has been investigated. The sintered prototypes have then been cut to small beams of a size of 25 by 4.5 by 1.5 mm for the mechanical strength evaluation as well as various sizes for the porosity measurement. For each sintering regime ten beams have been measured with the micrometer gauge and examined on a test machine from Zwick-Roell using the three point bending method. The measured dimensions and forces are shown in A. 12. The three point bending tensile strength was calculated using Equation 20.

$$\sigma = \frac{M_{b,\max}}{W} = \frac{3 \cdot F \cdot l}{2 \cdot b \cdot h^2}$$

Equation 20: calculation of the bending strength

The Weibull parameters have been determined graphically. For this the calculated bending strength values have been sorted in order and plotted against the corresponding probabilities of fracture in a Weibull diagram. From this diagram the characteristic Weibull strength values S_0 , the intercepts of the regression lines with $y=0$, could be extracted. The Weibull module m has been extracted from a different Weibull diagram where the strength is plotted logarithmically against $\ln[1/(1-F(\sigma_{B,i}))]$. The slope of the regression line of the data equals the Weibull modulus m . The determined Weibull parameters are displayed in Table 4.

Table 4: Weibull parameters of YSZ in dependency of the sintering temperature

sintering regime	Weibull strength	Weibull module
	S_0 [MPa]	m
N1350/30/6	741.83	12.315
N1360/30/6	778.65	12.780
N1370/30/6	751.56	11.805
N1380/30/6	875.72	12.156
N1390/30/6	901.05	11.244
N1400/30/6	878.24	10.546

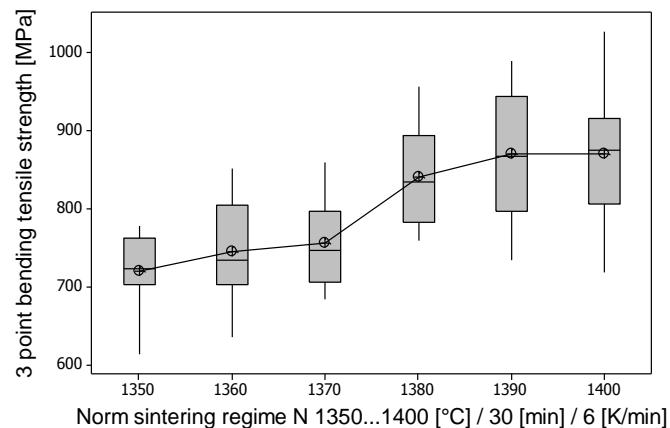


Figure 23: mechanical strength of YSZ in dependency of different norm sintering regimes

Figure 23 shows that the 3 point bending strength increases with higher sintering temperatures and reaches a maximum characteristic Weibull strength of approximately 900 MPa. The Weibull module can be determined to an average of 11.8, which is a sign for a good distribution of possible defects within the YSZ.

3 Material development

Next to the mechanical strength also the density of the YSZ has been pre-evaluated using Archimedes' principle. First the mass of the dried sample m_1 has been determined. The sintered samples have then been drenched with water using the vacuum method according to DIN 51056 [DIN85]. The air within the open pores is hereby suppressed by water. Then the water saturated sample m_2 is weighted. Using a non-absorbent cloth the sample is then slightly drained and weighted once more. The three measured masses are summarized in A. 14. The density of the water has been determined according to the measured temperature. The bulk density, the open porosity and the water absorption of the samples, that have been calculated with Equation 21 to Equation 23, are also shown in A. 14. The bulk density of the YSZ in dependency of the sintering temperature is displayed in Figure 24. With higher sintering temperature the bulk density increases slightly from 5.720 to 5.738 g/cm³. As shown in Figure 25 very low open porosity values of no more than 0.2 % have been determined for the YSZ. Altogether the pre-investigations have proven that the Yttrium stabilized zirconia has high mechanical strength values and a very dense structure within the investigated sintering temperatures from 1350 to 1400°C. Due to these properties it is suitable as structural base system for the PTC.

$$\rho_{bulk} = \frac{m_1}{m_3 - m_2} \cdot \rho_{fl} \quad \text{Equation 21: calculation of the bulk density}$$

$$P_o = \frac{\rho_{bulk} \cdot w}{\rho_{fl}} \cdot 100\% = \frac{m_3 - m_1}{m_3 - m_2} \cdot 100\% \quad \text{Equation 22: calculation of the open porosity}$$

$$w = \frac{m_3 - m_1}{m_1} \cdot 100\% \quad \text{Equation 23: calculation of the water absorption}$$

ρ_{bulk} :	bulk density of the sample	[g/cm ³]
ρ_{fl} :	density of the detection liquid, in this case water	[g/cm ³]
P_o :	open porosity of the sample	[%]
w :	water absorption of the sample	[%]
m_1 :	mass of the dried sample	[g]
m_2 :	apparent mass of the probe drenched in the detection liquid	[g]
m_3 :	mass of the drenched probe in air	[g]

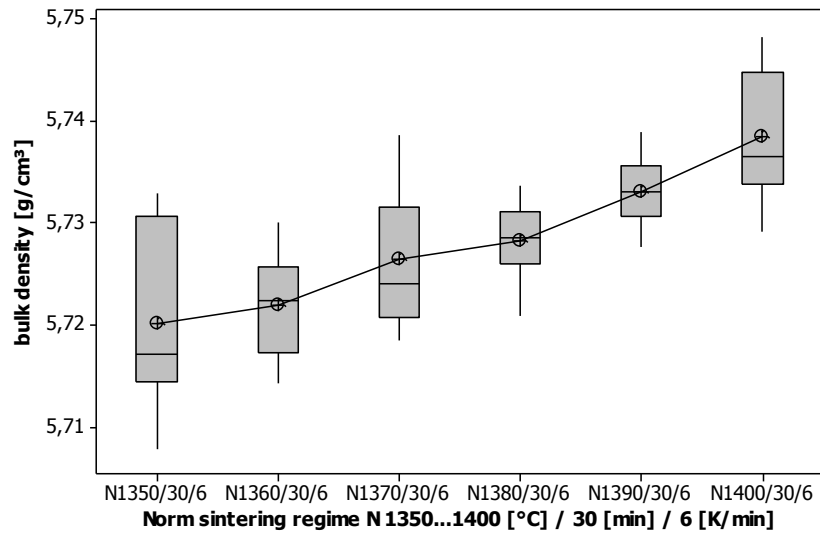


Figure 24: bulk density of YSZ in dependency of different norm sintering regimes

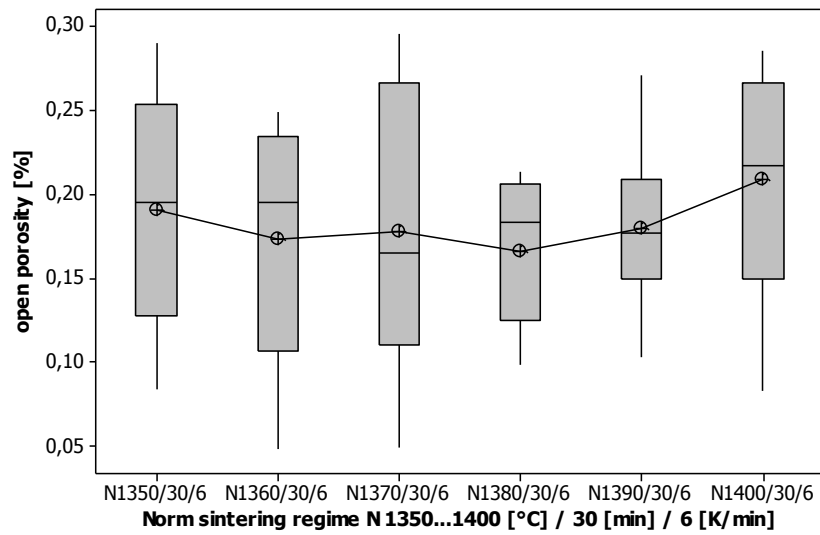


Figure 25: open porosity of YSZ in dependency of different norm sintering regimes

3 Material development

Mechanical strength:

The mechanical strength has been evaluated with the help of a regression analysis. From the processed YSZ powder substrates with a thickness of 2 mm and a green density of 2.5 g/cm³ have been pressed. The substrates have then been sintered in a muffle kiln using the norm sintering regime. According to the results of the pre-investigations the sintering temperature has been varied from 1360°C to 1400°C and the dwell time has been varied from 20 to 80 minutes. Small beams with a size of 25 x 1.80 x 3.5 mm have been cut from the sintered substrates and examined on a test machine from Zwick-Roell using the three point bending method. The measured dimensions and forces are summarized in A. 13. The three point bending tensile strength was calculated using Equation 20. The Weibull parameters, displayed in Table 5, have been determined graphically as described before. The YSZ shows within the investigated sintering range Weibull bending tensile strength values from 560 to 710 MPa.

Table 5: Weibull parameters of YSZ in dependency of different norm sintering regimes

sintering regime	Weibull strength	Weibull module
	S ₀ [MPa]	m
1: N1380/50/6	694.47	21.619
2: N1380/50/6	711.79	10.889
3: N1366/29/6	658.09	10.196
4: N1380/20/6	647.38	8.609
5: N1380/50/6	600.00	12.271
6: N1394/71/6	597.55	6.311
7: N1380/50/6	697.33	9.401
8: N1360/50/6	670.51	16.779
9: N1400/50/6	667.00	9.401
10: N1380/80/6	671.78	11.220
11: N1394/29/6	678.42	14.780
12: N1366/71/6	674.66	23.523
13: N1380/50/6	555.88	11.349
14: N1366/29/6	636.87	13.407
15: N1366/29/6	613.33	10.425
16: N1366/29/6	628.54	7.250
17: N1366/29/6	626.81	14.193

The conducted regression analysis is shown in Figure 26. The p-value for the regression is with 0.717 greater than 0. Thus the regression is not significant. The R² adjusted of 0 % also proves this. This is actually a good result, since it

proves that the mechanical strength of the YSZ is steadily high and independent from temperature and dwell time within the investigated sintering range.

Predictor	Coef	SE Coef	T	P
Constant	718.0	710.8	1.01	0.314
temperature	-0.0807	0.5193	-0.16	0.877
dwell time	0.2815	0.3462	0.81	0.417

S = 73.7852 R-Sq = 0.4% R-Sq(adj) = 0.0%

Analysis of Variance					
Source	DF	SS	MS	F	P
Regression	2	3628	1814	0.33	0.717
Residual Error	167	909190	5444		
Total	169	912818			

Source	DF	Seq SS
temperature	1	27
dwell time	1	3601

Figure 26: regression analysis of the mechanical strength of YSZ

Porosity measurement

Archimedes' principle has also been used for further investigations on the density of the YSZ. The samples have been produced and sintered as described for the mechanical strength measurement. Also the same sintering regimes with temperatures from 1360 to 1400°C and dwell times from 20 to 80 minutes have been used. The masses m_1 , m_2 and m_3 of ten samples for each sintering regime have been determined with the vacuum method according to DIN 51056 [DIN85] as described for the pre-investigations. The measured masses are summarized in A. 15 to A. 17. The density of the water has been determined according to the measured temperature. The bulk density, the open porosity and the water absorption of the samples have been calculated with equations 18 to 20 and are also shown in A. 15 to A. 17. The YSZ showed within the investigated sintering range a high bulk density of 5.7 g/cm³ and very low open porosities of lower than 0.5 %. The regression analysis that has been conducted on the bulk density values is shown in Figure 27 and Figure 28 shows the regression analysis of the open porosity. Both analyses yielded the same results. Both regression have p-values of 0 and are therefore significant. The p-value of the dwell time is in each case greater than 0.05. Thus the dwell time has neither a significant influence on the bulk density nor on the open porosity. The coefficients of determination are

3 Material development

very low with 8.9 and 4.9 %. Thus only low percentages of the measured values are on the determined regression lines. The explanation for this is that the influence of the temperature on both values is very low and thus both differ only slightly within the sintering range. This is furthermore a good sign since the YSZ has very high bulk densities and low open porosity values all over the investigates sintering range.

Predictor	Coef	SE Coef	T	P
Constant	4.5013	0.3079	14.62	0.000
temperature	0.0008751	0.0002249	3.89	0.000
dwel time	0.0001072	0.0001500	0.72	0.476

S = 0.0319623 R-Sq = 10.0% R-Sq(adj) = 8.9%

Analysis of Variance					
Source	DF	SS	MS	F	P
Regression	2	0.018974	0.009487	9.29	0.000
Residual Error	167	0.170605	0.001022		
Total	169	0.189579			

Source	DF	Seq SS
temperature	1	0.018451
dwel time	1	0.000522

Figure 27: regression analysis of the green density of YSZ

Predictor	Coef	SE Coef	T	P
Constant	10.499	3.115	3.37	0.001
temperature	-0.007396	0.002276	-3.25	0.001
dwel time	0.000797	0.001517	0.53	0.600

S = 0.323325 R-Sq = 6.0% R-Sq(adj) = 4.9%

Analysis of Variance					
Source	DF	SS	MS	F	P
Regression	2	1.1197	0.5599	5.36	0.006
Residual Error	167	17.4580	0.1045		
Total	169	18.5778			

Source	DF	Seq SS
temperature	1	1.0909
dwel time	1	0.0289

Figure 28: regression analysis of the open porosity of YSZ

Dilatometry measurements

Green pressed parts with a size of 3 by 3 by 25 mm have been heated in the dilatometer DIL 402CD together with a normal based on alumina. The shrinkage has been calculated from the measured change in length over temperature using Equation 9 as described in chapter 2.4.2. The shrinkage curves of the PTC mass

PTC mass A and the YSZ are displayed in Figure 29. The YSZ shows a slightly lower shrinkage than the PTC mass within the temperature interval up to 1200°C.

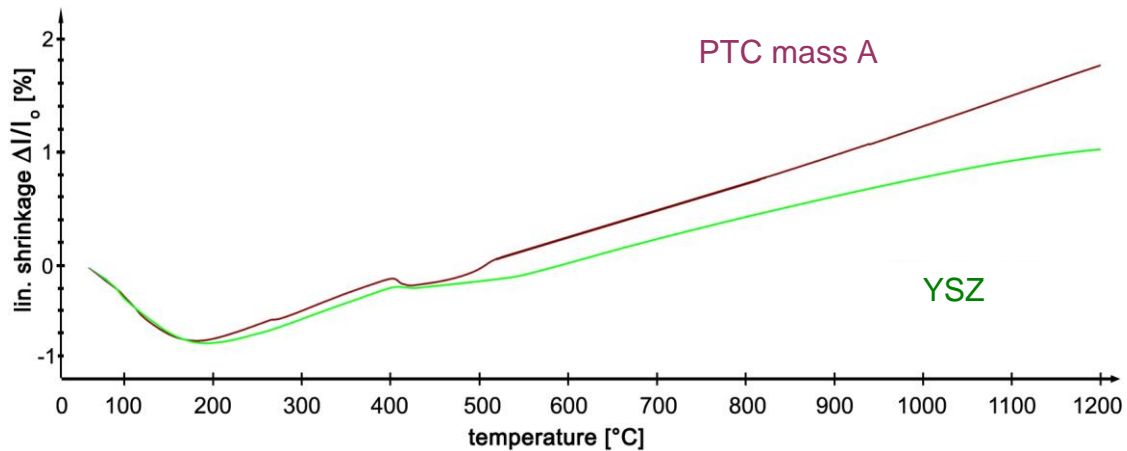


Figure 29: shrinkage measurement of PTC mass A and YSZ

Sintered samples of a length of 25 mm have been measured together with an alumina normal in the dilatometer DIL 402CD to determine the thermal expansion. The linear thermal expansion coefficient has been calculated from the measured change in length according to Equation 7. The thermal expansion coefficient in dependency of the temperature is shown in Figure 30. Since the thermal expansion of the YSZ has to be adjusted to the PTC mass, its curve is for comparison also shown in this diagram. The thermal expansion coefficient of the YSZ increases until 200°C and reaches then a relatively steady value of $5.26 \cdot 10^{-6}$ K. Below the curie temperature, the thermal expansion of the YSZ is a lot higher than the expansion of the PTC mass A. An adjustment of both within this temperature range is not possible, but fortunately there is no need for this. Due to the higher expansion the YSZ elongates more than the PTC thus the PTC layer gets under compressive stress. This even improves a firm composite since the PTC layer then has to overcome the enclosed compressive stress. This behaviour is also used for glass coating and enamels, where the coating has a lower thermal expansion coefficient than the metal to be protected. Above the Curie temperature the linear thermal expansion coefficient of the PTC can be determined to $7.70 \cdot 10^{-6}$ K. Thus an existing difference in the thermal expansion of $2.44 \cdot 10^{-6}$ K has to be accomplished with intermediate layers. According to

operating experience of the multilayer department at EPCOS OHG a firm interconnection of different ceramics can only be achieved with a difference in the thermal expansion no higher than $1 \cdot 10^{-6}$ K. Taking this into account at least two better three intermediate layers are required to achieve a stable material composition of PTC and YSZ. Of course the interconnection of both ceramics increases even more with less difference and therefore more intermediate layers, but at the same time the complexity, thickness of the composite as well as expenditure and costs increase dramatically. Owing to these economic reasons composites of two and three intermediate layers have been investigated further.

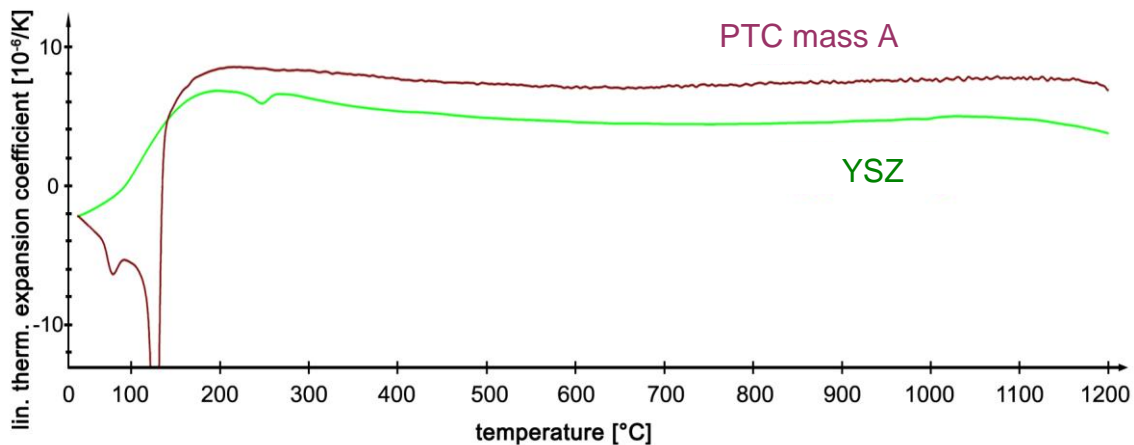


Figure 30: thermal expansion measurement of PTC mass A and YSZ

All in all the characterization proved that the YSZ has a high mechanical strength and a very dense structure within the sintering regime. Based on the evaluation of PTC and YSZ the optimal sintering regime for the material combination has been set up. The optimal sintering regime consists of a sintering temperature of 1400°C, a dwell time of 30 minutes and a cooling gradient of about 6 K/min. The sintering regime is characterized by high mechanical strength values of the zirconia and appropriate electrical characteristics of the PTC mass A.

3.1.3 Alumina

Next to zirconium dioxide also aluminium oxide (product name: UFX-DBM, supplier: Baikowski Malakoff, Inc.) has been investigated as structural ceramic layer. Table 3 shows the specified composition of the alumina powder. The specific surface area has been determined with the BET method to $12.61 \text{ m}^2 \text{ g}^{-1}$.

The loss on ignition has been determined to 0.74 wt.-%. The grain size distribution is shown in A. 18.

Table 6: composition of aluminium oxide

Analytic value (max %) specifications						
Al ₂ O ₃	Na ₂ O	SiO ₂	Fe ₂ O ₃	CaO	MgO	Ga ₂ O ₃
99,26	0.0096	0.0028	0.01	0.0063	0.0007	0.0021

3.1.4 Barium titanate

After the first investigations it was evident that diffusion and reactions take place between the PTC and the YSZ as well as between PTC and the Al₂O₃. As barrier layer a barium titanate layer was chosen as it is very similar to PTC, donor doped barium titanate. Thus its properties are similar and no third ceramic would make the composite even more complex. In opposition to the PTC mass the barium titanate does not contain any calcium or yttrium oxide. Due to this fact the diffusion of calcium and yttrium atoms could be lowered or absorbed within this barrier layer. The barium titanate powder (Product name: BTHP2, supplier: EPCOS) has been used for the investigations. In Figure 31 the scanning electron microscopy of the barium powder is shown.

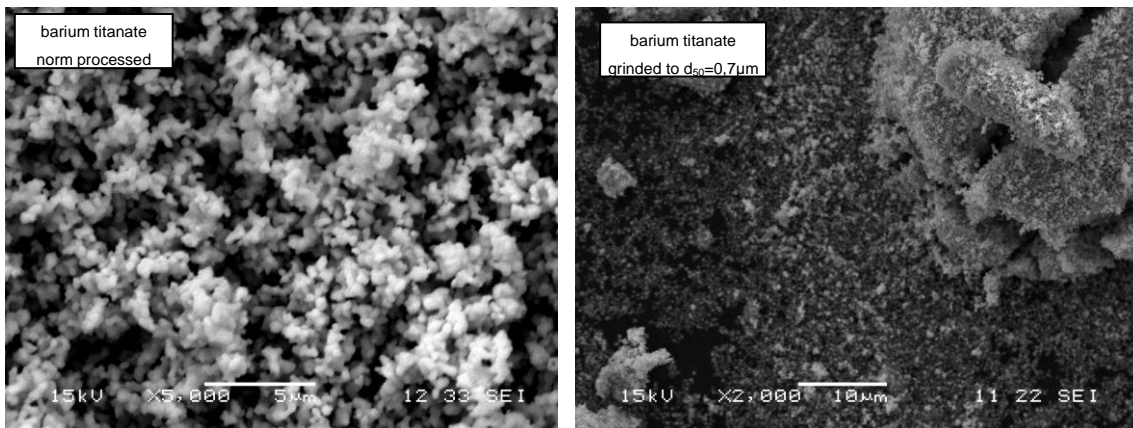


Figure 31: SEM picture of barium titanate powder (left: original, right: grinded to 0.7 μm)

3.2 Tape development

In order to produce prototypes by means of tape casting tapes based on the PTC mass PTC mass A, zirconium dioxide as well as molecular proportions of both had to be developed. First the slurry had to be produced from the ceramic powders.

Slurry production:

As described in chapter 2.5.2 for tape casting homogenous slurries with stability in time, a certain viscosity, pseudo plastic behaviour and a high solid content are needed. Thus a multi-component system of the ceramic powder and various organics has to be produced. For first trials a binder set based on NT-1008 has been used. Since particularly the produced zirconia tapes were too chapped and not treatable the binder set has been exchanged to Butyl acetate and Butyl cellosolve. Benzylbutylphthalat has been used as softening agent. The exact organic proportions for each tape have roughly been adapted beforehand and fine-tuned according to the resulting tapes. For example the amount of binder and softener had to be reduced for the PTC layer otherwise the tape would have been too sticky. The exact compositions of the slurries for each tape are summarized in Table 7 and Table 8.

Table 7: slurry composition of PTC mass A, YSZ and intermediate layers

component	unit	PTC mass A	YSZ	20% YSZ 80% PTC mass A	50% YSZ 50% PTC mass A	80% YSZ 20% PTC mass A
grinding balls	g	200.00				
PTC mass A	%	57.00	0.00	45.11	22.08	10.92
YSZ	%	0.00	54.05	11.28	33.11	43.69
Butyl acetate	%	29.64	31.23	29.97	30.61	30.92
Butyl cellosolve	%	7.41	7.81	7.49	7.65	7.73
Benzylbutylphthalat	%	1.85	2.59	2.00	2.30	2.45
BL-S	%	1.03	1.08	1.04	1.06	1.07
BM-S	%	2.05	2.16	2.07	2.12	2.14
BH-S	%	1.03	1.08	1.04	1.06	1.07

Table 8: slurry composition of PTC mass A, Al₂O₃ and intermediate layers

components	unit	Al ₂ O ₃	20% Al ₂ O ₃ 80% PTC mass A	60% Al ₂ O ₃ 40% PTC mass A	80% Al ₂ O ₃ 20% PTC mass A
grinding balls	g	200.00			
PTC mass A	%	0.00	46.85	30.92	12.97
Al ₂ O ₃	%	48.51	9.62	24.73	41.75
Butyl acetate	%	35.79	29.92	30.37	30.87
Butyl cellosolve	%	8.41	7.48	7.59	7.72
Benzylbutylphthalat	%	3.41	1.98	2.19	2.42
BL-S	%	1.94	1.04	1.05	1.07
BM-S	%	1.94	2.07	2.10	2.14
BH-S	%	0.00	1.04	1.05	1.07

The first step was to weigh in 200 g of grinding balls. Then the organic components Butyl acetate, Butyl cellosolve and Benzylbutylphthalat were added. Further on the ceramic mass was weighted in. Then the slurry has been shaken for 20 minutes using a single-arm shaker from Red Devil equipment Co. After that the components BL-S, BM-S and BH-S were added. Subsequently, the slurries have been shaken for another 60 minutes in steps of 20 minutes with a followed cooling.

Rheological behaviour:

The tape casting technology requires a preferably shear-thinning behaviour of the slurry. Particularly, the slurry shall light-bodily flow on the carrier under the shear stress caused by the doctor blade and shall set on the carrier, when the shear stress is zero. The rheological behaviour of the developed slurries has been determined using a cone disc viscosimeter from Brookfield. Exemplary the recorded viscosity values for the slurry based on yttria stabilized zirconia are summarized in Table 9. The corresponding viscosity by shear rate diagram is shown in Figure 32.

Table 9: recorded viscosity values for the YSZ slurry

Revolution speed [rpm]	Shear rate [1/s]	Viscosity [Pa·s]
5	2	4.24
10	4	3.5
20	8	2.8
50	20	2.2
100	40	1.71

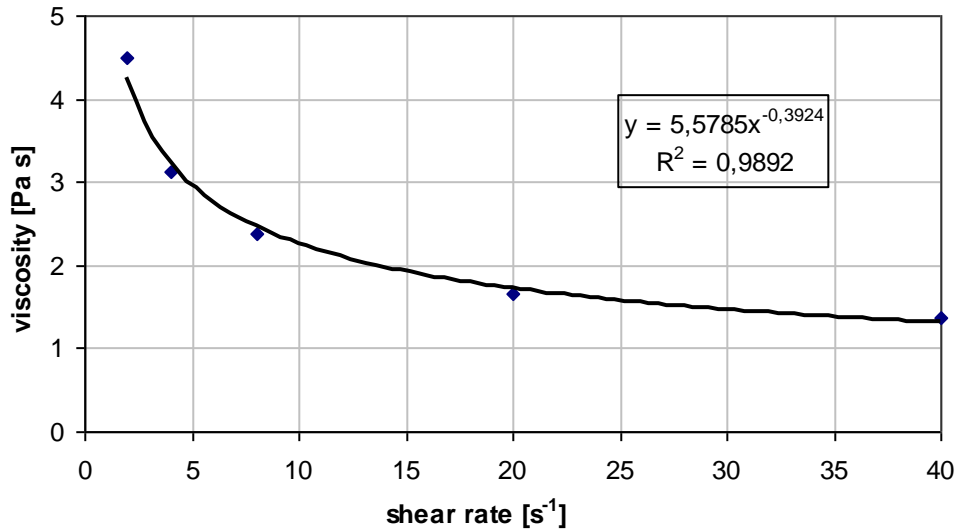


Figure 32: viscosity-shear rate diagram of the YSZ slurry

As displayed the slurry shows the desired shear-thinning behaviour, since the viscosity decreases with a higher shear rate. But it has to be acknowledged that the results of the used cone disc viscosimeter are not fully representative since only a small slurry drop is measured. Thus interferences like an additional wall friction and a possible evaporation of the solvent become more important.

Tape production:

After this procedure, the tapes have been casted on an organic carrier using doctor blades of 30, 200 and 300 μm . The tapes were then left to dry. The 30 μm thick tapes have been used to check the dispersity of the slurry. With the 200 μm doctor blade green tapes with a thickness of 60 to 70 μm could be produced. Using the 300 μm doctor blade 90 to 100 μm thin green tapes could be produced. Latter have been used for further investigations as well as the prototype production. The tapes have then been cut into pieces of 100 by 100 mm and separated from the organic carrier.

Dilatometry measurements

The single tapes have been stacked according to the desired assembly for the prototypes. For dilatometry measurements fifteen single tapes have been stacked together to form a sintered thickness of about 1 mm, the smallest

available normal size for the dilatometer. All tapes have been pressed together for 2 minutes with a pressure of 100 t and a temperature of 35°C. For the dilatometry measurements the stacks have been cut to samples of 3 by 6 mm. In order to compare the shrinkages green samples of each tape have repeatedly been measured in the dilatometer DIL 402CD together with a normal based on alumina. From the measured difference in length over temperature the shrinkage has then been calculated using Equation 9 (see chapter 2.4.2). A. 3 displays the shrinkage curves of tapes based on the PTC mass A and YSZ. All in all, it can be seen that the shrinkages of the zirconia layers are adapted to the barium titanate up to 1200°C. Above 1200°C first liquid phases are formed, that can compensate differences.

3.3 Investigations of the chemical interactions based on pressed powder mixtures

For the first investigations of the chemical interactions formed at the boundary layer between the PTC ceramic and the structural ceramic the following experimental design has been set up. Based on the PTC masses A and B 26 compositions as shown in Table 10 have been evaluated. Each mass has been added with 1 to 20 mol% yttria stabilized zirconia as well as aluminium oxide.

Table 10: experimental design of pressed powder mixtures

Experiment number	Reference	Doping with YSZ [mol%]						Doping with Al ₂ O ₃ [mol%]					
		1	3	5	10	15	20	1	3	5	10	15	20
PTC mass A	1	2	3	4	5	6	7	8	9	10	11	12	13
PTC mass B	14	15	16	17	18	19	20	21	22	23	24	25	26

Each composition has been spray dried with 4 wt.-% binder in order to achieve a free-flowing mass. Then discs with a diameter of 12 mm, a thickness of 2 mm have been pressed with a unilateral press. For characterisation of the pressed parts the dimensions have been measured with a micrometer gauge and the mass has been determined a microbalance. From both the green density of the samples has been calculated using Equation 21. The discs have then been sintered in a batch kiln from Linn High Therm GmbH. The disks have been

3 Material development

sintered in a rouleau on an alumina plate sprinkled with a thin zirconia layer to avoid reactions between parts and sintering aids. The sintered parts have been optically checked and the density has been calculated from size and weight measurements. Using Equation 9 the shrinkage has been calculated from the green and sintered sized.

The powder mixtures have been further investigated as follows. Shrinkage measurements have been carried out in the dilatometer DIL402CD. Electrical characteristics such as the resistance over temperature curve, the resistance at 25°C, the surface temperature, the residual current and the break down voltage have been determined. The three point bending tensile strength has been determined as mechanical characteristic. For analytical characterization a structure determination including Scanning electron microscopy (SEM) with EDX and x-ray diffraction analysis has been conducted.

The photographs of the sintered disks are shown in Figure 33 to Figure 34. Already from first view one can see the different grey and brownish shades of the PTC disks. Whereas the PTC references show a saturated grey colour the additions of zirconia or aluminium oxide turn them into a light brown colour. This is already a very good indication of the PTC characteristics. A saturated grey usually equals good PTC characteristics, such as a steep slope and low resistance. For donor doped barium titanate the brownish colour usually indicates an under sintered behaviour and poor PTC characteristics. The colour change from grey to brown can be observed between 5 to 10 mol% YSZ. PTC mass A shows this colour change already for 1 mol% alumina content. In opposition the PTC mass B shows this colour change between 5 to 10 mol% alumina.

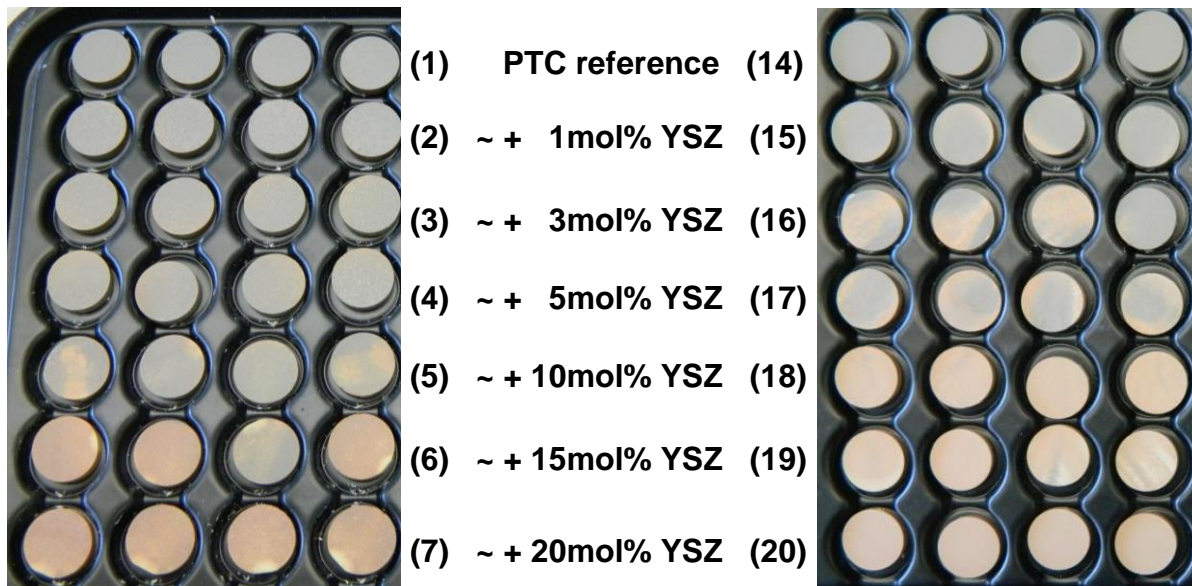


Figure 33: Sintered disks composed of YSZ and PTC (left: PTC mass A and right: mass B)

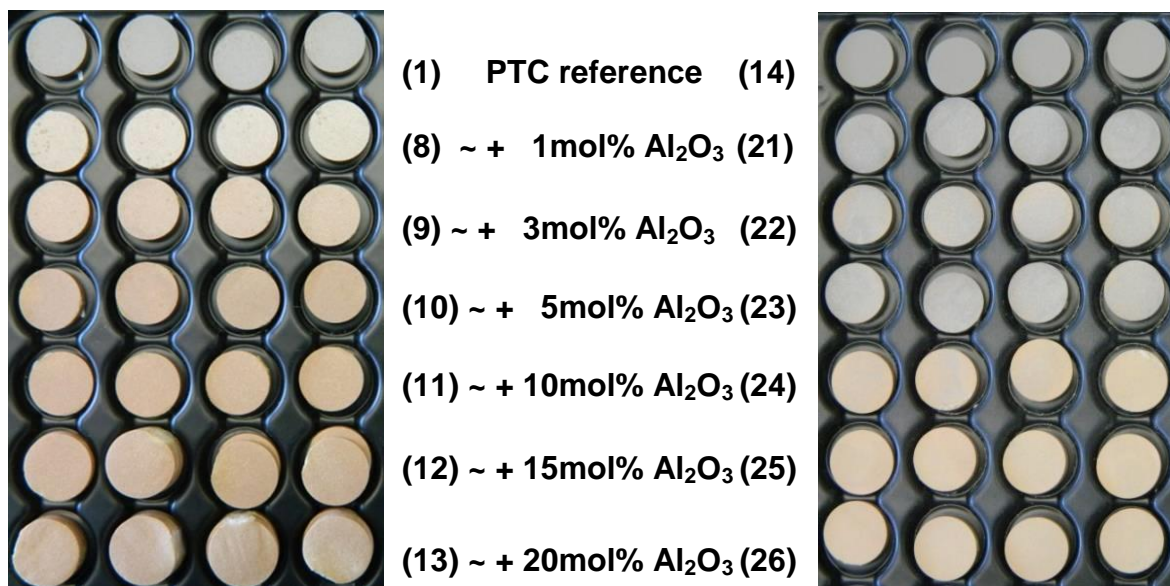


Figure 34: Sintered disks composed of Al₂O₃ and PTC (left: PTC mass A and right: mass B)

3.3.1 Thermal analysis and density measurements

The dimensions of the pressed and the sintered disks have been measured with a caliper. Furthermore their weight has been determined using a scale. From these measurements the geometrical densities have been determined using equation 3. Next to this the thermal expansion has been measured using the dilatometer

3 Material development

DIL402CD. For this specimen with the size of 25mm by 3mm have been sintered. Figure 35 shows the dilatometry measurements of the PTC mass A doped with alumina and YSZ. Figure 36 depicts the dilatometry measurements of PTC mass B with additions of YSZ and alumina. The dilatometry curves prove for both masses that an adaption towards pure alumina and pure YSZ can be done with intermediate layers composed of molar compositions of both ceramics.

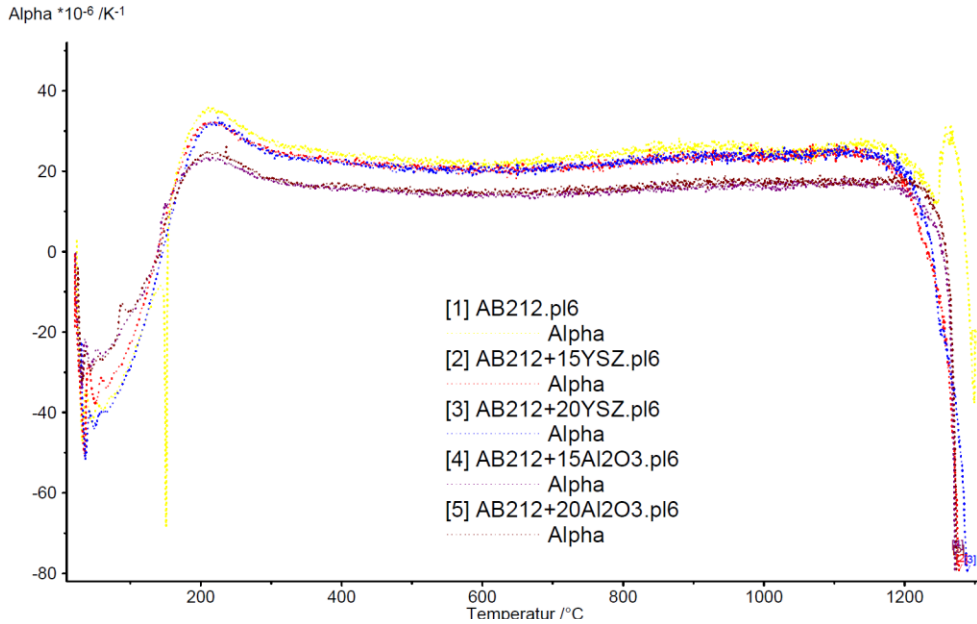


Figure 35: Dilatometry analysis of PTC mass A and YSZ and alumina

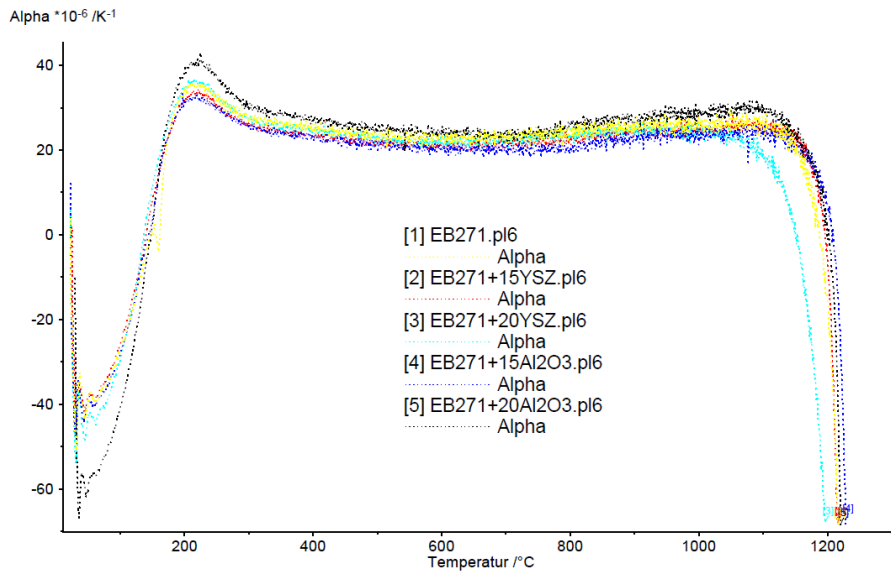


Figure 36: Dilatometry analysis of PTC mass B and YSZ and alumina

3.3.2 Electrical measurements

For electrical measurements the sintered disks have been sputtered with 1 μm layer composed of chrome, nickel and silver in the pilot sputter station Leibold-Heraeus Z400. After this sputtering process the specific electrical values have been determined. The Keithley 199 System DMM/Scanner was used to measure the electrical resistance R_{25} . The device has a clip on instrument for measuring the parts and was inside an air-conditioned room with the temperature of 25°C. The specific electrical resistance was calculated according to Equation 17. The electrical resistance in dependency of the temperature has been measured in the oil-filled tank Proline RP 18409. From the recorded R-T values the reference temperature and the temperature coefficient, the slope of the R-T curve have been calculated. The resistance over temperature curves of the PTC mass A and YSZ is shown in Figure 37. Figure 38 depicts the resistance in dependency of temperature of PTC mass A and Al_2O_3 . In Figure 39 the resistance over temperature curves of PTC mass B and YSZ is shown. Figure 40 shows the R-T-curve of PTC mass B and Al_2O_3 . One can see that with increasing YSZ or alumina content the PTC properties for both masses decrease. For YSZ the electrical values do not increase as much as for alumina. There is also a difference in the behaviour of the masses. PTC mass B shows a smaller decrease on the electrical values with same addition level. This can be seen as the composition of PTC mass A and 1 mol-% alumina has already an very high resistance at room temperature of $5,0\text{E}+06$ and a small PTC jump. For PTC mass B this behaviour occurs with additions of around 15 mol-% alumina content. One explanation for this behaviour is that the PTC mass A is silica free. Thus only a titanium rich glassy phase can occur during sintering. PTC mass B is additional composed of silicium. Thus next to the titanium rich melt also a silicium rich glassy phase can occur. This higher amount of melt can dissolve a higher amount of impurities in the secondary phases around the primary barium titanate grains. These impurities are then not yet incorporated into the barium titanate grains. This altogether results in better PTC behaviour seen in the measurements.

3 Material development

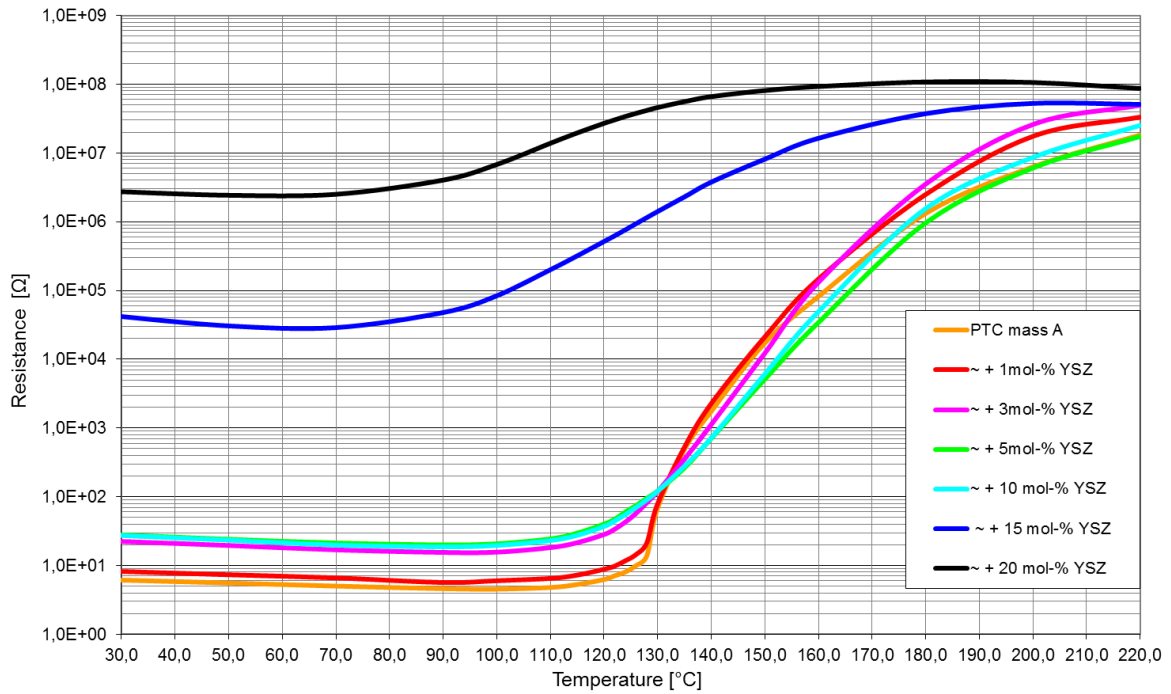


Figure 37: Resistance over temperature curve of PTC mass A+YSZ

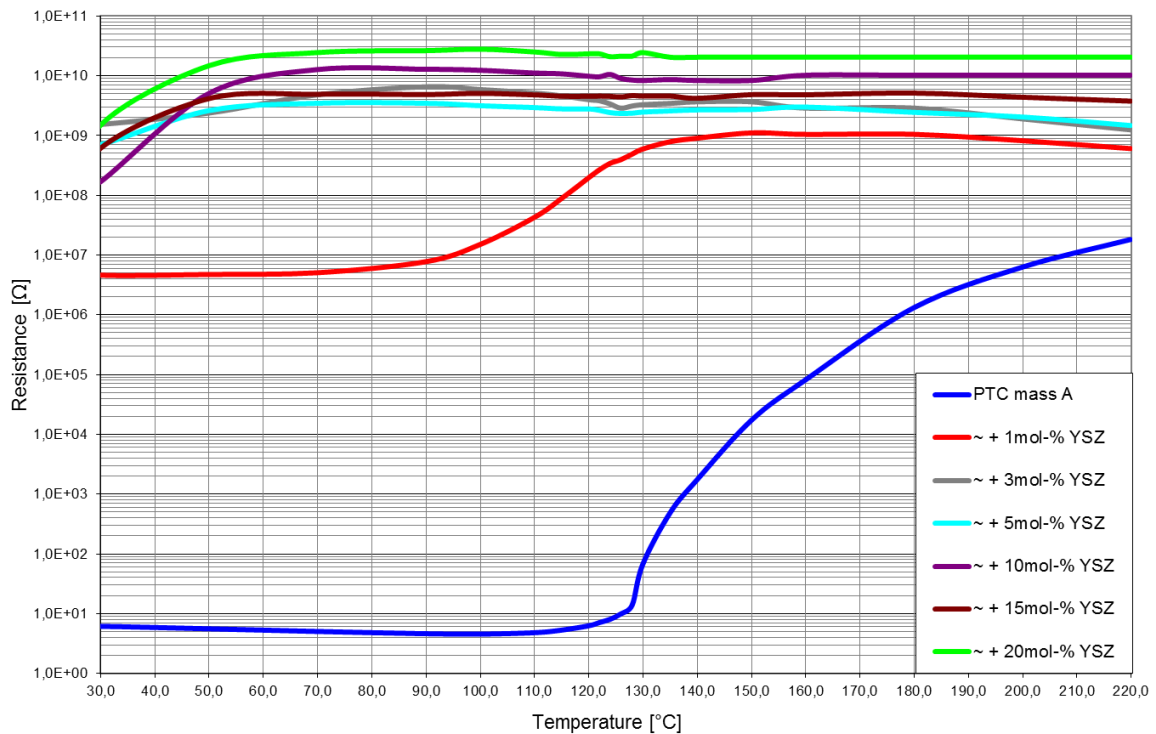


Figure 38: Resistance over temperature curve of PTC mass A+ Al_2O_3

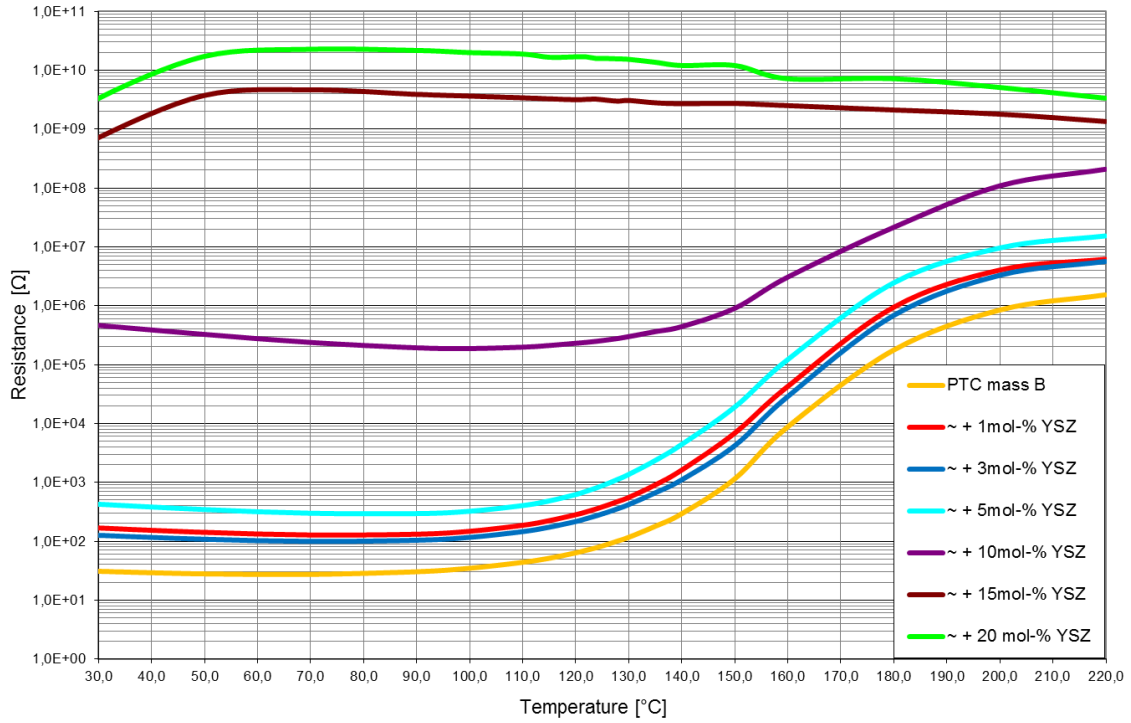


Figure 39: Resistance over temperature curve of PTC mass B+YSZ

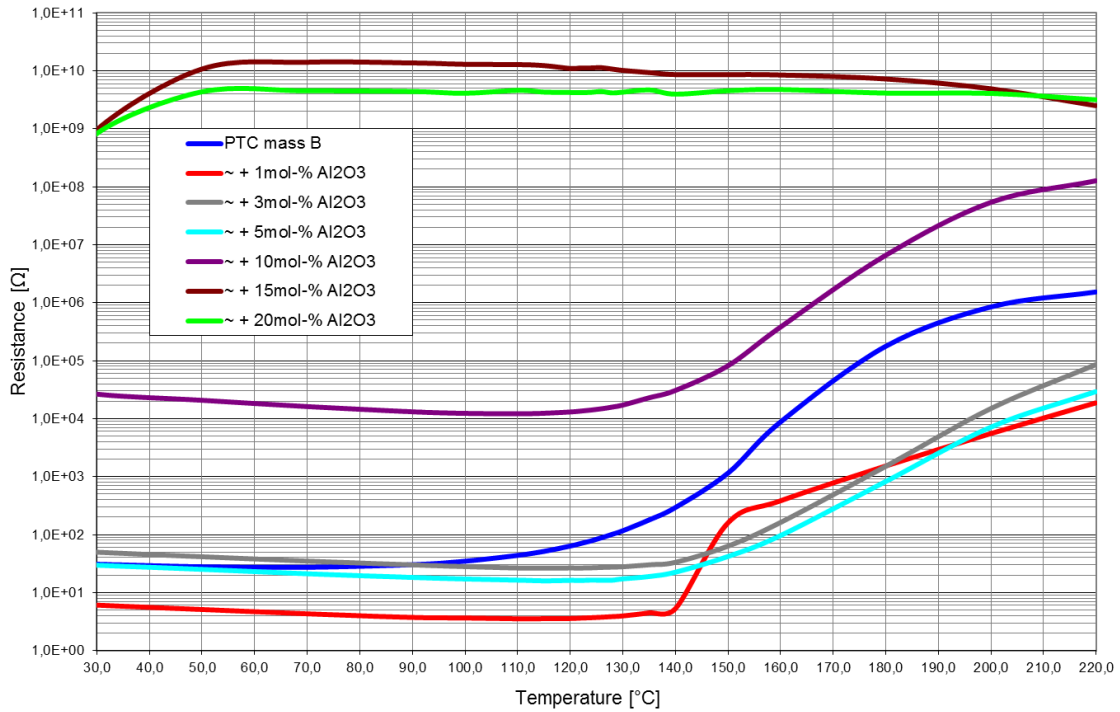


Figure 40: Resistance over temperature curve of PTC mass B+Al₂O₃

3.3.3 Mechanical measurements

For the mechanical strength measurements additional to the disks rods have been pressed and sintered. The sintered specimens were 25 mm long, 2.5 mm thick and 4.6 mm thick. The pressed parts for sample 7, PTC mass A with 20mol% YSZ as well as the samples 8-13, PTC mass A and Al_2O_3 reacted too much with the sintering setter, so that they could not been used for measurements. In opposition the disks had only a small contact area with the setter, so that specimen for the other measurements could be used. Using the Zwick Roell test machine the four point bending tensile strength has been measured of 30 prepared samples. The measured dimensions, forces and calculated bending tensile strength values of the samples are displayed in A. 19 to A. 22. From these the Weibull parameters have been determined graphically. For this the calculated bending strength values have been sorted in order and plotted against the corresponding probabilities of fracture in a Weibull diagram.

From this diagram, shown in

Figure 41, the characteristic Weibull strength values S_0 , the intercepts of the regression lines with $y=0$, could be extracted. The Weibull module m has been extracted from a different Weibull diagram where the strength is plotted logarithmically against $\ln\ln[1/(1-F(\sigma_{B,i}))]$. The slope of the regression line of the data equals the Weibull modulus m . The determined Weibull parameters are displayed in Table 11. The Weibull strength shows a maximum for the pure PTC masses and is lowered with each molar addition of YSZ or alumina. According to these results it is evident that the intermediate layers composed out of PTC and YSZ / alumina do not exhibit a contribution towards a higher mechanical strength of the composite. For PTC mass B one can see an increase in mechanical strength from 15 to 20 mol-% YSZ and alumina. Thus the minimum in mechanical strength can be recorded for PTC mass B with an addition of 15 mol-% YSZ or alumina.

Table 11: Weibull strength and Weibull modulus of pressed powder mixtures

Composition	Weibull strength	Weibull module	Composition	Weibull strength	Weibull module
	S ₀ [MPa]	m		S ₀ [MPa]	m
1: PTC mass A	103,01	14,304	14: PTC mass B	170,59	4,645
2: PTC mass A + 1mol-% YSZ	78,81	7,357	15: PTC mass B + 1mol-% YSZ	163,65	4,847
3: PTC mass A + 3 mol-% YSZ	77,55	10,352	16: PTC mass B + 3 mol-% YSZ	142,74	6,568
4: PTC mass A + 5 mol-% YSZ	69,17	4,604	17: PTC mass B + 5 mol-% YSZ	141,37	6,609
5: PTC mass A + 10mol-% YSZ	46,06	7,032	18: PTC mass B + 10mol-% YSZ	108,35	13,886
6: PTC mass A + 15mol-% YSZ	39,78	3,523	19: PTC mass B + 15mol-% YSZ	110,00	7,792
7: PTC mass A + 20mol-% YSZ	-	-	20: PTC mass B + 20mol-% YSZ	132,59	6,385
8: PTC mass A + 1mol-% Al ₂ O ₃	-	-	21: PTC mass B + 1mol-% Al ₂ O ₃	144,85	5,436
9: PTC mass A + 3mol-% Al ₂ O ₃	-	-	22: PTC mass B + 3mol-% Al ₂ O ₃	136,24	8,041
10: PTC mass A + 5mol-% Al ₂ O ₃	-	-	23: PTC mass B + 5mol-% Al ₂ O ₃	120,47	8,255
11: PTC mass A + 10mol-% Al ₂ O ₃	-	-	24: PTC mass B + 10mol-% Al ₂ O ₃	50,63	5,256
12: PTC mass A + 15mol-% Al ₂ O ₃	-	-	25: PTC mass B + 15mol-% Al ₂ O ₃	35,60	7,806
13: PTC mass A + 20mol-% Al ₂ O ₃	-	-	26: PTC mass B + 20mol-% Al ₂ O ₃	45,04	7,526

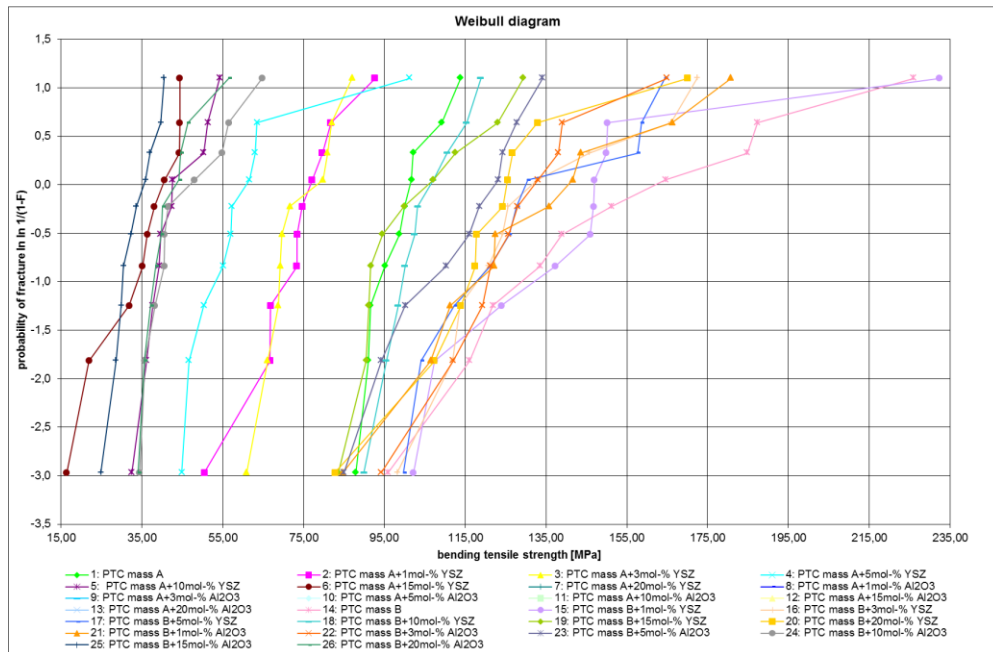


Figure 41: Weibull diagram of mechanical strength values of pressed powder mixtures

3.3.4 Microstructure evolution

For detailed characterisation of the microstructure cross sections have been made. First samples have been embedded in a synthetic resin Varidur 200, a cold embedding medium for the metallography from Bühler GmbH. The hardened samples have then been grinded and polished using grinding discs of different grits. The finished samples have then been observed under the optical microscope OLYMPUS BX51M. The micrograph of PTC mass A and 20 mol-% YSZ is shown in Figure 42. Figure 43 depicts the micrograph of PTC mass A and 20 mol-% Al_2O_3 . In Figure 44 the micrograph of PTC mass B and 20 mol-% YSZ is shown. Figure 45 shows the R-T-curve of PTC mass B and 20 mol-% Al_2O_3 . For both PTC masses A and B a formation of harder phases can be seen with additions of YSZ. With additions of alumina a formation of glassy secondary phases can be observed for both PTC masses.

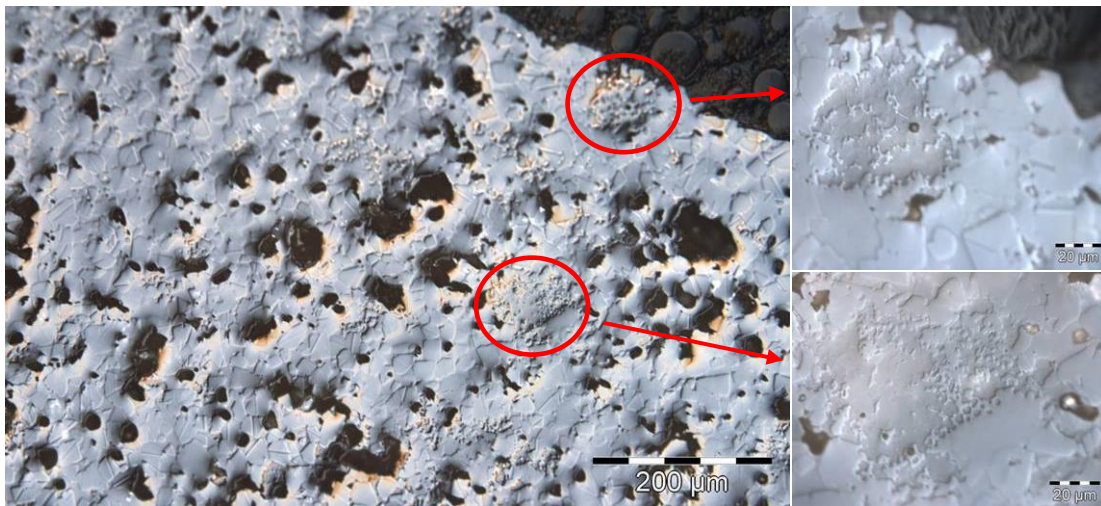


Figure 42: micrographs of PTC mass A and 20 mol-% YSZ

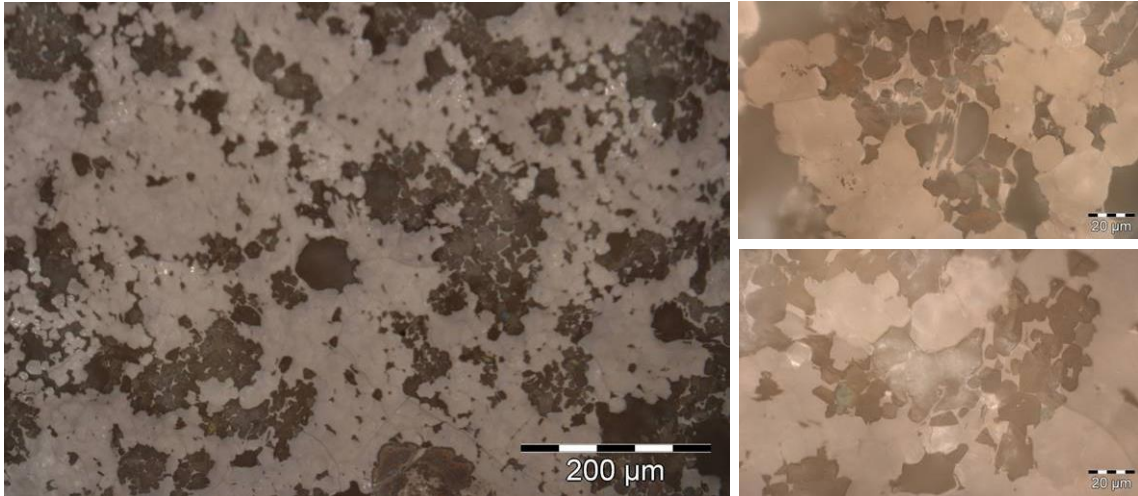


Figure 43: micrographs of PTC mass A and 20 mol-% Al₂O₃

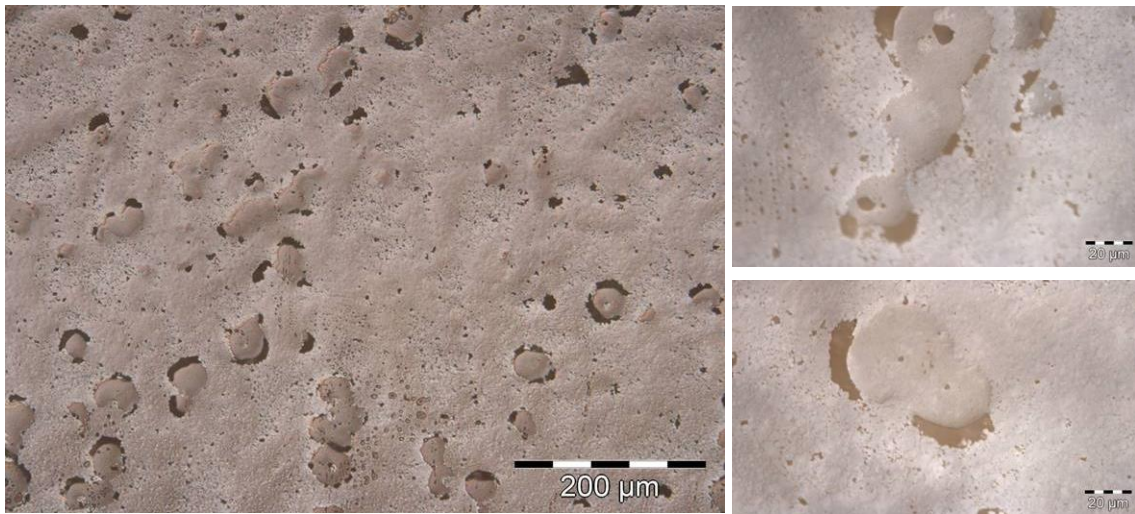


Figure 44: micrographs of PTC mass B and 20 mol-% YSZ

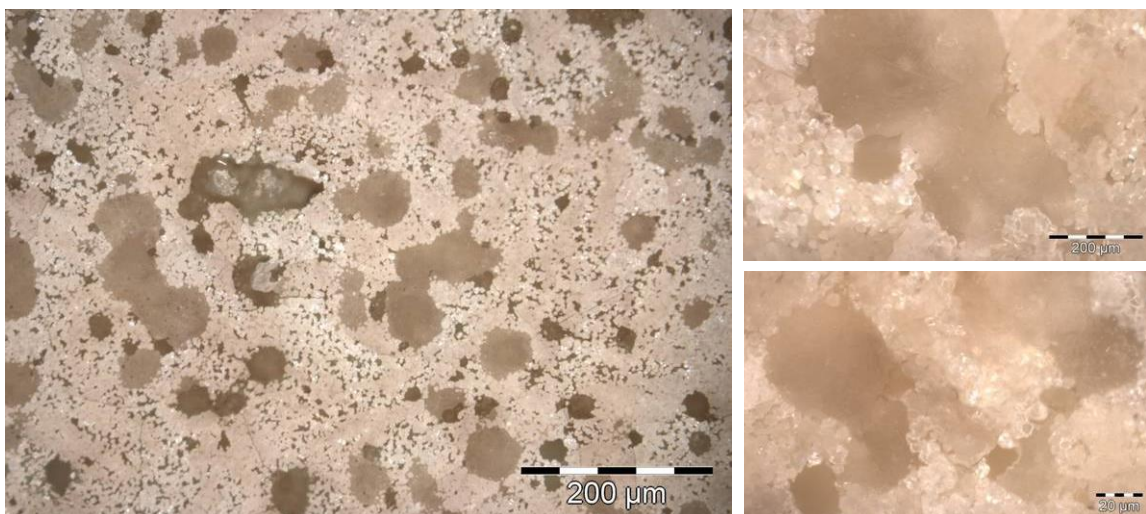
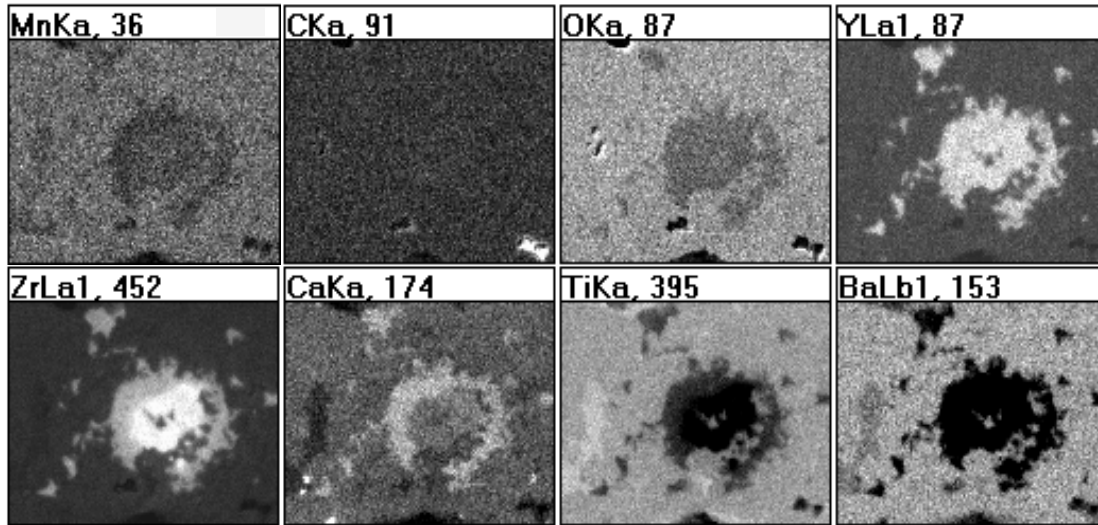
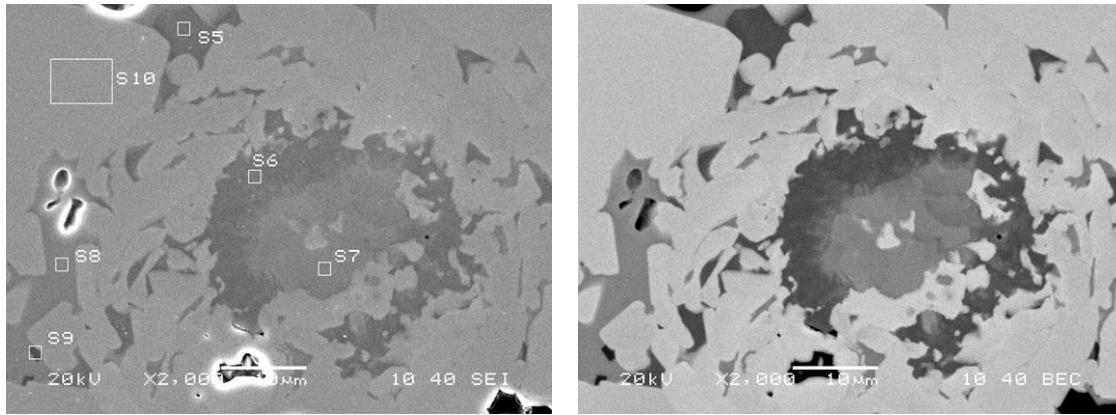


Figure 45: micrographs of PTC mass B and 20 mol-% Al₂O₃

3.3.5 SEM analysis

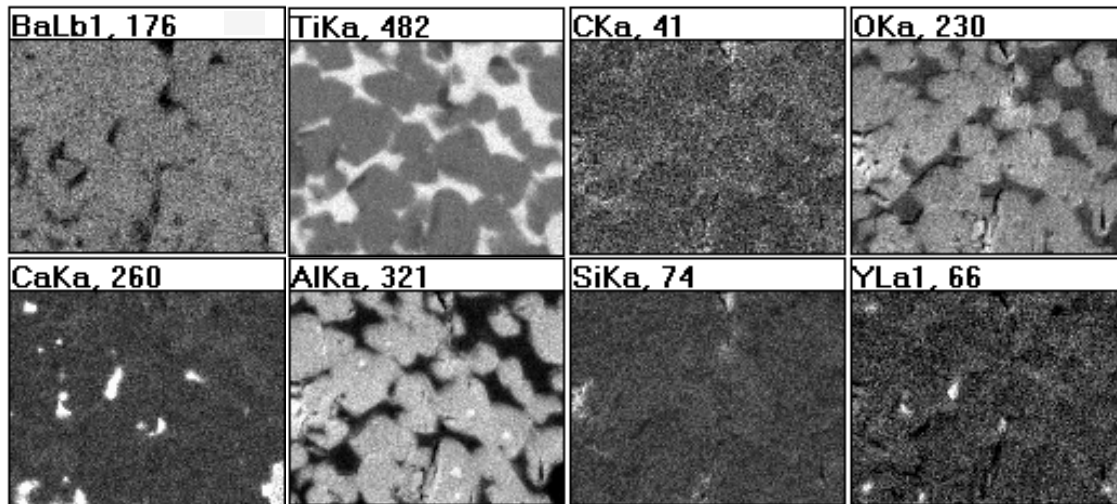
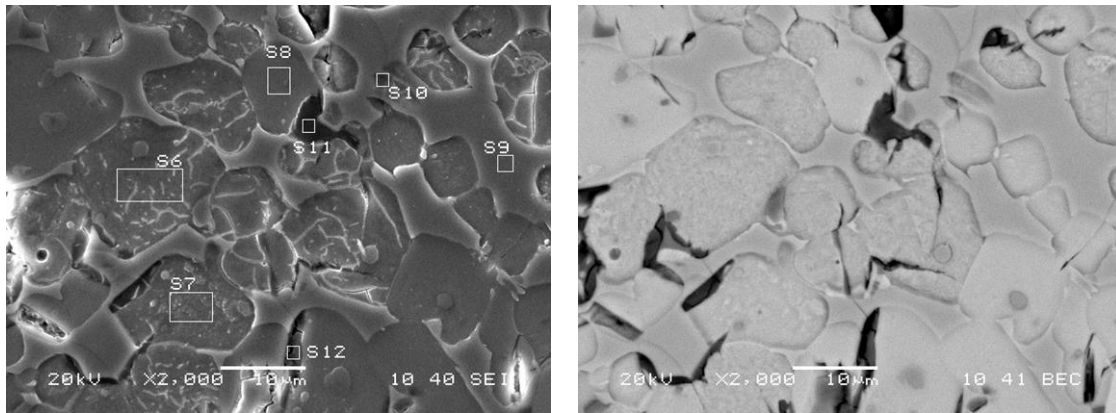
For more detailed analysis the samples have been investigated with a Scanning Electron Microscope (SEM). Using the built in energy dispersive x-ray analysis EDX an element mapping as well as different measurement points over the cross section have been conducted. With the help of this scan diffusion phenomena can be investigated further. As shown in Figure 46 zirconia and yttrium rich areas are surrounded by clouds enriched of calcium. In opposition to this the barium and titanium content is lowered. These areas are later identified by x-ray diffraction as zirconium titanates such as zirconolite and zirconium titanium oxide. In Figure 47 the PTC mass A and alumina is shown. It can be seen that the structure consists of a highly titanium rich secondary phase surrounding alumina and barium rich grain matrix. These grains are identified by x-ray diffraction as hexagonal barium aluminium oxide. Figure 48 shows the SEM analysis of PTC mass B and YSZ. The structure shows a zirconia grain inside a barium titanate grain structure. Between the grains a titanium rich secondary phase is formed. At the bottom of the analysis picture an even titanium richer secondary phase can be seen. This secondary phase reacted with the zirconia grain forming a needle structure composed of zirconium and titanium, growing into the inside of the zirconia grain. These phases are later identified with x-ray diffraction as zirconolite and other secondary barium titanate phases. In the last Figure 49 the analysis of PTC mass B and alumina is shown. The composition consists of alumina rich grains inside the barium titanate matrix. Around the alumina grains a barium, titanium and aluminium rich boundary layer is formed. This is by x-ray identified as Barium aluminium titanium oxide.



Element Label	Ba	Ti	Ca	Zr	Y	O	Mn	Hf
	mol%							
S5	9.88	22.12	6.27	17.08	18.40	25.92	0.11	0.22
S6	1.20	20.33	6.95	23.81	18.12	28.91	0.04	0.64
S7	0.63	7.21	4.18	48.25	16.56	21.87	0.13	1.17
S8	37.51	32.12	1.01	3.36	0.06	25.59	0.06	0.29
S9	20.68	30.28	12.71	1.22	8.15	26.54	0.05	0.37
S10	54.06	19.14	2.95	4.74	0.01	19.01	0.06	0.03

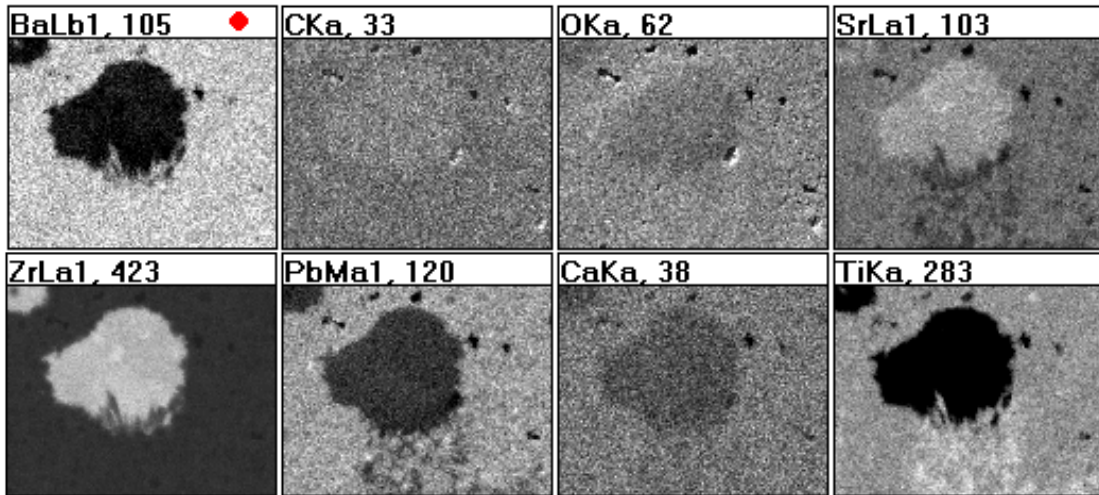
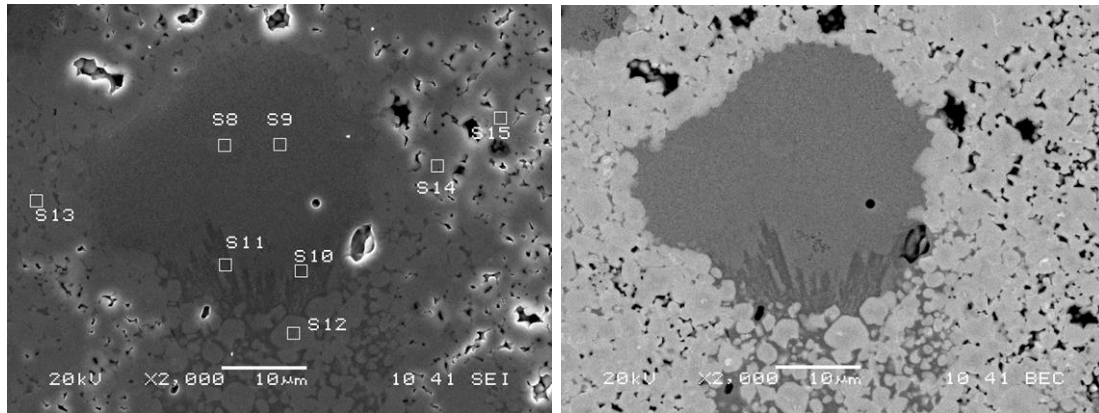
Figure 46: SEM analysis of PTC mass A + 20mol% YSZ

3 Material development



Element Label	Ba	Ti	Ca	Al	Si	Y	O	Mn
	mol%							
S6	51.61	0.70	0.37	20.29	0.31	0.05	26.52	0.15
S7	53.21	0.95	0.12	20.51	0.20	0.10	24.81	0.10
S8	53.05	1.22	0.27	20.14	0.25	0.33	24.65	0.09
S9	36.21	31.45	0.68	2.74	0.09	0.00	28.69	0.14
S10	34.80	30.43	0.67	4.39	0.40	0.22	29.07	0.02
S11	28.80	4.60	0.59	17.71	2.49	0.28	45.51	0.02
S12	39.92	9.09	0.61	14.37	1.52	0.48	33.99	0.02

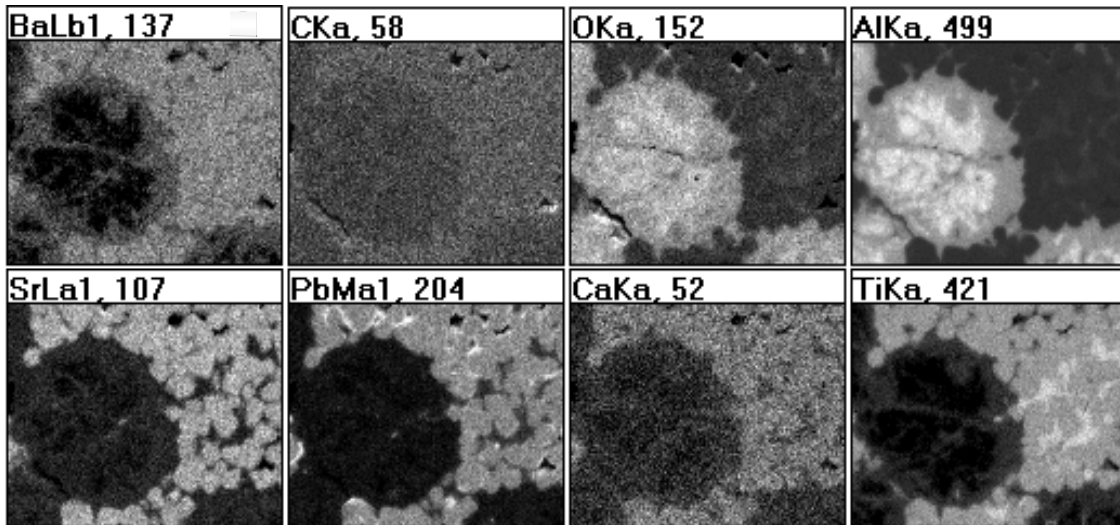
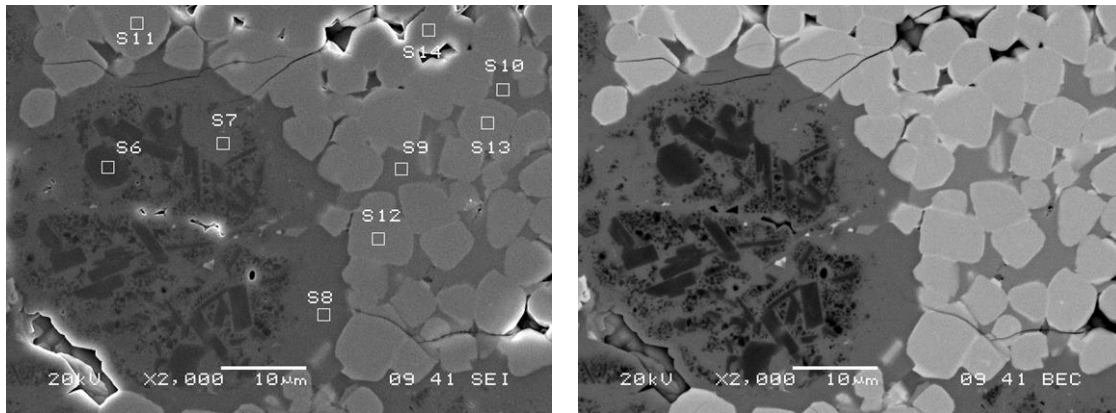
Figure 47: SEM analysis of PTC mass A + 20mol% Al₂O₃



Element Label	Ba	Ti	Ca	Zr	Pb	Sr	O	Hf
	mol%							
S8	0.33	3.28	0.29	64.01	3.01	6.15	17.98	5.15
S9	0.80	4.26	0.41	59.74	2.30	4.53	23.25	4.71
S10	26.95	25.43	0.24	25.10	3.06	0.30	18.62	0.30
S11	26.88	25.07	0.31	23.52	2.86	0.12	21.12	0.12
S12	40.91	19.88	0.67	1.33	14.51	6.13	16.54	0.03
S13	37.92	18.23	0.66	4.48	15.08	6.75	16.81	0.07
S14	36.93	18.98	0.63	3.91	15.58	6.70	17.17	0.10
S15	37.24	18.71	0.58	4.74	15.84	6.30	16.55	0.04

Figure 48: SEM analysis of PTC mass B + 20mol% YSZ

3 Material development



Element Label	Ba	Ti	Ca	Al	Pb	Sr	O
	mol%						
S6	18.77	0.74	0.02	41.99	1.05	0.25	37.18
S7	36.19	4.28	0.15	26.63	2.34	1.29	29.12
S8	36.72	5.06	0.05	25.62	1.75	1.52	29.28
S9	34.55	31.60	0.06	3.02	4.53	0.23	26.01
S10	34.04	30.82	0.22	3.00	5.38	0.45	26.09
S11	36.09	21.92	0.89	0.17	15.38	8.44	17.11
S12	36.74	22.03	0.72	0.21	15.44	7.14	17.72
S13	37.87	21.44	0.63	0.17	15.20	7.53	17.16
S14	34.39	22.45	0.87	0.23	15.61	8.19	18.26

Figure 49: SEM analysis of PTC mass B + 20mol% Al₂O₃

3.3.6 X-ray diffraction analysis

In order to analyse the chemical interactions, sintered disks have been grinded to powder. Then a powder diffraction analysis has been conducted with the Panalytical X'Pert PRO powder diffractometer with Co-K α -Radiation. For the measurements a source voltage of 45 kV, a current of 40 mA and a 2Θ -range between 15° and 100° with a step size of 0.004° has been used. The Bruker software program Diffrac Plus EVA (version 12.0) has been used for analysis. The X-ray diffraction pattern of the PTC mass A reference powder is shown in Figure 50. The reflexes can be fully assigned to tetragonal Barium Titanium Oxide (BaTiO_3), PDF 00-005-0626, with the unit cell parameters of $a=3.96404$, $b=3.96404$, $c=4.01444$ and $\gamma=90^\circ$. This proves that the barium titanate formation from the raw materials titanium dioxide and barium carbonate has been quite good. In Figure 51 the reflexes of the second PTC mass B are depicted. In this case the powder consists of two phases the main phase is again the tetragonal BaTiO_3 , PDF 00-005-0626, and as second phase monoclinic Ba_2TiO_4 , PDF 00-035-0813 with the unit cell parameters of $a=10.65510$, $b=7.67350$, $c=6.14240$, $\alpha=90^\circ$, $\beta=93.182^\circ$ and $\gamma=90^\circ$, can be identified. The presence of Ba_2TiO_4 has also been verified by wet chemical testing. The powder has been dissolved in water and monitored with a pH-meter, which showed a fast rise to a pH level of 8. This is due to the fast solubility of Ba_2TiO_4 giving a fast rise into basic pH levels. Contrary to this a testing with PTC mass A showed no fast increase in pH-level.

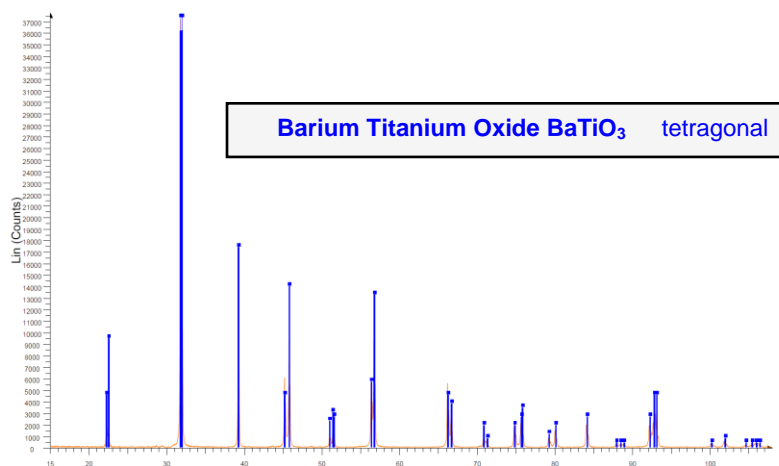


Figure 50: X-ray diffraction pattern of PTC mass A

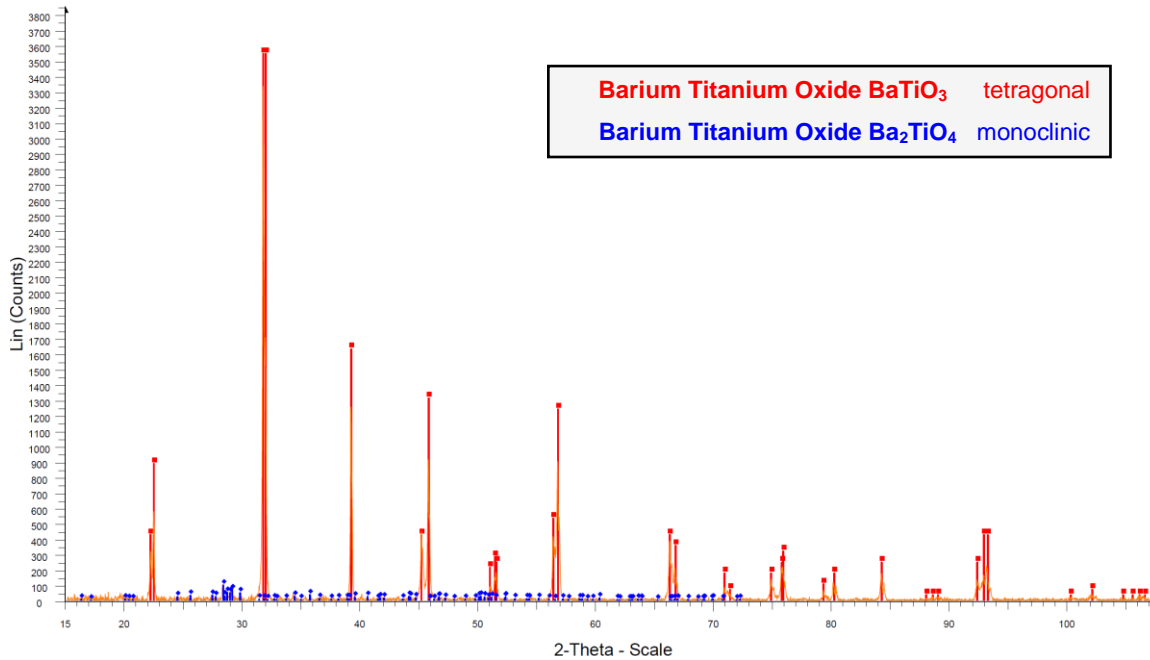


Figure 51: X-ray diffraction pattern of PTC mass B

PTC mass A and YSZ:

The diffraction patterns of the samples composed of the PTC mass A and yttria stabilized zirconia are summed up together in Figure 54. The diffraction patterns of the individual powders showed no difference but that with increasing YSZ portion a displacement of the barium titanate reflexes occurs and that the amount of secondary phases increases. The BaTiO_3 unit cell distorts from a tetragonal to a more cubic unit cell with $a=b=4.02701$, $c=4.02087$ with an addition of 20 mol% YSZ. Additionally secondary phases such as barium titanate rich (B_2T , B_6T_{17} , B_2T_5 and BT_2) and zirconium rich phases (Z , ZT and CZT_2) are formed. The barium titanate phases are in detail orthorhombic Ba_2TiO_4 , monoclinic BaTi_2O_7 , monoclinic $\text{Ba}_2\text{Ti}_5\text{O}_{12}$ and monoclinic $\text{Ba}_6\text{Ti}_{17}\text{O}_{40}$. The zirconium rich phases are tetragonal zirconia ZrO_2 , monoclinic Zirconolite $\text{CaZrTi}_2\text{O}_7$, orthorhombic Zirconium Titanium Oxide ZrTiO_4 . The detailed analysis of sample 7, PTC mass A and 20 mol% YSZ, is shown in Figure 55. The wet chemical testing also showed a fast increase in pH level to 8.5, proving the Ba_2TiO_4 .

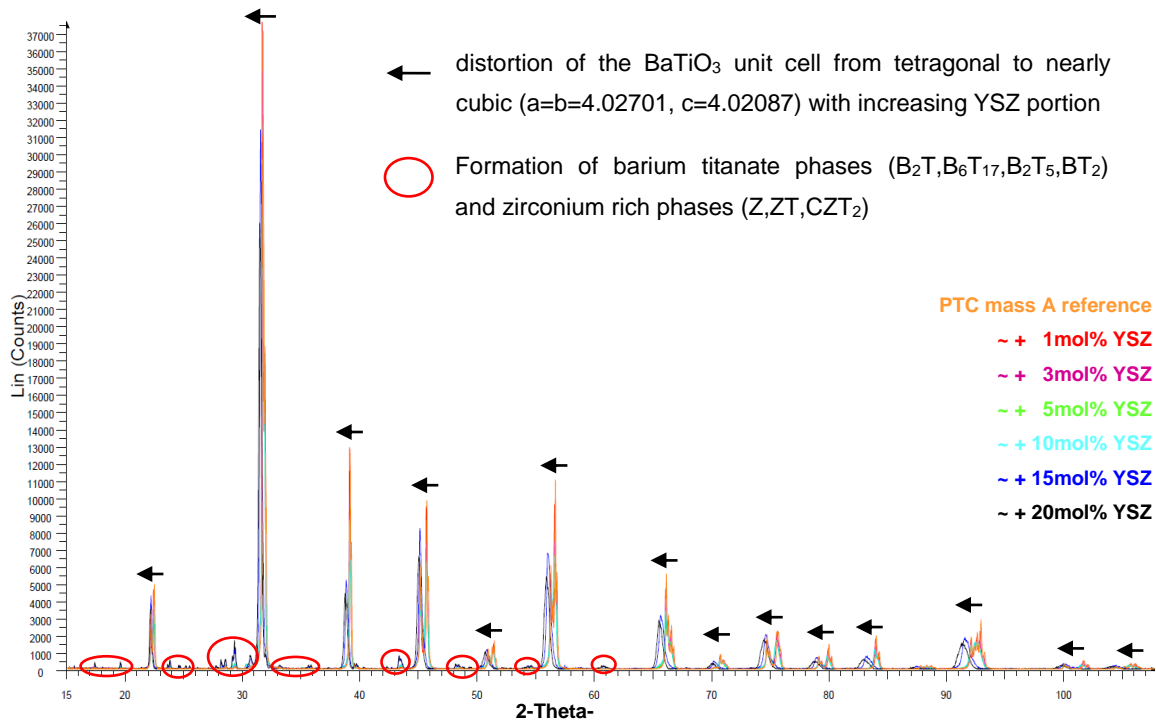


Figure 52: X-ray diffraction pattern of PTC mass A and YSZ

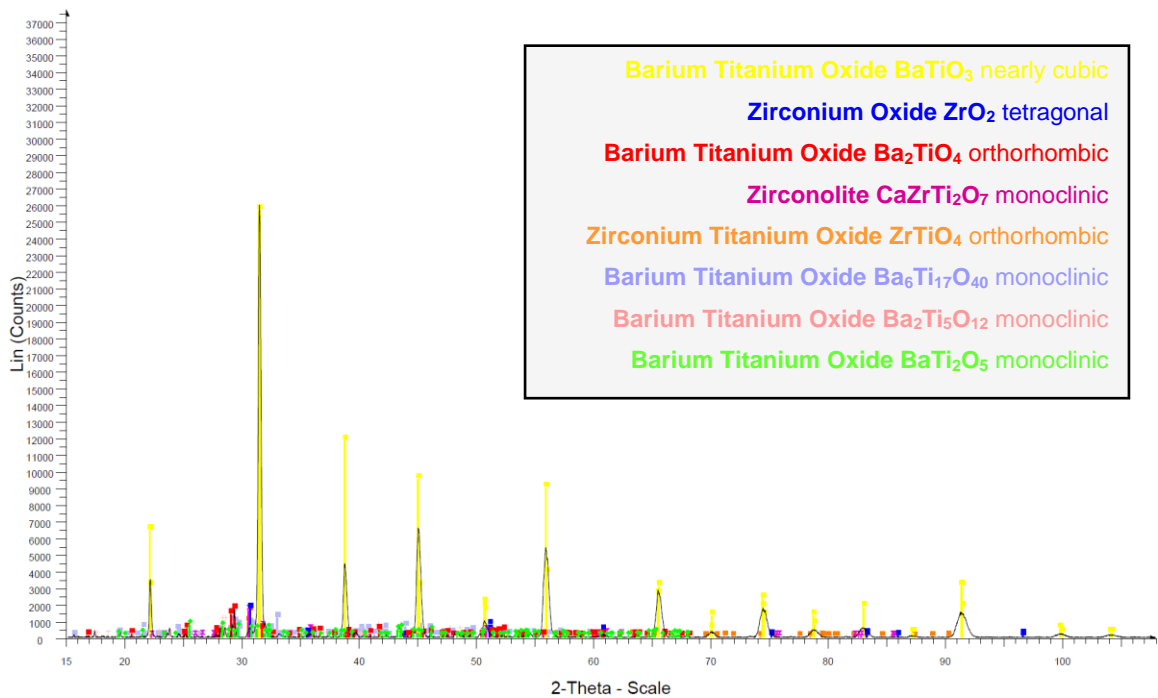


Figure 53: X-ray diffraction pattern of PTC mass A and 20mol-% YSZ

PTC mass B and YSZ:

The diffraction patterns of the samples composed of the PTC mass B and yttria stabilized zirconia are summed up together in Figure 54. The diffraction patterns of the individual powders also showed no difference but that with increasing YSZ portion a displacement of the barium titanate reflexes occurs and that the amount of secondary phases increases. The BaTiO_3 unit cell distorts from a tetragonal to a more cubic unit cell with $a=b=3.98536$, $c=4.02109$ with an addition of 20 mol% YSZ. Additionally secondary phases such as barium titanate rich (B_2T , B_6T_{17} , B_2T_5 and BT_2) and the monoclinic Zirconolite $\text{CaZrTi}_2\text{O}_7$ are formed. The barium titanate phases are in detail orthorhombic Ba_2TiO_4 , monoclinic BaTi_2O_7 , monoclinic $\text{Ba}_2\text{Ti}_5\text{O}_{12}$ and monoclinic $\text{Ba}_6\text{Ti}_{17}\text{O}_{40}$. The detailed analysis of sample 13, PTC mass B and 20 mol% YSZ, is shown in Figure 55. The wet chemical testing also showed a fast pH level increase to 8.5 due to the Ba_2TiO_4 .

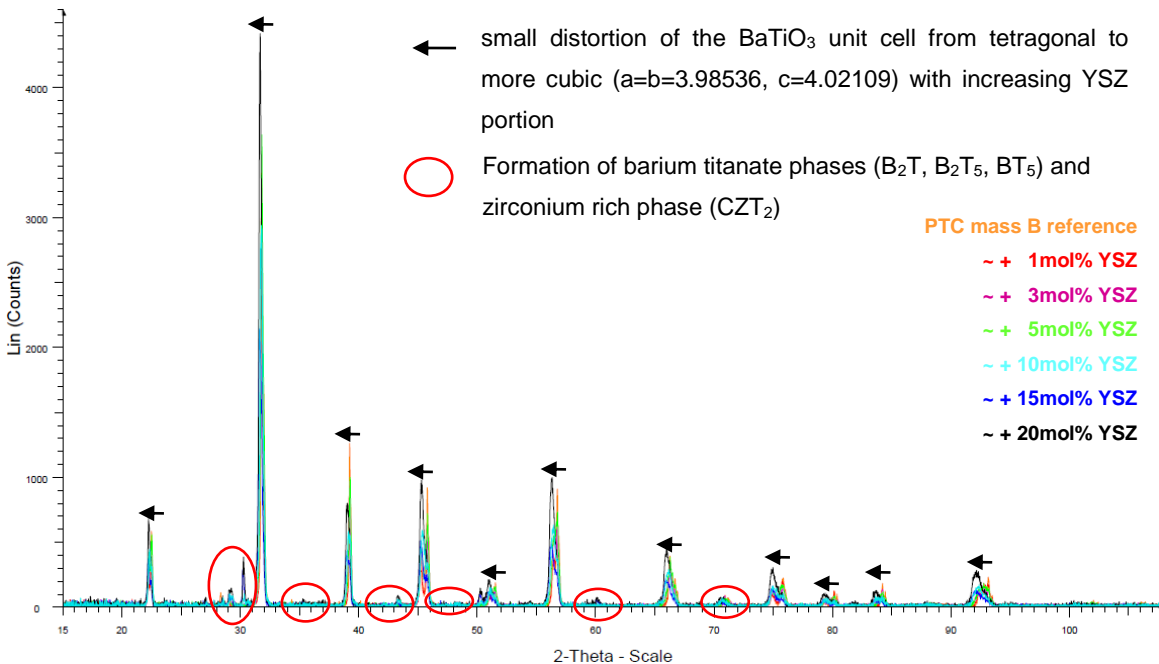
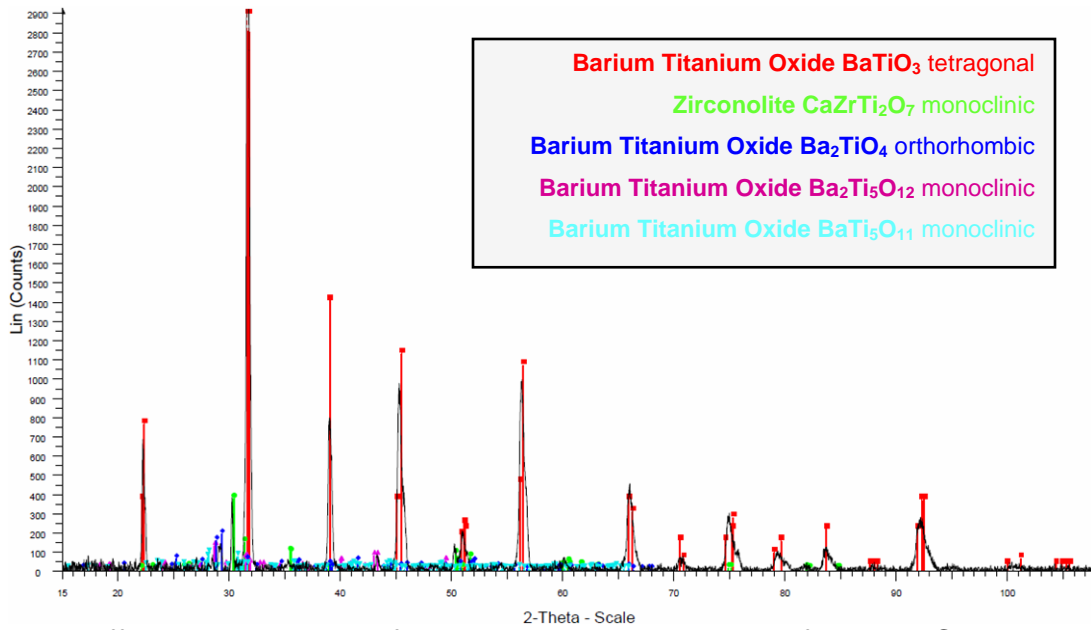


Figure 54: X-ray diffraction pattern of PTC mass B and YSZ



The diffraction patterns of the samples composed of the PTC mass A and alumina are summed up together in Figure 56. With increasing alumina content a secondary phase consisting of the hexagonal BaAl_2O_4 and the monoclinic $\text{Ba}_2\text{Ti}_5\text{O}_{12}$ is formed. The diffraction pattern of sample 20, composed of the PTC mass A and 20 mol% Al_2O_3 , is shown in Figure 57.

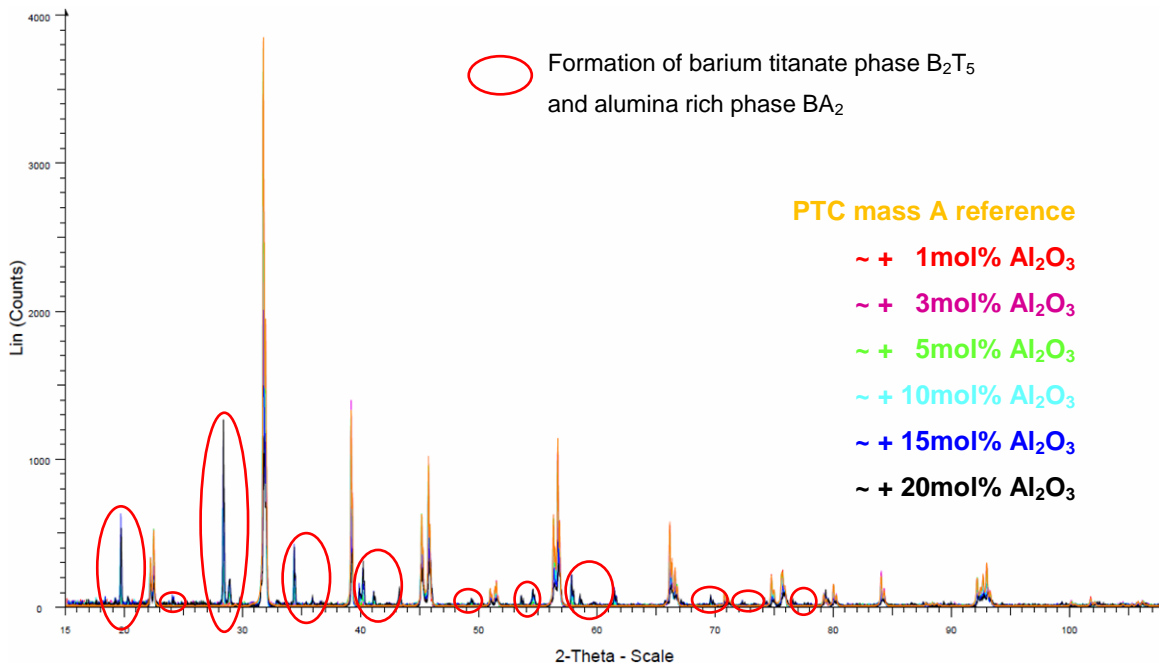


Figure 56: X-ray diffraction pattern of PTC mass A and Al_2O_3

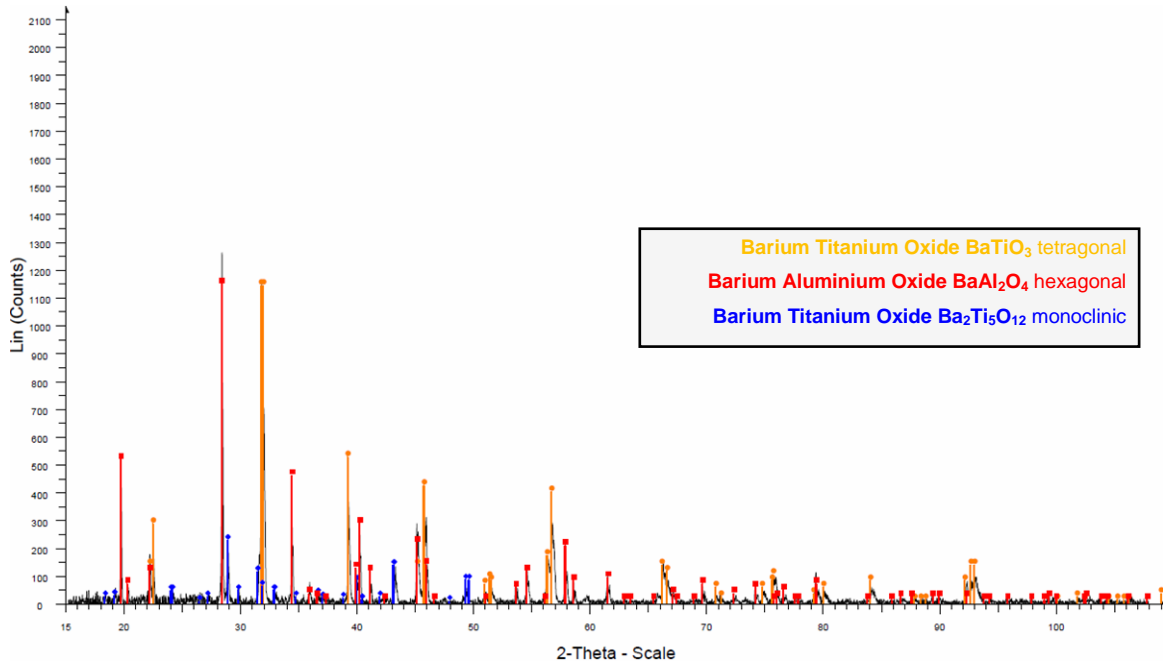


Figure 57: X-ray diffraction pattern of PTC mass A and 20mol-% Al₂O₃

PTC mass B and Al₂O₃:

In Figure 58 the diffraction patterns of the samples composed of the PTC mass B and alumina are summed up together. With increasing alumina content the monoclinic Ba₃Al₁₀TiO₂₀ is formed as secondary phase. The diffraction pattern of sample 26, composed of the PTC mass B and 20 mol% Al₂O₃, is shown in Figure 59. The formation of Barium aluminium titanium oxide has also been observed by Hari and Kutty [Har98]. They added up to 10 mol% Al₂O₃ to Nb-doped BaTiO₃. Their samples were sintered in air at 1377°C. They observed that for additions of 3 mol%Al₂O₃, second phases of BaAl₆TiO₁₂ and Ba₃Al₁₀TiO₂₀ appeared at the grain boundaries and triple junctions.

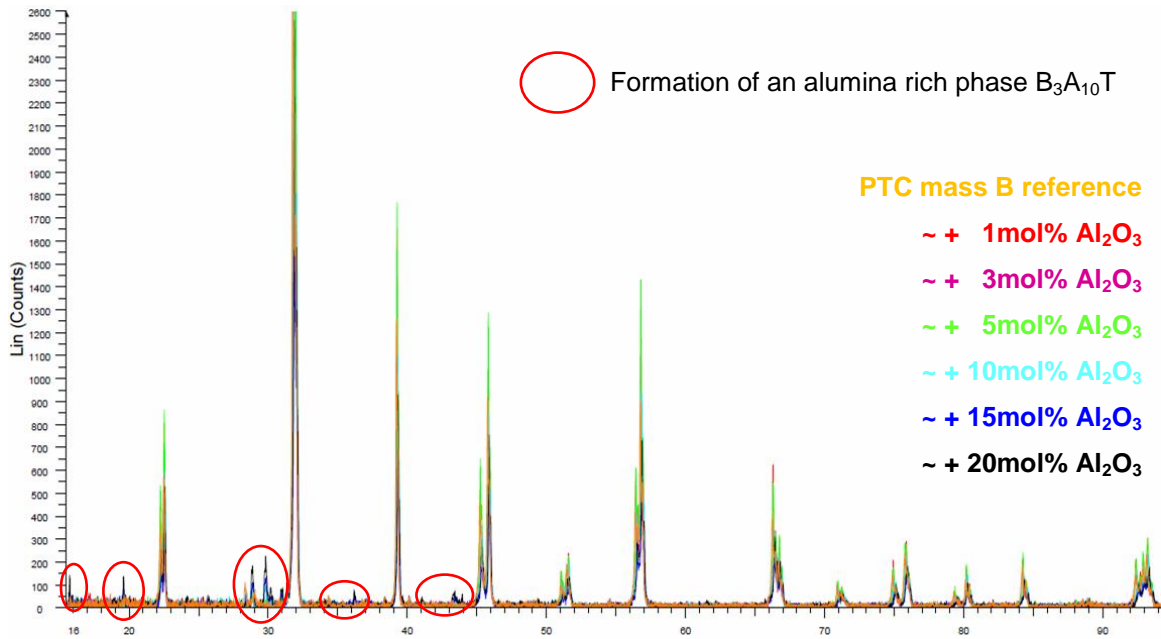


Figure 58: X-ray diffraction pattern of PTC mass B and Al_2O_3

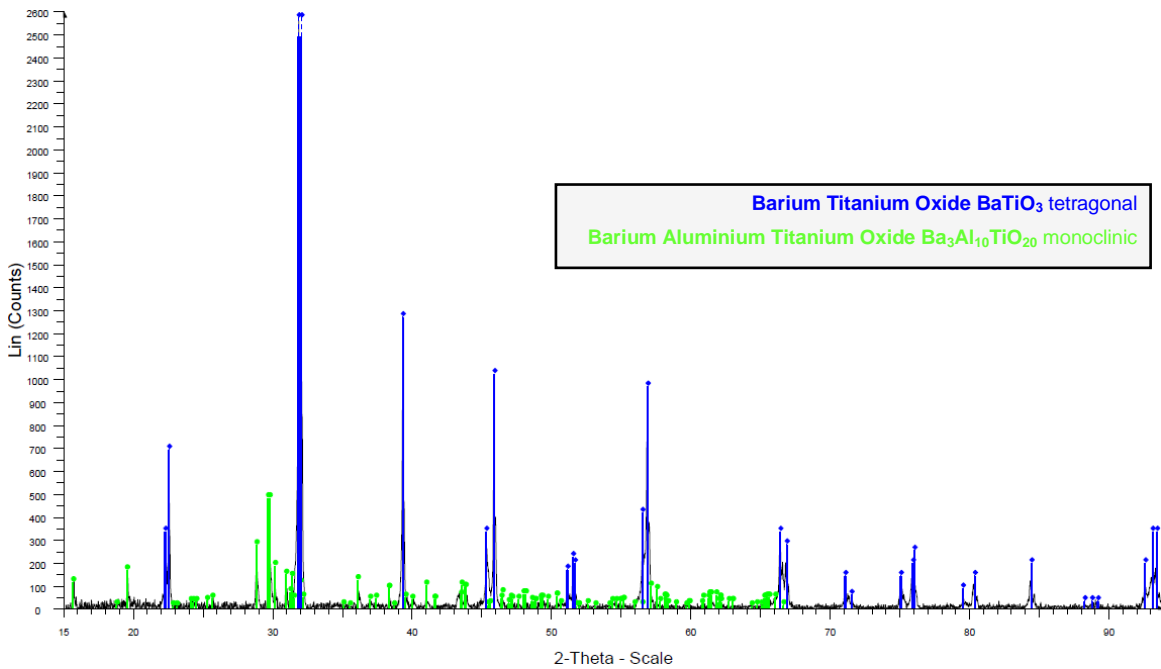


Figure 59: X-ray diffraction pattern of PTC mass B and 20 mol% Al_2O_3

4 Prototypes

For evaluation of the material combination various types of prototypes have been produced. This chapter is dedicated to their shaping, the adjustment of the following process steps such as debinding and sintering for a stable material combination as well as the verification of electrical and mechanical properties and a structure analysis of them.

4.1 Thin PTC heater bonded on alumina

4.1.1 Production and electrode development

For the first investigations a demonstrator has been built up. For this a standard pressed PTC substrate has been lapped to 200 μm thickness. This PTC layer has then been bonded on a 1 mm thick aluminium oxide substrate to achieve a two component heater. As adhesive a high temperature and high purity Al_2O_3 adhesive (product name: Resbond 989FS, supplier: Cotronics) has been used. For comparison also a pressed PTC with a sintered thickness of 1.2 mm has been produced. For electrical termination of the more component heater a new electrode layout had to be developed. The standard termination for PTCs is a full sized metallisation on opposite sides. This could only be done on the very thin sides, shown in Figure 60 left, as the other side is occupied by the substrate ceramic. Inner electrodes or vias as they are used for other multilayer ceramics are not possible, since the PTC has to be sintered in oxygen atmospheres at temperatures greater than 1300°C. An inner electrode would then oxidize or melt during sintering of the PTC. A full metallisation on the thin sides would also be problematic because of a long distance between the electrodes, thus a high resistance, and the difficult metallisation process itself. A different approach can be achieved by only a slight movement of both electrodes onto the top side of the PTC as shown in Figure 61 right. Two straight line electrodes would thus be already a good termination method, but the distance between the electrodes should be as short as possible. Also the electrode itself has to be as small as possible as the current takes the way of the lowest resistance, usually the shortest distance, and thus the area under the

electrode does not effectively contribute to the heat output. In order to optimize the effective heating volume a finger electrode design has been designed. The developed layout on the produced thin PTC heater is shown in Figure 61. The sides of the fingers are that large due to the experimental soldering and clamping method. For the production design this area can be very small and only in the opposite corners and the residual area can be fully used for finger electrodes. The electrode can also be extended over the sides of the composite and there connected with the circuit.

The finger electrode layout has also its disadvantages. Since both electrodes are one side a shortage by a conducting media, such as a liquid or a metal, is problematic. A second disadvantage is that if cracks occur the cracked area will not work properly anymore and in worst case larger areas are affected. For a fully metallised PTC cracks are not that problematic as the pieces are all in parallel circuit, so that cracked areas will still heat properly.

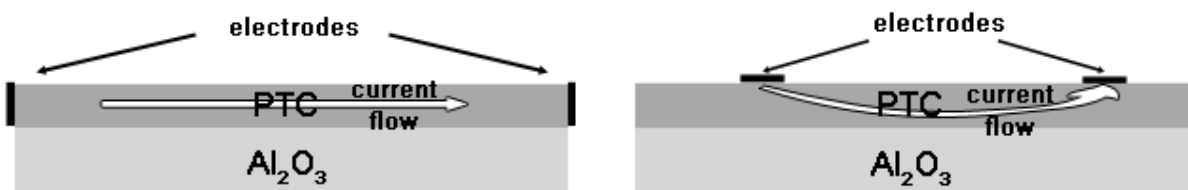


Figure 60: possible electrode layouts for the demonstrator

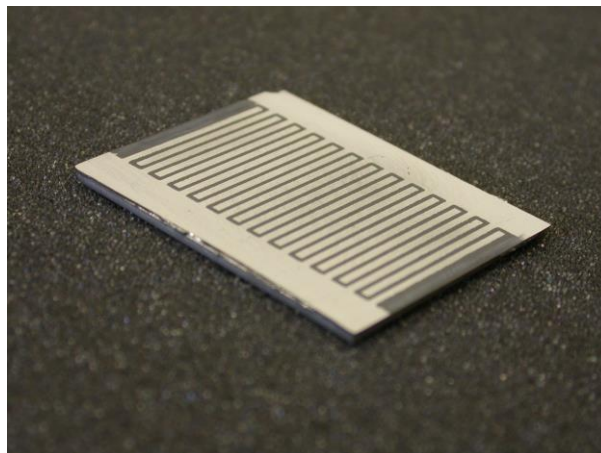


Figure 61: demonstrator with developed finger electrode layout

4.1.2 Electrical results

For electrical characteristics the resistance over temperature curve has been recorded with a voltage of 0.01V. In Figure 62 the R-T-curve of the demonstrator is shown. The resistance at 25°C has been measured with 1.20 Ω. From the measured R-T-values summarized in Table 12 the slope of the R-T curve has been calculated to 0.27 K⁻¹ and the reference temperature has been determined to 130.4°C. In Figure 63 the current voltage curve is shown together with the temperatures of the PTC and Al₂O₃ side measured by a k-thermocouple. The inrush current can be determined to 1.4 A and it asymptotical reaches a residual current of 0.38 A.

Table 12: measured resistance over temperature values

temperature	°C	30,06	39,81	49,96	59,88	69,96	79,94	89,94	99,96	105,13
resistance	Ω	1,22	1,20	1,21	1,23	1,21	1,23	1,25	1,30	1,33
temperature	°C	110,11	115,15	120,13	125,06	130,06	135,13	140,17	145,09	150,00
resistance	Ω	1,37	1,43	1,52	1,71	2,26	11,24	22,14	50,65	87,03

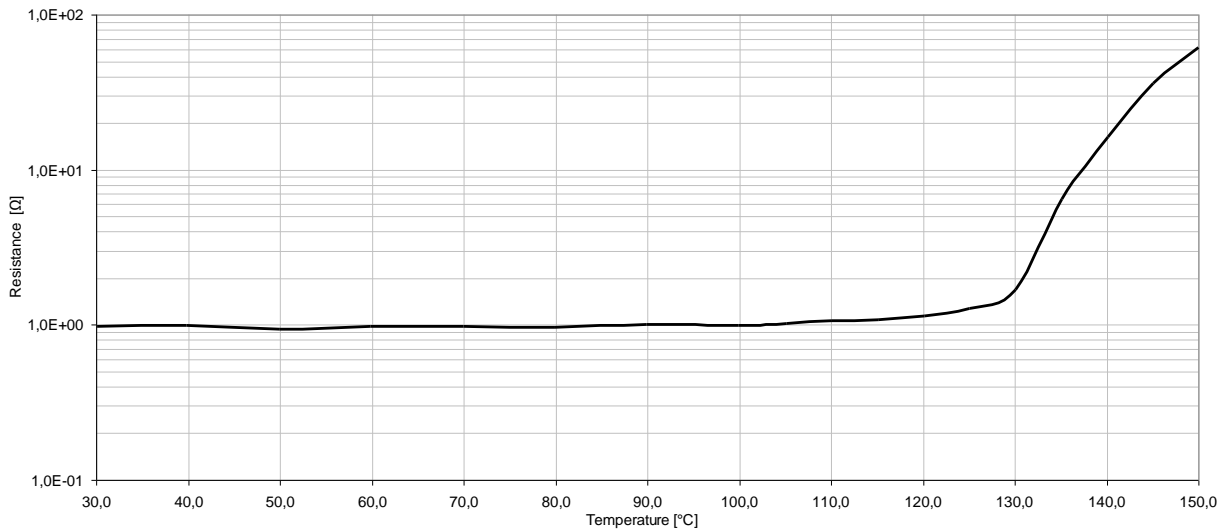


Figure 62: resistance over temperature curve of demonstrator

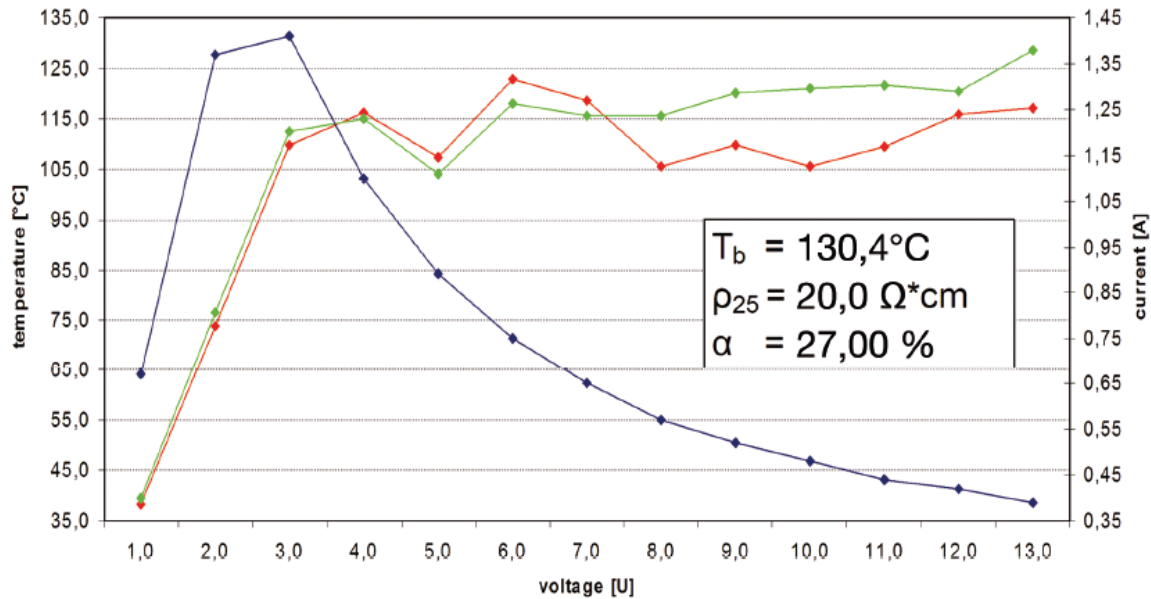


Figure 63: current and temperature measured with k-type thermocouple on PTC and Al_2O_3 side as a function of applied voltage

4.1.3 Calorimetric results

In order to compare the heating properties of the demonstrator and the standard PTC a calorimetric measuring device, also known as Junker's calorimeter, has been built up. For this the large heat capacity of water has been used. As first step a water reservoir, with about 10l water, has been used for temperature homogenization. From this reservoir, the water is flowing through the calorimetric measuring device shown in Figure 64. The measuring device has been based on a water cooler for CPU chips (supplier: Innovatek GmbH). This cooler consisting of an aluminium plate for heat exchange is placed directly on the alumina side, respectively on the standard pressed PTC. The PTC itself can be electrically contacted in two ways. Either from two small copper stripes for the developed finger electrode or on opposite sides, aluminium cooler and the copper stripes, for the standard pressed PTC. The distance between the aluminium cooler and the sample is kept as low as possible by fastening of windings and a thin layer of thermally conductive paste (supplier: Silmore) has been applied. The exactness of the developed measuring equipment has been checked by calculating the efficiency between the electric power and the heat capacity. An accuracy of up to 99,7% has been achieved. The heat capacity itself has been calculated using Equation 24. As

5 Discussion of results

shown in Table 13 the measurement revealed that the heat capacity per active area of the composite is 1.8 times higher than a conventional PTC substrate sputtered on both sides. But the absolute heat extraction is only half as much as a conventional PTC. As already discussed the electrode layout of the demonstrator has not been optimized with respect to a high active PTC area. This can for e.g. be done by modifying the borders to a minimum viable size 0.5mm and lowering the electrode size from 0.7 to 0.1mm. Regarding the 23.95 W cm^{-2} this increase in the active PTC area will result in an absolute heat capacity of 166W, which is about 10% higher than the conventional PTC substrate.

$$Q = m_w \cdot c_w \cdot \Delta T = \frac{V_w \cdot \rho_w}{t} \cdot c_w \cdot (T_{out} - T_{in}) \quad \text{Equation 24: calculation of the heat capacity}$$

Q:	heat capacity	[W]
m_w	mass of water heated water	[kg]
V_w	volume of water flowing through the calorimeter	[l]
c_w	specific heat capacity of water (interpolated between T_{in} and T_{out})	[J kg ⁻¹ K ⁻¹]
ρ_w :	density of water (interpolated between T_{in} and T_{out})	[kg·l ⁻¹]
T_{in} :	temperature of the water flowing in the calorimeter	[°C]
T_{out}	temperature of the water flowing out of the calorimeter	[°C]
t	stopped time	[s]

Table 13: Measured electric and calorimetric characteristics

sample	electrical values			calorimetric values (water)					Heat capacity	Heat capacity per area	Heat capacity per volume	time	efficiency
	voltage	current	power	thermal capacity	density	volume	input temp.	output temp.					
	U [V]	I [A]	P [W]	C_w [KJ/K·Kg]	ρ_w [kg/l]	V_w [l]	T_{ein} [°C]	T_{aus} [°C]					
1.2mm PTC	12.0	12.90	154.80	4.1823	1.0083	0.062	21.0	56.3	153.82	13.33	11.11	60	99.4
0.2 PTC + 1mm Al ₂ O ₃	12.0	6.17	74.04	4.1797	1.0050	0.062	22.5	39.5	73.79	23.95	960.98	60	99.6



Figure 64: developed calorimetric measuring device

Table 14: Temperature dependent density and specific heat capacity values

temperature	density	specific heat capacity	temperature	density	specific heat capacity
T [°C]	ρ_w [kg/l]	c_w [KJ/K·Kg]	T [°C]	ρ_w [kg/l]	c_w [KJ/K·Kg]
20,0	1,0018	4,1819	42,0		4,1789
21,0	1,0020	4,1813	43,0		4,1791
22,0	1,0022	4,1808	44,0		4,1792
23,0	1,0025	4,1804	45,0	1,0099	4,1795
24,0	1,0027	4,1800	46,0		4,1797
25,0	1,0030	4,1796	47,0		4,1799
26,0	1,0032	4,1793	48,0		4,1802
27,0	1,0035	4,1790	49,0		4,1804
28,0	1,0038	4,1788	50,0	1,0121	4,1807
29,0	1,0041	4,1786	51,0		4,1810
30,0	1,0044	4,1785	52,0		4,1814
31,0	1,0047	4,1784	53,0		4,1817
32,0	1,0050	4,1783	54,0		4,1820
33,0	1,0053	4,1783	55,0	1,0145	4,1824
34,0	1,0057	4,1782	56,0		4,1828
35,0	1,0060	4,1782	57,0		4,1832
36,0	1,0064	4,1783	58,0		4,1836
37,0	1,0067	4,1783	59,0		4,1840
38,0	1,0071	4,1784	60,0	1,0171	4,1844
39,0	1,0075	4,1785	61,0		4,1849
40,0	1,0079	4,1786	62,0		4,1853
41,0		4,1787	65,0	1,0198	4,1868

Thermo camera investigation:

The demonstrator has also been investigated with a thermo camera 42S from FLIR. Particularly the switching-on and switching-off process has been recorded. The switching-on process is shown in Figure 65, taken just as the power supply has been

switched on, and Figure 66, taken after 15 seconds of heating. On the left sides of the pictures the PTC side is recorded and on the right side the view on the alumina side is shown. The camera recording shows the effectiveness of the electrode layout as all electrode fingers are heated uniformly. The camera recordings also prove a homogeneous and fast developing temperature distribution particularly on alumina side. They further confirmed that heat is mainly produced in within the active proportion of the PTC layer below the electrode gap. It also proves a very fast heating of the demonstrator as already after 15 seconds the reference temperature is achieved.

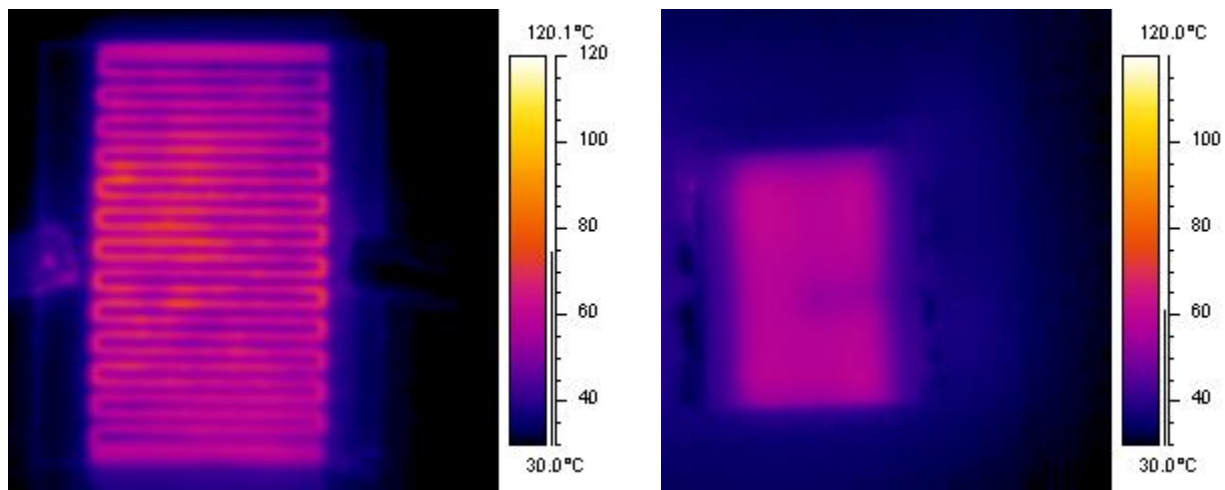


Figure 65: thermo camera recording of the swichting-on of the demonstrator (t=0s)

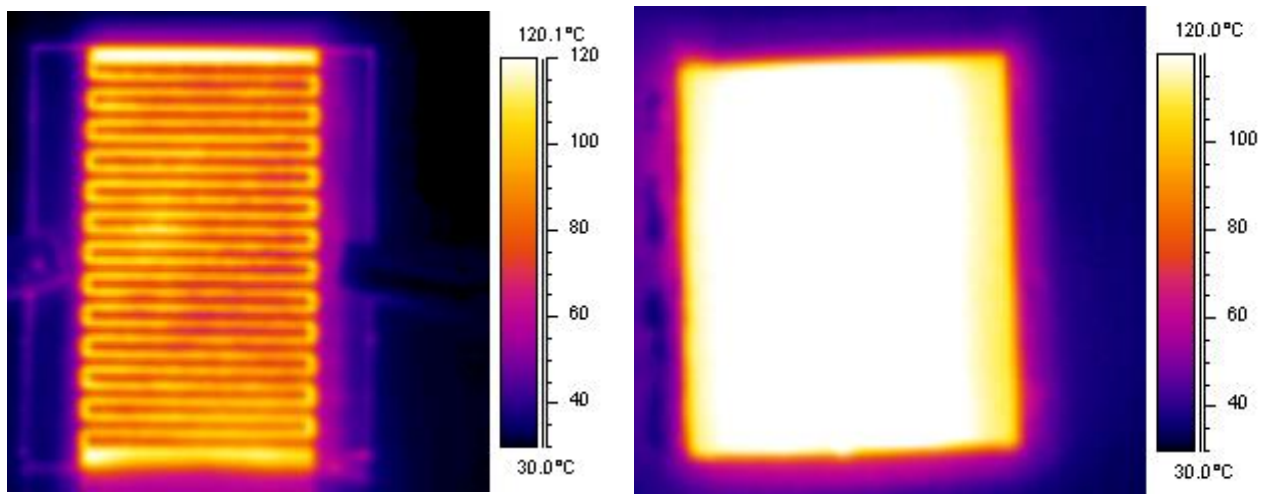


Figure 66: thermo camera recording of the swichting-on of the demonstrator (t~15s)

All in all the demonstrator has shown that a heater based on a thin PTC layer and a substrate ceramic such as Al_2O_3 has promising electrical and calorimetric properties.

4.2 Prototypes based on Yttria stabilized Zirconia

4.2.1 Production

Using the tape casting technology prototypes based on yttrium dioxide stabilized zirconia have been assembled. The different tapes have been produced as described in chapter 3.2. According to the results of the tape development also three intermediate layers of 20 mol-%, 50 mol-% and 80 mol-% YSZ have been used. The exact tape assembly is shown in Figure 67. Investigations from Dr. Andrea Testino on diffusion phenomena of magnesium oxide into barium titanate showed a diffusion layer of about 100 μm [Tes09]. Taking this into account each intermediate layer has been set up with two layers of tape. All tapes have been pressed together for 2 minutes with a pressure of 100 t and a temperature of 35°C. A stacked prototype is shown in Figure 68.

PTC mass A	(7 layers of tape)
20% YSZ / 80% PTC mass A	(2 layers of tape)
50% YSZ / 50% PTC mass A	(2 layers of tape)
80% YSZ / 20% PTC mass A	(2 layers of tape)
YSZ	(7 layers of tape)

Figure 67: tape assembly with three intermediate layers

Subsequently the prototypes have been thermally debinded within a debinding kiln from Tridelta Thermprozess GmbH. The furnace has a thermal afterburning, so that binder rests in the exhaust are burned at a temperature of 700°C. The amount of air flowing through the furnace has been adjusted to 100 l/min and the used debinding regime is shown in Table 15.

Table 15: debinding regime

Step	process	time	Gradient [K/min]	Temperature [°C]
1	heat	1:30:00	2	200
2	heat	8:20:00	0.5	450
3	dwel	0:30:00	0	450
4	cool	4:10:00	1	200
5	cool	1:30:00	2	20
		16:00:00 (Sum)		

Following the parts have been sintered in an electrical heated muffle kiln from CM INC. Bloomfield N.J.. The Sintering curve has been adapted according to the results of the material characterisation. Most characteristic are a sintering temperature of 1400°C, the dwell time of 30 minutes and the cooling gradient of 3 K/min.

Table 16: Adapted sintering regime

gradient [K/min]	5	0.5	3	3	0.5	3	1	0.5
temperature [°C]	100	450	900	1000	1400	900	450	0
dwell time [min]	0	0	0	0	30	0	0	0

Since a higher cooling gradient is known for an increase of the PTC effect and a lowering of the specific electrical resistance at room temperature also a cooling rate of 6 K/min has been investigated. A sintered prototype is shown in Figure 68.

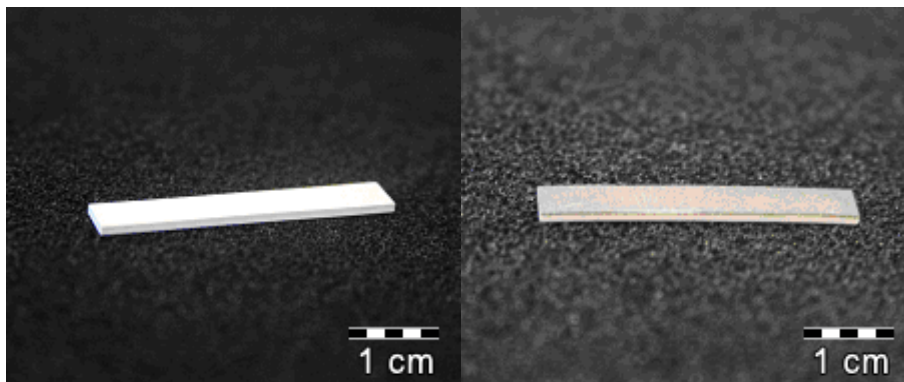


Figure 68: tape casted prototype based on YSZ (left: green and right: sintered)

4.2.2 Structural analysis

The structure of the parts has been observed under the optical microscope OLYMPUS BX51M. As shown in Figure 69 a stable material combination could be achieved. The micro section also shows that the PTC layer is more porous and less dense than the zirconia layer. In order to investigate the diffusion phenomena more the prototype has been observed with a Scanning electron microscope (SEM). Using the built in energy dispersive x-ray analysis EDX a Line-Scan of the prototypes' cross section has been

conducted. With the help of this scan diffusion phenomena can be investigated further. The SEM recording of the investigated part is shown in Figure 70. The recorded cross section of the Line-Scan is additionally marked. The Line-Scan itself is shown in Figure 71. For a better overview the different intermediate layers are marked by vertical lines. The recorded Line-scan is only qualitative, thus does not allow conclusions on the underlying quantities but for each element a trend over the cross section can be identified. The elements C, O, Zr, Ca, Ba and Ti have been investigated. Unfortunately the investigation of yttrium is very imprecise since it is overlaid with zirconia due to their chemical affinity. Because of that yttrium has not been investigated in this qualitative Line-Scan. Carbon has been investigated to show micro-cracks. During the preparation the cold embedding medium would flow into these defects, which can now be seen as higher amounts in carbon. This effect can be seen on the sides of the sample, but no micro crack can be identified here. The PTC layer on the right side is rich of barium and titanate and the amount of both lowers within the intermediate layers. Near the boundary of the zirconia layer the amount of barium and titanate sharply drops, thus no diffusion of barium or titanate into the zirconia layer can be detected. In opposition a diffusion of zirconium atoms into the PTC layer can be identified as a slowly declining line.

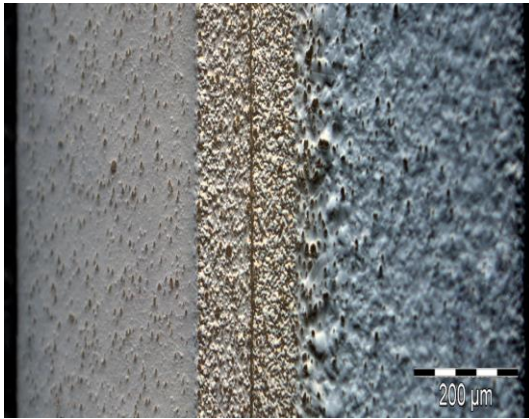


Figure 69: optical microscopy of prototype based on YSZ(zirconia left, PTC right)

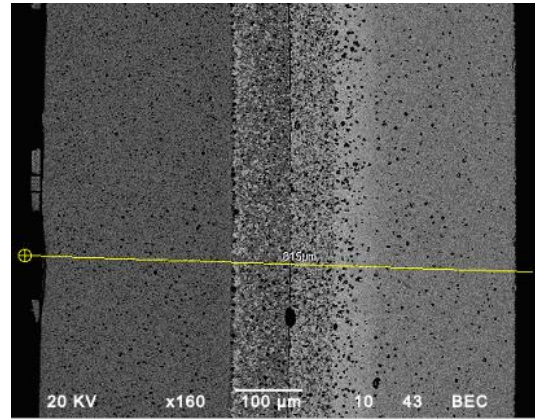


Figure 70: SEM analysis with marked line scan of YSZ(zirconia left, PTC right)

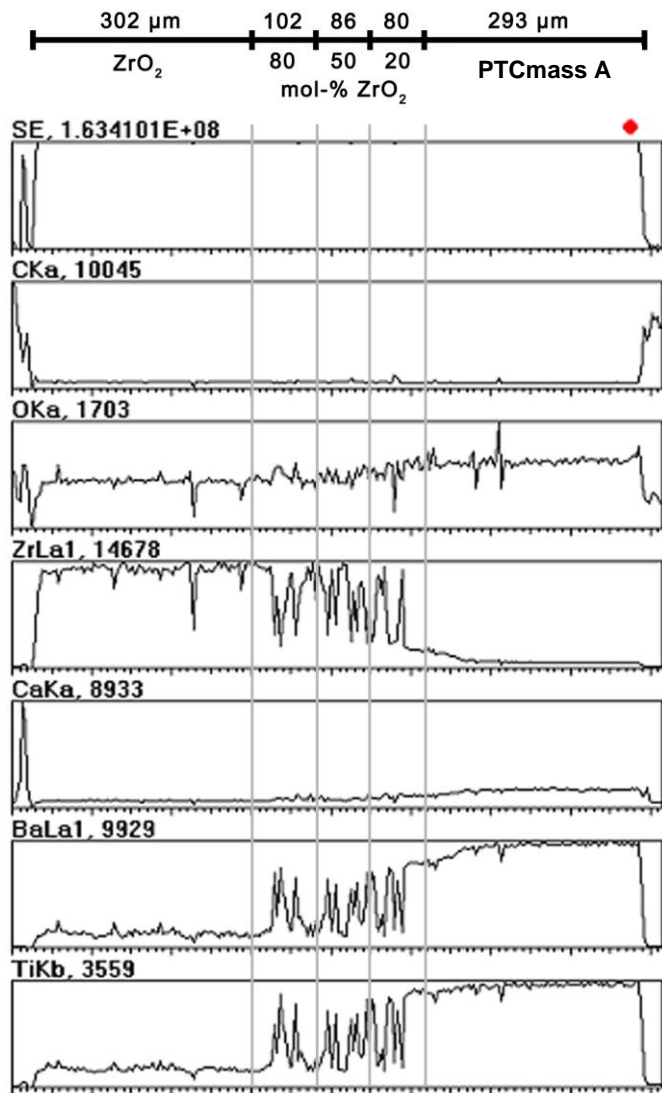


Figure 71: EDX line scan of tape casted prototype based on YSZ

4.2.3 Mechanical strength

For evaluation of the mechanical strength 20 tape casted prototypes have been produced using three intermediate layers as well as the optimal debinding and sintering regime as described earlier. Next their dimensions were taken using the micrometer gauge. As strength evaluation the 3 point bending strength has been measured using a test machine by Zwick-Roell. The parts were tested as sintered. Due to the described direction dependency of the bending tensile strength of composites half of the prototypes were measured with zirconia side on top and the other half was investigated with PTC side on top. The measured dimensions and forces are shown in A. 23. The three point bending tensile strength was calculated using Equation 20. The Weibull parameters have been determined graphically. The sorted bending strength values and the corresponding probabilities of fracture are displayed in Table 17. Both values are then plotted in the Weibull diagram shown in Figure 72. From this diagram the characteristic Weibull strength values S_0 , the intercepts of the regression lines with $y=0$, could be extracted. The Weibull module m can be extracted from a different Weibull diagram where the strength is plotted logarithmically against $\ln\ln[1/(1-F(\sigma_{B,i}))]$. The slope of the regression line of the data equals the Weibull modulus m . The determined Weibull parameters are displayed in Table 18. One can see that the characteristic Weibull strength as well as the Weibull modulus of both assemblies differentiate and therefore are oriented as discussed. The higher values of $S_0 = 401.62$ MPa and $m=16$ are reached when the PTC mass A layer is on top. Thus a 4.5 times higher characteristic Weibull strength and a 1.8 times higher Weibull module can be achieved when the zirconia side is charged with the higher bending load. This also conforms to the measurement of the single materials as well as the structural analysis. The measured 88.5 MPa compare to the three point bending tensile strength of the single PTC ceramic of about 100 MPa. The structural analysis concluded that the PTC layer is more porous and less dense, thus the PTC layer has more critical defects. This would result in a higher spreading in mechanical strength, which could be verified by the lower Weibull module of 9.6.

Table 17: calculated mechanical strength of tape casted prototypes based on YSZ

i	probability of fracture		YSZ on top		PTC mass A on top	
	F($\sigma_{B,i}$) [%]	lnln[1/(1-F($\sigma_{B,i}$))]	bending strength			
			$\sigma_{B,i}$ [MPa]	ln($\sigma_{B,i}$)	$\sigma_{B,i}$ [MPa]	ln($\sigma_{B,i}$)
1	5.00	-2.970	66.65	4.1994	341.48	5.8333
2	15.00	-1.817	72.43	4.2826	345.11	5.8439
3	25.00	-1.246	77.36	4.3485	383.41	5.9491
4	35.00	-0.842	79.32	4.3735	387.64	5.9601
5	45.00	-0.514	79.97	4.3817	390.59	5.9677
6	55.00	-0.225	88.60	4.4841	392.59	5.9728
7	65.00	0.049	90.22	4.5022	394.11	5.9766
8	75.00	0.327	92.98	4.5324	407.02	6.0089
9	85.00	0.640	94.13	4.5447	414.47	6.0270
10	95.00	1.097	96.89	4.5735	431.05	6.0662

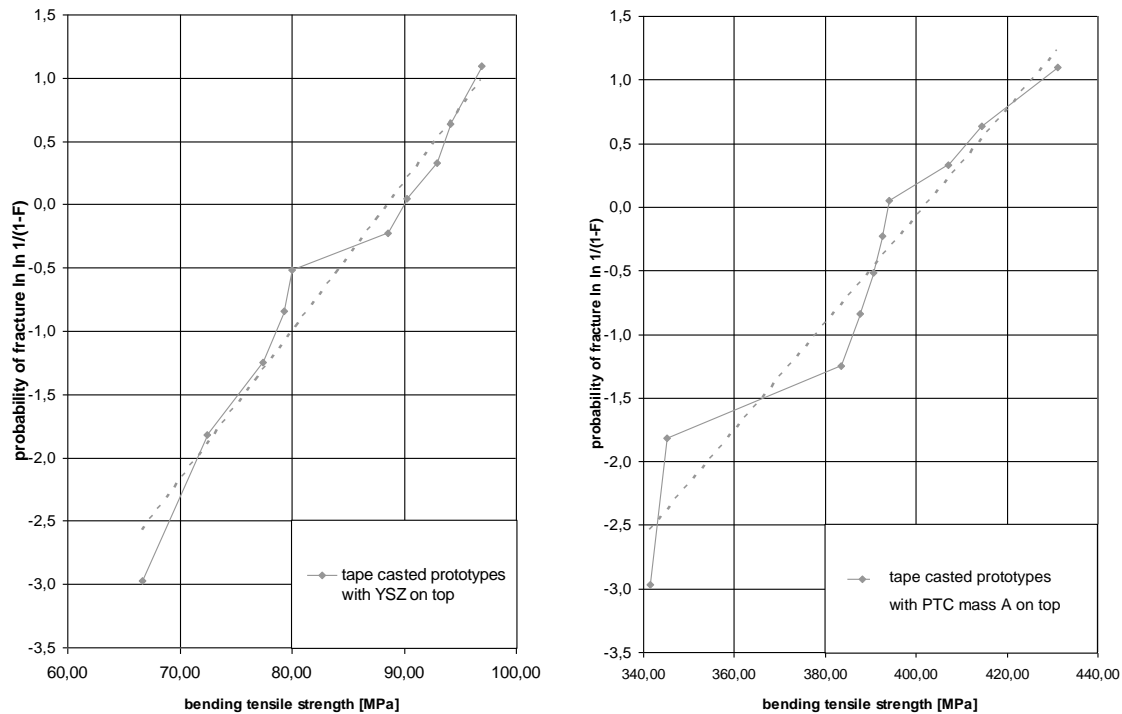


Figure 72: Weibull diagram of bending tensile strength of tape casted prototypes based on YSZ

Table 18: characteristic Weibull strength and Weibull module of tape casted prototypes based on YSZ

Arrangement	Weibull strength	Weibull module
	S_0 [MPa]	m
YSZ on top	88.50	9.649
PTC mass A on top	401.62	16.004

4.2.4 Electrical characteristics

In order to measure the electrical characteristics ten prototypes have been cut into smaller pieces. The parts dimensions have then been determined using the optical microscope OLYMPUS BX51M. After sputtering the specific electrical values have been determined. At first the resistance at room temperature R_{25} has been determined using the Keithley 199 System DMM/Scanner and the specific electrical resistance ρ_{25} was calculated according to Equation 17. Further on the electrical resistance in dependency of the temperature has been measured in the oil-filled tank Proline RP 18409. From the recorded R-T-characteristic curve the reference temperature and the temperature coefficient, the slope of the R-T-curve above the reference temperature have been calculated. As described in chapter 2.1.3 the reference temperature T_B is near the Curie temperature but experimentally easier determined, since it is defined as the temperature, where the PTC reaches twice the lowest resistance. The measured electrical values are shown in Table 19, exemplary R-T curves are displayed in Figure 73 and the underlying R(T) values are displayed in A. 24. Two different sintering curves with cooling rates of 3 and 6 K/min have been investigated. By increasing the cooling rate the specific electrical resistance could be lowered for about one decimal power. Nevertheless the specific electric resistance values are relatively high with lowest 5324.2 Ωcm . The reference temperatures have a low spreading and are all about 120°C just as the PTC mass A. The slope of the R-T curve varies from 12.6 to 26.0 %/K. All in all the PTC characteristics could be verified on the tape casted prototypes based on YSZ.

Table 19: electrical measurements of tape casted prototypes based on YSZ

sintering regime	nr	measurement				resistance		slope of R-T-curve alpha	T(R _b)
		width	height	thickness	area	R ₂₅	ρ ₂₅		
-	-	μm	μm	mm	mm ²	Ω	kΩ*cm	1/K	°C
Sintering curve 1400/30/3	1	25404.4	301.0	3.75	7.65	3.33E+07	6783.93	0.1257	120.2
	2	25390.1	293.0	3.54	7.44	3.72E+07	7812.73	0.1674	121.7
Sintering curve 1400/30/6	3	4149.7	315.6	1.20	1.31	3.77E+06	411.62	0.1508	121.1
	4	4197.6	280.2	0.84	1.18	4.05E+06	567.56	0.1537	120.6
	5	4174.5	272.1	0.85	1.14	2.21E+06	70.86	0.1643	120.0
	6	4196.9	283.0	1.99	1.19	2.32E+07	1384.47	0.1656	120.7
	7	4162.2	299.8	1.27	1.25	5.25E+06	516.05	0.1213	122.1
	8	4200.5	307.4	1.85	1.29	4.85E+06	338.74	0.1282	118.8
	9	4181.4	291.2	2.47	1.22	1.53E+05	5.32	0.2595	118.0
	10	4171.6	283.1	1.65	1.18	6.96E+06	497.86	0.1337	120.0

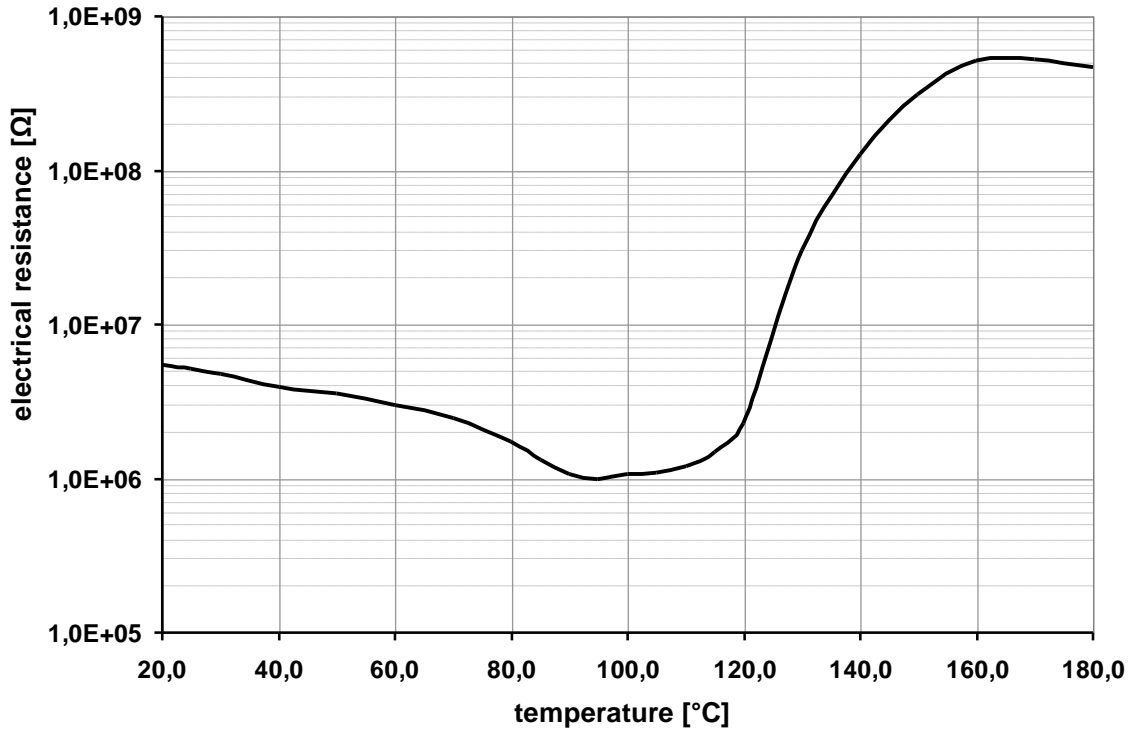


Figure 73: exemplary R(T) curve of tape casted prototype based on YSZ

4.3 Prototypes based on YSZ, barium titanate and PTC

4.3.1 Production

According to the rather high-ohmic electrical results and identified diffusional phenomena of the zirconia and PTC composite, it was evident that some barrier layer, which prevents or suppresses the diffusion had to be included. As the structural and mechanical investigations showed rather good results for the adaptation of shrinkage and expansion coefficients a similar material for the barrier layer was desired. Barium titanate as the undoped PTC version was further investigated. Due to the absence of yttrium and calcium inside the barium titanate layer the diffusion shall be lowered by doping the pure barium titanate layer during diffusion. Using the tape casting technology prototypes based on yttrium dioxide stabilized zirconia have been assembled. The different tapes have been produced as described in chapter 3.2. According to the results of the tape development also three intermediate layers of 20 mol-%, 50 mol-% and 80 mol-% YSZ have been used. The exact tape assembly is shown in Figure 67. Investigations from Dr. Andrea Testino on diffusion phenomena of magnesium oxide into barium titanate showed a diffusion layer of about 100 μm [Tes09]. Taking this into account each intermediate layer has been set up with two layers of tape. All tapes have been pressed together for 2 minutes with a pressure of 100 t and a temperature of 35°C.

PTC mass A	(7 layers of tape)
Barium titanate layer	(2 layers of tape)
20% YSZ / 80% PTC mass A	(2 layers of tape)
50% YSZ / 50% PTC mass A	(2 layers of tape)
80% YSZ / 20% PTC mass A	(2 layers of tape)
YSZ	(7 layers of tape)

Figure 74: tape assembly with three intermediate layers

Subsequently the prototypes have been thermally debinded within a debinding kiln from Tridelta Thermprozess GmbH. The furnace has a thermal afterburning, so that binder rests in the exhaust are burned at a temperature of 700°C. The amount of air

flowing through the furnace has been adjusted to 100 l/min and the used debinding regime is shown in Table 15.

Table 20: debinding regime

Step	process	time	Gradient [K/min]	Temperature [°C]
1	heat	1:30:00	2	200
2	heat	8:20:00	0.5	450
3	dwel	0:30:00	0	450
4	cool	4:10:00	1	200
5	cool	1:30:00	2	20
		16:00:00 (Sum)		

Following the parts have been sintered in an electrical heated muffle kiln from CM INC. Bloomfield N.J.. The Sintering curve has been adapted according to the results of the material characterisation. Most characteristic are a sintering temperature of 1400°C, the dwell time of 30 minutes and the cooling gradient of 3 K/min.

Table 21: Adapted sintering regime

gradient [K/min]	5	0.5	3	3	0.5	3	1	0.5
temperature [°C]	100	450	900	1000	1400	900	450	0
dwell time [min]	0	0	0	0	30	0	0	0

Since a higher cooling gradient is known for an increase of the PTC effect and a lowering of the specific electrical resistance at room temperature also a cooling rate of 6 K/min has been investigated.

4.3.2 Structural analysis

For first structural analysis the optical microscope OLYMPUS BX51M has been used. Figure 75 shows the micrograph of a prototype with barium titanate as barrier layer. In general this micrograph depicts a good material composite but also already identifies two problems: a high porosity inside the barium titanate and PTC layer and diffusional phenomena into the pure zirconia layer. In Figure 76 the dentrical into the zirconia layer are further shown.

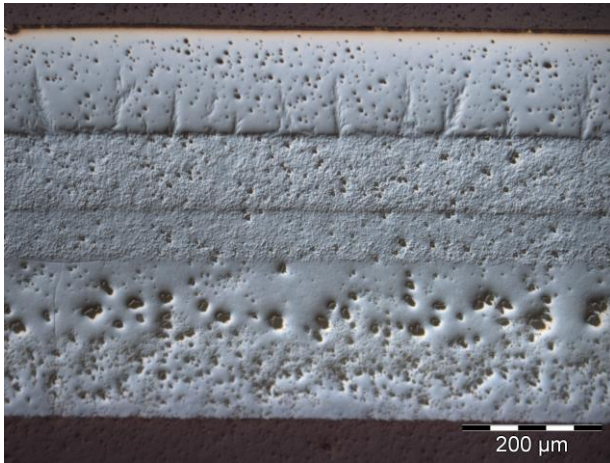


Figure 75: micrograph of PTC, BT, YSZ prototype

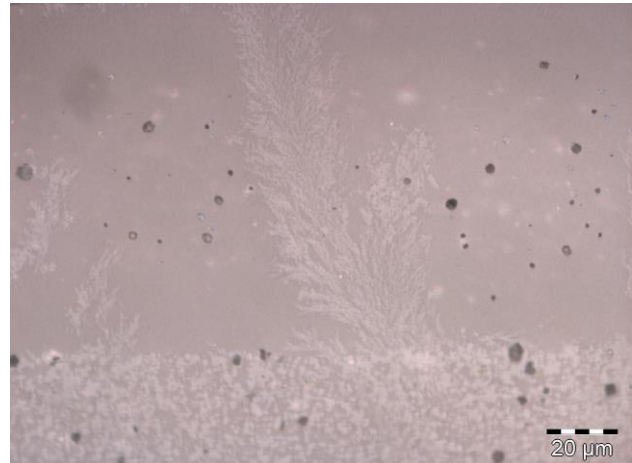


Figure 76: micrograph of needles in YSZ layer

SEM analysis:

Using the SEM the microstructure and composition has been investigated further. For more detailed analysis the samples have been investigated with a Scanning Electron Microscope (SEM). Using the built in energy dispersive x-ray analysis EDX an element mapping as well as different measurement points over the cross section have been conducted. With the help of this scan diffusion phenomena can be investigated further. The diffusional properties into the

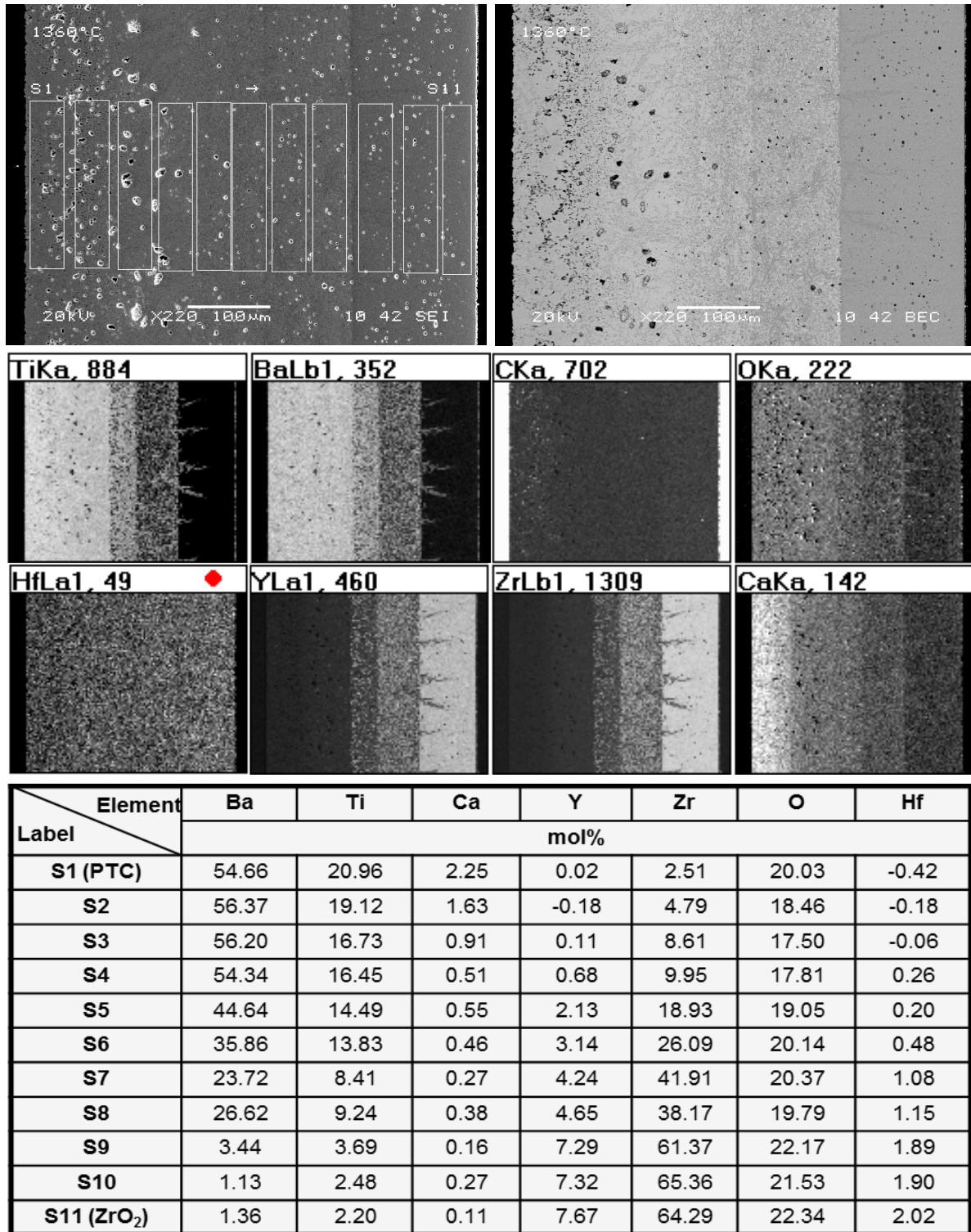
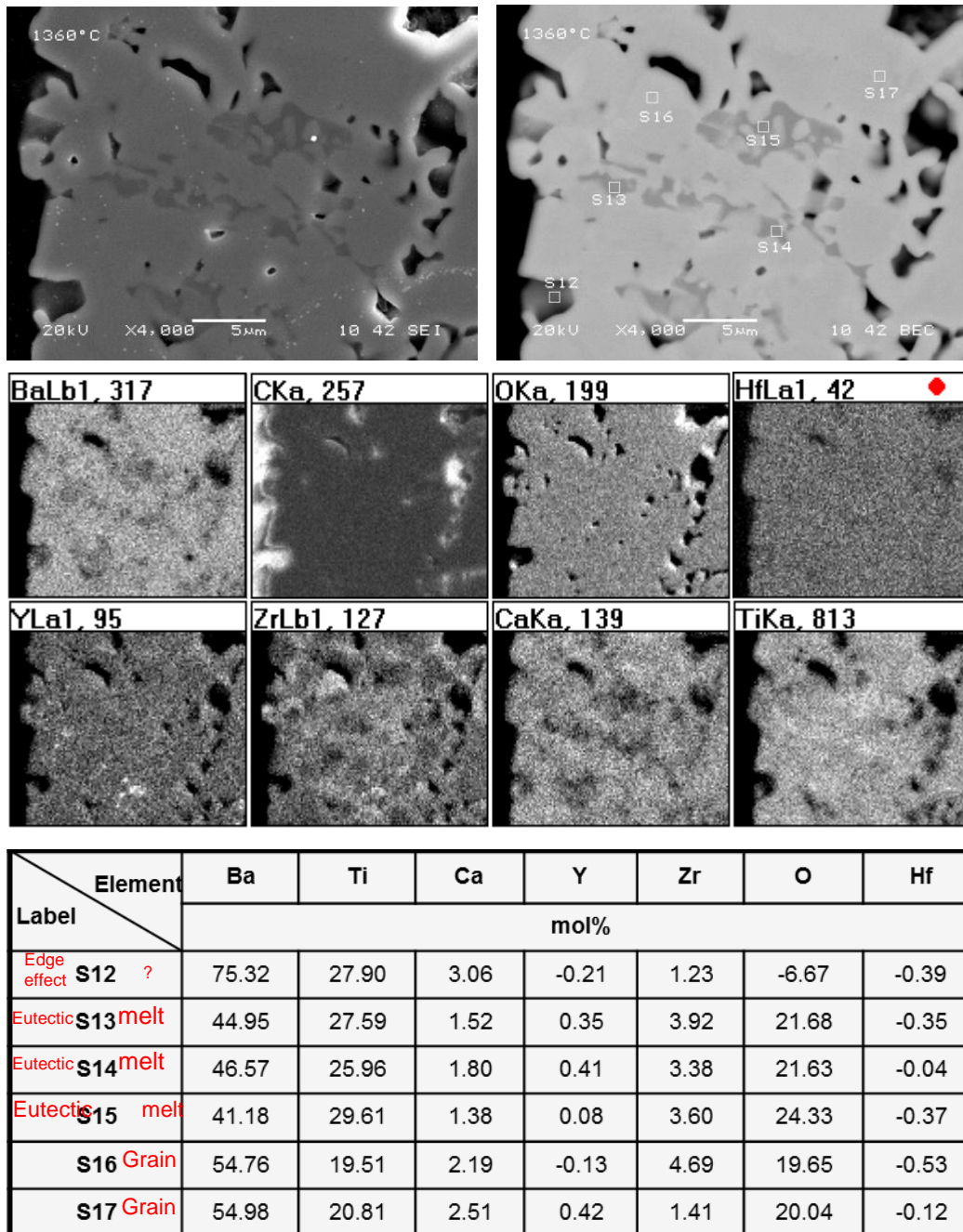


Figure 77: SEM analysis of PTC, BT, ZrO₂ composite

Figure 78: SEM analysis of PTC layer of PTC, BT, ZrO₂ composite

5 Discussion of results

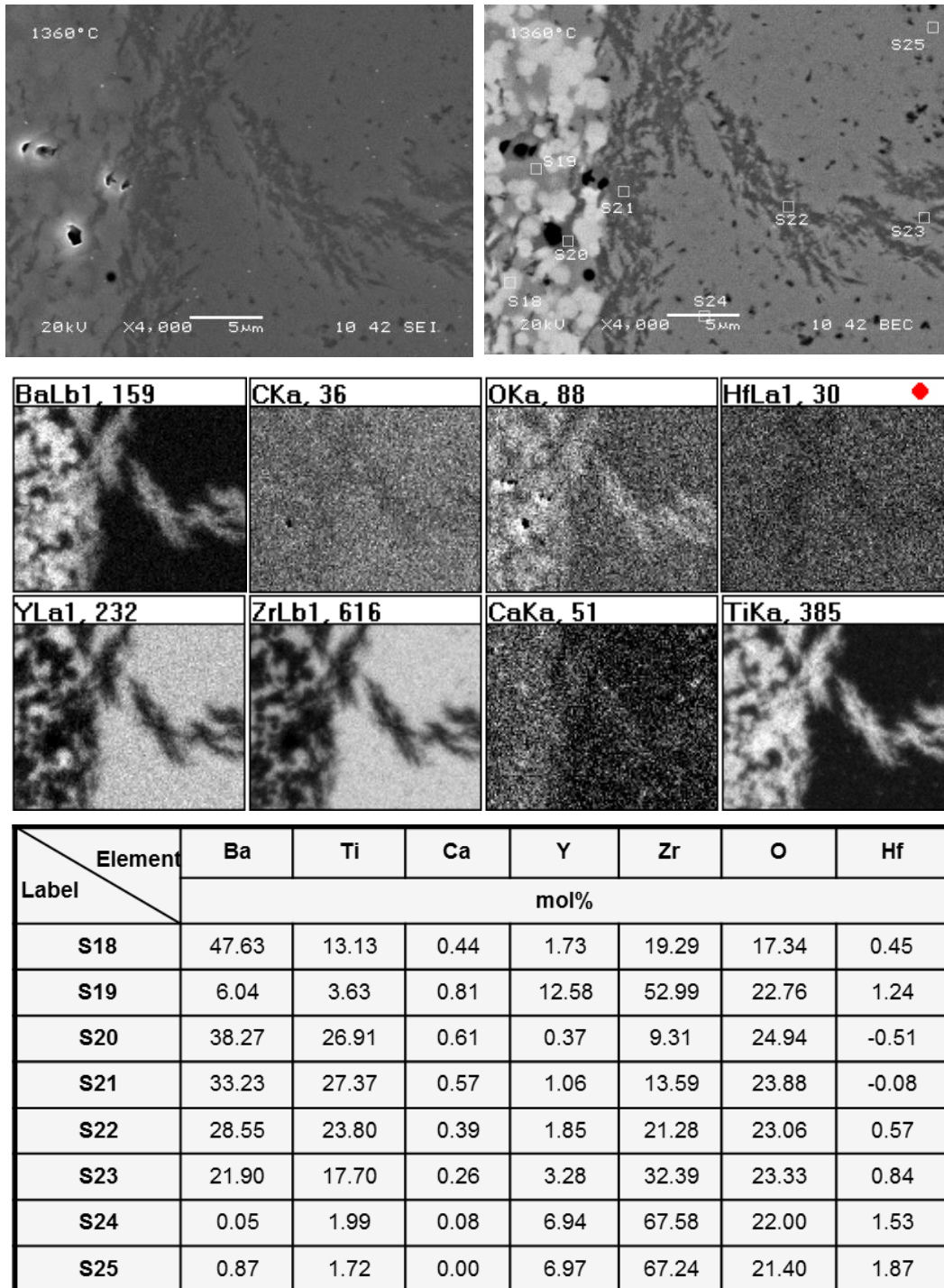


Figure 79: SEM analysis of intermediate layer of PTC, BT, ZrO₂ composite

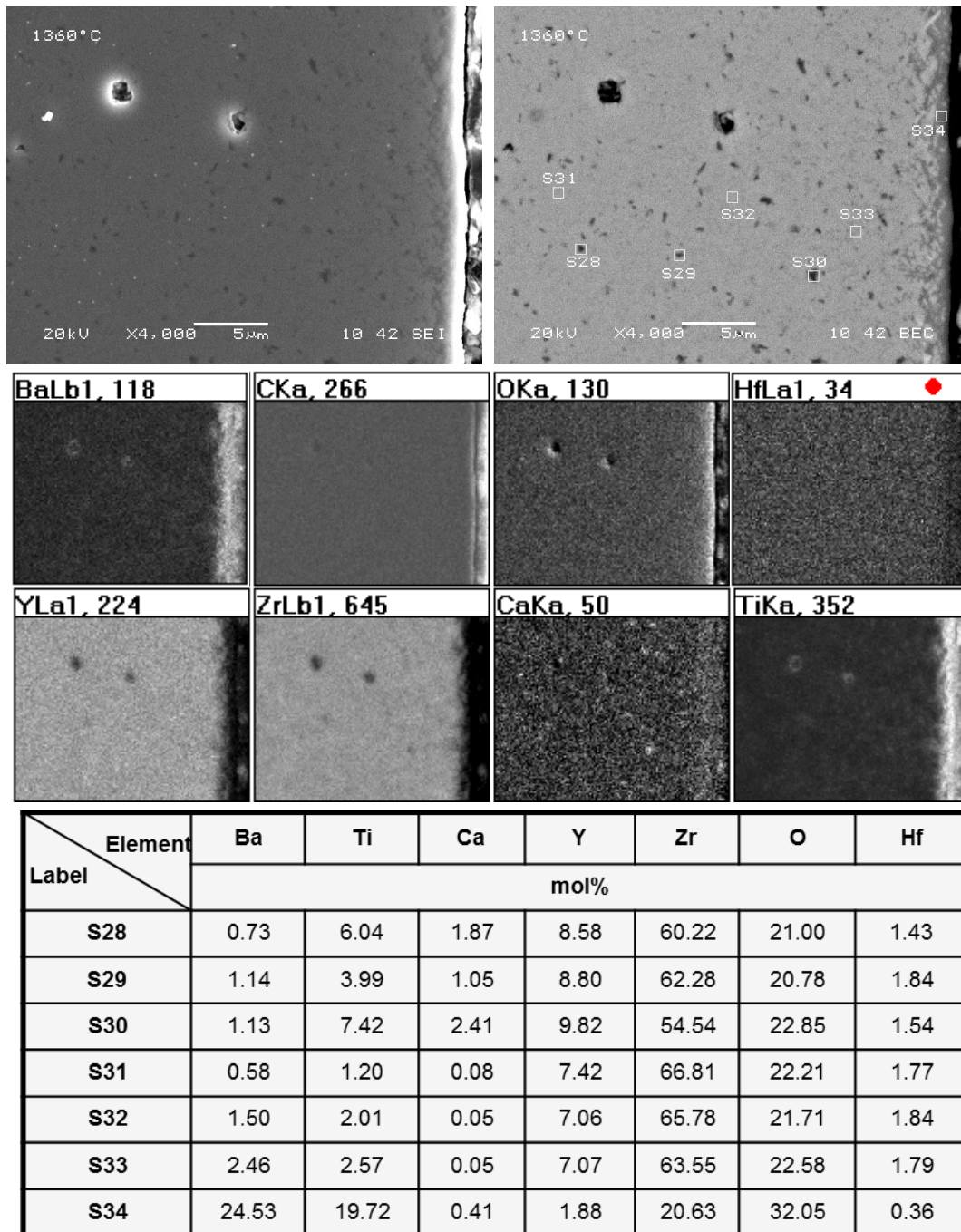


Figure 80: SEM analysis of ZrO₂ layer of PTC, BT, ZrO₂ composite

Detailed analysis of the intermediate layer:

For more detailed analysis the intermediate layers have been further investigated. Figure 81 shows the sem analysis of the intermediate layer.

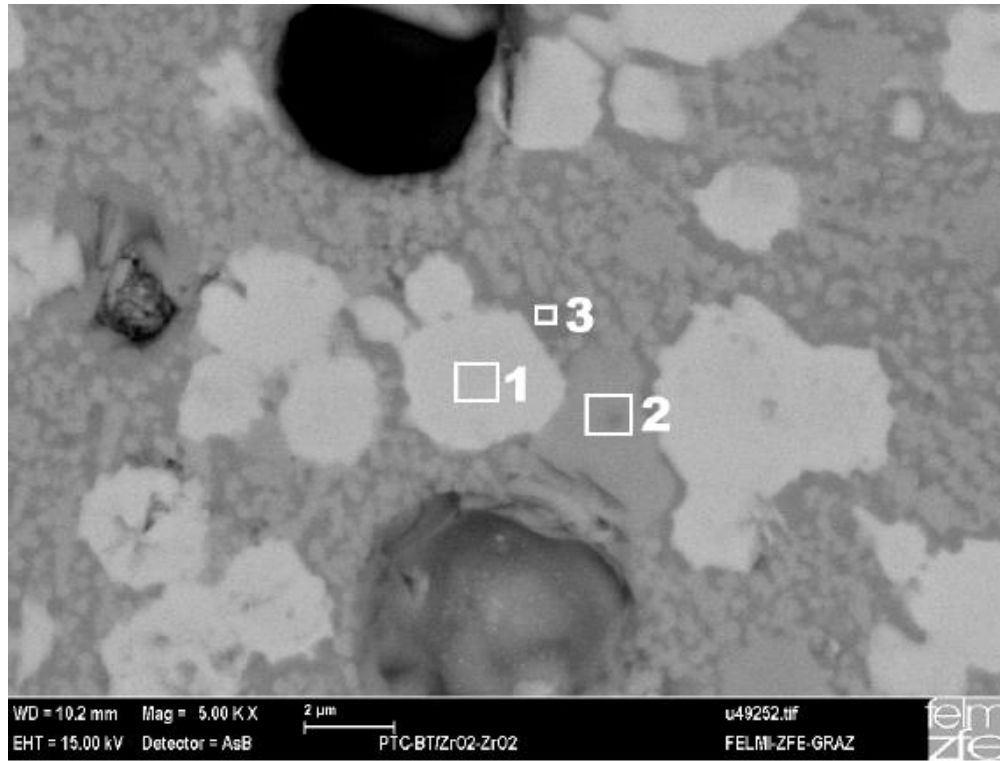


Figure 81: SEM analysis intermediate layer YSZ, BT, PTC

Investigations on different PTC and BT layer thicknesses:

For further testing of the diffusion phenomena into the PTC layer and their influence on the PTC characteristics prototypes with different thicknesses of the barium titanate have been assembled. The thickness of the pure barium titanate layer has been varied from 100 to 200 μm . As third prototype also an thicker PTC layer of 300 has been investigated. In Figure 82 the micrograph of the three different thicknesses are compared with each other. It can be seen that the Kirkendall porosity is for the lowest PTC and barium titanate thickness is at the edge of the PTC layer. With increased barium titanate layer this porosity shifts inside the barium titanate layer. Figure 83 depicts the corresponding R-t curves of the assembled prototypes. These curves correspond with the micrographs and show that assembly XII shows the best electrical results. Lowest resistance and highest slope of the R-T curve compared with the

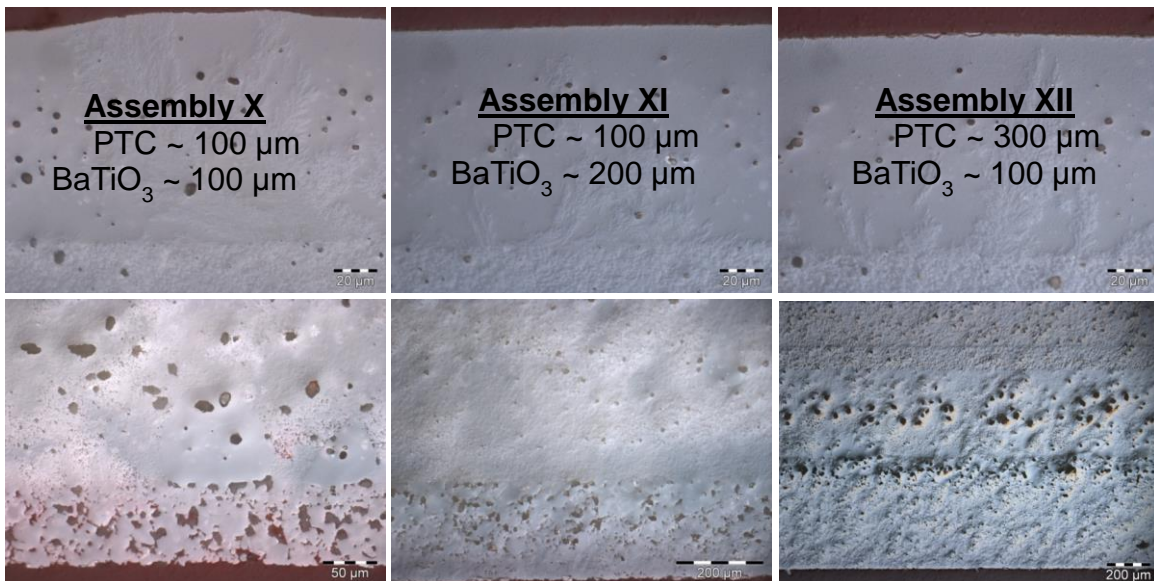


Figure 82: micrographs of YSZ, BT, PTC with different BT and PTC layer thicknesses

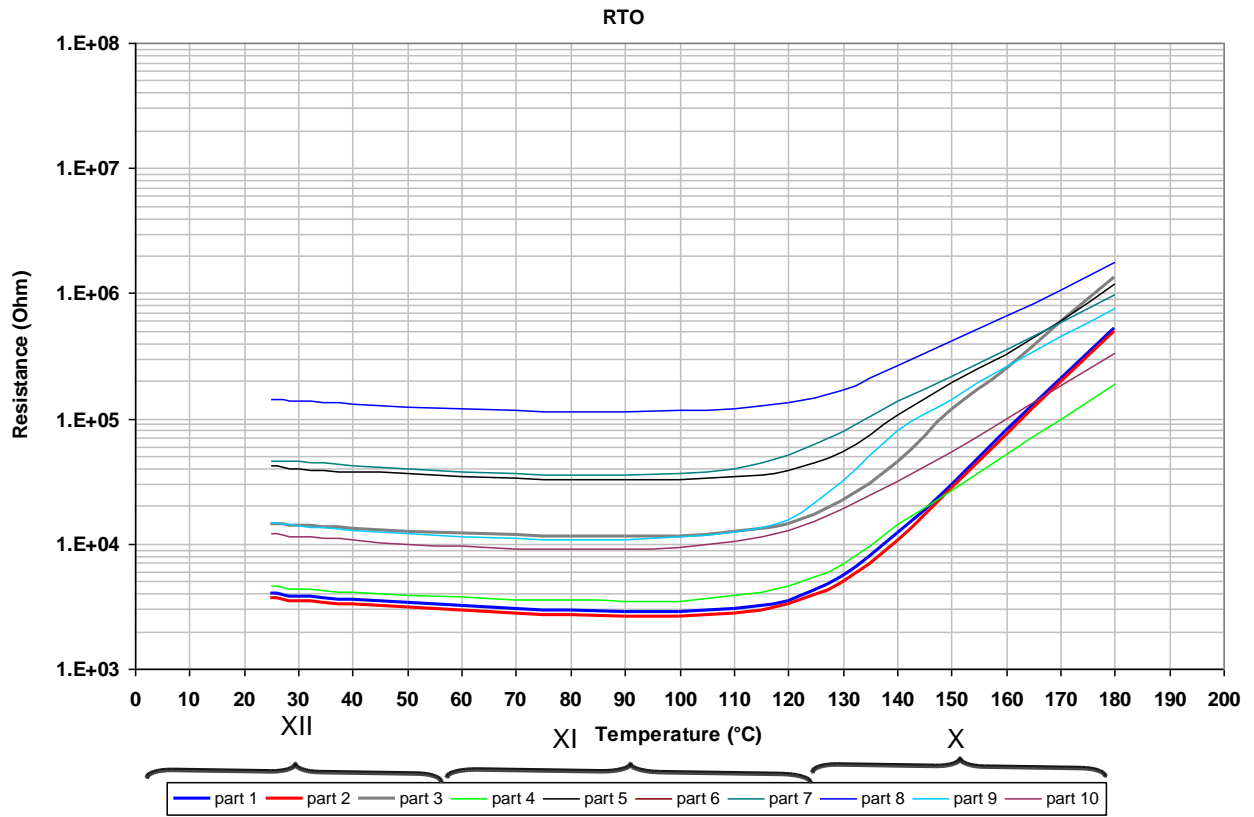


Figure 83: R-t curves of YSZ, BT, PTC with different BT and PTC layer thicknesses

4.4 Prototypes based on alumina

4.4.1 Production

With the developed alumina and PTC tapes also prototypes have been produced. A difference of 5 ppm in the thermal expansion can be seen in the dilatometry measurements. From operating experience a difference of $\Delta\alpha = 1 \cdot 10^{-6} \text{ K}^{-1}$ between 2 layers can be compensated to form a stable composite. According to this difference of 5 ppm a minimum of 4 intermediate layers are needed. Because of this prototypes with 3, 4 and 5 intermediate layers have been assembled for investigations.

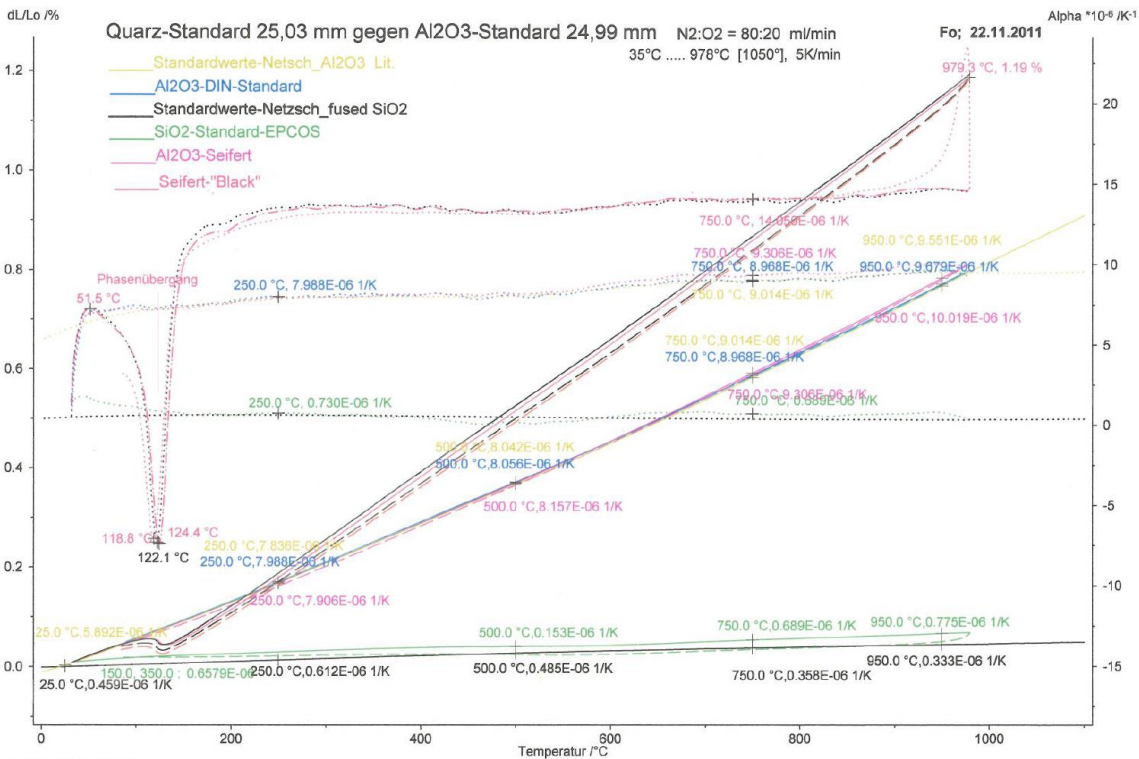


Figure 84: Thermal shrinkage and expansion analysis of PTC and alumina tapes

PTC	PTC	PTC
75% PTC & 25% Al ₂ O ₃	80% PTC & 20% Al ₂ O ₃	83% PTC & 17% Al ₂ O ₃
50% PTC & 50% Al ₂ O ₃	60% PTC & 40% Al ₂ O ₃	66% PTC & 34% Al ₂ O ₃
25% PTC & 75% Al ₂ O ₃	40% PTC & 60% Al ₂ O ₃	50% PTC & 50% Al ₂ O ₃
Al ₂ O ₃	20% PTC & 80% Al ₂ O ₃	34% PTC & 66% Al ₂ O ₃
	Al ₂ O ₃	17% PTC & 83% Al ₂ O ₃
		Al ₂ O ₃

Figure 85: Different assemblies of 3, 4 and 5 intermediate layers

5 Discussion of results

The assembled prototypes have been thermally debinded within a debinding kiln from Tridelta Thermprozess GmbH. The furnace has a thermal afterburning, so that binder rests in the exhaust are burned at a temperature of 700°C. The amount of air flowing through the furnace has been adjusted to 100 l/min and the used debinding regime is shown in Table 15.

Table 22: debinding regime

Step	process	time	Gradient [K/min]	Temperature [°C]
1	heat	1:30:00	2	200
2	heat	8:20:00	0.5	450
3	dwel	0:30:00	0	450
4	cool	4:10:00	1	200
5	cool	1:30:00	2	20
		16:00:00 (Sum)		

Following the parts have been sintered in an electrical heated muffle kiln from CM INC. Bloomfield N.J.. The Sintering curve has been adapted according to the results of the material characterisation. Most characteristic are a sintering temperature of 1400°C, the dwell time of 30 minutes and the cooling gradient of 3 K/min.

Table 23: Adapted sintering regime

gradient [K/min]	5	0.5	3	3	0.5	3	1	0.5
temperature [°C]	100	450	900	1000	1400	900	450	0
dwell time [min]	0	0	0	0	30	0	0	0

Since a higher cooling gradient is known for an increase of the PTC effect and a lowering of the specific electrical resistance at room temperature also a cooling rate of 6 K/min has been investigated.

4.4.2 Structural analysis

SEM analysis:

Using the SEM the microstructure and composition has been investigated further. For more detailed analysis the samples have been investigated with a Scanning Electron Microscope (SEM). Using the built in energy dispersive x-ray analysis EDX an element mapping as well as different measurement points over the cross section have been conducted. With the help of this scan diffusion phenomena can be investigated further. As shown in Figure 46 zirconia and yttrium rich areas are surrounded by clouds enriched of calcium.

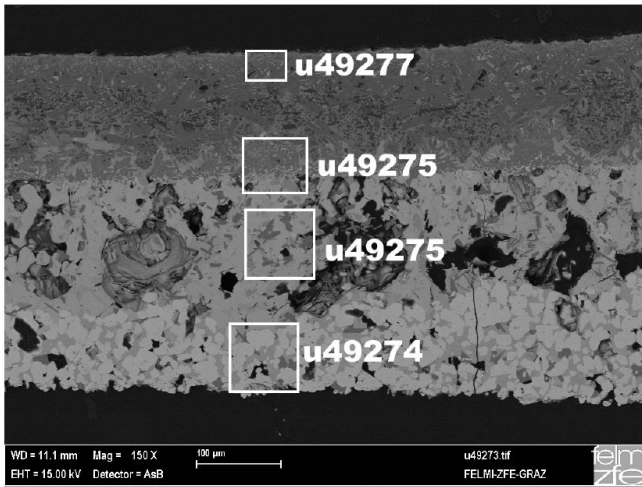


Figure 86: Analysis of PTC, BT, Al₂O₃ composite

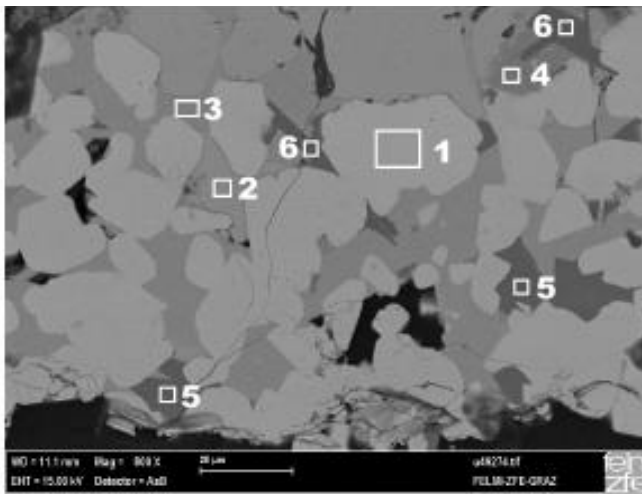


Figure 87: analysis of Al₂O₃ layer – u49274

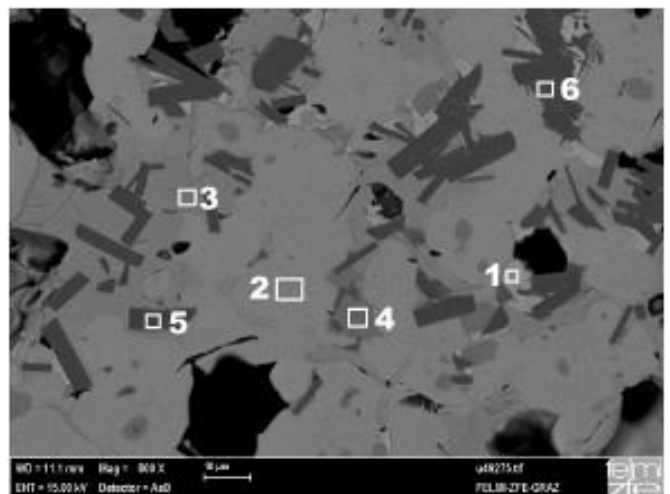


Figure 88: analysis of intermediate layer – u49275

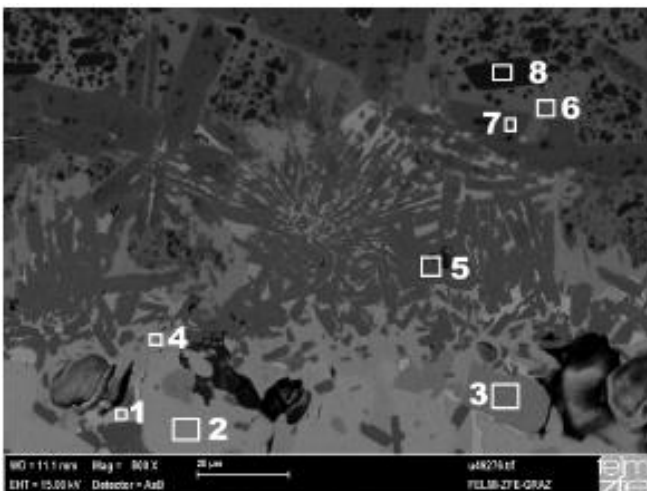


Figure 89: analysis intermediate layer - u49276

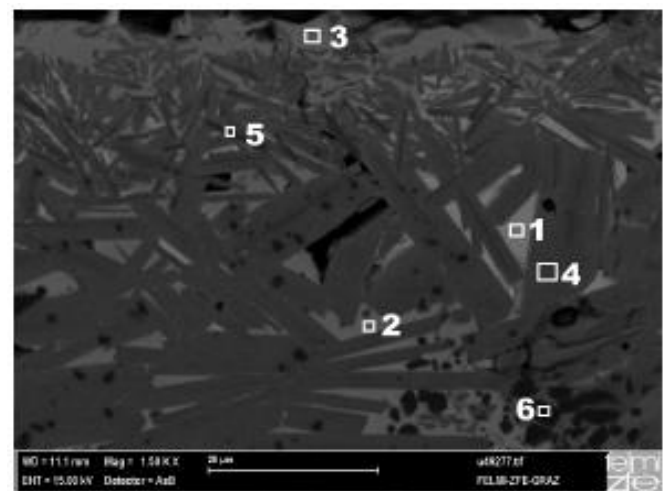


Figure 90: analysis of Al₂O₃ layer – u49277

4.5 Investigations on the sintering of the material composite

4.5.1 Heating microscope evaluation

The samples have been investigated in a heating microscope in order to investigate the macroscopic changes during the sintering process. The samples have been heated up to a maximum 1400°C with a heating gradient of 10 K/min and every 50K a picture is made. Each individual image has been analyzed using computer software Adobe Photoshop. As shown in Figure 91 for each image the length of the top layer (PTC), the length of the bottom layer (zirconia or alumina) and the height of the prototype have been determined. For bended parts the length has been determined with a small detour. A circle has been manually adapted to the part. Then the arc length, which is matching the part's length, has been calculated according to Equation 25. For this the angle between the outside points of the part and the radius of the subsidiary circle has been used.

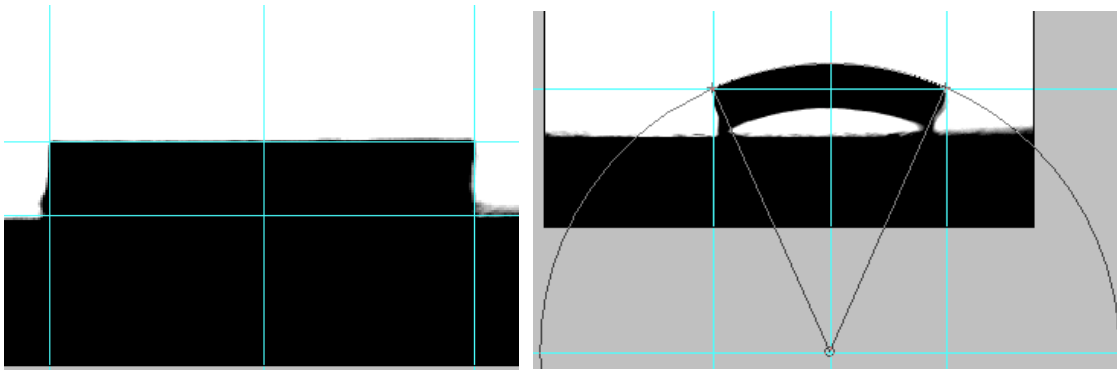


Figure 91: exemplary image analysis of the PTC/ZrO₂ prototype (left: 500 and right: 1300°C)

$$b = \frac{\pi \cdot r \cdot \alpha}{180^\circ}$$

Equation 25: calculation of the arc length

b	arc length of subsidiary circle (equals the part's length)	[px]
r	radius of the subsidiary circle	[px]
α	angle of the subsidiary circle	[px]

The HT-microscopy pictures of the thin PTC heater are shown in A. 25 to A. 32 and the analyzed sizes are shown in A. 60 to A. 63. The HT-microscopy pictures of the PTC-ZrO₂ prototype are shown in A. 33 to A. 38 and the analyzed sizes are shown in A. 52 to

A. 55. The HT-microscopy pictures of the PTC-BT-ZrO₂ prototype are shown in A. 39 to A. 44 and the analyzed sizes are shown in A. 56 to A. 59. The HT-microscopy pictures of the PTC-Al₂O₃ prototype are shown in A. 45 to A. 51. By comparing all measured lengths and heights to the initial lengths and heights using Equation 9 the shrinkage has been calculated. The shrinkages are summarized in Figure 92. For comparison the shrinkages of YSZ and PTC recorded in the dilatometer DIL402CD are inserted in the diagram with dashed lines.

From the first view one can see that the change in height is characteristically greater for each prototype than the change in length. On the one hand this is due to the exactness of the analysis method. As the height values are comparatively smaller than the length values, already a small change in height results in a larger percentage value. On the other hand are the diffusion and reaction phenomena between the individual material layers more intense in direction of the height. Based on this the change in height gives a good indication on the chemical interactions during sintering. It can be observed that all dimensions increase until about 1000°C. This is due to the positive thermal expansion of the materials. Beginning at 1000°C shrinkage of the dimensions can be observed. The exact starting temperature, in other words the onset temperature, is different for each prototype and thus can be shifted with the exact layer construction.

For the pure PTC prototype, displayed with a black solid line, the shrinkage occurs at 1100°C and uniformly shrinks further to a total shrinkage value of about -18,70%. Only one small delay at 1270°C and about -4,2% shrinkage can be seen during the uniform shrinkage process. Interestingly this delay can be seen for all materials at similar shrinkage values but different temperatures.

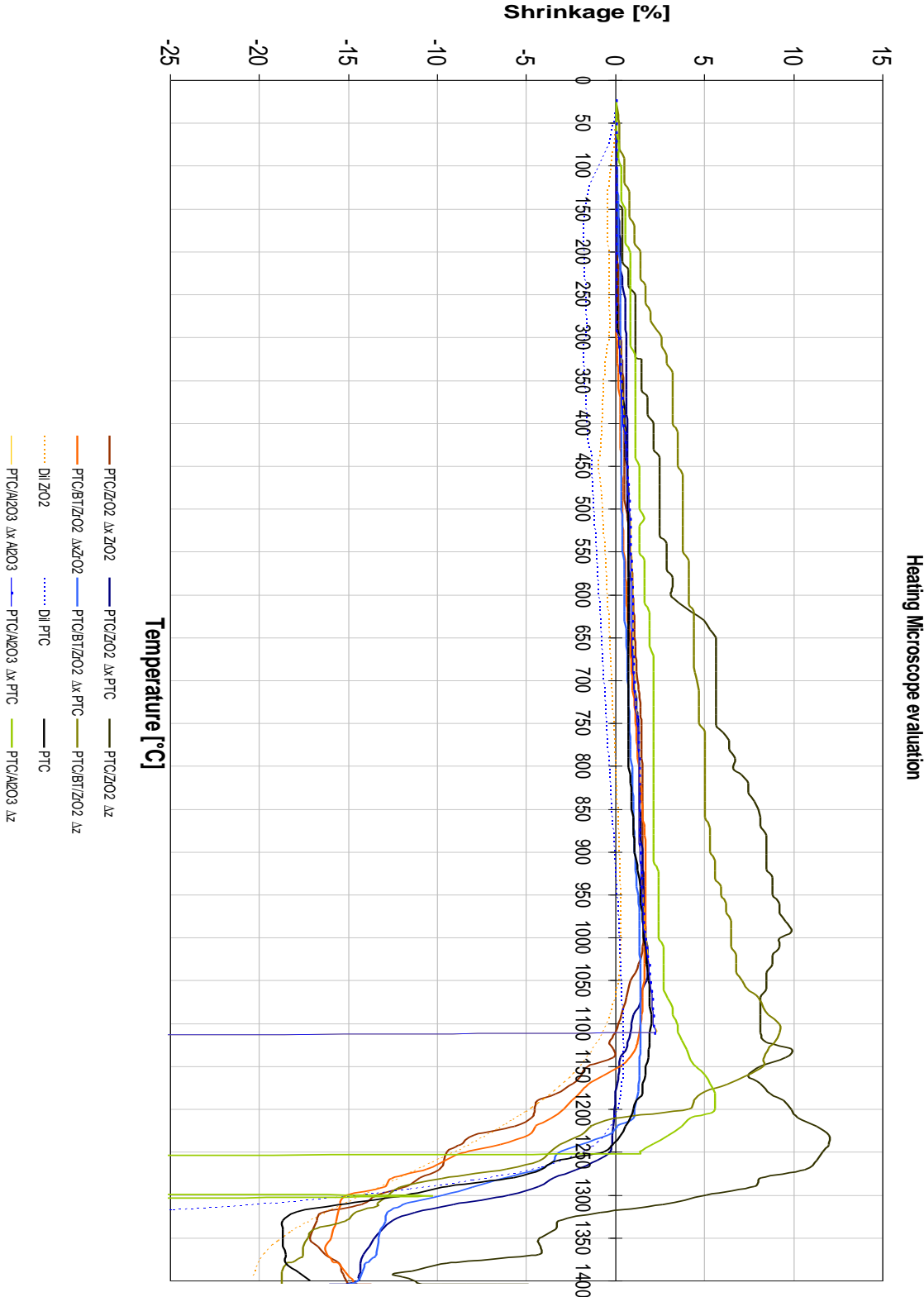
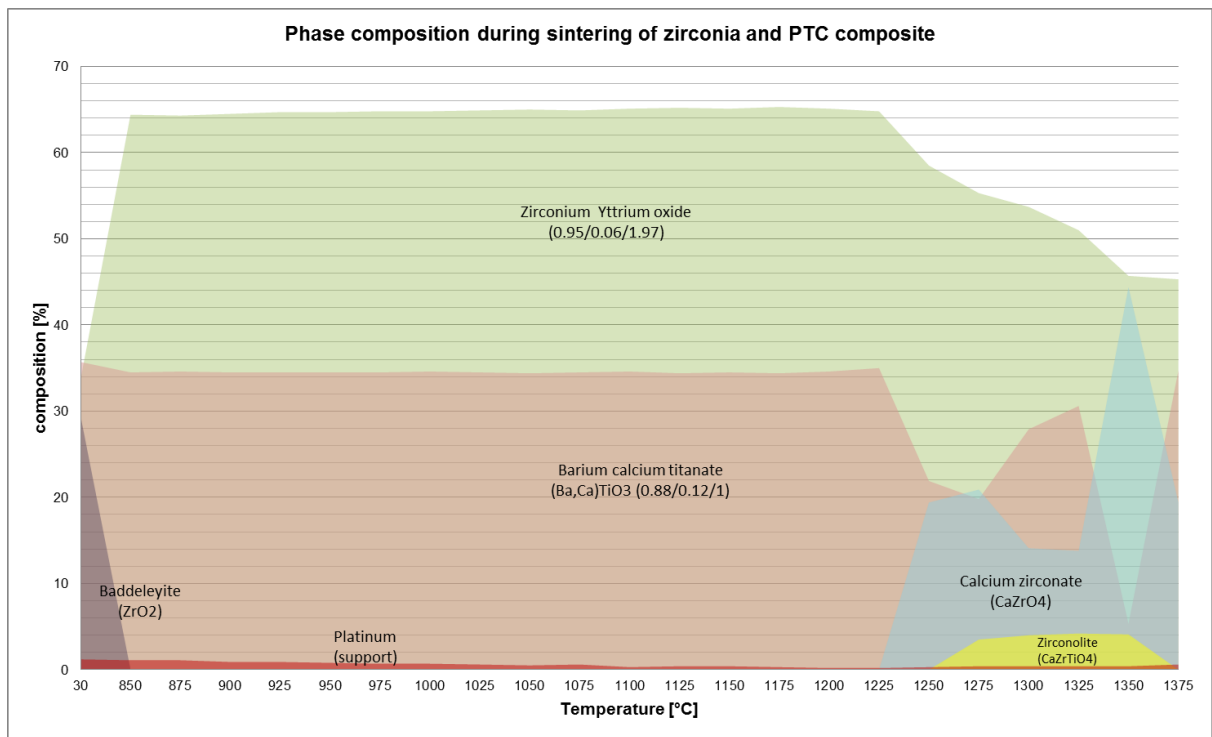


Figure 92: heating microscope evaluation

4.5.2 High temperature x-ray diffraction analysis (HT-XRD)

In order to investigate the chemical interactions between the ceramic materials during the sintering process a high temperature x-ray diffraction analysis has been conducted. For this the prototypes have been heated up with 10K/min up to 1400°C, dwelled for 30 minutes and cooled down. Starting and ending at 850°C every 25°C an x-ray diffraction pattern has been recorded during the sintering process.



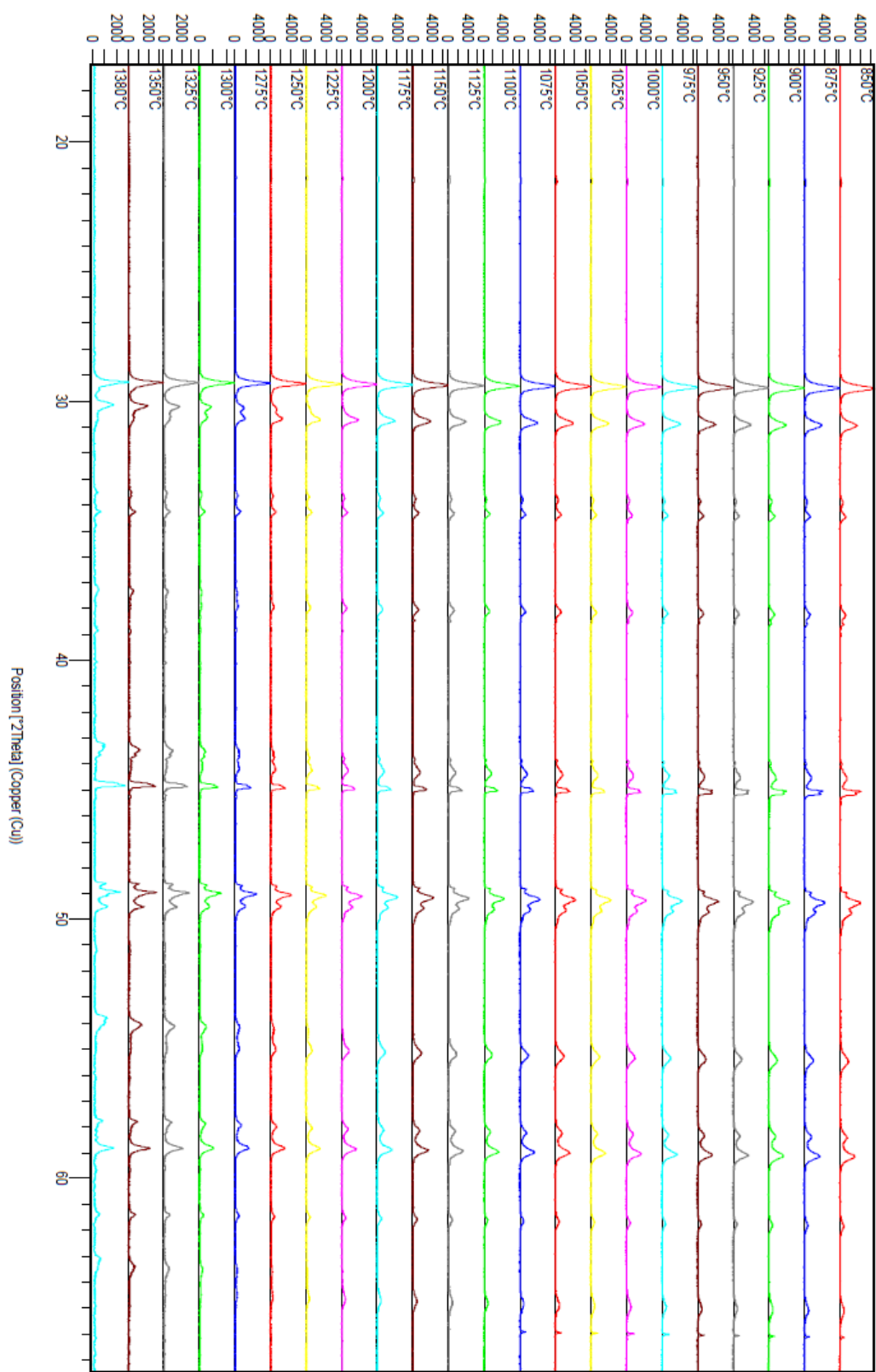


Figure 94: X-ray diffraction patterns during heating of zirconia and PTC composite

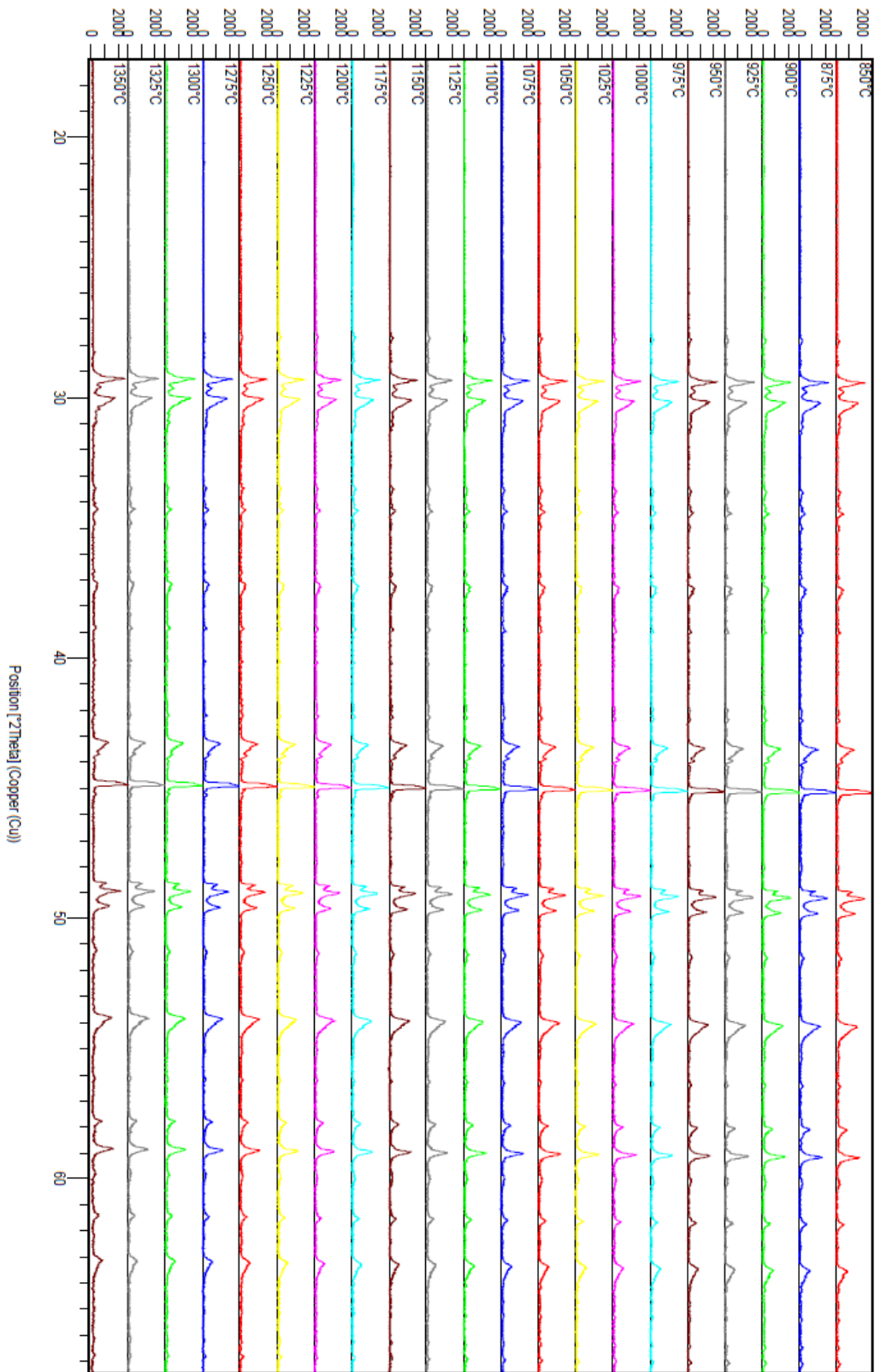


Figure 95: X-ray diffraction patterns during cooling of zirconia and PTC composite

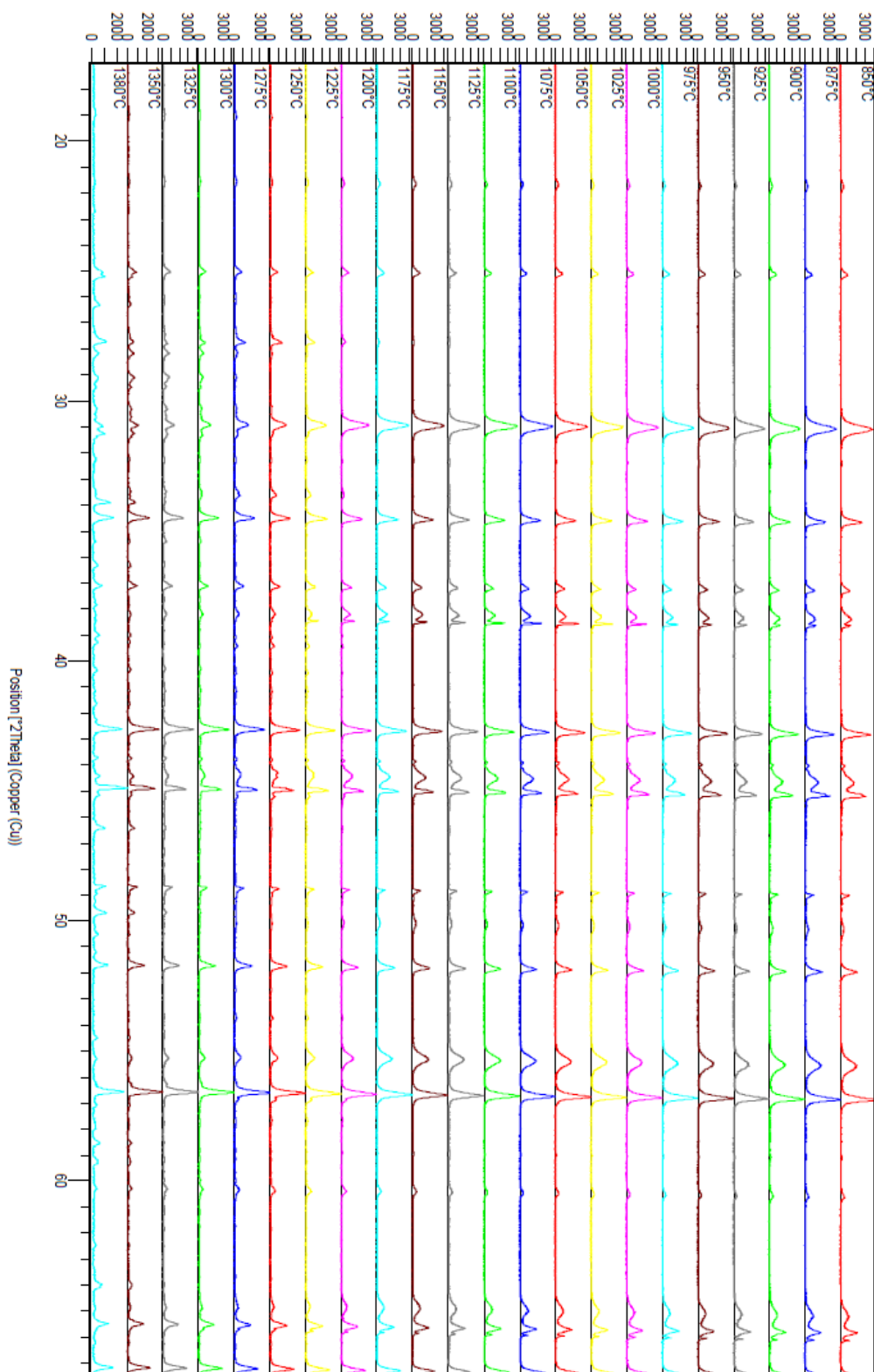


Figure 96: X-ray diffraction patterns during heating of alumina and PTC composite

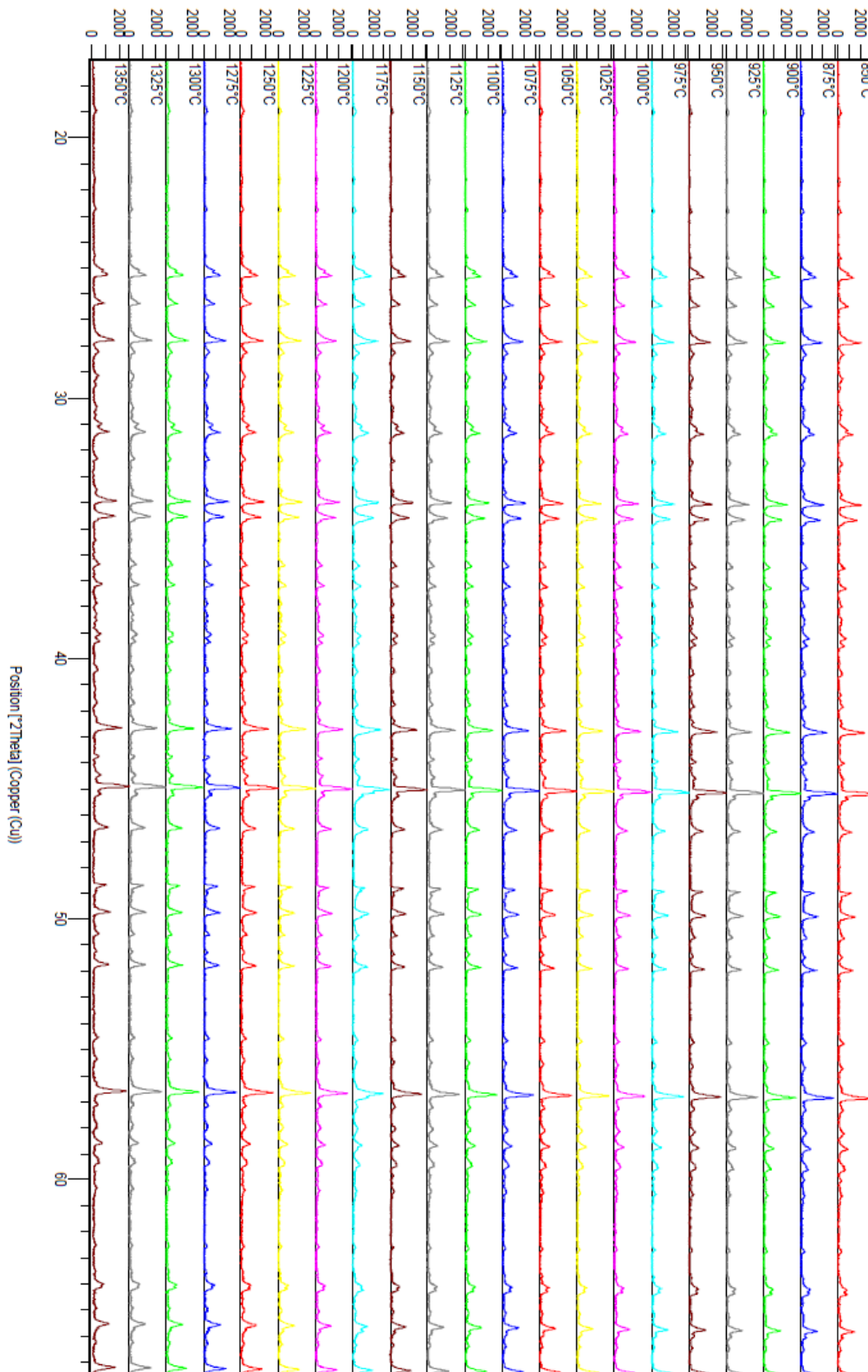


Figure 97: X-ray diffraction patterns during cooling of alumina and PTC composite

5 Discussion of results

5.1 Material development

Within this doctoral thesis the barium titanate rich PTC mass A, yttria stabilized zirconia (YSZ) and aluminium oxide (Al_2O_3) have been investigated.

First the ceramic powders have been characterized according to grain size distribution and specific surface area. With normal powder processing of the PTC mass A, used at EPCOS OHG, a grain size distribution with a d_{50} of 2.5 μm and a specific surface area of 3.48 m^2/g has been produced. The YSZ powder possesses a d_{50} of 0.7 μm and a specific surface area of 16.3 m^2/g . The barium titanate powder has a medium grain size of 0.7 μm and a specific surface area of 11.2 m^2/g . The Al_2O_3 powder has a medium grain size of 0.7 μm and a specific surface area of 11.2 m^2/g .

Furthermore the electrical properties of the sintered PTC mass A as well as the mechanical strength and porosity values for the sintered zirconia have been evaluated. As electrical criteria particularly the specific electrical resistance, the slope of the resistance by temperature curve and the reference temperature have been determined with the help of statistical investigations. On the bases of the norm sintering regime the sintering temperature has been varied from 1360 to 1400°C and the dwell time has been varied from 20 to 80 minutes. Within the investigated sintering interval the reference temperature is very stable at about 125°C and shifts only for 3 K to 122°C with the lowest sintering temperature of 1360°C. The highest specific electrical resistance of 2200 $\Omega\cdot\text{cm}$ has been measured with a sinter temperature of 1360°C. With increasing sinter temperature as well as a short dwell time the specific electrical resistance can be lowered to 20 $\Omega\cdot\text{cm}$. The slope of the R-T-curve varies from 35.2 to a maximum of 75.4 %/K with longer dwell times. All in all the PTC mass A shows a low specific electrical resistance and a suitable R-T-curve.

The yttrium stabilized zirconia showed within the investigated sintering range bending tensile strength values from 560 to 710 MPa, a high bulk density of 5.7 g/cm^3 and very low open porosities of lower than 0.5 %. Altogether the YSZ showed high mechanical strength values and a very dense structure.

Based on the described investigations the optimal sintering regime for the material combination has been defined. The optimal sintering regime consists of a sintering temperature of 1400°C, a dwell time of 30 minutes and a cooling gradient of about 6 K/min. The sintering regime is characterized by high mechanical strength values of the zirconia and appropriate electrical characteristics of the PTC mass A.

In general a stable material composite can be achieved by harmonizing the thermal expansion and shrinkage. Dilatometry measurements have been carried out to determine the ceramics' shrinkages and thermal expansions. The measurement of the shrinkage of the pressed parts has shown that the shrinkages are very similar and reach up to 2% at 1200°C. A further harmonization has been achieved by adjusting the ceramics' particle characteristics such as grain size distribution as well as the binder content.

The thermal expansion measurement of the PTC revealed a change in the thermal expansion coefficient at 130°C, which compares to the Curie temperature. The PTC mass contracts until the Curie temperature is reached, then the crystal lattice transforms, which results in a change in the thermal expansion coefficient. Above the Curie temperature the linear thermal expansion coefficient is comparatively steady and can be determined to $7.70 \cdot 10^{-6}$ K. The thermal expansion coefficient of the YSZ has been determined to $5.26 \cdot 10^{-6}$ K. Thus an existing difference in the thermal expansion of $2.44 \cdot 10^{-6}$ K has to be accomplished with intermediate layers. According to operating experience of the multilayer department at EPCOS OHG a firm interconnection of different ceramics can only be achieved with a difference in the thermal expansion no higher than $1 \cdot 10^{-6}$ K. Taking this into account at least two better three intermediate layers are required to achieve a stable material composition of PTC and YSZ. Of course the interconnection of both ceramics increases even more with less difference and therefore more intermediate layers, but at the same time the complexity, thickness of the composite as well as expenditure and costs increase dramatically. Owing to these economic reasons composites of three intermediate layers have been investigated further.

Using the characterized ceramic masses slurries have been prepared according to a developed recipe. As quality criteria their rheology has been measured. The slurries showed a desirable shear-thinning behaviour. Thus the viscosity decreases with a higher shear rate. This is preferable for tape casting, since the slurry shall easily flow on the organic carrier under the doctor blade but shall then set. Based on these slurries tapes have been casted and characterized further. Dilatometry measurements of the single tapes showed that shrinkage and thermal expansion of the individual ceramics have been harmonized.

5.2 Prototypes

Based on the results of the conducted material development three different prototypes have been produced to further investigate the material combination. Using multilayer pressing prototypes based on yttrium stabilized zirconia (YSZ) have been produced. Composites have also been stacked using the developed ceramic tapes based on YSZ and Al_2O_3 .

The respective production steps have been adjusted for each prototype - starting with the powder processing such as grinding and spray drying.

Tape casted prototypes based on YSZ showed a characteristic Weibull strength of 400 MPa and a Weibull module of 16, when the barium titanate layer is on top during measurement. With the zirconia layer on top a 3 point bending strength of 88.5 MPa and a Weibull module of 9.6 has been measured. The latter compares to the three point bending tensile strength of a monolithic PTC of about 100 MPa. The direction dependency of the mechanical strength has been revealed for both kind of tape casted prototypes and can be explained as follows. The strength of a composite is a resulting strength of the single materials. Depending on the part's alignment during testing one material is exposed to a higher bending force. As barium titanate has a much lower bending strength than zirconia it will result in different bending tensile strength values. The specific electrical resistance of the tape casted prototypes based on YSZ could be determined to a lowest of 5324 Ωcm . Furthermore a temperature coefficient of utmost 26 %/K and a reference temperature of 120°C have been achieved.

All in all the manufactured prototypes confirmed the harmonization of the different materials and featured both high mechanical strength values and appropriate PTC characteristics.

6 Conclusion and prospect

The main aim of this thesis has been the development of a ceramic system based on a structural ceramic with a high mechanical strength and a good chemical consistency and an electro ceramic with a self-levelling of the electrical resistance. For this composite material a barium titanate rich mass with a reference temperature of 120°C and a specific resistance of 100 Ωcm (PTC mass A) has been selected and as structural ceramic an yttria stabilized zirconia and alumina have been chosen. First the ceramic powders have been characterized and their electrical and mechanical properties after processing have been determined with the help of statistical investigations. Based on the results the optimal sintering regime for the composite material has been defined.

Various tools of Six Sigma have been applied to analyze the material development according to different aspects. Quality criteria for the composite material such as freedom from defects, a harmonized shrinkage and thermal expansion and a concurrent sinterability have been determined. Also possible causes of defects have been identified and described. In general a stable material combination can be achieved by harmonizing the thermal expansion and shrinkage. The latter has been achieved by adapting the materials' particle characteristics such as the grain size distribution. The different thermal expansion coefficients of barium titanate and zirconia have been harmonized by means of intermediate layers composed of molecular portions of both ceramics.

The accomplished material harmonization has been confirmed with tape casted prototypes. The prototypes featured a high mechanical strength as well as appropriate PTC characteristics. A firm connection of the composites' layers has been supported by a structural analysis. Furthermore a diffusion of zirconium atoms into the barium titanate layer and a diffusion of barium and titanate atoms into the zirconia layer have been revealed.

7 Index

7.1 Index of sources

- [All08] Allmann, R.; Röntgenpulverdiffraktometrie: Rechnergestützte Auswertung, Phasenanalyse und Strukturbestimmung; 2008
- [Arb07] Arburg GmbH & Co. KG; Produktinformation Anwendungskompetenz in der Spritzgießtechnik – Innovative Technologien konsequent nutzen; Lossburg; 2007
- [Bel07] Bellaform Extrusionstechnik GmbH; Prospekt; Bellaform-Scherwalzen BSW; Ingelheim; 2007.
- [Dan79] Daniels. J.; Härdtl. K. H.; Wernicke. R.; Der PTC-Effekt von BaTiO₃; Philips Technische Rundschau; 38. Jahrgang; 1979
- [DIN06] DIN-EN 843: Hochleistungskeramik - Mechanische Eigenschaften monolithischer Keramik bei Raumtemperatur; 2006
- [DIN76] DIN 51045: Bestimmung der Längenänderung fester Körper unter Wärmeinwirkung, 1976
- [DIN85] DIN 51056: Prüfung keramischer Roh- und Werkstoffe; Bestimmung der Wasseraufnahme und offenen Porosität, 1985
- [Epc07] EPCOS Arbeitsanweisung Fehlermöglichkeits- und Einfluss-Analyse (FMEA); Keramische Bauelemente, 2007
- [Epc08] Kirsten, L.; Method for the production of a PTC Component; Patent: EP20030747078; EPCOS AG; 02.07.2008
- [Epc09] EPCOS Data Book 2009 PTC Thermistors; published by EPCOS AG; Corporate Center; 2008
- [Gab01] Gablenz, S.; Sprühtrocknung und Sprühydrolyse - neue Methoden zur Herstellung von Metalloxiden und zur Modifizierung von BaTiO₃; Dissertation Martin-Luther-Universität; 2001; Halle-Wittenberg
- [Gau00] Gauckler, Prof. Dr. L. J.; Ingenieurkeramik II Herstellung von

-
- Keramik; Band 2; ETH Zürich Nichtmetallische Werkstoffe; 2000
- [Gau01] Gauckler, Prof. Dr. L. J.; Ingenieurkeramik III Funktionskeramik; ETH Zürich Nichtmetallische Werkstoffe; 2001
- [Haa60] Haase, Dr. phil. nat. T.; Keramik; VEB Deutscher Verlag der Wissenschaften; Berlin; 1960
- [Har61] Harrison, L.G.; Trans. Faraday Soc. 57, 1191; 1961
- [Har98] Hari,N.S.; Kutty,T.R.N; Effect of Secondary-Phase Segregation on the Positive Temperature Coefficient in Resistance Characteristics of n-BaTiO₃ Ceramics; J. Mater. Sci. 33, 3275–84; 1998
- [Hey61] Heywang, W.; Bariumtitanat als Sperrschichtableiter; Pergamon Press Vol. 3; 1961
- [Hey71] Heywang, W.; Semiconducting Barium Titanate; Journal of Materials Science 6; 1971
- [Kai88] Kainz, Gerald; Kaltleiter: Technik - Funktion und Anwendung; Siemens; 1988
- [Ker06] Keramische Zeitschrift 6/06 November-Dezember; 58.Jahrgang; DVS Verlag; Düsseldorf.
- [Kra88] Krause, E.; Berger. I.; Plaul. T.; Schulle. W.; Technologie der Keramik; Band 2 Mechanische Prozesse; VEB Verlag für Bauwesen; Berlin; 1988
- [Kol01] Kollenberg, W.; M. v. Witzleben; Keramikpulver spritzgießen – Anforderungen und Voraussetzungen für Kunststoffverarbeiter; Kunststoffe; 2001
- [Kol04] Kollenberg, W.; Technische Keramik, Grundlagen, Werkstoffe, Verfahrenstechnik; Vulkan-Verlag; Essen; 2004
- [Meh07] Mehrer, H.; Diffusion in Solids; Springer; 2007
- [Mou03] Moulson, A.J.; Herbert, J. M.; Electroceramics Materials Properties Applications; Wiley; New York; 2003
- [Pap01] Papula, L.; Mathematik für Ingenieure und Naturwissenschaftler; Band 3; Vieweg Verlag; 4. verbesserte Auflage; 2001

- [Pet90] Petzold, Armin; Ulbricht, Joachim; Aluminiumoxid; Deutscher Verlag für Grundstoffindustrie: Leipzig; 1990
- [Qui98] Quirnbach, S.; Schwartz, S.; Keramischer Spritzguß (CIM): Potentielle Fertigungstechnologie in existierenden und neuen Anwendungsbereichen; Cfi/Ber; DKG 75 ; No.1/2; 1988
- [Ree94] Reed, J. S.; Principles of ceramics processing; Wiley; 1994
- [Ruf29] Ruff, O.; Ebert, F.; Stephen, E.; Contributions to the ceramics of highly refractory materials: System Zirconia-lime; Z. anorg. Allg. Chemie; Vol. 180; 1929
- [Sal82] Salmang, H.; Scholze, H.; Keramik Band 1 – Allgemeine Grundlagen und wichtige Eigenschaften; 6. Auflage Springer Verlag; Berlin; 1982
- [Sal83] Salmang, H.; Scholze, H.; Keramik Band 2 – Keramische Werkstoffe; 6. Auflage; Springer Verlag; Berlin; 1983
- [Sch78] Schmelz. Dr. H.; Ruehlmann. K.; Sinterführung von Heizkaltleitern; 2.Teil. Bleiabdampf und Gefügeausbildung; Siemens; 1978
- [Sch94] Schaumburg. Hanno; Werkstoffe und Bauelemente der Elektrotechnik Keramik; B. G. Teubner; Stuttgart; 1994
- [Sei09] Seifert, T.; Optimierung der Entbinderungs- und Sinterprozesse für spritzgegossene Kaltleiterwiderstände, Studienarbeit TU Bergakademie Freiberg, 2008
- [Sei10] Seifert, T.; Material development of a multicomponent heating element based on barium titanate ceramics: diploma thesis; TU Bergakademie Freiberg, 2008
- [Ste09] Fortschritte in der PTCR-Entwicklung; TDK-EPC Corporate Material R&D; Dr. Bernhard Steinberger; Deutschlandsberg; 2009
- [Stu75] Sturhahn, H. H.; Dawihl, W.; Thamerus, G.; Anwendungsmöglichkeiten und Werkstoffeigenschaften von Zirkonoxid-Sintererzeugnissen, DKG 52; 1975
- [Spr11] Sprengel, W.; composition formation and diffusion in materials;

- lecture notes; 2011
- [Tes09] High Performance Varactor; TDK-EPC Corporate Material R&D; Dr. Andrea Testino; Deutschlandsberg; 2009
- [Teq06] TEQ Technologietransfer & Qualitätssicherung GmbH; Trainingsprogramm Six Sigma Black Belt; Chemnitz; 2006
- [Wap06] Wappis. Johann; Jung. Berndt; Taschenbuch Null-Fehler-Management; Umsetzung von Six Sigma; Carl Hanser Verlag München; Wien; 2006
- [Van80] Van der Zwan, J.; Siskens, C.A.M; The compaction and mechanical properties of some spray-dried ceramic materials, Science of Ceramic 10; 1980
- [Wag00] Wagner, M.; Stiegelschmitt, A.; Roosen, A.; Mehrlagen-Foliengießen zur direkten Herstellung geschichteter keramischer Verbundstrukturen und Untersuchung ihrer mechanischen Eigenschaften; Keramische Zeitschrift 52; 2000

7.2 Index of figures

Figure 1: BaO-TiO ₂ system according to Roy und Osborn [Haa60].....	11
Figure 2: process map of the mix-oxide-method.....	11
Figure 3: BaCO ₃ -TiO ₂ -system (left), BaTiO ₃ genesis according to Niepce und Mutin (right).....	12
Figure 4: oblique projection of Barium titanate's perovskite structure [Gab01].....	13
Figure 5: change in modification of barium titanate	13
Figure 6: displacement of the Ti ⁴⁺ -Ion in tetragonal modification [Gab01]	14
Figure 7: hysteresis of BaTiO ₃ : above T _c (left) and below T _c (right).....	14
Figure 8: composition of the crystal's overall resistance	15
Figure 9: Resistance-temperature-curve of a PTC	16
Figure 10: Adaption of reference temperature by doping with strontium or lead [Gau01]	18
Figure 11: Kirkendall effect [Spr11].....	27

Figure 12: Harrison's type A,B and C diffusion regimes in a polycrystal [Meh07].....	28
Figure 13: process steps of dry pressing	30
Figure 14: tape casting line [Ree94]	32
Figure 15: SEM analysis of PTC powder (left: norm processed, right: grinded)	35
Figure 16: ρ_{25} of PTC mass A in dependency of different norm sintering regimes.....	37
Figure 17: R-T-curve of PTC mass A sintered with N 1400/50/6	38
Figure 18: regression analysis of the specific electrical resistance of PTC mass A.....	39
Figure 19: regression analysis of the slope of the R-T-curve of PTC mass A	39
Figure 20: shrinkage measurement of PTC mass A	40
Figure 21: thermal expansion measurement of PTC mass A	41
Figure 22: SEM analysis of zirconia powder.....	42
Figure 23: mechanical strength of YSZ in dependency of different norm sintering regimes	43
Figure 24: bulk density of YSZ in dependency of different norm sintering regimes.....	45
Figure 25: open porosity of YSZ in dependency of different norm sintering regimes.....	45
Figure 26: regression analysis of the mechanical strength of YSZ	47
Figure 27: regression analysis of the green density of YSZ.....	48
Figure 28: regression analysis of the open porosity of YSZ.....	48
Figure 29: shrinkage measurement of PTC mass A and YSZ	49
Figure 30: thermal expansion measurement of PTC mass A and YSZ.....	50
Figure 31: SEM picture of barium titanate powder (left: original, right: grinded to 0.7 μ m)	51
Figure 32: viscosity-shear rate diagram of the YSZ slurry	54

Figure 33: sintered disks composed of YSZ and PTC (left: PTC mass A and right: mass B).....	57
Figure 34: sintered disks composed of Al_2O_3 and PTC (left: PTC mass A and right: mass B).....	57
Figure 35: Resistance over temperature curve of PTC mass A+YSZ.....	60
Figure 36: Resistance over temperature curve of PTC mass A+ Al_2O_3	60
Figure 37: Resistance over temperature curve of PTC mass B+YSZ.....	61
Figure 38: Resistance over temperature curve of PTC mass B+ Al_2O_3	61
Figure 39: Weibull diagram of mechanical strength values of pressed powder mixtures	63
Figure 40: Comparison of mechanical strength values of pressed powder mixtures	Fehler! Textmarke nicht definiert.
Figure 41: micrographs of PTC mass A and 20 mol% YSZ	64
Figure 42: micrographs of PTC mass A and 20 mol% Al_2O_3	65
Figure 43: micrographs of PTC mass B and 20 mol% YSZ	65
Figure 44: micrographs of PTC mass B and 20 mol% Al_2O_3	65
Figure 45: SEM analysis of PTC mass A + 20mol% YSZ	67
Figure 46: SEM analysis of PTC mass A + 20mol% Al_2O_3	68
Figure 47: SEM analysis of PTC mass B + 20mol% YSZ	69
Figure 48: SEM analysis of PTC mass B + 20mol% Al_2O_3	70
Figure 49: X-ray diffraction pattern of PTC mass A	71
Figure 50: X-ray diffraction pattern of PTC mass B	72
Figure 51: X-ray diffraction pattern of PTC mass A and YSZ.....	73
Figure 52: X-ray diffraction pattern of PTC mass A and 20mol% YSZ.....	73
Figure 53: X-ray diffraction pattern of PTC mass B and YSZ.....	74
Figure 54: X-ray diffraction pattern of PTC mass B and 20mol% YSZ.....	75
Figure 55: X-ray diffraction pattern of PTC mass A and Al_2O_3	75
Figure 56: X-ray diffraction pattern of PTC mass A and 20mol% Al_2O_3	76
Figure 57: X-ray diffraction pattern of PTC mass B and Al_2O_3	77
Figure 58: X-ray diffraction pattern of PTC mass B and 20mol% Al_2O_3	77

Figure 59: possible electrode layouts for the demonstrator	79
Figure 60: demonstrator with developed finger electrode layout.....	79
Figure 61: resistance over temperature curve of demonstrator	80
Figure 62: current and temperature measured with k-type thermocouple on PTC and Al ₂ O ₃ side as a function of applied voltage	81
Figure 63: developed calorimetric measuring device.....	83
Figure 64: thermo camera recording of the swichting-on of the demonstrator (t~0s)	84
Figure 65: thermo camera recording of the swichting-on of the demonstrator (t~15s)	84
Figure 66: tape assembly with three intermediate layers.....	85
Figure 67: tape casted prototype based on YSZ (left: green and right: sintered).....	86
Figure 68: optical microscopy of prototype based on YSZ(zirconia left, PTC right)	88
Figure 69: SEM analysis with marked line scan of YSZ(zirconia left, PTC right)	88
Figure 70: EDX line scan of tape casted prototype based on YSZ	88
Figure 71: Weibull diagram of bending tensile strength of tape casted prototypes based on YSZ	90
Figure 72: exemplary R(T) curve of tape casted prototype based on YSZ	92
Figure 73: exemplary image analysis of the PTC/ZrO ₂ prototype (left: 500 and right: 1300°C).....	107

7.3 Index of tables

Table 1: molecular proportions of the cations of PTC masses.....	34
Table 2: Norm sintering regime.....	36
Table 3: composition of yttria stabilized zirconia Melox3Y	41
Table 4: Weibull parameters of YSZ in dependency of the sintering temperature	43

Table 5: Weibull parameters of YSZ in dependency of different norm sintering regimes	46
Table 6: composition of aluminium oxide	51
Table 7: slurry composition of PTC mass A, YSZ and intermediate layers	52
Table 8: slurry composition of PTC mass A, Al ₂ O ₃ and intermediate layers ..	53
Table 9: recorded viscosity values for the YSZ slurry	53
Table 10: experimental design of pressed powder mixtures	55
Table 11: Weibull strength and Weibull modulus of pressed powder mixtures	63
Table 12: measured resistance over temperature values	80
Table 13: Measured electric and calorimetric characteristics.....	82
Table 14: Temperature dependent density and specific heat capacity values	83
Table 15: debinding regime	85
Table 16: Adapted sintering regime	86
Table 17: calculated mechanical strength of tape casted prototypes based on YSZ.....	90
Table 18: characteristic Weibull strength and Weibull module of tape casted prototypes based on YSZ.....	90
Table 19: electrical measurements of tape casted prototypes based on YSZ.....	92

7.4 Index of equations

Equation 1: production of BaTiO ₃	12
Equation 2: Curie Weiss law	15
Equation 3: calculation of reference resistance	17
Equation 4: calculation of the temperature coefficient α	17
Equation 5: production of ZrO ₂	20
Equation 6: Bayer process.....	21
Equation 7: calculation of the linear thermal expansion coefficient α	23

Equation 8: calculation of the volume thermal expansion coefficient β	23
Equation 9: calculation of the linear shrinkage.....	24
Equation 10: calculation of the volume shrinkage.....	25
Equation 11: Fick's first law	25
Equation 11: arhenius relation of diffusion.....	26
Equation 11: conditions for type A kinetics	28
Equation 12: conditions for type B kinetics	28
Equation 13: conditions for type C kinetics	28
Equation 14: calculation of the specific electrical resistance.....	36
Equation 15: regression equation for the specific electrical resistance of PTC mass A.....	39
Equation 16: regression equation for the slope of the R-T-curve of PTC mass A.....	40
Equation 17: calculation of the bending strength	43
Equation 18: calculation of the bulk density	44
Equation 19: calculation of the open porosity	44
Equation 20: calculation of the water absorption	44
Equation 21: calculation of the heat capacity.....	82
Equation 22: calculation of the arc length	107

7.5 Index of appendix

A. 1: grain size distribution of normally processed PTC mass A.....	132
A. 2: grain size distribution of granulated PTC mass A.....	133
A. 3: Pre-investigations on specific electrical resistance of PTC mass A (sintering temperatures 1300 ... 1350°C).....	134
A. 4: Pre-investigations on specific electrical resistance of PTC mass A (sintering temperatures 1360 ... 1400°C).....	135
A. 5: Investigations on specific electrical resistance of PTC mass A (runs 1 to 6)	136
A. 6: Investigations on specific electrical resistance of PTC mass A (runs 7 to 12)	137
A. 7: Investigations on specific electrical resistance of PTC mass A (runs 13 to 17)	138
A. 8: Investigations on the slope of the R-T-curve of PTC mass A (runs 1 to 6)	139
A. 9: Investigations on the slope of the R-T-curve of PTC mass A (runs 7 to 12)	140
A. 10: Investigations on the slope of the R-T-curve of PTC mass A (runs 13 to 17)	141
A. 11: grain size distribution of YSZ.....	142
A. 12: Pre-investigations on mechanical strength of YSZ	143
A. 13: Investigations on mechanical strength of YSZ.....	144
A. 14: Pre-investigations on porosity of YSZ.....	145
A. 15: Investigations on porosity of YSZ (runs 1 to 6).....	146
A. 16: Investigations on porosity of YSZ (runs 7 to 12).....	147
A. 17: Investigations on porosity of YSZ (runs 13 to 17).....	148
A. 18: Mechanical strength measurements of powder mixtures - PTC mass A+YSZ.....	150
A. 19: Mechanical strength measurements of powder mixtures - PTC mass A+Al ₂ O ₃	151

A. 20: Mechanical strength measurements of powder mixtures - PTC mass B+YSZ.....	152
A. 21: Mechanical strength measurements of powder mixtures - PTC mass B+Al ₂ O ₃	153
A. 22: Mechanical strength measurements of prototypes	154
A. 23: R(T) measurement of prototypes based on YSZ	155
A. 24: High temperature microscopy of thin PTC prototype (25-200°C)	156
A. 25: High temperature microscopy of thin PTC prototype (210-390°C)	157
A. 26: High temperature microscopy of thin PTC prototype (400-580°C)	158
A. 27: High temperature microscopy of thin PTC prototype (590-700°C)	159
A. 28: High temperature microscopy of thin PTC prototype (700-870°C)	160
A. 29: High temperature microscopy of thin PTC prototype (880-1040°C)	161
A. 30: High temperature microscopy of thin PTC prototype (1050-1270°C)	162
A. 31: High temperature microscopy of thin PTC prototype (1280-1400°C)	163
A. 32: High temperature microscopy of PTC/ZrO ₂ prototype (35-270°C)	164
A. 33: High temperature microscopy of PTC/ZrO ₂ prototype (280-500°C) ..	165
A. 34: High temperature microscopy of PTC/ZrO ₂ prototype (510-740°C) ..	166
A. 35: High temperature microscopy of PTC/ZrO ₂ prototype (750-980°C) ..	167
A. 36: High temperature microscopy of PTC/ZrO ₂ prototype (990-1220°C)	168
A. 37: High temperature microscopy of PTC/ZrO ₂ prototype (1230- 1400°C)	169
A. 38: High temperature microscopy of PTC/BT/ZrO ₂ prototype (25- 270°C)	170
A. 39: High temperature microscopy of PTC/BT/ZrO ₂ prototype (280- 510°C)	171
A. 40: High temperature microscopy of PTC/BT/ZrO ₂ prototype (520- 750°C)	172
A. 41: High temperature microscopy of PTC/BT/ZrO ₂ prototype (760- 990°C)	173

A. 42: High temperature microscopy of PTC/BT/ZrO ₂ prototype (1000-1220°C)	174
A. 43: High temperature microscopy of PTC/BT/ZrO ₂ prototype (1230-1400°C)	175
A. 44: High temperature microscopy of PTC/Al ₂ O ₃ prototype (25-270°C) ..	176
A. 45: High temperature microscopy of PTC/Al ₂ O ₃ prototype (280-510°C)	177
A. 46: High temperature microscopy of PTC/Al ₂ O ₃ prototype (520-750°C)	178
A. 47: High temperature microscopy of PTC/Al ₂ O ₃ prototype (760-990°C)	179
A. 48: High temperature microscopy of PTC/Al ₂ O ₃ prototype (1000-1220°C)	180
A. 49: High temperature microscopy of PTC/Al ₂ O ₃ prototype (1230-1380°C)	181
A. 50: High temperature microscopy of PTC/Al ₂ O ₃ prototype (1280-1400°C)	182
A. 51:heating microscope analysis of PTC/ZrO ₂ prototype (35-270°C).....	182
A. 52:heating microscope analysis of PTC/ZrO ₂ prototype (280-690°C).....	183
A. 53:heating microscope analysis of PTC/ZrO ₂ prototype (700-1122°C)...	184
A. 54:heating microscope analysis of PTC/ZrO ₂ prototype (1130-1400°C).	185
A. 55:heating microscope analysis of PTC/BT/ZrO ₂ prototype (25-460°C) .	186
A. 56:heating microscope analysis of PTC/BT/ZrO ₂ prototype (470-890°C)	187
A. 57:heating microscope analysis of PTC/BT/ZrO ₂ prototype (900-1310°C)	188
A. 58:heating microscope analysis of PTC/BT/ZrO ₂ prototype (1310-1400°C)	189
A. 59:heating microscope analysis of thin PTC prototype (25-230°C)	189
A. 60:heating microscope analysis of thin PTC prototype (240-660°C)	190
A. 61:heating microscope analysis of thin PTC prototype (670-1090°C)	191
A. 62:heating microscope analysis of thin PTC prototype (1100-1400°C) ...	192

A Appendix

A.1 Material characterisation



Result Analysis Report

Sample Name: PTC mass A
Sample Source & type: KPP PT = SPC
Sample bulk lot ref:

SOP Name: _Standard
Measured by: Fertigung
Result Source: Averaged

Particle Name: Fraunhofer
Particle RI: 0.000
Dispersant Name: Water

Accessory Name: Hydro 2000G (A)
Absorption: 0
Dispersant RI: 1.330

Analysis model: General purpose
Size range: 0.020 to 2000.000 μm
Weighted Residual: 0.220 %

Sensitivity: Enhanced
Obscuration: 17.48 %
Result Emulation: Off

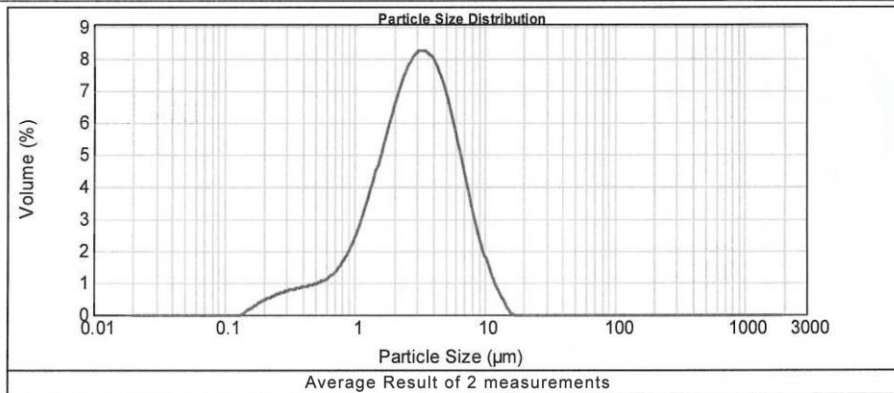
Concentration: 0.0047 %Vol
Specific Surface Area: 3.48 m^2/g

Span : 2.060
Surface Weighted Mean D[3,2]: 1.724 μm

Uniformity: 0.638
Vol. Weighted Mean D[4,3]: 3.525 μm

Result units: Volume

d(0.1): 0.888 μm d(0.5): 2.941 μm d(0.9): 6.945 μm



Size (μm)	Volume In %	Size (μm)	Volume In %	Size (μm)	Volume In %	Size (μm)	Volume In %	Size (μm)	Volume In %	Size (μm)	Volume In %
0.010	0.00	0.105	0.00	1.093	2.85	11.482	0.77	120.226	0.00	1258.925	0.00
0.011	0.00	0.120	0.00	1.259	3.58	13.183	0.37	138.038	0.00	1445.440	0.00
0.013	0.00	0.136	0.00	1.445	4.37	15.136	0.03	158.489	0.00	1659.587	0.00
0.015	0.00	0.155	0.10	1.660	5.19	17.378	0.00	181.970	0.00	1905.461	0.00
0.017	0.00	0.182	0.23	1.905	5.97	19.953	0.00	208.930	0.00	2187.762	0.00
0.020	0.00	0.209	0.38	2.188	6.64	22.909	0.00	239.883	0.00	2511.886	0.00
0.023	0.00	0.240	0.49	2.512	7.14	26.303	0.00	275.423	0.00	2884.032	0.00
0.026	0.00	0.275	0.67	2.884	7.42	30.200	0.00	316.228	0.00	3311.311	0.00
0.030	0.00	0.316	0.73	3.311	7.44	34.674	0.00	363.078	0.00	3801.894	0.00
0.035	0.00	0.363	0.78	3.802	7.18	39.811	0.00	416.869	0.00	4365.158	0.00
0.040	0.00	0.417	0.82	4.365	6.64	45.709	0.00	478.630	0.00	5011.872	0.00
0.046	0.00	0.479	0.89	5.012	5.88	52.481	0.00	549.541	0.00	5754.399	0.00
0.052	0.00	0.550	0.99	5.754	4.95	60.256	0.00	630.957	0.00	6606.934	0.00
0.060	0.00	0.631	1.15	6.607	3.96	69.183	0.00	724.436	0.00	7585.776	0.00
0.069	0.00	0.724	1.40	7.586	2.97	79.433	0.00	831.764	0.00	8709.636	0.00
0.079	0.00	0.832	1.76	8.710	2.10	91.201	0.00	954.993	0.00	10000.000	0.00
0.091	0.00	0.955	2.25	10.000	1.35	104.713	0.00	1095.478	0.00		
0.105	0.00	1.096		11.482		120.226	0.00	1258.925	0.00		

A. 1: grain size distribution of normally processed PTC mass A



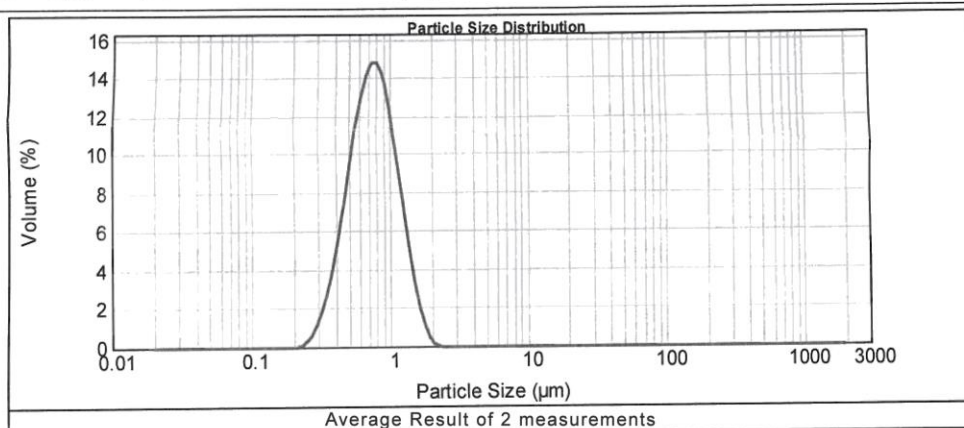
Result Analysis Report

Sample Name: PTC mass A granulated
Sample Source & type: KPP PT = SPC
Sample bulk lot ref:
SOP Name: _Standard
Measured by: Fertigung
Result Source: Averaged

Particle Name: Fraunhofer	Accessory Name: Hydro 2000G (A)	Analysis model: General purpose	Sensitivity: Enhanced
Particle RI: 0.000	Absorption: 0	Size range: 0.020 to 2000.000 um	Obscuration: 17.87 %
Dispersant Name: Water	Dispersant RI: 1.330	Weighted Residual: 2.989 %	Result Emulation: Off

Concentration: 0.0019 %Vol	Span : 1.055	Uniformity: 0.33	Result units: Volume
Specific Surface Area: 8.77 m ² /g	Surface Weighted Mean D[3,2]: 0.684 um	Vol. Weighted Mean D[4,3]: 0.798 um	

d(0.1): 0.438 um d(0.5): 0.748 um d(0.9): 1.227 um



Size (µm)	Volume In %	Size (µm)	Volume In %	Size (µm)	Volume In %	Size (µm)	Volume In %	Size (µm)	Volume In %	Size (µm)	Volume In %
0.010	0.00	0.105	0.00	1.096	7.78	11.482	0.00	120.226	0.00	1258.925	0.00
0.011	0.00	0.120	0.00	1.259	4.93	13.183	0.00	138.038	0.00	1445.440	0.00
0.013	0.00	0.138	0.00	1.445	2.61	15.136	0.00	158.489	0.00	1659.587	0.00
0.015	0.00	0.158	0.00	1.660	1.04	17.378	0.00	181.970	0.00	1905.461	0.00
0.017	0.00	0.182	0.00	1.905	0.21	19.953	0.00	208.930	0.00	2187.762	0.00
0.020	0.00	0.209	0.03	2.188	0.00	22.909	0.00	238.883	0.00	2511.886	0.00
0.023	0.00	0.240	0.40	2.512	0.00	26.303	0.00	275.423	0.00	2884.032	0.00
0.026	0.00	0.275	1.13	2.884	0.00	30.200	0.00	316.228	0.00	3311.311	0.00
0.030	0.00	0.316	2.36	3.311	0.00	34.674	0.00	363.078	0.00	3801.894	0.00
0.035	0.00	0.363	4.09	3.802	0.00	39.811	0.00	416.869	0.00	4365.158	0.00
0.040	0.00	0.417	6.30	4.365	0.00	45.709	0.00	478.630	0.00	5011.872	0.00
0.046	0.00	0.479	8.74	5.012	0.00	52.481	0.00	549.541	0.00	5754.399	0.00
0.052	0.00	0.550	11.08	5.754	0.00	60.256	0.00	630.957	0.00	6606.934	0.00
0.060	0.00	0.631	12.78	6.607	0.00	69.183	0.00	724.436	0.00	7585.776	0.00
0.069	0.00	0.724	13.38	7.596	0.00	79.433	0.00	831.764	0.00	8709.636	0.00
0.079	0.00	0.832	12.60	8.710	0.00	91.201	0.00	954.993	0.00	10000.000	0.00
0.091	0.00	0.955	10.55	10.000	0.00	104.713	0.00	1096.478	0.00		
0.105	0.00	1.096	10.55	11.482	0.00	120.226	0.00	1258.925	0.00		

A. 2: grain size distribution of granulated PTC mass A

sintering regime	Nr.	dimensions			electrical resistance		
		diameter mm	thickness mm	area mm ²	R ₂₅ Ω	ρ ₂₅ Ω*cm	ρ ₂₅ Ω*cm
N 1300/30/6	1	12,640	2,875	125,6504	6,687E+07	2,922E+08	3,081E+08
	2	12,629	2,862	125,4318	6,130E+07	2,687E+08	
	3	12,640	2,859	125,6504	5,596E+07	2,460E+08	
	4	12,636	2,853	125,5709	5,791E+07	2,549E+08	
	5	12,615	2,855	125,1539	7,800E+07	3,419E+08	
	6	12,644	2,876	125,7299	8,267E+07	3,614E+08	
	7	12,618	2,855	125,2134	5,826E+07	2,555E+08	
	8	12,653	2,872	125,9090	6,360E+07	2,788E+08	
	9	12,645	2,860	125,7498	8,557E+07	3,762E+08	
	10	12,644	2,866	125,7299	9,229E+07	4,049E+08	
N 1310/30/6	1	12,365	2,784	120,2425	-	-	-
	2	12,395	2,799	120,8267	-	-	
	3	12,361	2,794	120,1647	-	-	
	4	12,355	2,793	120,0481	-	-	
	5	12,357	2,794	120,0870	-	-	
	6	12,378	2,810	120,4955	-	-	
	7	12,367	2,785	120,2814	-	-	
	8	12,373	2,779	120,3981	-	-	
	9	12,343	2,774	119,8150	-	-	
	10	12,353	2,802	120,0092	-	-	
N 1320/30/6	1	12,172	2,739	116,5182	-	-	-
	2	12,168	2,749	116,4416	-	-	
	3	12,168	2,733	116,4416	-	-	
	4	12,176	2,748	116,5948	-	-	
	5	12,166	2,748	116,4033	-	-	
	6	12,171	2,729	116,4990	-	-	
	7	12,165	2,738	116,3842	-	-	
	8	12,162	2,744	116,3268	-	-	
	9	12,167	2,736	116,4225	-	-	
	10	12,169	2,753	116,4607	-	-	
N 1330/30/6	1	12,036	2,710	113,9289	-	-	-
	2	12,041	2,719	114,0236	-	-	
	3	12,044	2,718	114,0805	-	-	
	4	12,053	2,720	114,2510	-	-	
	5	12,045	2,722	114,0994	-	-	
	6	12,067	2,717	114,5166	-	-	
	7	12,055	2,710	114,2889	-	-	
	8	12,054	2,733	114,2700	-	-	
	9	12,045	2,721	114,0994	-	-	
	10	12,053	2,716	114,2510	-	-	
N 1340/30/6	1	11,931	2,690	111,9498	9878,000	41109,308	41057,101
	2	11,934	2,699	112,0061	11348,000	47093,205	
	3	11,955	2,694	112,4007	10172,000	42440,223	
	4	11,938	2,692	112,0812	7305,000	30414,316	
	5	11,948	2,696	112,2691	9702,000	40401,877	
	6	11,936	2,681	112,0437	6120,000	25576,550	
	7	11,933	2,694	111,9874	8921,000	37083,863	
	8	11,938	2,707	112,0812	12628,000	52285,252	
	9	11,941	2,708	112,1376	11255,000	46606,659	
	10	11,943	2,690	112,1751	11405,000	47559,755	
N 1350/30/6	1	11,954	2,685	112,3819	23,890	99,993	95,458
	2	11,918	2,704	111,7060	22,879	94,516	
	3	11,936	2,703	112,0437	22,628	93,797	
	4	11,943	2,695	112,1751	22,631	94,198	
	5	11,959	2,686	112,4759	22,019	92,204	
	6	11,936	2,697	112,0437	23,440	97,379	
	7	11,942	2,694	112,1564	22,594	94,063	
	8	11,954	2,705	112,3819	22,790	94,683	
	9	11,956	2,699	112,4195	23,120	96,300	
	10	11,938	2,696	112,0812	23,440	97,447	

A. 3: Pre-investigations on specific electrical resistance of PTC mass A (sintering temperatures 1300 ... 1350°C)

sintering regime	Nr.	dimensions			electrical resistance		
		diameter	thickness	area	R ₂₅	ρ ₂₅	ρ ₂₅
-	-	mm	mm	mm ²	Ω	Ω*cm	Ω*cm
N 1360/30/6	1	11,991	2,709	113,0786	7,360	30,722	30,903
	2	11,951	2,689	112,3255	7,763	32,428	
	3	11,973	2,682	112,7394	7,605	31,968	
	4	11,968	2,689	112,6453	7,290	30,539	
	5	11,965	2,684	112,5888	7,295	30,601	
	6	11,963	2,703	112,5512	7,289	30,351	
	7	11,964	2,701	112,5700	7,203	30,020	
	8	11,971	2,691	112,7017	7,360	30,824	
	9	11,965	2,696	112,5888	7,231	30,198	
	10	11,969	2,687	112,6641	7,483	31,376	
N 1370/30/6	1	11,968	2,689	112,6453	4,908	20,560	19,001
	2	11,980	2,691	112,8713	4,688	19,663	
	3	11,965	2,699	112,5888	4,611	19,235	
	4	11,983	2,697	112,9278	4,448	18,625	
	5	11,962	2,700	112,5323	4,289	17,876	
	6	11,968	2,689	112,6453	4,735	19,835	
	7	11,963	2,697	112,5530	4,464	18,629	
	8	11,967	2,702	112,6264	4,398	18,332	
	9	11,965	2,687	112,5888	4,456	18,671	
	10	11,974	2,706	112,7582	4,459	18,581	
N 1380/30/6	1	11,954	2,710	112,3819	4,519	18,740	18,063
	2	11,987	2,687	113,0032	4,413	18,559	
	3	11,986	2,703	112,9843	4,242	17,731	
	4	11,967	2,714	112,6264	4,258	17,670	
	5	11,972	2,700	112,7206	4,165	17,388	
	6	11,956	2,707	112,4195	4,304	17,874	
	7	11,976	2,695	112,7959	4,501	18,838	
	8	11,978	2,700	112,8336	4,437	18,542	
	9	11,973	2,717	112,7394	4,522	18,764	
	10	11,978	2,693	112,8336	3,943	16,521	
N 1390/30/6	1	11,973	2,706	112,7394	4,174	17,390	17,059
	2	11,977	2,702	112,8147	3,917	16,354	
	3	11,980	2,702	112,8713	4,151	17,340	
	4	11,992	2,697	113,0975	4,057	17,013	
	5	11,981	2,713	112,8901	4,252	17,693	
	6	11,986	2,701	112,9843	3,948	16,515	
	7	11,973	2,713	112,7394	4,286	17,811	
	8	11,976	2,714	112,7959	3,959	16,454	
	9	11,993	2,716	113,1164	3,954	16,468	
	10	11,980	2,693	112,8713	4,187	17,549	
N 1400/30/6	1	12,004	2,712	113,3240	3,691	15,423	15,555
	2	12,000	2,699	113,2484	3,792	15,911	
	3	11,993	2,708	113,1164	3,682	15,380	
	4	11,997	2,702	113,1918	3,792	15,885	
	5	11,996	2,698	113,1730	3,700	15,520	
	6	11,981	2,714	112,8901	3,684	15,324	
	7	11,977	2,713	112,8147	3,697	15,373	
	8	11,994	2,696	113,1352	3,748	15,728	
	9	11,992	2,700	113,0975	3,732	15,633	
	10	11,985	2,705	112,9655	3,680	15,368	

A. 4: Pre-investigations on specific electrical resistance of PTC mass A (sintering temperatures 1360 ... 1400°C)

sintering regime	Nr.	measurement			resistance		
		diameter	thickness	area	R ₂₅	ρ ₂₅	ρ ₂₅
	-	mm	mm	mm ²	Ω	Ω*cm	Ω*cm
1. N 1380/50/6	1	11,988	2,716	113,0221	19,669	81,849	75,709
	2	11,975	2,702	112,7771	18,080	75,463	
	3	11,980	2,695	112,8713	18,398	77,054	
	4	11,959	2,711	112,4759	17,635	73,165	
	5	11,986	2,702	112,9843	18,659	78,023	
	6	11,981	2,702	112,8901	18,310	76,500	
	7	11,936	2,708	112,0437	18,093	74,860	
	8	11,965	2,706	112,5888	17,470	72,688	
	9	11,966	2,710	112,6076	17,670	73,423	
	10	11,976	2,712	112,7959	17,808	74,066	
2. N 1380/50/6	1	11,954	2,714	112,3819	18,980	78,593	79,795
	2	11,974	2,696	112,7582	20,284	84,836	
	3	11,964	2,701	112,5700	18,804	78,370	
	4	11,961	2,712	112,5135	18,192	75,474	
	5	11,972	2,705	112,7206	19,651	81,888	
	6	11,960	2,711	112,4947	19,321	80,174	
	7	11,976	2,694	112,7959	18,594	77,852	
	8	11,979	2,705	112,8524	18,972	79,151	
	9	11,956	2,708	112,4195	18,213	75,609	
	10	11,985	2,705	112,9655	20,593	86,000	
3. N 1366/29/6	1	11,955	2,694	112,4007	42,450	177,112	178,632
	2	11,948	2,701	112,2691	41,745	173,516	
	3	11,936	2,688	112,0437	45,217	188,478	
	4	11,955	2,692	112,4007	40,515	169,165	
	5	11,943	2,702	112,1751	40,945	169,986	
	6	11,944	2,703	112,1939	43,782	181,727	
	7	11,936	2,702	112,0437	40,631	168,484	
	8	11,956	2,716	112,4195	44,985	186,200	
	9	11,958	2,692	112,4571	41,601	173,786	
	10	11,949	2,703	112,2879	47,631	197,868	
4. N 1380/20/6	1	11,965	2,713	112,5888	6,461	26,813	27,472
	2	11,974	2,706	112,7582	6,298	26,244	
	3	11,947	2,697	112,2503	6,130	25,513	
	4	11,959	2,699	112,4759	6,632	27,638	
	5	11,964	2,700	112,5700	6,460	26,933	
	6	11,959	2,697	112,4759	7,820	32,613	
	7	11,952	2,699	112,3443	6,145	25,578	
	8	11,967	2,691	112,6264	6,308	26,401	
	9	11,953	2,703	112,3631	6,708	27,885	
	10	11,971	2,691	112,7017	6,949	29,103	
5. N 1380/50/6	1	11,964	2,713	112,5700	23,660	98,172	91,964
	2	11,968	2,714	112,6453	20,631	85,629	
	3	11,976	2,707	112,7959	21,345	88,941	
	4	11,988	2,703	113,0221	22,353	93,466	
	5	12,032	2,707	113,8532	21,967	92,391	
	6	12,003	2,696	113,3051	20,262	85,155	
	7	12,121	2,694	115,5438	20,901	89,643	
	8	11,971	2,708	112,7017	23,895	99,446	
	9	11,974	2,707	112,7582	24,491	102,016	
	10	11,971	2,700	112,7017	20,310	84,777	
6. N 1394/71/6	1	11,989	2,708	113,0409	17,261	72,053	73,144
	2	11,982	2,710	112,9089	17,881	74,499	
	3	11,975	2,715	112,7771	19,613	81,469	
	4	11,975	2,706	112,7771	17,016	70,917	
	5	11,985	2,695	112,9655	17,021	71,346	
	6	12,000	2,690	113,2484	16,541	69,637	
	7	11,973	2,740	112,7394	18,761	77,194	
	8	12,005	2,698	113,3428	17,386	73,038	
	9	12,010	2,707	113,4373	17,010	71,281	
	10	11,983	2,695	112,9278	16,707	70,007	

A. 5: Investigations on specific electrical resistance of PTC mass A (runs 1 to 6)

sintering regime	Nr.	measurement			resistance		
		diameter	thickness	area	R_{25}	ρ_{25}	ρ_{25}
	-	mm	mm	mm ²	Ω	$\Omega \cdot \text{cm}$	$\Omega \cdot \text{cm}$
7. N 1380/50/6	1	11,985	2,699	112,9655	23,120	96,768	95,513
	2	11,977	2,719	112,8147	22,942	95,189	
	3	11,971	2,703	112,7017	24,412	101,786	
	4	11,979	2,695	112,8524	22,000	92,124	
	5	11,985	2,708	112,9655	22,482	93,785	
	6	11,968	2,707	112,6453	24,891	103,578	
	7	11,980	2,701	112,8713	22,074	92,244	
	8	11,969	2,695	112,6641	21,849	91,339	
	9	11,976	2,691	112,7959	23,497	98,490	
	10	11,965	2,705	112,5888	21,581	89,825	
8. N 1360/50/6	1	11,944	2,700	112,1939	414,000	1720,307	2292,100
	2	11,936	2,683	112,0437	548,000	2288,481	
	3	11,925	2,691	111,8373	483,000	2007,335	
	4	11,942	2,686	112,1564	517,000	2158,780	
	5	11,949	2,700	112,2879	419,000	1742,541	
	6	11,932	2,683	111,9686	403,000	1681,824	
	7	11,925	2,704	111,8373	708,000	2928,283	
	8	12,060	2,707	114,3838	461,000	1947,946	
	9	11,929	2,697	111,9123	930,000	3859,045	
	10	11,949	2,696	112,2879	621,000	2586,453	
9. N 1400/50/6	1	11,976	2,715	112,7959	10,375	43,103	43,484
	2	11,975	2,720	112,7771	9,938	41,205	
	3	11,966	2,716	112,6076	11,112	46,071	
	4	11,981	2,694	112,8901	10,570	44,293	
	5	11,993	2,710	113,1164	11,361	47,421	
	6	11,976	2,716	112,7959	9,979	41,443	
	7	11,975	2,707	112,7771	10,371	43,207	
	8	11,970	2,717	112,6829	10,270	42,593	
	9	11,970	2,710	112,6829	10,028	41,697	
	10	11,963	2,714	112,5512	10,563	43,805	
10. N 1380/80/6	1	11,963	2,713	112,5512	85,921	356,451	364,971
	2	11,985	2,719	112,9655	80,801	335,702	
	3	11,994	2,707	113,1352	84,350	352,529	
	4	11,988	2,715	113,0221	83,198	346,343	
	5	11,984	2,701	112,9466	90,938	380,272	
	6	11,980	2,700	112,8713	86,732	362,576	
	7	11,974	2,709	112,7582	99,120	412,573	
	8	11,981	2,707	112,8901	88,572	369,372	
	9	11,976	2,718	112,7959	88,432	366,989	
	10	11,978	2,703	112,8336	87,894	366,903	
11. N 1394/29/6	1	11,994	2,700	113,1352	5,175	21,684	20,817
	2	11,960	2,716	112,4947	5,312	22,002	
	3	11,959	2,712	112,4759	4,840	20,073	
	4	11,972	2,695	112,7206	4,864	20,344	
	5	11,969	2,710	112,6641	5,002	20,795	
	6	11,957	2,753	112,4383	5,021	20,507	
	7	11,961	2,714	112,5135	5,496	22,785	
	8	11,984	2,708	112,9466	4,837	20,174	
	9	11,967	2,714	112,6264	4,830	20,044	
	10	11,975	2,717	112,7771	4,760	19,758	
12. N 1366/71/6	1	11,963	2,705	112,5512	481,000	2001,372	2149,018
	2	11,948	2,718	112,2691	452,000	1867,021	
	3	11,953	2,716	112,3631	587,000	2428,465	
	4	12,004	2,703	113,3240	476,000	1995,642	
	5	11,954	2,709	112,3819	553,000	2294,100	
	6	11,959	2,715	112,4759	527,000	2183,234	
	7	11,977	2,702	112,8147	509,000	2125,192	
	8	11,969	2,701	112,6641	448,000	1868,697	
	9	11,957	2,712	112,4383	448,000	1857,388	
	10	11,959	2,705	112,4759	690,000	2869,071	

A. 6: Investigations on specific electrical resistance of PTC mass A (runs 7 to 12)

sintering regime	Nr.	measurement			resistance		
		diameter	thickness	area	R ₂₅	ρ ₂₅	ρ ₂₅
-	-	mm	mm	mm ²	Ω	Ω*cm	Ω*cm
13. N 1380/50/6	1	11,995	2,716	113,1541	35,681	148,654	148,726
	2	11,959	2,716	112,4759	33,843	140,152	
	3	11,960	2,697	112,4947	37,642	157,009	
	4	11,941	2,714	112,1376	34,060	140,730	
	5	11,961	2,701	112,5135	36,356	151,445	
	6	11,958	2,705	112,4571	36,082	150,007	
	7	11,966	2,720	112,6076	35,820	148,294	
	8	11,949	2,723	112,2879	36,992	152,543	
	9	11,967	2,703	112,6264	35,800	149,169	
	10	11,978	2,701	112,8336	35,730	149,261	
14. N 1366/29/6	1	11,979	2,698	112,8524	280,823	1174,631	1067,677
	2	11,928	2,684	111,8935	339,000	1413,260	
	3	11,926	2,707	111,8560	180,872	747,382	
	4	11,934	2,701	112,0061	170,840	708,446	
	5	11,921	2,702	111,7622	202,610	838,051	
	6	11,943	2,694	112,1751	441,000	1836,274	
	7	11,950	2,696	112,3067	145,221	604,944	
	8	11,914	2,700	111,6310	231,510	957,174	
	9	11,935	2,701	112,0249	159,690	662,320	
	10	11,915	2,691	111,6498	418,000	1734,285	
15. N 1366/29/6	1	11,939	2,693	112,1000	334,000	1390,323	944,906
	2	11,928	2,696	111,8935	162,232	673,320	
	3	11,915	2,706	111,6498	128,810	531,471	
	4	11,926	2,695	111,8560	460,245	1910,248	
	5	11,937	2,714	112,0625	146,641	605,488	
	6	11,942	2,690	112,1564	158,726	661,789	
	7	11,935	2,690	112,0249	224,771	936,058	
	8	11,922	2,707	111,7810	198,438	819,416	
	9	11,919	2,700	111,7247	275,012	1137,987	
	10	11,924	2,695	111,8185	188,705	782,958	
16. N 1366/29/6	1	11,927	2,692	111,8748	288,543	1199,134	780,838
	2	11,934	2,693	112,0061	173,268	720,649	
	3	11,944	2,701	112,1939	127,758	530,680	
	4	11,935	2,690	112,0249	162,401	676,318	
	5	11,910	2,701	111,5561	243,223	1004,554	
	6	11,935	2,709	112,0249	114,742	474,491	
	7	11,913	2,702	111,6123	268,091	1107,411	
	8	11,926	2,706	111,8560	211,280	873,353	
	9	11,916	2,704	111,6685	157,541	650,605	
	10	11,937	2,700	112,0625	137,620	571,186	
17. N 1366/29/6	1	11,927	2,690	111,8748	264,810	1101,322	747,272
	2	11,930	2,698	111,9311	143,511	595,379	
	3	11,921	2,708	111,7622	200,080	825,753	
	4	11,937	2,687	112,0625	109,230	455,548	
	5	11,933	2,709	111,9874	132,572	548,039	
	6	11,930	2,692	111,9311	163,701	680,655	
	7	11,923	2,708	111,7997	189,071	780,579	
	8	11,920	2,703	111,7435	333,154	1377,277	
	9	11,925	2,704	111,8373	145,502	601,795	
	10	11,930	2,703	111,9311	122,282	506,369	

A. 7: Investigations on specific electrical resistance of PTC mass A (runs 13 to 17)

sintering regime	Nr.	measurement			slope of the R-T curve		ref. Temperature	
		diameter	thickness	area	α	α	T_{ref}	T_{ref}
-	-	mm	mm	mm ²	1/K	1/K	°C	°C
1. N 1380/50/6	1	11,988	2,716	113,0221	0,530	0,525	125,1	125,0
	2	11,975	2,702	112,7771	0,527		125,1	
	3	11,980	2,695	112,8713	0,524		125,1	
	4	11,959	2,711	112,4759	0,526		125,2	
	5	11,986	2,702	112,9843	0,528		125,1	
	6	11,981	2,702	112,8901	0,527		125,1	
	7	11,936	2,708	112,0437	0,524		123,3	
	8	11,965	2,706	112,5888	0,522		125,2	
	9	11,966	2,710	112,6076	0,524		125,2	
	10	11,976	2,712	112,7959	0,524		125,2	
2. N 1380/50/6	1	11,954	2,714	112,3819	0,517	0,527	125,2	124,5
	2	11,974	2,696	112,7582	0,548		125,1	
	3	11,964	2,701	112,5700	0,526		125,2	
	4	11,961	2,712	112,5135	0,520		125,2	
	5	11,972	2,705	112,7206	0,524		125,1	
	6	11,960	2,711	112,4947	0,540		118,7	
	7	11,976	2,694	112,7959	0,524		125,1	
	8	11,979	2,705	112,8524	0,523		125,1	
	9	11,956	2,708	112,4195	0,516		125,2	
	10	11,985	2,705	112,9655	0,530		125,2	
3. N 1366/29/6	1	11,955	2,694	112,4007	0,378	0,375	123,3	123,5
	2	11,948	2,701	112,2691	0,378		123,4	
	3	11,936	2,688	112,0437	0,375		123,3	
	4	11,955	2,692	112,4007	0,376		123,4	
	5	11,943	2,702	112,1751	0,375		123,4	
	6	11,944	2,703	112,1939	0,375		123,3	
	7	11,936	2,702	112,0437	0,370		123,2	
	8	11,956	2,716	112,4195	0,370		125,1	
	9	11,958	2,692	112,4571	0,376		123,3	
	10	11,949	2,703	112,2879	0,374		123,3	
4. N 1380/20/6	1	11,965	2,713	112,5888	0,316	0,314	125,2	125,2
	2	11,974	2,706	112,7582	0,311		125,2	
	3	11,947	2,697	112,2503	0,309		125,2	
	4	11,959	2,699	112,4759	0,316		125,2	
	5	11,964	2,700	112,5700	0,314		125,2	
	6	11,959	2,697	112,4759	0,318		125,0	
	7	11,952	2,699	112,3443	0,310		125,2	
	8	11,967	2,691	112,6264	0,307		125,2	
	9	11,953	2,703	112,3631	0,314		125,2	
	10	11,971	2,691	112,7017	0,321		125,2	
5. N 1380/50/6	1	11,964	2,713	112,5700	0,522	0,531	125,0	125,1
	2	11,968	2,714	112,6453	0,536		125,2	
	3	11,976	2,707	112,7959	0,536		125,1	
	4	11,988	2,703	113,0221	0,536		125,1	
	5	12,032	2,707	113,8532	0,521		125,2	
	6	12,003	2,696	113,3051	0,522		125,1	
	7	12,121	2,694	115,5438	0,534		125,1	
	8	11,971	2,708	112,7017	0,553		125,1	
	9	11,974	2,707	112,7582	0,531		125,2	
	10	11,971	2,700	112,7017	0,522		125,1	
6. N 1394/71/6	1	11,989	2,708	113,0409	0,618	0,633	125,1	125,1
	2	11,982	2,710	112,9089	0,623		125,1	
	3	11,975	2,715	112,7771	0,664		125,1	
	4	11,975	2,706	112,7771	0,632		125,1	
	5	11,985	2,695	112,9655	0,631		125,1	
	6	12,000	2,690	113,2484	0,623		125,1	
	7	11,973	2,740	112,7394	0,643		125,0	
	8	12,005	2,698	113,3428	0,636		125,1	
	9	12,010	2,707	113,4373	0,628		125,1	
	10	11,983	2,695	112,9278	0,631		125,1	

A. 8: Investigations on the slope of the R-T-curve of PTC mass A (runs 1 to 6)

sintering regime	Nr.	measurement			slope of the R-T curve α 1/K	ref. Temperature T_{ref} °C	T_{ref} °C
		diameter mm	thickness mm	area mm ²			
7. N 1380/50/6	1	11,985	2,699	112,9655	0,546	125,1	125,1
	2	11,977	2,719	112,8147	0,571	125,1	
	3	11,971	2,703	112,7017	0,562	125,1	
	4	11,979	2,695	112,8524	0,547	125,1	
	5	11,985	2,708	112,9655	0,533	125,1	
	6	11,968	2,707	112,6453	0,536	125,4	
	7	11,980	2,701	112,8713	0,540	125,1	
	8	11,969	2,695	112,6641	0,534	125,2	
	9	11,976	2,691	112,7959	0,562	125,1	
	10	11,965	2,705	112,5888	0,536	125,1	
8. N 1360/50/6	1	11,944	2,700	112,1939	0,537	122,1	122,2
	2	11,936	2,683	112,0437	0,528	121,9	
	3	11,925	2,691	111,8373	0,531	122,1	
	4	11,942	2,686	112,1564	0,529	122,0	
	5	11,949	2,700	112,2879	0,542	122,1	
	6	11,932	2,683	111,9686	0,544	123,7	
	7	11,925	2,704	111,8373	0,523	121,9	
	8	12,060	2,707	114,3838	0,537	122,1	
	9	11,929	2,697	111,9123	0,520	121,7	
	10	11,949	2,696	112,2879	0,525	122,0	
9. N 1400/50/6	1	11,976	2,715	112,7959	0,512	125,2	125,2
	2	11,975	2,720	112,7771	0,498	125,2	
	3	11,966	2,716	112,6076	0,520	125,1	
	4	11,981	2,694	112,8901	0,504	125,2	
	5	11,993	2,710	113,1164	0,521	125,1	
	6	11,976	2,716	112,7959	0,495	125,2	
	7	11,975	2,707	112,7771	0,512	125,2	
	8	11,970	2,717	112,6829	0,510	125,2	
	9	11,970	2,710	112,6829	0,508	125,2	
	10	11,963	2,714	112,5512	0,510	125,2	
10. N 1380/80/6	1	11,963	2,713	112,5512	0,742	123,9	124,9
	2	11,985	2,719	112,9655	0,754	125,0	
	3	11,994	2,707	113,1352	0,758	125,0	
	4	11,988	2,715	113,0221	0,762	125,0	
	5	11,984	2,701	112,9466	0,755	125,1	
	6	11,980	2,700	112,8713	0,752	124,6	
	7	11,974	2,709	112,7582	0,766	125,0	
	8	11,981	2,707	112,8901	0,752	125,0	
	9	11,976	2,718	112,7959	0,746	125,0	
	10	11,978	2,703	112,8336	0,751	125,0	
11. N 1394/29/6	1	11,994	2,700	113,1352	0,357	125,3	125,3
	2	11,960	2,716	112,4947	0,349	125,3	
	3	11,959	2,712	112,4759	0,351	125,3	
	4	11,972	2,695	112,7206	0,353	125,3	
	5	11,969	2,710	112,6641	0,351	125,3	
	6	11,957	2,753	112,4383	0,350	125,3	
	7	11,961	2,714	112,5135	0,348	125,3	
	8	11,984	2,708	112,9466	0,350	125,3	
	9	11,967	2,714	112,6264	0,353	125,3	
	10	11,975	2,717	112,7771	0,353	125,3	
12. N 1366/71/6	1	11,963	2,705	112,5512	0,730	122,1	122,0
	2	11,948	2,718	112,2691	0,732	122,1	
	3	11,953	2,716	112,3631	0,707	122,1	
	4	12,004	2,703	113,3240	0,730	122,1	
	5	11,954	2,709	112,3819	0,713	122,1	
	6	11,959	2,715	112,4759	0,734	122,0	
	7	11,977	2,702	112,8147	0,722	122,0	
	8	11,969	2,701	112,6641	0,729	121,8	
	9	11,957	2,712	112,4383	0,729	122,0	
	10	11,959	2,705	112,4759	0,719	121,9	

A. 9: Investigations on the slope of the R-T-curve of PTC mass A (runs 7 to 12)

sintering regime	Nr.	measurement			slope of the R-T curve		ref. Temperature	
		diameter	thickness	area	α	α	T_{ref}	T_{ref}
	-	mm	mm	mm ²	1/K	1/K	°C	°C
13. N 1380/50/6	1	11,995	2,716	113,1541	0,573	0,569	125,0	125,0
	2	11,959	2,716	112,4759	0,564		125,0	
	3	11,960	2,697	112,4947	0,567		124,5	
	4	11,941	2,714	112,1376	0,570		125,0	
	5	11,961	2,701	112,5135	0,564		125,0	
	6	11,958	2,705	112,4571	0,572		125,0	
	7	11,966	2,720	112,6076	0,567		125,0	
	8	11,949	2,723	112,2879	0,567		125,0	
	9	11,967	2,703	112,6264	0,569		125,0	
	10	11,978	2,701	112,8336	0,573		125,0	
14. N 1366/29/6	1	11,979	2,698	112,8524	0,355	0,355	122,0	122,8
	2	11,928	2,684	111,8935	0,354		122,0	
	3	11,926	2,707	111,8560	0,351		122,4	
	4	11,934	2,701	112,0061	0,354		122,4	
	5	11,921	2,702	111,7622	0,352		122,3	
	6	11,943	2,694	112,1751	0,382		125,6	
	7	11,950	2,696	112,3067	0,345		124,8	
	8	11,914	2,700	111,6310	0,350		122,2	
	9	11,935	2,701	112,0249	0,353		122,4	
	10	11,915	2,691	111,6498	0,351		122,2	
15. N 1366/29/6	1	11,939	2,693	112,1000	0,355	0,354	122,0	122,2
	2	11,928	2,696	111,8935	0,355		122,4	
	3	11,915	2,706	111,6498	0,356		122,5	
	4	11,926	2,695	111,8560	0,351		121,8	
	5	11,937	2,714	112,0625	0,355		122,4	
	6	11,942	2,690	112,1564	0,355		122,3	
	7	11,935	2,690	112,0249	0,353		122,2	
	8	11,922	2,707	111,7810	0,352		122,3	
	9	11,919	2,700	111,7247	0,354		122,1	
	10	11,924	2,695	111,8185	0,354		122,3	
16. N 1366/29/6	1	11,927	2,692	111,8748	0,355	0,355	122,1	122,2
	2	11,934	2,693	112,0061	0,356		122,3	
	3	11,944	2,701	112,1939	0,358		122,5	
	4	11,935	2,690	112,0249	0,355		122,3	
	5	11,910	2,701	111,5561	0,352		122,2	
	6	11,935	2,709	112,0249	0,353		122,3	
	7	11,913	2,702	111,6123	0,355		121,7	
	8	11,926	2,706	111,8560	0,353		122,2	
	9	11,916	2,704	111,6685	0,355		122,3	
	10	11,937	2,700	112,0625	0,357		122,3	
17. N 1366/29/6	1	11,927	2,690	111,8748	0,356	0,355	121,9	122,2
	2	11,930	2,698	111,9311	0,356		122,3	
	3	11,921	2,708	111,7622	0,352		122,1	
	4	11,937	2,687	112,0625	0,357		122,4	
	5	11,933	2,709	111,9874	0,355		122,3	
	6	11,930	2,692	111,9311	0,354		122,2	
	7	11,923	2,708	111,7997	0,353		122,2	
	8	11,920	2,703	111,7435	0,353		121,8	
	9	11,925	2,704	111,8373	0,356		122,3	
	10	11,930	2,703	111,9311	0,359		122,4	

A. 10: Investigations on the slope of the R-T-curve of PTC mass A (runs 13 to 17)



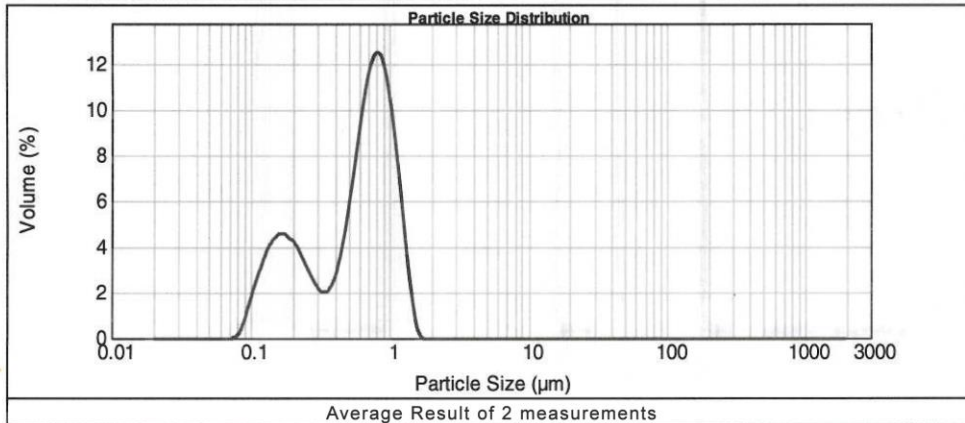
Result Analysis Report

Sample Name: Y2O3-ZrO2
Sample Source & type: KPP PT = SPC
Sample bulk lot ref:
SOP Name: _Standard
Measured by: Fertigung
Result Source: Averaged

Particle Name: Fraunhofer
Particle RI: 0.000
Dispersant Name: Water
Accessory Name: Hydro 2000G (A)
Absorption: 0
Dispersant RI: 1.330
Analysis model: General purpose
Size range: 0.020 to 2000.000 um
Weighted Residual: 6.316 %
Sensitivity: Enhanced
Obscuration: 17.22 %
Result Emulation: Off

Concentration: 0.0010 %Vol
Specific Surface Area: 16.3 m²/g
Span : 1.466
Surface Weighted Mean D[3,2]: 0.368 um
Uniformity: 0.464
Vol. Weighted Mean D[4,3]: 0.625 um
Result units: Volume

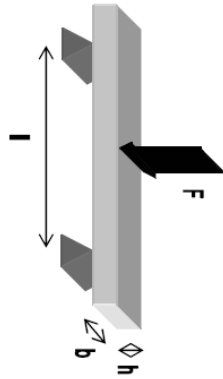
d(0.1): 0.150 um d(0.5): 0.643 um d(0.9): 1.092 um



Size (µm)	Volume In %	Size (µm)	Volume In %	Size (µm)	Volume In %	Size (µm)	Volume In %	Size (µm)	Volume In %	Size (µm)	Volume In %
0.010	0.00	0.105	2.46	1.096	6.20	11.482	0.00	120.226	0.00	1258.925	0.00
0.011	0.00	0.120	3.37	1.259	3.01	13.183	0.00	138.038	0.00	1445.440	0.00
0.013	0.00	0.138	3.97	1.445	0.57	15.136	0.00	158.489	0.00	1659.587	0.00
0.015	0.00	0.158	4.16	1.660	0.00	17.378	0.00	181.970	0.00	1905.461	0.00
0.017	0.00	0.182	3.92	1.905	0.00	19.953	0.00	208.930	0.00	2187.762	0.00
0.020	0.00	0.209	3.36	2.188	0.00	22.909	0.00	239.883	0.00	2511.886	0.00
0.023	0.00	0.240	2.64	2.512	0.00	26.303	0.00	275.423	0.00	2884.032	0.00
0.026	0.00	0.275	2.03	2.884	0.00	30.200	0.00	316.228	0.00	3311.311	0.00
0.030	0.00	0.316	1.83	3.311	0.00	34.674	0.00	363.078	0.00	3801.894	0.00
0.035	0.00	0.363	2.29	3.802	0.00	39.811	0.00	416.869	0.00	4365.158	0.00
0.040	0.00	0.417	3.56	4.365	0.00	45.709	0.00	478.630	0.00	5011.872	0.00
0.046	0.00	0.479	5.54	5.012	0.00	52.481	0.00	549.541	0.00	5754.399	0.00
0.052	0.00	0.550	7.93	5.754	0.00	60.256	0.00	630.957	0.00	6606.934	0.00
0.060	0.00	0.631	10.06	6.607	0.00	69.183	0.00	724.436	0.00	7585.776	0.00
0.069	0.00	0.724	11.27	7.586	0.00	79.433	0.00	831.764	0.00	8709.636	0.00
0.079	0.36	0.832	10.99	8.710	0.00	91.201	0.00	954.993	0.00	10000.000	0.00
0.091	1.39	0.955	9.11	10.000	0.00	104.713	0.00	1096.478	0.00		
0.105		1.096		11.482	0.00	120.226	0.00	1258.925	0.00		

A. 11: grain size distribution of YSZ

temperature: 25,9 °C
humidity: 48%

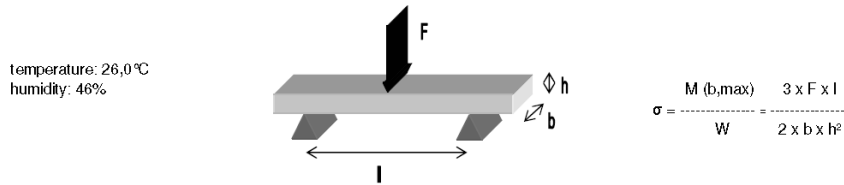


$$\sigma = \frac{M(b, \max)}{W} = \frac{3 \times F \times l}{2 \times b \times h^2}$$

sintering regime	description	unit	1	2	3	4	5	6	7	8	9	10
-	bearing distance l	mm	1,532	1,521	1,513	1,483	1,555	1,492	1,508	1,501	1,511	1,507
1: N1350/30/6	thickness h	mm	4,170	4,135	4,190	4,184	4,187	4,128	4,073	4,142	3,976	4,113
	width b	mm	234,02	232,00	232,39	215,28	262,12	187,71	216,38	239,54	229,56	220,37
	force F	N	717,33	727,57	726,85	701,86	776,71	612,82	700,84	770,07	758,65	707,76
2: N1360/30/6	bending strength σ	10^6 N/m^2	1,537	1,531	1,541	1,539	1,532	1,507	1,511	1,518	1,505	1,534
	thickness h	mm	4,103	4,147	4,170	4,173	4,090	4,182	4,149	4,070	4,135	4,009
	width b	mm	237,74	257,31	236,61	280,41	234,32	208,95	200,28	240,37	224,94	281,38
3: N1370/30/6	force F	N	736,82	794,13	716,82	851,12	732,30	660,01	634,29	768,89	720,51	831,20
	bending strength σ	10^6 N/m^2	1,528	1,518	1,549	1,510	1,526	1,498	1,546	1,525	1,484	1,527
	thickness h	mm	4,070	4,164	4,211	4,065	4,092	4,207	4,033	4,128	4,122	4,173
4: N1380/30/6	width b	mm	229,53	190,13	230,26	226,93	224,03	206,65	224,70	225,77	239,03	278,57
	force F	N	724,64	596,02	683,68	734,51	705,31	656,69	699,32	705,52	789,95	868,87
	bending strength σ	10^6 N/m^2	1,521	1,511	1,483	1,516	1,517	1,508	1,547	1,510	1,496	1,559
5: N1390/30/6	thickness h	mm	4,101	4,136	4,150	4,102	4,127	4,137	4,094	4,139	4,139	4,056
	width b	mm	302,27	256,03	204,66	238,46	280,08	260,09	291,34	267,48	255,12	294,63
	force F	N	955,80	819,75	672,70	758,83	884,70	829,39	892,06	850,28	839,42	896,62
6: N1400/30/6	bending strength σ	10^6 N/m^2	1,548	1,490	1,546	1,521	1,501	1,511	1,490	1,526	1,501	1,532
	thickness h	mm	4,100	4,131	3,996	4,220	4,057	4,151	4,090	3,946	4,147	4,038
	width b	mm	230,56	228,31	311,61	301,19	212,66	256,23	221,81	285,36	246,31	312,42
7: N1400/30/6	force F	N	887,22	746,82	978,79	925,53	697,98	811,09	732,84	931,64	790,88	988,95
	bending strength σ	10^6 N/m^2	1,526	1,522	1,463	1,507	1,455	1,489	1,501	1,500	1,505	1,503
	thickness h	mm	4,189	4,192	4,028	4,155	4,057	4,108	4,143	4,135	4,098	4,159
8: N1400/30/6	width b	mm	264,64	291,39	217,82	244,65	205,36	228,34	243,65	263,43	276,07	321,50
	force F	N	813,87	900,21	757,95	777,80	717,31	772,73	783,09	849,43	892,27	1026,59
	bending strength σ	10^6 N/m^2	1,521	1,511	1,483	1,516	1,517	1,508	1,547	1,510	1,496	1,559

A.

A Appendix



sintering regime	description	unit	1	2	3	4	5	6	7	8	9	10
-	bearing distance l	mm	20,00									
1: N1380/50/6	thickness h	mm	1,516	1,493	1,497	1,534	1,479	1,535	1,516	1,508	1,536	1,525
	width b	mm	2,981	3,414	3,448	3,391	3,384	3,462	3,460	3,170	3,204	3,343
	force F	N	155,46	171,47	171,11	160,89	161,21	188,31	172,40	176,53	181,70	180,45
	bending strength σ	10^6 N/m^2	680,74	675,97	664,33	604,88	653,35	692,55	650,41	734,65	721,11	696,31
2: N1380/50/6	thickness h	mm	1,556	1,538	1,556	1,526	1,536	1,492	1,476	1,500	1,481	1,509
	width b	mm	3,439	3,366	3,428	3,376	3,385	3,466	3,271	3,404	3,484	3,436
	force F	N	208,96	204,68	185,43	156,06	198,64	147,86	157,21	151,11	171,29	188,16
	bending strength σ	10^6 N/m^2	752,89	771,21	670,26	595,53	746,19	574,92	661,83	591,89	672,46	721,47
3: N1366/29/6	thickness h	mm	1,482	1,479	1,501	1,504	1,512	1,519	1,515	1,487	1,524	1,522
	width b	mm	3,251	3,412	3,255	3,497	3,664	3,310	3,434	3,268	3,467	3,497
	force F	N	145,42	160,07	151,41	154,86	181,23	165,14	176,91	127,61	137,03	205,77
	bending strength σ	10^6 N/m^2	610,99	643,41	619,39	587,31	649,07	648,68	673,36	529,79	510,52	762,04
4: N1380/20/6	thickness h	mm	1,497	1,537	1,536	1,546	1,518	1,529	1,532	1,493	1,539	1,500
	width b	mm	3,237	3,361	3,441	3,459	3,390	3,450	3,344	3,516	3,349	3,385
	force F	N	145,19	163,02	168,69	167,76	161,58	187,71	168,63	139,53	187,60	111,93
	bending strength σ	10^6 N/m^2	600,44	615,95	623,37	608,75	620,53	698,19	644,57	534,10	709,52	440,89
5: N1380/50/6	thickness h	mm	1,494	1,516	1,537	1,511	1,538	1,532	1,524	1,539	1,490	1,538
	width b	mm	2,857	2,945	2,876	2,915	3,227	2,818	2,970	2,830	2,878	2,838
	force F	N	124,04	149,13	140,20	126,17	130,15	130,98	118,20	141,00	120,34	111,12
	bending strength σ	10^6 N/m^2	583,54	661,00	619,06	568,73	511,51	594,11	514,06	631,07	565,03	496,58
6: N1394/71/6	thickness h	mm	1,510	1,506	1,505	1,505	1,532	1,521	1,518	1,523	1,536	1,535
	width b	mm	3,039	2,819	2,978	2,796	2,735	3,070	3,017	2,843	3,208	2,853
	force F	N	96,94	91,24	138,66	122,04	92,42	132,16	154,10	138,52	129,23	147,51
	bending strength σ	10^6 N/m^2	419,71	428,09	616,68	578,11	431,92	558,26	664,96	630,19	512,25	658,30
7: N1380/50/6	thickness h	mm	1,530	1,513	1,529	1,526	1,516	1,528	1,525	1,525	1,533	1,520
	width b	mm	3,119	3,067	2,962	2,827	3,067	3,083	3,085	3,096	2,998	3,077
	force F	N	164,55	125,77	170,06	163,79	155,68	179,14	156,52	126,81	155,63	157,87
	bending strength σ	10^6 N/m^2	676,13	537,42	736,76	746,40	682,58	746,60	654,47	528,34	662,67	666,18
8: N1360/50/6	thickness h	mm	1,509	1,528	1,507	1,508	1,523	1,533	1,516	1,514	1,526	1,524
	width b	mm	3,203	3,120	3,202	3,181	2,973	3,141	3,167	3,093	2,825	3,150
	force F	N	158,70	178,76	154,15	155,16	154,09	142,16	142,41	155,72	143,40	165,02
	bending strength σ	10^6 N/m^2	652,78	736,21	635,95	643,46	670,35	577,77	586,95	658,91	653,94	676,65
9: N1400/50/6	thickness h	mm	1,523	1,498	1,511	1,525	1,539	1,529	1,499	1,535	1,510	1,545
	width b	mm	3,458	3,335	3,478	3,507	3,400	3,373	3,522	3,570	3,266	3,561
	force F	N	195,59	157,16	155,97	175,10	179,77	165,18	160,61	197,13	147,09	180,36
	bending strength σ	10^6 N/m^2	731,53	630,00	589,27	644,05	669,70	628,42	608,84	703,05	592,56	636,55
10: N1380/80/6	thickness h	mm	1,528	1,512	1,500	1,503	1,531	1,528	1,528	1,507	1,520	1,521
	width b	mm	3,110	3,114	3,314	3,104	3,138	3,242	3,175	2,984	3,139	2,971
	force F	N	174,67	130,01	165,10	141,95	140,10	157,51	164,60	134,27	149,36	175,11
	bending strength σ	10^6 N/m^2	721,65	547,87	664,25	607,32	571,40	624,26	666,14	594,41	617,82	764,33
11: N1394/29/6	thickness h	mm	1,514	1,513	1,510	1,524	1,540	1,509	1,509	1,525	1,509	1,526
	width b	mm	2,944	3,071	3,171	3,097	3,069	3,133	2,966	3,105	2,831	3,166
	force F	N	156,47	152,87	161,80	165,14	134,23	157,32	159,80	147,96	151,15	146,57
	bending strength σ	10^6 N/m^2	695,62	652,37	671,37	688,73	553,25	661,54	709,81	614,69	703,40	596,40
12: N1366/71/6	thickness h	mm	1,541	1,522	1,530	1,533	1,526	1,516	1,533	1,520	1,519	1,533
	width b	mm	3,036	3,078	3,092	2,946	3,121	2,962	3,127	3,056	2,982	3,128
	force F	N	173,99	159,71	157,43	155,43	149,47	152,73	150,17	149,39	153,16	161,67
	bending strength σ	10^6 N/m^2	723,98	671,98	652,52	673,51	616,96	673,06	613,03	634,75	667,79	659,76
13: N1380/50/6	thickness h	mm	1,492	1,500	1,499	1,491	1,513	1,516	1,494	1,502	1,497	1,499
	width b	mm	3,484	2,996	3,025	3,500	3,473	3,459	3,260	3,478	3,086	2,902
	force F	N	119,80	124,08	125,02	114,86	143,11	164,02	138,64	131,11	112,66	125,09
	bending strength σ	10^6 N/m^2	463,40	552,22	551,79	442,84	540,01	618,98	571,61	501,28	488,71	575,48
14: N1366/29/6	thickness h	mm	1,537	1,526	1,527	1,534	1,523	1,505	1,520	1,527	1,534	1,528
	width b	mm	3,537	3,389	3,544	3,507	3,176	3,564	3,784	3,495	3,391	3,539
	force F	N	192,28	176,90	177,70	162,74	161,61	150,99	164,42	150,73	150,85	170,96
	bending strength σ	10^6 N/m^2	690,36	672,47	645,11	591,59	658,14	561,13	564,21	554,86	567,14	620,71
15: N1366/29/6	thickness h	mm	1,495	1,528	1,511	1,498	1,527	1,524	1,527	1,529	1,505	1,509
	width b	mm	3,538	3,328	3,650	3,482	3,675	3,499	3,107	3,595	3,400	3,532
	force F	N	159,92	166,06	157,25	128,49	184,93	144,94	141,57	160,29	175,51	129,62
	bending strength σ	10^6 N/m^2	606,71	641,15	566,11	493,33	647,44	535,04	586,22	572,16	683,69	483,50
16: N1366/29/6	thickness h	mm	1,535	1,551	1,544	1,546	1,537	1,535	1,549	1,549	1,546	1,549
	width b	mm	3,500	3,258	3,391	3,294	3,356	3,509	3,348	3,219	3,314	3,254
	force F	N	107,49	142,21	148,83	174,14	177,75	176,96	163,61	147,87	171,18	155,10
	bending strength σ	10^6 N/m^2	391,01	544,34	552,30	663,55	672,61	642,08	611,01	574,35	648,34	595,95
17: N1366/29/6	thickness h	mm	1,512	1,521	1,501	1,505	1,506	1,528	1,524	1,507	1,525	1,521
	width b	mm	3,183	3,394	3,525	3,458	3,413	3,169	3,285	3,529	3,365	3,458
	force F	N	141,30	150,39	137,86	157,58	145,56	174,61	160,10	158,80	163,29	168,25
	bending strength σ	10^6 N/m^2	582,52	574,61	520,76	603,55	564,11	707,97	629,52	594,40	625,97	630,95

A. 13: Investigations on mechanical strength of YSZ

m_1 = mass of the dried probe

m_2 = apparent mass of the probe drenched in the detection liquid

m_3 = mass of the drenched probe in air

sintering regime	Nr.	temperature	density of detection liquid ρ_{li}	mass			bulk density		water absorption		open porosity	
				m_1	m_2	m_3	ρ_{roh}	$\mu [\rho_{roh}]$	w	$\mu [w]$	P_o	$\mu [P_o]$
	-	°C	g/cm ³	g	g	g	g/cm ³	g/cm ³	%	%	%	%
1. N 1350/30/6	1	26,0	0,99678	3,4321	2,8340	3,4326	5,715	5,720	0,01	0,03	0,08	0,19
	2			3,4837	2,8775	3,4850	5,716		0,04		0,21	
	3			2,6284	2,1722	2,6292	5,733		0,03		0,18	
	4			3,5745	2,9546	3,5763	5,731		0,05		0,29	
	5			2,4529	2,0256	2,4535	5,714		0,02		0,14	
	6			3,4706	2,8662	3,4713	5,717		0,02		0,12	
	7			3,5418	2,9269	3,5430	5,730		0,03		0,19	
	8			3,5369	2,9220	3,5386	5,718		0,05		0,28	
	9			2,4835	2,0508	2,4845	5,708		0,04		0,23	
2. N 1360/30/6	1	26,0	0,99678	3,5285	2,9145	3,5300	5,714	5,722	0,04	0,03	0,24	0,17
	2			3,4998	2,8917	3,5009	5,726		0,03		0,18	
	3			2,5155	2,0777	2,5164	5,716		0,04		0,21	
	4			2,5587	2,1140	2,5597	5,722		0,04		0,22	
	5			3,4651	2,8628	3,4666	5,720		0,04		0,25	
	6			3,5516	2,9334	3,5519	5,724		0,01		0,05	
	7			2,4939	2,0602	2,4944	5,725		0,02		0,12	
	8			3,5233	2,9110	3,5239	5,730		0,02		0,10	
	9			3,5252	2,9120	3,5264	5,719		0,03		0,20	
3. N 1370/30/6	1	26,0	0,99678	3,5245	2,9126	3,5248	5,739	5,726	0,01	0,03	0,05	0,18
	2			3,5457	2,9294	3,5462	5,730		0,01		0,08	
	3			2,4560	2,0290	2,4571	5,719		0,04		0,26	
	4			3,6001	2,9750	3,6012	5,731		0,03		0,18	
	5			2,4366	2,0130	2,4373	5,724		0,03		0,16	
	6			3,5020	2,8936	3,5038	5,721		0,05		0,29	
	7			2,4816	2,0507	2,4822	5,733		0,02		0,14	
	8			3,5069	2,8970	3,5079	5,722		0,03		0,16	
	9			3,5395	2,9245	3,5412	5,721		0,05		0,28	
4. N 1380/30/6	1	26,0	0,99678	3,6259	2,9958	3,6268	5,728	5,728	0,02	0,03	0,14	0,17
	2			2,3820	1,9686	2,3828	5,732		0,03		0,19	
	3			3,5052	2,8962	3,5065	5,725		0,04		0,21	
	4			3,5146	2,9035	3,5152	5,727		0,02		0,10	
	5			2,5448	2,1029	2,5457	5,729		0,04		0,20	
	6			3,4571	2,8572	3,4582	5,734		0,03		0,18	
	7			3,5767	2,9558	3,5780	5,730		0,04		0,21	
	8			3,5278	2,9148	3,5286	5,729		0,02		0,13	
	9			2,4071	1,9882	2,4076	5,721		0,02		0,12	
5. N 1390/30/6	1	23,5	0,99742	3,3566	2,7734	3,3572	5,735	5,733	0,02	0,03	0,10	0,18
	2			2,7772	2,2948	2,7779	5,734		0,03		0,14	
	3			3,3950	2,8054	3,3966	5,728		0,05		0,27	
	4			2,9240	2,4160	2,9249	5,731		0,03		0,18	
	5			3,3700	2,7852	3,3709	5,739		0,03		0,15	
	6			3,2341	2,6722	3,2351	5,731		0,03		0,18	
	7			2,6268	2,1706	2,6276	5,733		0,03		0,18	
	8			2,4982	2,0645	2,4992	5,732		0,04		0,23	
	9			2,1487	1,7758	2,1494	5,736		0,03		0,19	
6. N 1400/30/6	1	28,0	0,99626	2,9077	2,4050	2,9090	5,748	5,738	0,04	0,04	0,26	0,21
	2			2,8245	2,3356	2,8259	5,739		0,05		0,29	
	3			3,7802	3,1255	3,7820	5,737		0,05		0,27	
	4			2,8080	2,3209	2,8089	5,733		0,03		0,18	
	5			3,0407	2,5136	3,0418	5,735		0,04		0,21	
	6			3,6753	3,0378	3,6769	5,729		0,04		0,25	
	7			4,0446	3,3444	4,0454	5,748		0,02		0,11	
	8			2,7866	2,3035	2,7870	5,742		0,01		0,08	
	9			2,6586	2,1978	2,6596	5,736		0,04		0,22	

A. 14: Pre-investigations on porosity of YSZ

A Appendix

sintering regime	Nr.	temperature °C	density of detection liquid ρ_{fl} g/cm ³	mass			bulk density		water absorption		open porosity	
				m1 g	m2 g	m3 g	ρ_{roh} %	μ [ρ_{roh}] %	WA %	μ [WA] %	OP %	μ [OP] %
1. N 1380/50/6	1	21,5	0,99788	0,4840	0,4002	0,4845	5,729	5,702	0,10	0,08	0,59	0,44
	2			0,3915	0,3230	0,3919	5,670		0,10		0,58	
	3			0,7342	0,6068	0,7356	5,688		0,19		1,09	
	4			0,4600	0,3800	0,4610	5,667		0,22		1,23	
	5			0,4523	0,3738	0,4526	5,728		0,07		0,38	
	6			0,9709	0,8012	0,9712	5,699		0,03		0,18	
	7			0,6945	0,5740	0,6945	5,751		0,00		0,00	
	8			0,1640	0,1350	0,1641	5,624		0,06		0,34	
	9			0,5570	0,4600	0,5570	5,730		0,00		0,00	
	10			0,6215	0,5134	0,6215	5,737		0,00		0,00	
2. N 1380/50/6	1	21,5	0,99788	0,4586	0,3789	0,4593	5,692	5,733	0,15	0,05	0,87	0,27
	2			0,3763	0,3109	0,3763	5,742		0,00		0,00	
	3			0,7493	0,6196	0,7500	5,734		0,09		0,54	
	4			0,3632	0,3000	0,3636	5,699		0,11		0,63	
	5			0,8998	0,7435	0,8999	5,741		0,01		0,06	
	6			0,5416	0,4475	0,5419	5,725		0,06		0,32	
	7			0,7193	0,5945	0,7194	5,747		0,01		0,08	
	8			0,7729	0,6386	0,7729	5,743		0,00		0,00	
	9			0,6094	0,5034	0,6096	5,726		0,03		0,19	
	10			0,4615	0,3818	0,4615	5,778		0,00		0,00	
3. N 1366/29/6	1	21,5	0,99788	0,3942	0,3258	0,3943	5,743	5,733	0,03	0,05	0,15	0,27
	2			0,7402	0,6127	0,7404	5,784		0,03		0,16	
	3			0,4788	0,3952	0,4793	5,681		0,10		0,59	
	4			0,3745	0,3095	0,3746	5,738		0,03		0,20	
	5			0,3745	0,3095	0,3747	5,732		0,05		0,31	
	6			0,9522	0,7870	0,9526	5,738		0,04		0,24	
	7			0,8931	0,7378	0,8933	5,731		0,02		0,13	
	8			0,4897	0,4047	0,4901	5,722		0,08		0,47	
	9			0,6660	0,5505	0,6662	5,744		0,03		0,17	
	10			0,5597	0,4623	0,5600	5,717		0,05		0,31	
4. N 1380/20/6	1	21,5	0,99788	0,7740	0,6394	0,7744	5,721	5,720	0,05	0,04	0,30	0,21
	2			0,4229	0,3493	0,4230	5,726		0,02		0,14	
	3			0,3426	0,2830	0,3428	5,717		0,06		0,33	
	4			0,4622	0,3816	0,4626	5,694		0,09		0,49	
	5			0,7951	0,6562	0,7952	5,708		0,01		0,07	
	6			0,7129	0,5900	0,7130	5,784		0,01		0,08	
	7			0,7827	0,6467	0,7827	5,743		0,00		0,00	
	8			0,4409	0,3640	0,4410	5,714		0,02		0,13	
	9			0,4678	0,3860	0,4682	5,679		0,09		0,49	
	10			0,7581	0,6259	0,7582	5,718		0,01		0,08	
5. N 1380/50/6	1	21,5	0,99788	0,4873	0,4026	0,4873	5,741	5,735	0,00	0,04	0,00	0,24
	2			0,4275	0,3532	0,4276	5,734		0,02		0,13	
	3			0,5206	0,4304	0,5212	5,721		0,12		0,66	
	4			0,4154	0,3433	0,4158	5,718		0,10		0,55	
	5			0,4932	0,4083	0,4933	5,790		0,02		0,12	
	6			1,4219	1,1748	1,4228	5,721		0,06		0,36	
	7			1,0210	0,8444	1,0211	5,766		0,01		0,06	
	8			0,8031	0,6631	0,8034	5,712		0,04		0,21	
	9			0,7493	0,6188	0,7494	5,725		0,01		0,08	
	10			0,6319	0,5220	0,6322	5,722		0,05		0,27	
6. N 1394/71/6	1	21,5	0,99788	0,8247	0,6818	0,8248	5,755	5,736	0,01	0,05	0,07	0,29
	2			0,7973	0,6593	0,7974	5,761		0,01		0,07	
	3			0,4326	0,3575	0,4328	5,733		0,05		0,27	
	4			0,5693	0,4706	0,5696	5,738		0,05		0,30	
	5			0,6544	0,5410	0,6544	5,758		0,00		0,00	
	6			0,7723	0,6382	0,7724	5,743		0,01		0,07	
	7			0,7333	0,6066	0,7341	5,739		0,11		0,63	
	8			0,4899	0,4043	0,4901	5,698		0,04		0,23	
	9			0,8033	0,6633	0,8039	5,701		0,07		0,43	
	10			0,5322	0,4403	0,5330	5,729		0,15		0,86	

A. 15: Investigations on porosity of YSZ (runs 1 to 6)

sintering regime	Nr.	temperature °C	density of detection liquid ρ_{fl} g/cm ³	mass			bulk density		water absorption		open porosity	
				m1 g	m2 g	m3 g	ρ_{boh} %	μ [ρ_{boh}] %	WA %	μ [WA] %	OP %	μ [OP] %
7. N 1380/50/6	1	20	0,9982	0,4153	0,3432	0,4154	5,742	5,688	0,02	0,07	0,14	0,41
	2			0,4339	0,3569	0,4340	5,618		0,02		0,13	
	3			0,7852	0,6480	0,7853	5,709		0,01		0,07	
	4			0,6394	0,5270	0,6394	5,678		0,00		0,00	
	5			0,8042	0,6641	0,8043	5,726		0,01		0,07	
	6			0,4524	0,3730	0,4530	5,645		0,13		0,75	
	7			0,9625	0,7937	0,9641	5,638		0,17		0,94	
	8			1,1149	0,9213	1,1155	5,731		0,05		0,31	
	9			0,6308	0,5215	0,6320	5,698		0,19		1,09	
	10			0,4613	0,3810	0,4618	5,699		0,11		0,62	
8. N 1360/50/6	1	20,5	0,9981	0,4454	0,3682	0,4459	5,721	5,692	0,11	0,11	0,64	0,62
	2			0,4384	0,3616	0,4392	5,639		0,18		1,03	
	3			1,2316	1,0168	1,2322	5,707		0,05		0,28	
	4			0,9432	0,7794	0,9434	5,740		0,02		0,12	
	5			0,4076	0,3369	0,4076	5,754		0,00		0,00	
	6			1,1052	0,9124	1,1090	5,611		0,34		1,93	
	7			0,9160	0,7568	0,9166	5,721		0,07		0,38	
	8			0,5782	0,4770	0,5790	5,658		0,14		0,78	
	9			0,6074	0,5014	0,6085	5,661		0,18		1,03	
	10			0,4516	0,3727	0,4516	5,713		0,00		0,00	
9. N 1400/50/6	1	22	0,99777	0,3679	0,3038	0,3680	5,718	5,725	0,03	0,03	0,16	0,19
	2			0,4473	0,3696	0,4476	5,722		0,07		0,38	
	3			0,6460	0,5330	0,6460	5,704		0,00		0,00	
	4			0,2934	0,2419	0,2936	5,662		0,07		0,39	
	5			0,9101	0,7525	0,9104	5,751		0,03		0,19	
	6			1,0632	0,8788	1,0640	5,728		0,08		0,43	
	7			0,6266	0,5182	0,6267	5,762		0,02		0,09	
	8			0,3959	0,3269	0,3959	5,725		0,00		0,00	
	9			0,6402	0,5290	0,6404	5,734		0,03		0,18	
	10			0,4574	0,3780	0,4575	5,741		0,02		0,13	
10. N 1380/80/6	1	20,5	0,9981	0,5950	0,4916	0,5951	5,738	5,731	0,02	0,03	0,10	0,19
	2			0,3252	0,2686	0,3252	5,735		0,00		0,00	
	3			0,8525	0,7045	0,8527	5,741		0,02		0,13	
	4			1,2815	1,0577	1,2815	5,715		0,00		0,00	
	5			0,4498	0,3717	0,4502	5,719		0,09		0,51	
	6			0,8636	0,7139	0,8641	5,739		0,06		0,33	
	7			0,4726	0,3903	0,4730	5,704		0,08		0,48	
	8			0,4871	0,4026	0,4872	5,747		0,02		0,12	
	9			0,9446	0,7803	0,9447	5,735		0,01		0,06	
	10			0,7490	0,6188	0,7492	5,733		0,03		0,15	
11. N 1394/29/6	1	20,5	0,9981	0,6778	0,5598	0,6780	5,723	5,723	0,03	0,05	0,17	0,27
	2			0,7196	0,5948	0,7200	5,737		0,06		0,32	
	3			1,3592	1,1226	1,3600	5,714		0,06		0,34	
	4			0,4537	0,3748	0,4538	5,732		0,02		0,13	
	5			0,4176	0,3450	0,4177	5,733		0,02		0,14	
	6			0,4797	0,3965	0,4800	5,734		0,06		0,36	
	7			0,5293	0,4371	0,5294	5,724		0,02		0,11	
	8			0,3837	0,3168	0,3840	5,699		0,08		0,45	
	9			1,2936	1,0685	1,2939	5,728		0,02		0,13	
	10			0,5389	0,4452	0,5394	5,710		0,09		0,53	
12. N 1366/71/6	1	21	0,9981	0,5191	0,4282	0,5192	5,694	5,692	0,02	0,08	0,11	0,46
	2			0,5270	0,4350	0,5282	5,644		0,23		1,29	
	3			0,7153	0,5908	0,7155	5,725		0,03		0,16	
	4			0,4487	0,3707	0,4493	5,698		0,13		0,76	
	5			0,5557	0,4582	0,5558	5,683		0,02		0,10	
	6			0,4420	0,3645	0,4421	5,685		0,02		0,13	
	7			0,8493	0,7012	0,8504	5,682		0,13		0,74	
	8			1,2733	1,0515	1,2750	5,686		0,13		0,76	
	9			1,1927	0,9850	1,1928	5,729		0,01		0,05	
	10			0,4156	0,3432	0,4160	5,698		0,10		0,55	

A. 16: Investigations on porosity of YSZ (runs 7 to 12)

A Appendix

sintering regime	Nr.	temperature °C	density of detection liquid ρ_{fl} g/cm ³	mass			bulk density		water absorption		open porosity	
				m1 g	m2 g	m3 g	ρ_{roh} %	μ [ρ_{roh}] %	WA %	μ [WA] %	OP %	μ [OP] %
13. N 1380/50/6	1	21	0,9981	0,4798	0,3962	0,4802	5,701	5,707	0,08	0,07	0,48	0,39
	2			0,8045	0,6642	0,8048	5,711		0,04		0,21	
	3			0,5666	0,4670	0,5671	5,650		0,09		0,50	
	4			0,5846	0,4829	0,5856	5,681		0,17		0,97	
	5			0,3626	0,2997	0,3626	5,754		0,00		0,00	
	6			0,5482	0,4531	0,5484	5,741		0,04		0,21	
	7			0,5556	0,4590	0,5556	5,741		0,00		0,00	
	8			0,8879	0,7336	0,8883	5,729		0,05		0,26	
	9			0,7492	0,6188	0,7495	5,721		0,04		0,23	
	10			0,5091	0,4200	0,5100	5,646		0,18		1,00	
14. N 1366/29/6	1	21,5	0,99788	0,4626	0,3815	0,4627	5,685	5,680	0,02	0,09	0,12	0,54
	2			0,3763	0,3108	0,3767	5,698		0,11		0,61	
	3			0,3286	0,2713	0,3289	5,693		0,09		0,52	
	4			0,3652	0,3014	0,3659	5,650		0,19		1,09	
	5			0,7128	0,5885	0,7130	5,713		0,03		0,16	
	6			0,7526	0,6210	0,7533	5,677		0,09		0,53	
	7			0,8344	0,6888	0,8349	5,699		0,06		0,34	
	8			0,5139	0,4239	0,5151	5,623		0,23		1,32	
	9			0,6455	0,5325	0,6459	5,680		0,06		0,35	
	10			0,5305	0,4376	0,5308	5,680		0,06		0,32	
15. N 1366/29/6	1	21,5	0,99788	0,3543	0,2924	0,3544	5,702	5,693	0,03	0,08	0,16	0,48
	2			0,4790	0,3952	0,4794	5,677		0,08		0,48	
	3			0,4592	0,3794	0,4600	5,685		0,17		0,99	
	4			0,8139	0,6719	0,8151	5,672		0,15		0,84	
	5			0,8370	0,6910	0,8378	5,690		0,10		0,54	
	6			0,6998	0,5776	0,7000	5,705		0,03		0,16	
	7			0,5766	0,4760	0,5769	5,702		0,05		0,30	
	8			0,5290	0,4368	0,5298	5,676		0,15		0,86	
	9			0,8114	0,6696	0,8118	5,694		0,05		0,28	
	10			0,5303	0,4381	0,5305	5,727		0,04		0,22	
16. N 1366/29/6	1	21,5	0,99788	0,4907	0,4050	0,4908	5,707	5,703	0,02	0,07	0,12	0,41
	2			0,3529	0,2912	0,3530	5,698		0,03		0,16	
	3			0,7451	0,6156	0,7457	5,715		0,08		0,46	
	4			0,5508	0,4560	0,5515	5,755		0,13		0,73	
	5			0,9460	0,7812	0,9464	5,714		0,04		0,24	
	6			0,9116	0,7526	0,9120	5,707		0,04		0,25	
	7			0,6226	0,5146	0,6234	5,710		0,13		0,74	
	8			0,6098	0,5030	0,6108	5,645		0,16		0,93	
	9			0,5160	0,4255	0,5163	5,671		0,06		0,33	
	10			0,6661	0,5498	0,6663	5,705		0,03		0,17	
17. N 1366/29/6	1	22	0,99777	0,4677	0,3860	0,4680	5,691	5,698	0,06	0,05	0,37	0,30
	2			0,3358	0,2769	0,3362	5,650		0,12		0,67	
	3			0,8036	0,6635	0,8038	5,715		0,02		0,14	
	4			0,4769	0,3934	0,4774	5,665		0,10		0,60	
	5			0,8667	0,7162	0,8667	5,746		0,00		0,00	
	6			0,8672	0,7154	0,8672	5,700		0,00		0,00	
	7			0,4883	0,4032	0,4887	5,698		0,08		0,47	
	8			0,6251	0,5162	0,6256	5,701		0,08		0,46	
	9			0,6761	0,5576	0,6763	5,683		0,03		0,17	
	10			0,6270	0,5179	0,6271	5,729		0,02		0,09	

A. 17: Investigations on porosity of YSZ (runs 13 to 17)



MASTERSIZER 2000

Result Analysis Report

Sample Name:
AL2O3 UFX DBM - Average

Sample Source & type:
KPP PT = SPC

Sample bulk lot ref:
3BM-2680 30minPM100

SOP Name:
Al2O3

Measured by:
Fertigung

Result Source:
Averaged

Measured:
Donnerstag, 22. April 2010 09:44:27

Analysed:
Donnerstag, 22. April 2010 09:44:28

Particle Name:
Al2O3

Particle RI:
1.780

Dispersant Name:
Water

Accessory Name:
Hydro 2000G (A)

Absorption:
0.01

Dispersant RI:
1.330

Analysis model:
General purpose

Size range:
0.020 to 2000.000 um

Weighted Residual:
2.660 %

Sensitivity:
Enhanced

Obscuration:
12.53 %

Result Emulation:
Off

Concentration:
0.0033 %Vol

Span :
2.527

Uniformity:
0.918

Result units:
Volume

Specific Surface Area:
52.3 m²/g

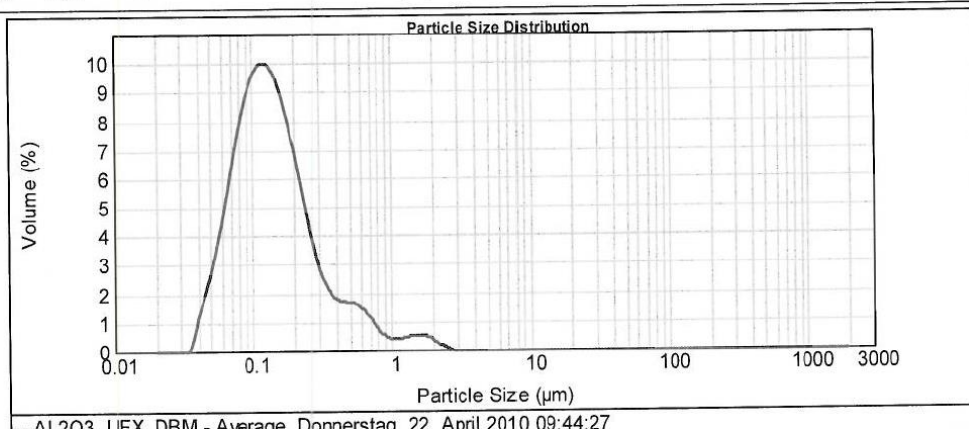
Surface Weighted Mean D[3,2]:
0.115 um

Vol. Weighted Mean D[4,3]:
0.210 um

d(0.1): 0.065 um

d(0.5): 0.132 um

d(0.9): 0.400 um



—AL2O3 UFX DBM - Average, Donnerstag, 22. April 2010 09:44:27

Size (µm)	Volume In %	Size (µm)	Volume In %	Size (µm)	Volume In %	Size (µm)	Volume In %	Size (µm)	Volume In %	Size (µm)	Volume In %
0.010	0.00	0.105	8.95	1.095	0.39	11.482	0.00	120.225	0.00	1258.925	0.00
0.011	0.00	0.120	8.98	1.259	0.45	13.183	0.00	138.038	0.00	1445.440	0.00
0.013	0.00	0.138	8.98	1.445	0.45	15.136	0.00	158.489	0.00	1659.587	0.00
0.015	0.00	0.158	8.54	1.660	0.50	17.378	0.00	181.970	0.00	1905.461	0.00
0.017	0.00	0.182	7.57	1.905	0.46	19.953	0.00	208.930	0.00	2187.762	0.00
0.020	0.00	0.209	6.46	2.188	0.33	22.909	0.00	239.883	0.00	2511.886	0.00
0.023	0.00	0.240	5.07	2.512	0.15	26.303	0.00	275.423	0.00	2884.032	0.00
0.026	0.00	0.275	3.73	2.894	0.01	30.200	0.00	316.228	0.00	3311.311	0.00
0.030	0.00	0.316	2.88	3.311	0.00	34.674	0.00	363.078	0.00	3801.894	0.00
0.035	0.00	0.363	2.00	3.802	0.00	39.811	0.00	416.869	0.00	4365.158	0.00
0.040	0.42	0.417	1.57	4.385	0.00	45.709	0.00	478.630	0.00	5011.872	0.00
0.046	1.40	0.479	1.55	5.012	0.00	52.481	0.00	549.541	0.00	5754.399	0.00
0.052	2.31	0.550	1.52	5.754	0.00	60.256	0.00	630.957	0.00	6606.934	0.00
0.060	3.44	0.631	1.39	6.607	0.00	69.183	0.00	724.436	0.00	7585.776	0.00
0.069	4.78	0.724	1.12	7.586	0.00	79.433	0.00	831.764	0.00	8709.636	0.00
0.079	6.31	0.832	0.77	8.710	0.00	91.201	0.00	954.093	0.00	10000.000	0.00
0.091	7.59	0.955	0.50	10.000	0.00	104.713	0.00	1096.478	0.00		
0.105	8.49	1.095	0.37	11.482	0.00	120.226	0.00	1258.925	0.00		

Operator notes:

A. 18: grain size distribution of alumina

A.2 Material development

temperature: 26.21°C
 humidity: 48%

$M(l, \max) = \frac{3 \times F \times l}{4 \times b \times h^2}$

composition	description	unit	20.00																						
			1	2	3	4	5	6	7	8	9	10													
1: PTC mass A	thickness h	mm	4.800	4.850	4.800	4.850	4.850	4.890	4.890	4.890	4.890	4.890	4.890	4.890	4.890	4.890	4.890	4.890	4.890	4.890	4.890				
	width b	mm	2.640	2.620	2.610	2.490	2.690	2.600	2.600	2.600	2.640	2.610	2.610	2.610	2.600	2.600	2.600	2.600	2.600	2.600	2.600	2.600	2.600		
	force F	N	176.76	156.69	193.28	199.89	189.13	190.78	180.74	180.42	176.35	169.27	169.27	169.27	169.27	169.27	169.27	169.27	169.27	169.27	169.27	169.27	169.27	169.27	
2: PTC mass A +5moFs YSZ	bending strength σ	10^4 N/m^2	86.86	87.82	108.17	113.79	101.71	91.56	102.08	91.01	100.01	96.12	96.12	96.12	96.12	96.12	96.12	96.12	96.12	96.12	96.12	96.12	96.12	96.12	
	thickness h	mm	4.610	4.690	4.690	4.610	4.620	4.630	4.630	4.630	4.630	4.630	4.630	4.630	4.630	4.630	4.630	4.630	4.630	4.630	4.630	4.630	4.630	4.630	4.630
	width b	mm	2.690	2.690	2.690	2.620	2.640	2.640	2.640	2.640	2.640	2.640	2.640	2.640	2.640	2.640	2.640	2.640	2.640	2.640	2.640	2.640	2.640	2.640	2.640
3: PTC mass A +3moFs YSZ	force F	N	168.02	136.96	143.36	148.02	91.28	133.29	120.66	129.91	120.79	124.38	124.38	124.38	124.38	124.38	124.38	124.38	124.38	124.38	124.38	124.38	124.38	124.38	124.38
	bending strength σ	10^4 N/m^2	92.68	77.16	79.84	81.79	60.61	73.44	66.70	73.36	68.84	74.88	74.88	74.88	74.88	74.88	74.88	74.88	74.88	74.88	74.88	74.88	74.88	74.88	74.88
	thickness h	mm	4.630	4.640	4.640	4.620	4.630	4.620	4.620	4.620	4.620	4.620	4.620	4.620	4.620	4.620	4.620	4.620	4.620	4.620	4.620	4.620	4.620	4.620	4.620
4: PTC mass A +5moFs YSZ	width b	mm	2.540	2.540	2.550	2.550	2.530	2.540	2.540	2.540	2.540	2.540	2.540	2.540	2.540	2.540	2.540	2.540	2.540	2.540	2.540	2.540	2.540	2.540	2.540
	force F	N	167.98	120.48	142.76	129.97	128.97	110.10	143.65	147.02	144.43	148.11	148.11	148.11	148.11	148.11	148.11	148.11	148.11	148.11	148.11	148.11	148.11	148.11	148.11
	bending strength σ	10^4 N/m^2	87.04	66.09	69.71	71.64	69.68	60.92	79.80	82.00	80.50	69.24	69.24	69.24	69.24	69.24	69.24	69.24	69.24	69.24	69.24	69.24	69.24	69.24	69.24
5: PTC mass A +10moFs YSZ	thickness h	mm	4.880	4.850	4.840	4.850	4.850	4.850	4.850	4.850	4.850	4.850	4.850	4.850	4.850	4.850	4.850	4.850	4.850	4.850	4.850	4.850	4.850	4.850	4.850
	width b	mm	2.660	2.640	2.650	2.650	2.670	2.650	2.650	2.650	2.650	2.650	2.650	2.650	2.650	2.650	2.650	2.650	2.650	2.650	2.650	2.650	2.650	2.650	2.650
	force F	N	108.11	188.34	100.82	115.80	99.20	98.40	82.20	105.12	116.16	113.27	113.27	113.27	113.27	113.27	113.27	113.27	113.27	113.27	113.27	113.27	113.27	113.27	113.27
6: PTC mass A +15moFs YSZ	bending strength σ	10^4 N/m^2	67.26	101.24	66.09	63.01	60.31	48.63	66.97	63.47	61.63	61.63	61.63	61.63	61.63	61.63	61.63	61.63	61.63	61.63	61.63	61.63	61.63	61.63	61.63
	thickness h	mm	4.750	4.720	4.690	4.750	4.730	4.720	4.720	4.720	4.720	4.720	4.720	4.720	4.720	4.720	4.720	4.720	4.720	4.720	4.720	4.720	4.720	4.720	4.720
	width b	mm	2.610	2.690	2.690	2.690	2.610	2.600	2.600	2.600	2.600	2.600	2.600	2.600	2.600	2.600	2.600	2.600	2.600	2.600	2.600	2.600	2.600	2.600	2.600
7: PTC mass A +20moFs YSZ	force F	N	70.37	81.60	97.48	63.25	97.89	76.82	101.61	73.61	77.16	83.28	83.28	83.28	83.28	83.28	83.28	83.28	83.28	83.28	83.28	83.28	83.28	83.28	83.28
	bending strength σ	10^4 N/m^2	36.15	42.57	51.24	32.47	60.29	39.27	54.26	37.69	39.64	42.61	42.61	42.61	42.61	42.61	42.61	42.61	42.61	42.61	42.61	42.61	42.61	42.61	42.61
	thickness h	mm	4.750	4.940	4.940	4.710	4.800	4.790	4.790	4.790	4.790	4.790	4.790	4.790	4.790	4.790	4.790	4.790	4.790	4.790	4.790	4.790	4.790	4.790	4.790
7: PTC mass A +20moFs YSZ	width b	mm	2.630	2.600	2.610	2.660	2.660	2.670	2.670	2.670	2.670	2.670	2.670	2.670	2.670	2.670	2.670	2.670	2.670	2.670	2.670	2.670	2.670	2.670	2.670
	force F	N	72.28	67.95	86.21	84.03	93.46	49.92	70.77	71.29	82.61	82.61	82.61	82.61	82.61	82.61	82.61	82.61	82.61	82.61	82.61	82.61	82.61	82.61	82.61
	bending strength σ	10^4 N/m^2	38.96	31.84	40.61	44.39	18.38	21.94	36.18	44.42	36.33	44.22	44.22	44.22	44.22	44.22	44.22	44.22	44.22	44.22	44.22	44.22	44.22	44.22	44.22

A. 19: Mechanical strength measurements of powder mixtures - PTC mass A+YSZ

8: PTC mass A +1mol% Al ₂ O ₃	thickness h	mm
	width b	mm
	force F	N
9: PTC mass A +3mol% Al ₂ O ₃	bending strength σ	10^8 N/m^2
	thickness h	mm
	width b	mm
10: PTC mass A +5mol% Al ₂ O ₃	force F	N
	bending strength σ	10^8 N/m^2
	thickness h	mm
11: PTC mass A +10mol% Al ₂ O ₃	width b	mm
	force F	N
	bending strength σ	10^8 N/m^2
12: PTC mass A +16mol% Al ₂ O ₃	thickness h	mm
	width b	mm
	force F	N
13: PTC mass A +20mol% Al ₂ O ₃	bending strength σ	10^8 N/m^2
	thickness h	mm
	width b	mm
	force F	N
	bending strength σ	10^8 N/m^2

A. 20: Mechanical strength measurements of powder mixtures - PTC mass A+Al₂O₃

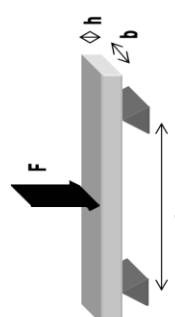
14: PTC mass B +10mol% YSZ	thickness h	mm	2.610	2.630	2.620	2.600	2.600	2.480	2.620	2.600	2.630	2.640	2.610
	width b	mm	4.620	4.620	4.630	4.640	4.630	4.650	4.620	4.620	4.630	4.630	4.630
	force F	N	93.06	131.69	161.28	117.82	110.17	222.37	145.62	137.19	193.96	162.08	162.08
	bending strength σ	10^6 N/m^2	95.92	133.49	164.96	121.88	116.07	226.91	151.19	139.88	194.76	167.46	167.46
15: PTC mass B +1mol% YSZ	thickness h	mm	2.620	2.640	2.630	2.640	2.650	2.650	2.620	2.600	2.630	2.640	2.620
	width b	mm	4.640	4.640	4.650	4.640	4.640	4.650	4.630	4.630	4.630	4.640	4.630
	force F	N	147.63	123.69	136.21	149.91	146.80	147.67	141.65	106.12	231.77	100.18	100.18
	bending strength σ	10^6 N/m^2	148.99	123.96	137.29	150.24	146.97	149.92	146.76	107.43	232.27	102.22	102.22
16: PTC mass B +3mol% YSZ	thickness h	mm	2.630	2.620	2.630	2.620	2.620	2.620	2.620	2.620	2.620	2.620	2.620
	width b	mm	4.700	4.660	4.690	4.700	4.690	4.710	4.720	4.650	4.660	4.660	4.700
	force F	N	124.62	173.71	118.04	149.37	128.67	101.08	139.18	166.92	122.65	114.92	114.92
	bending strength σ	10^6 N/m^2	124.17	172.96	119.67	146.04	126.69	98.24	132.90	166.92	120.74	111.93	111.93
17: PTC mass B +5mol% YSZ	thickness h	mm	2.610	2.620	2.620	2.640	2.620	2.620	2.630	2.640	2.630	2.620	2.620
	width b	mm	4.690	4.650	4.660	4.650	4.690	4.690	4.690	4.640	4.720	4.700	4.700
	force F	N	126.78	166.13	123.30	130.47	163.19	149.36	104.12	126.69	102.08	114.47	114.47
	bending strength σ	10^6 N/m^2	127.71	167.60	121.08	130.47	164.38	149.68	104.12	126.69	99.77	112.36	112.36
18: PTC mass B +10mol% YSZ	thickness h	mm	2.620	2.630	2.630	2.620	2.620	2.620	2.620	2.620	2.620	2.610	2.620
	width b	mm	4.740	4.790	4.750	4.730	4.780	4.780	4.780	4.780	4.780	4.780	4.770
	force F	N	110.06	105.63	96.74	105.91	116.37	93.91	102.06	113.95	119.82	99.37	99.37
	bending strength σ	10^6 N/m^2	107.13	103.26	95.46	102.60	110.49	89.93	100.07	116.26	119.87	98.42	98.42
19: PTC mass B +15mol% YSZ	thickness h	mm	2.600	2.640	2.620	2.630	2.620	2.620	2.620	2.620	2.620	2.620	2.620
	width b	mm	4.760	4.740	4.790	4.800	4.800	4.760	4.760	4.760	4.760	4.780	4.780
	force F	N	114.88	126.43	92.80	132.60	104.74	97.48	117.06	93.20	85.26	84.39	84.39
	bending strength σ	10^6 N/m^2	107.10	123.04	91.62	129.38	99.88	94.48	112.68	90.62	83.69	91.11	91.11
20: PTC mass B +20mol% YSZ	thickness h	mm	2.640	2.740	2.640	2.680	2.680	2.680	2.650	2.640	2.650	2.640	2.670
	width b	mm	4.780	4.740	4.740	4.780	4.770	4.720	4.730	4.730	4.730	4.760	4.760
	force F	N	110.34	133.49	93.74	122.61	124.66	173.96	127.63	129.88	116.62	130.03	130.03
	bending strength σ	10^6 N/m^2	107.34	132.92	92.80	117.42	117.79	170.03	126.48	126.69	113.92	124.34	124.34

A. 21: Mechanical strength measurements of powder mixtures - PTC mass B+YSZ

21: PTC mass B +1mol% Al2O3	thickness h	mm	2.540	2.520	2.510	2.520	2.540	2.530	2.530	2.530	2.530	2.530	2.520	2.520	2.520	2.520	2.520
	width b	mm	4.000	4.090	4.090	4.090	4.090	4.090	4.070	4.090	4.070	4.090	4.090	4.070	4.070	4.090	4.090
22: PTC mass B +3mol% Al2O3	force F	N	143.06	134.74	138.19	110.49	86.28	106.05	122.22	121.79	106.02	176.79	180.69	137.38	131.38	138.04	138.04
	bending strength σ	10^4 N/m^2	143.06	135.72	141.63	111.28	84.73	106.43	122.13	122.42	106.22	180.69	180.69	137.38	131.38	138.04	138.04
23: PTC mass B +5mol% Al2O3	thickness h	mm	2.610	2.650	2.620	2.630	2.630	2.630	2.600	2.600	2.600	2.620	2.630	2.620	2.630	2.630	2.630
	width b	mm	4.720	4.660	4.690	4.700	4.670	4.670	4.670	4.670	4.670	4.690	4.670	4.690	4.670	4.690	4.690
24: PTC mass B +10mol% Al2O3	force F	N	137.77	129.82	124.77	133.34	93.98	109.96	104.08	120.32	118.93	131.38	131.38	131.38	131.38	131.38	131.38
	bending strength σ	10^4 N/m^2	138.99	127.98	125.68	132.97	94.20	111.99	104.92	121.20	119.26	138.04	138.04	137.38	131.38	138.04	138.04
25: PTC mass B +19mol% Al2O3	thickness h	mm	2.630	2.670	2.660	2.660	2.660	2.660	2.630	2.630	2.630	2.650	2.660	2.660	2.660	2.660	2.660
	width b	mm	4.700	4.770	4.740	4.770	4.770	4.770	4.770	4.770	4.770	4.790	4.770	4.790	4.770	4.790	4.790
26: PTC mass B +20mol% Al2O3	force F	N	84.66	129.37	118.17	103.63	106.03	140.48	119.94	126.16	140.01	132.62	132.62	132.62	132.62	132.62	132.62
	bending strength σ	10^4 N/m^2	84.98	123.18	116.00	94.23	100.18	127.73	110.27	119.62	134.08	134.08	134.08	134.08	134.08	134.08	134.08
26: PTC mass B +19mol% Al2O3	thickness h	mm	2.690	2.600	2.630	2.630	2.720	2.620	2.620	2.630	2.630	2.630	2.630	2.630	2.630	2.630	2.630
	width b	mm	4.770	4.860	4.760	4.770	4.830	4.830	4.820	4.790	4.840	4.790	4.840	4.840	4.790	4.840	4.840
26: PTC mass B +19mol% Al2O3	force F	N	61.23	44.46	60.14	42.02	41.03	44.72	46.75	73.40	61.65	39.15	39.15	39.15	39.15	39.15	39.15
	bending strength σ	10^4 N/m^2	49.03	40.60	64.80	38.21	34.46	40.56	41.43	64.79	60.48	35.73	35.73	35.73	35.73	35.73	35.73
26: PTC mass B +19mol% Al2O3	thickness h	mm	2.670	2.620	2.620	2.690	2.670	2.670	2.670	2.670	2.670	2.690	2.690	2.690	2.690	2.690	2.690
	width b	mm	4.960	4.820	4.820	4.830	4.870	4.870	4.880	4.880	4.840	4.830	4.830	4.830	4.830	4.830	4.830
26: PTC mass B +19mol% Al2O3	force F	N	33.02	28.02	44.76	34.03	37.33	46.01	34.91	36.08	41.28	39.78	39.78	39.78	39.78	39.78	39.78
	bending strength σ	10^4 N/m^2	26.69	24.94	40.50	29.87	32.26	39.68	30.46	33.63	36.99	36.91	36.91	36.91	36.91	36.91	36.91
26: PTC mass B +19mol% Al2O3	thickness h	mm	2.630	2.610	2.600	2.600	2.600	2.600	2.600	2.600	2.600	2.620	2.620	2.620	2.620	2.620	2.620
	width b	mm	4.960	4.960	4.990	4.970	4.970	4.970	4.970	4.970	4.990	4.970	4.990	4.990	4.970	4.990	4.990
26: PTC mass B +19mol% Al2O3	force F	N	61.23	44.77	43.13	63.26	61.88	41.67	49.96	44.50	41.47	40.40	40.40	40.40	40.40	40.40	40.40
	bending strength σ	10^4 N/m^2	44.62	39.76	38.43	60.49	46.39	37.21	44.21	40.12	36.65	36.14	36.14	36.14	36.14	36.14	36.14

A. 22: Mechanical strength measurements of powder mixtures - PTC mass B+Al₂O₃

A.3 Prototypes



temperature: 26 °C
humidity: 45%

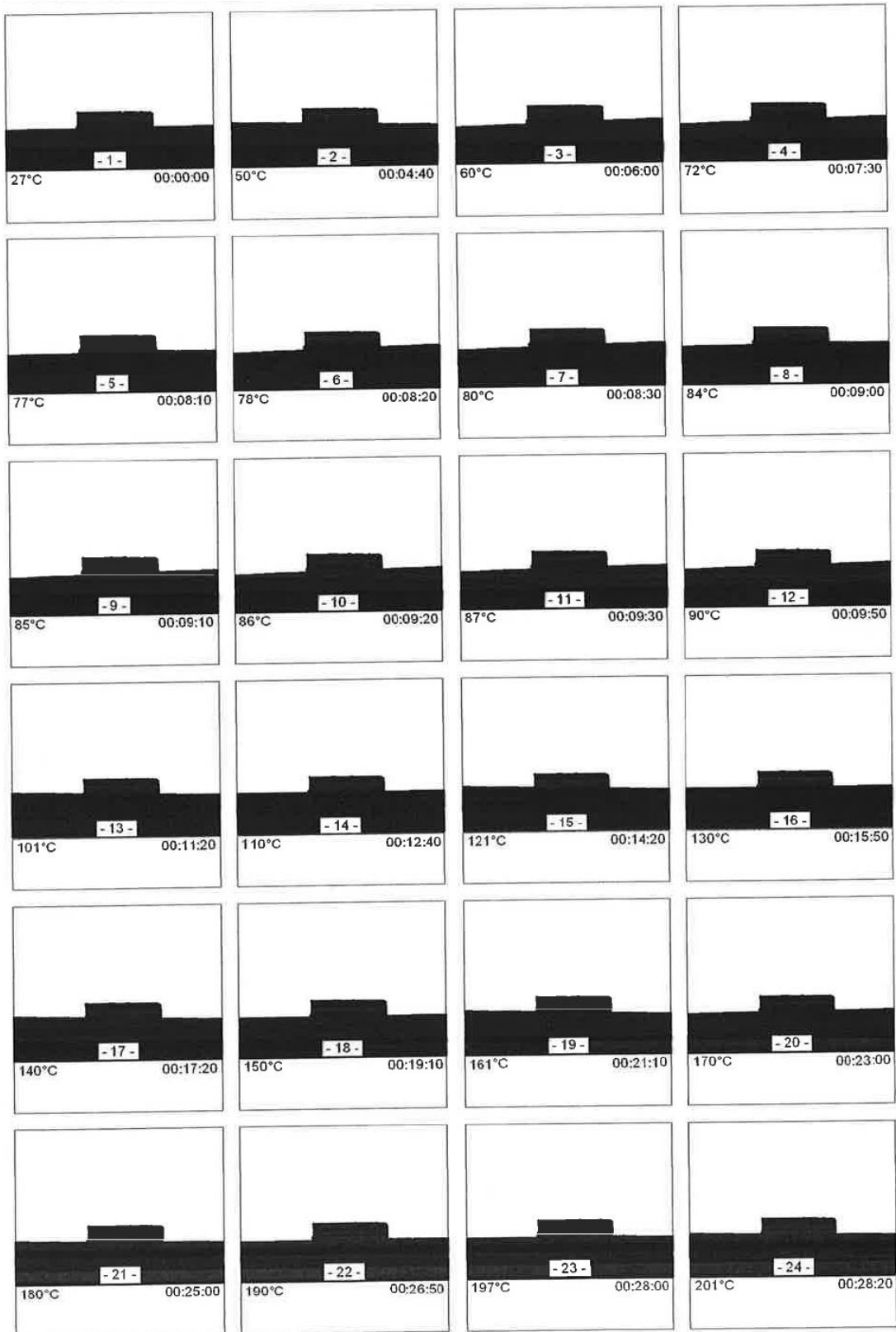
$$\sigma = \frac{M (b, \max)}{W} = \frac{3 \times F \times l}{2 \times b \times h^2}$$

part	description	unit	10,00										remarks
			1	2	3	4	5	6	7	8	9	10	
pressed prototype Y2O3-ZrO2 AB212 on top N1400/30/6	bearing distance l	mm	3,655	3,568	3,557	3,555	3,574	3,629	3,541	3,550	3,573	3,658	
	thickness h	mm	1,068	1,053	1,150	1,211	1,240	1,060	1,052	1,085	1,240	1,146	
	force F	N	480,00	480,00	480,00	480,00	480,00	480,00	480,00	480,00	480,00	480,00	max. force of 480 N hasn't led to breakage of parts!
pressed prototype Y2O3-ZrO2 ZrO2 on top N1400/30/6	bending strength σ	10 ⁶ N/m ²	504,65	537,10	494,84	470,45	454,57	515,77	545,84	526,56	454,83	469,53	
	thickness h	mm	3,655	3,568	3,557	3,555	3,574	3,629	3,541	3,550	3,573	3,658	
	width b	mm	1,150	1,235	1,102	1,081	1,210	1,166	1,105	1,157	1,105	1,246	
tape casted prototype CaO-ZrO2 AB212 on top N1400/30/6	force F	N	480,00	480,00	480,00	480,00	480,00	480,00	480,00	480,00	480,00	480,00	
	bending strength σ	10 ⁶ N/m ²	468,66	457,95	516,40	527,02	465,84	468,88	545,84	493,79	510,39	431,84	
	thickness h	mm	0,845	0,733	0,833	0,833	0,835	0,845	0,822	0,824	0,831	0,827	
tape casted prototype CaO-ZrO2 ZrO2 on top N1400/30/6	width b	mm	4,242	4,181	4,161	4,180	4,167	4,190	4,163	4,191	4,166	4,163	
	force F	N	17,82	19,42	18,20	17,45	23,20	19,93	18,91	18,35	19,40	14,56	
	bending strength σ	10 ⁶ N/m ²	88,23	129,68	94,53	90,22	119,78	99,92	100,36	96,70	101,15	76,72	
tape casted prototype Y2O3-ZrO2 AB212 on top N1400/30/6	thickness h	mm	0,855	0,836	0,843	0,856	0,850	0,845	0,821	0,739	0,883	0,836	
	width b	mm	4,189	4,167	4,185	4,193	4,188	4,193	4,163	4,222	4,246	4,224	
	force F	N	4,79	4,96	4,27	6,00	4,98	3,90	4,31	3,57	3,81	4,16	
tape casted prototype Y2O3-ZrO2 AB212 on top N1400/30/6	bending strength σ	10 ⁶ N/m ²	23,47	25,54	21,54	29,30	24,70	19,55	22,95	23,23	17,24	21,13	
	thickness h	mm	0,883	0,865	0,900	0,865	0,901	0,878	0,917	0,975	0,924	0,945	
	width b	mm	4,223	4,257	4,258	4,224	4,258	4,226	4,255	4,240	4,243	4,257	
tape casted prototype Y2O3-ZrO2 ZrO2 on top N1400/30/6	force F	N	85,09	83,69	93,59	87,33	78,69	83,27	93,21	92,73	94,33	109,25	
	bending strength σ	10 ⁶ N/m ²	387,64	394,11	407,02	414,47	341,48	383,41	392,59	345,11	390,59	431,05	
	thickness h	mm	0,899	0,897	0,916	0,917	0,928	0,896	0,952	0,873	0,910	0,927	
tape casted prototype Y2O3-ZrO2 ZrO2 on top N1400/30/6	width b	mm	4,222	4,223	4,268	4,259	4,273	4,239	4,290	4,231	4,256	4,229	
	force F	N	22,04	20,07	18,47	21,54	16,35	18,14	24,10	20,24	18,64	17,55	
	bending strength σ	10 ⁶ N/m ²	96,89	88,60	77,36	90,22	66,65	79,97	92,98	94,13	79,32	72,43	

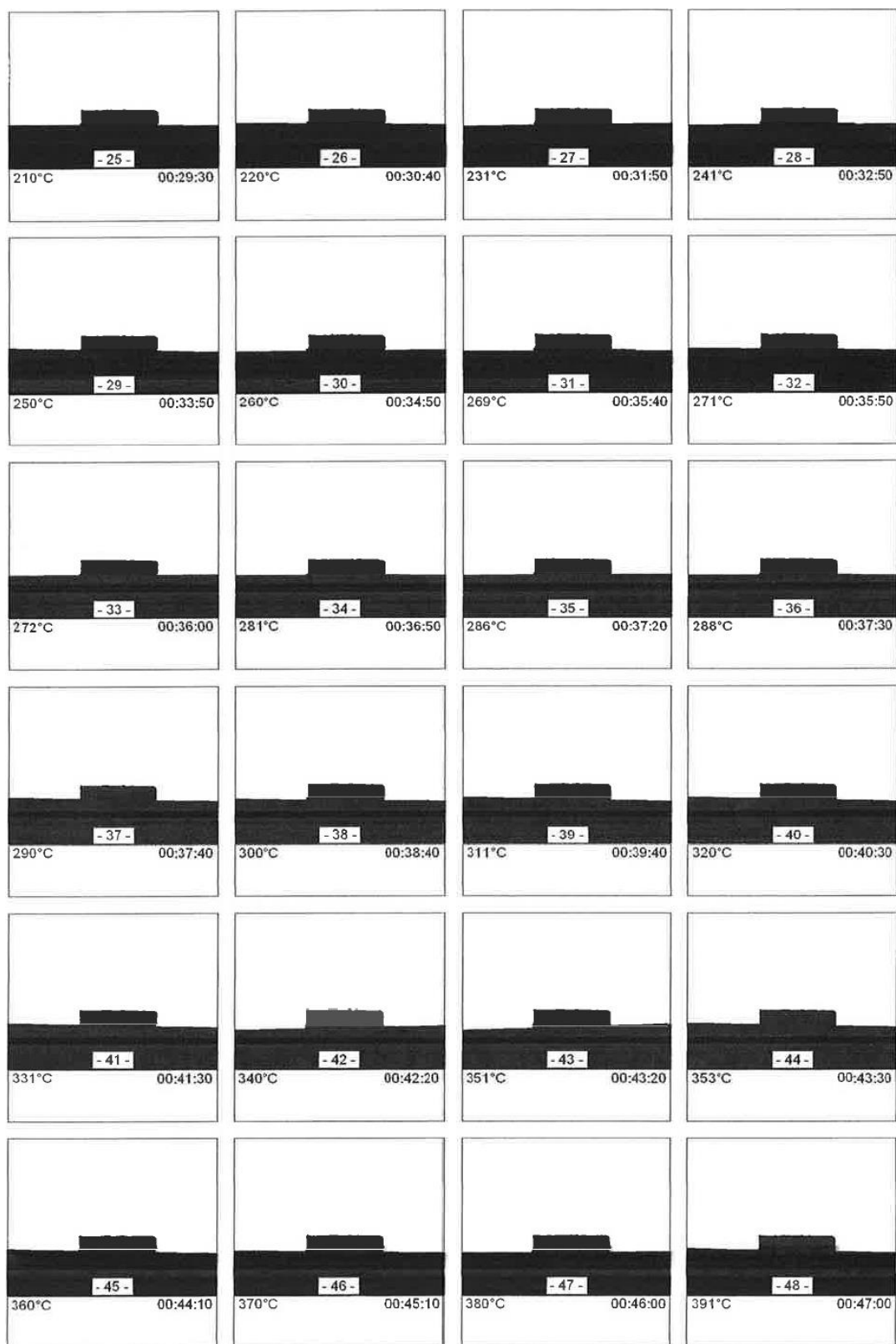
A. 23: Mechanical strength measurements of prototypes

sintering regime	KLSUBLANG 1400/30/6									
part	1	2	3	4	5	6	7	8	9	10
temperature °C	resistance Ω									
-0,07	2,87E+07	8,830E+06	5,374E+06	5,841E+06	3,021E+06	3,241E+07	6,457E+06	6,042E+06	7,331E+06	8,791E+06
10,00	3,32E+07	1,191E+07	4,729E+06	5,185E+06	2,739E+06	2,891E+07	6,128E+06	6,189E+06	6,391E+06	8,406E+06
19,99	3,53E+07	2,086E+07	4,070E+06	4,451E+06	2,395E+06	2,543E+07	5,555E+06	5,456E+06	5,492E+06	7,463E+06
25,00	3,33E+07	3,718E+07	3,772E+06	4,053E+06	2,215E+06	2,320E+07	5,252E+06	4,853E+06	5,141E+06	6,956E+06
29,99	3,13E+07	5,021E+07	3,458E+06	3,728E+06	2,052E+06	2,093E+07	4,824E+06	4,235E+06	4,747E+06	6,375E+06
40,01	2,23E+07	3,688E+07	2,892E+06	3,014E+06	1,703E+06	1,352E+07	4,012E+06	3,211E+06	3,941E+06	5,256E+06
50,00	1,85E+07	2,433E+07	2,367E+06	2,616E+06	1,414E+06	8,235E+06	3,166E+06	2,806E+06	3,541E+06	4,184E+06
59,97	1,42E+07	1,665E+07	2,037E+06	2,230E+06	1,212E+06	6,300E+06	2,670E+06	2,456E+06	3,004E+06	3,556E+06
69,97	1,14E+07	1,172E+07	1,822E+06	1,934E+06	1,029E+06	5,182E+06	2,330E+06	2,134E+06	2,445E+06	3,092E+06
79,97	7,90E+06	8,731E+06	1,646E+06	1,723E+06	8,919E+05	4,867E+06	1,979E+06	1,914E+06	1,751E+06	2,676E+06
84,97	6,64E+06	7,499E+06	1,613E+06	1,676E+06	9,175E+05	4,810E+06	1,786E+06	1,792E+06	1,329E+06	2,569E+06
89,97	5,39E+06	6,291E+06	1,600E+06	1,629E+06	1,002E+06	4,779E+06	1,827E+06	1,645E+06	1,070E+06	2,467E+06
94,96	4,44E+06	5,320E+06	1,586E+06	1,619E+06	1,004E+06	4,716E+06	1,879E+06	1,599E+06	9,831E+05	2,378E+06
99,96	3,00E+06	4,752E+06	1,585E+06	1,645E+06	9,253E+05	4,916E+06	1,950E+06	1,562E+06	1,062E+06	2,454E+06
104,94	1,97E+06	4,420E+06	1,635E+06	1,698E+06	1,047E+06	4,881E+06	2,023E+06	1,568E+06	1,096E+06	2,579E+06
109,96	1,20E+06	4,203E+06	1,710E+06	1,815E+06	1,090E+06	5,290E+06	2,134E+06	1,742E+06	1,212E+06	2,839E+06
114,94	1,17E+06	4,017E+06	1,864E+06	2,086E+06	1,315E+06	5,763E+06	2,254E+06	2,121E+06	1,490E+06	3,241E+06
119,97	2,20E+06	4,622E+06	2,293E+06	2,656E+06	1,767E+06	7,180E+06	2,539E+06	3,423E+06	2,276E+06	4,715E+06
129,94	7,53E+06	2,452E+07	1,031E+07	1,229E+07	9,095E+06	3,741E+07	7,337E+06	1,229E+07	3,025E+07	1,788E+07
139,94	9,18E+06	1,108E+08	1,931E+07	1,837E+07	1,572E+07	2,606E+07	2,128E+07	1,746E+07	1,266E+08	2,096E+07
149,94	6,72E+06	2,229E+08	2,482E+07	1,513E+07	1,362E+07	2,370E+07	3,224E+07	1,615E+07	3,139E+08	1,523E+07
159,95	5,32E+06	2,951E+08	1,991E+07	1,115E+07	1,028E+07	8,071E+07	1,086E+08	1,125E+07	5,195E+08	1,096E+07
169,97	5,94E+06	3,023E+08	1,509E+07	9,869E+06	7,503E+06	6,427E+07	1,441E+08	7,857E+06	5,247E+08	7,990E+06
179,97	7,62E+06	2,534E+08	1,101E+07	6,957E+06	5,426E+06	4,612E+07	1,559E+08	6,257E+06	4,721E+08	5,980E+06

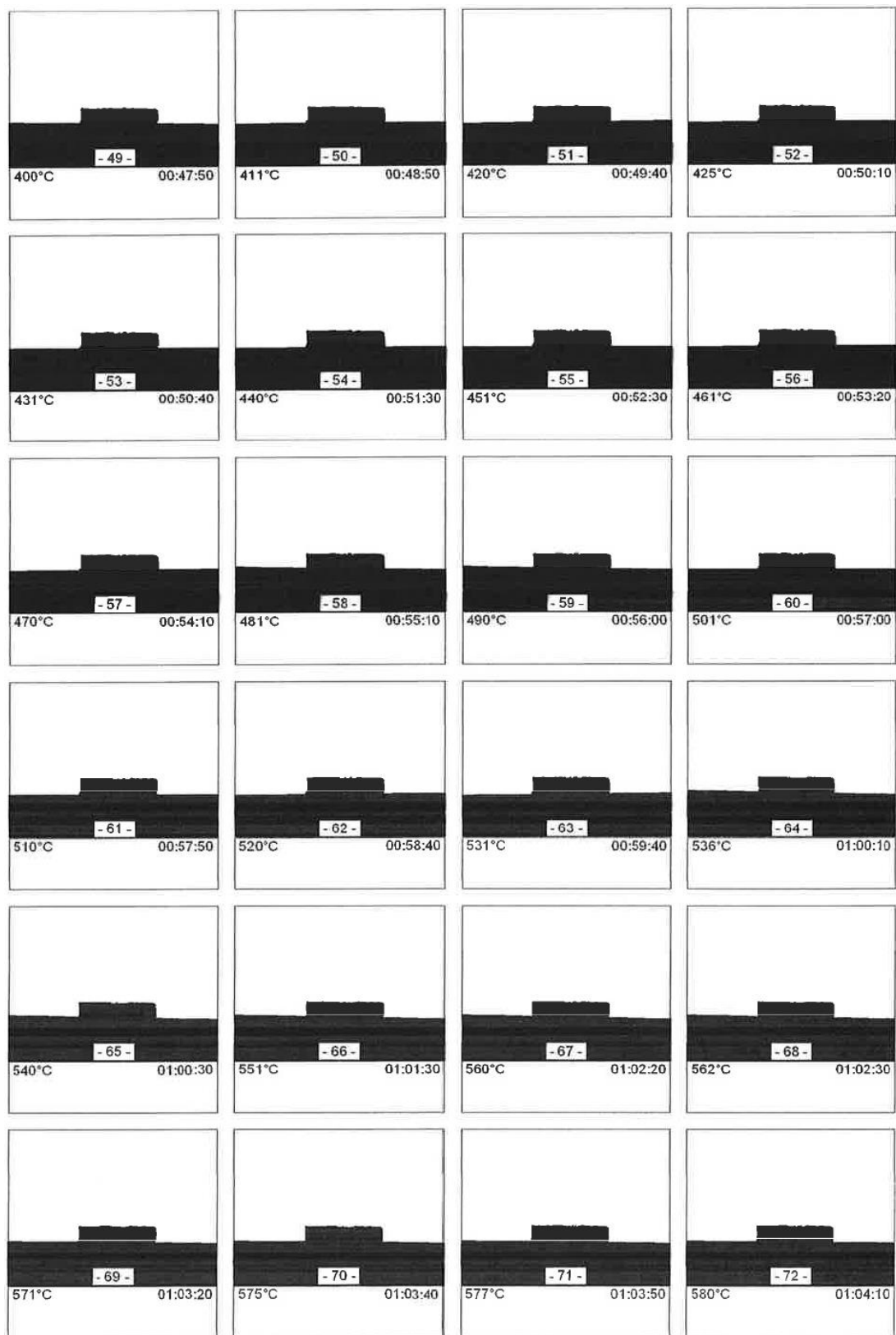
A. 24: R(T) measurement of prototypes based on YSZ



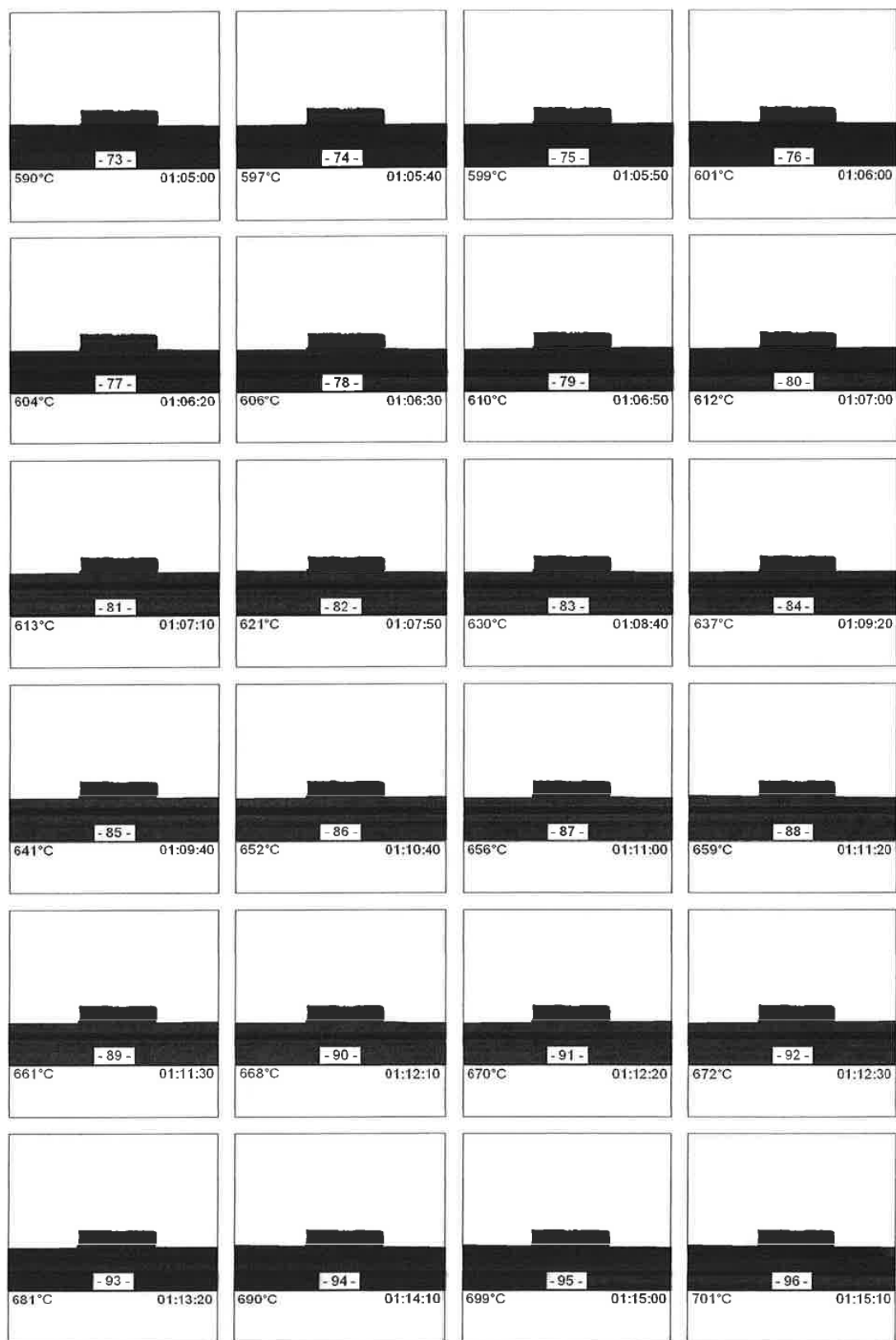
A. 25: Heating microscopy of thin PTC prototype (25-200°C)



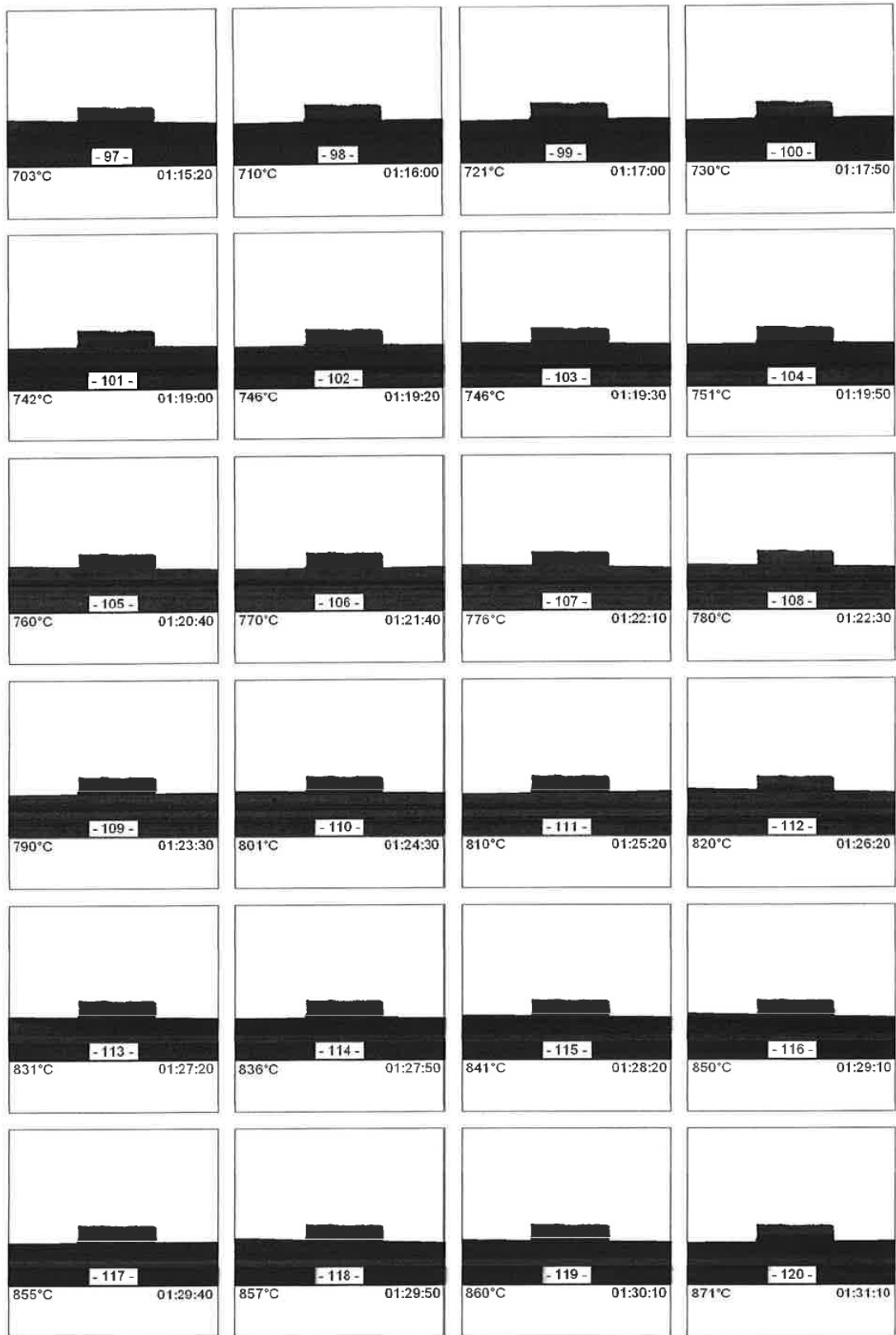
A. 26: Heating microscopy of thin PTC prototype (210-390°C)



A. 27: Heating microscopy of thin PTC prototype (400-580°C)



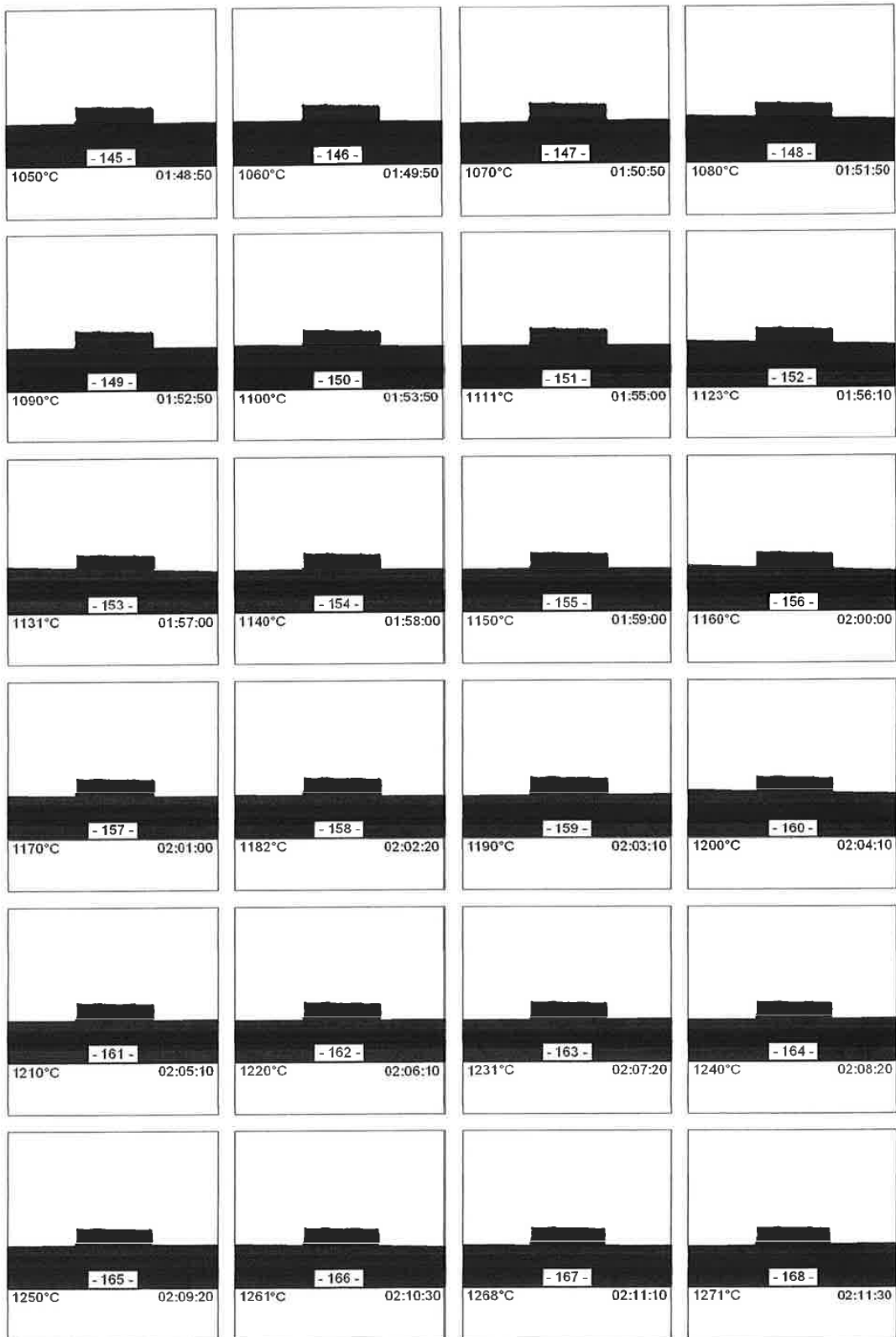
A. 28: Heating microscopy of thin PTC prototype (590-700°C)



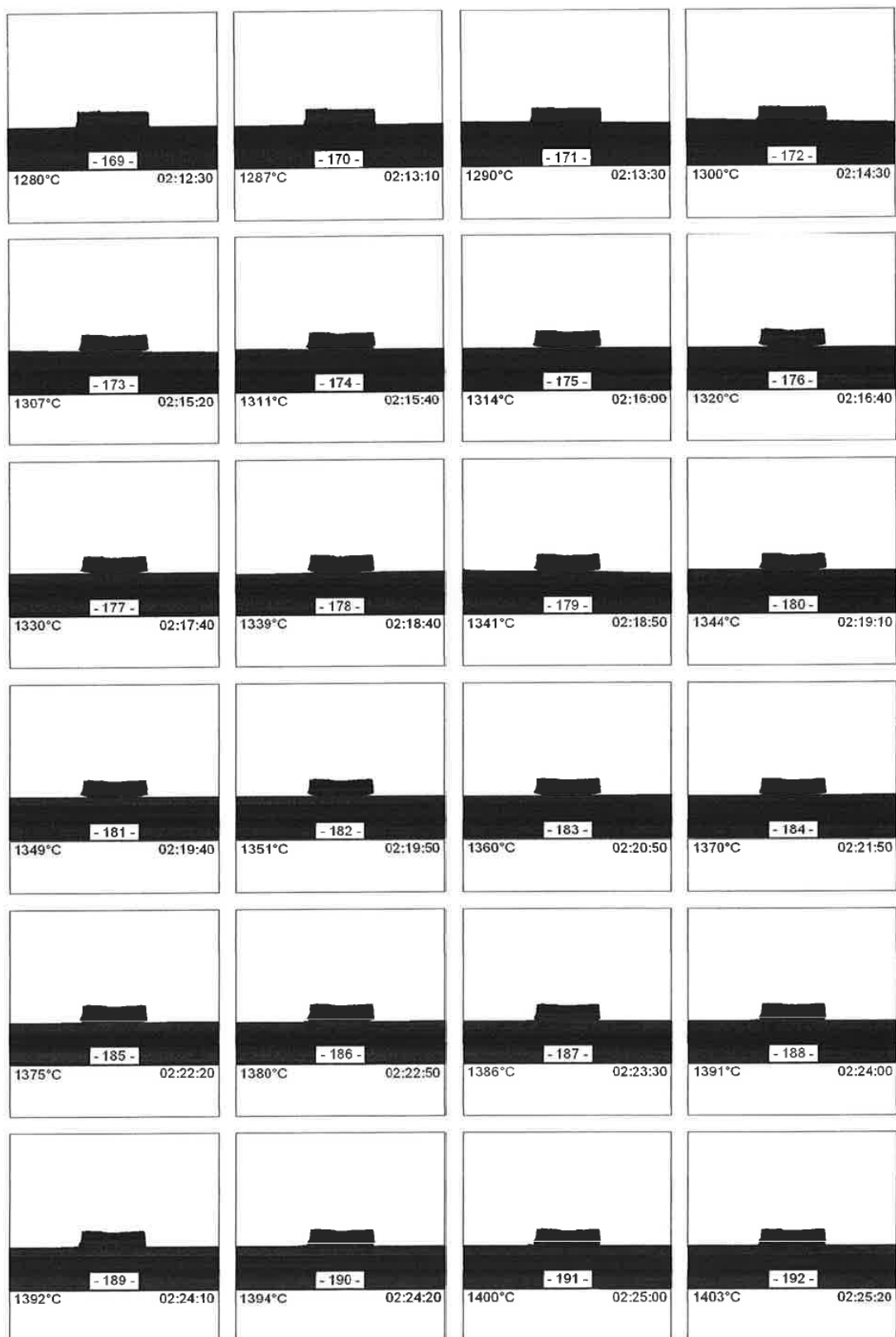
A. 29: Heating microscopy of thin PTC prototype (700-870°C)



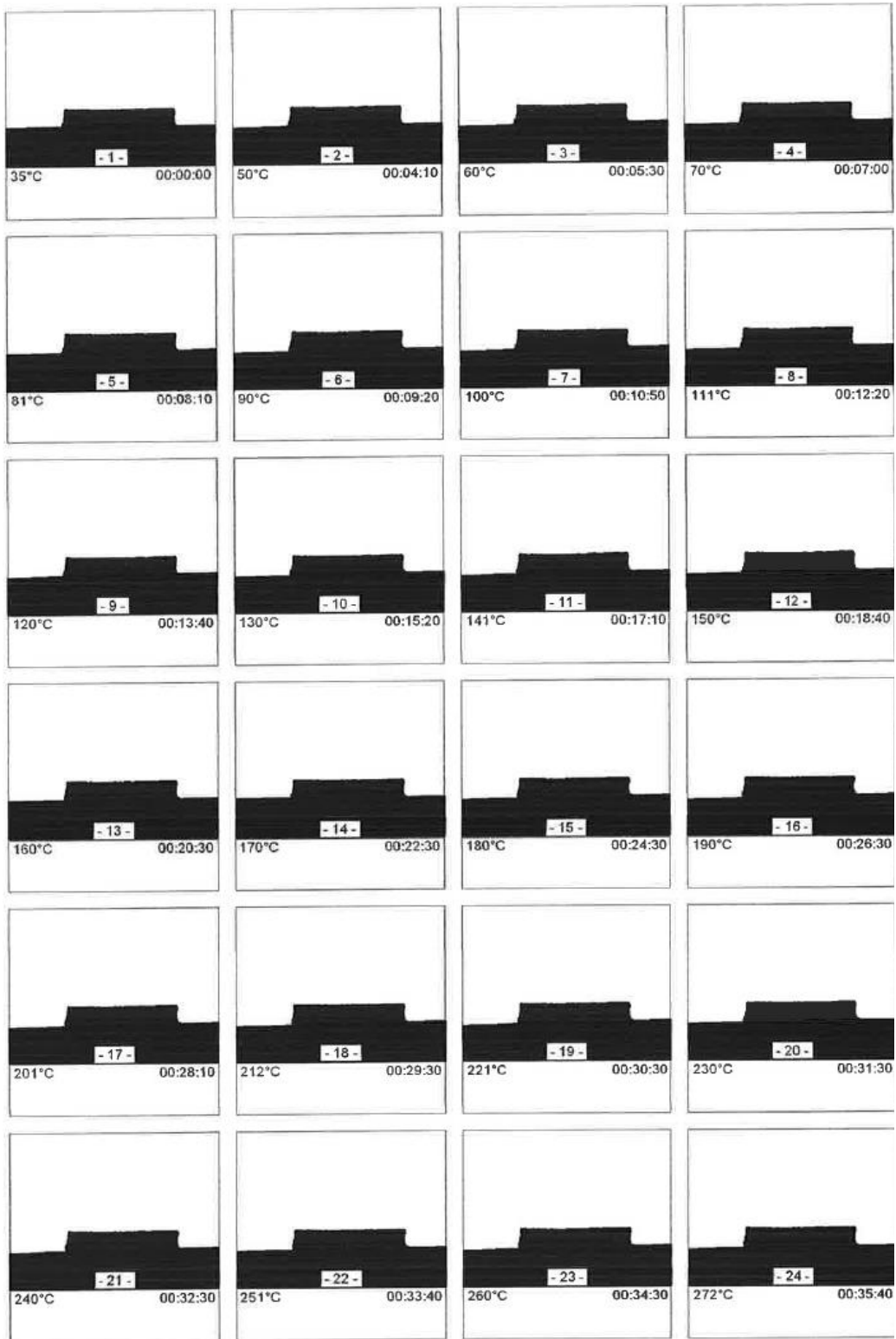
A. 30: Heating microscopy of thin PTC prototype (8800-1040°C)



A. 31: Heating microscopy of thin PTC prototype (1050-1270°C)

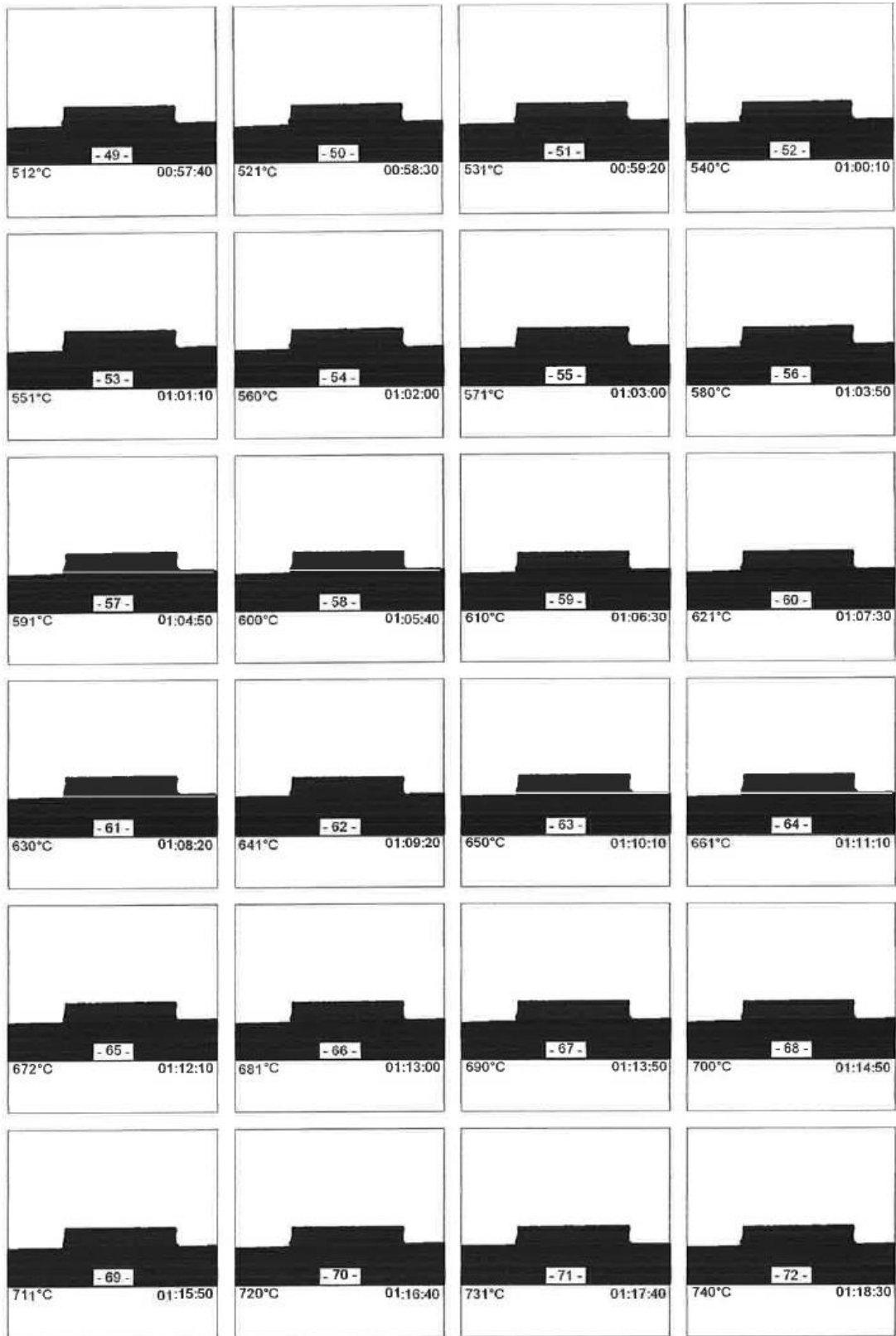


A. 32: Heating microscopy of thin PTC prototype (1280-1400°C)

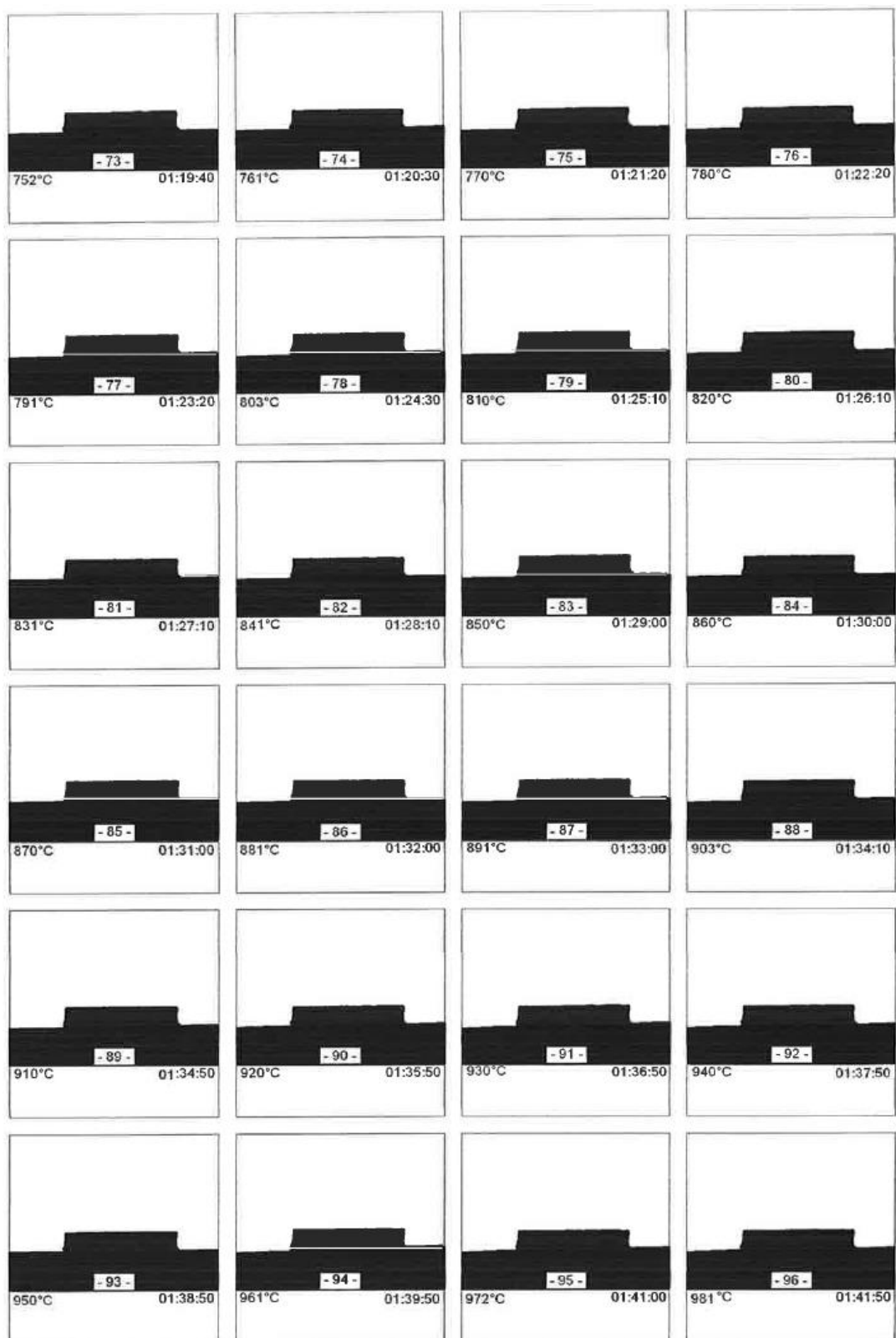


A. 33: Heating microscopy of PTC-ZrO₂ prototype (35-270°C)

A. 34: Heating microscopy of PTC-ZrO₂ prototype (280-500°C)



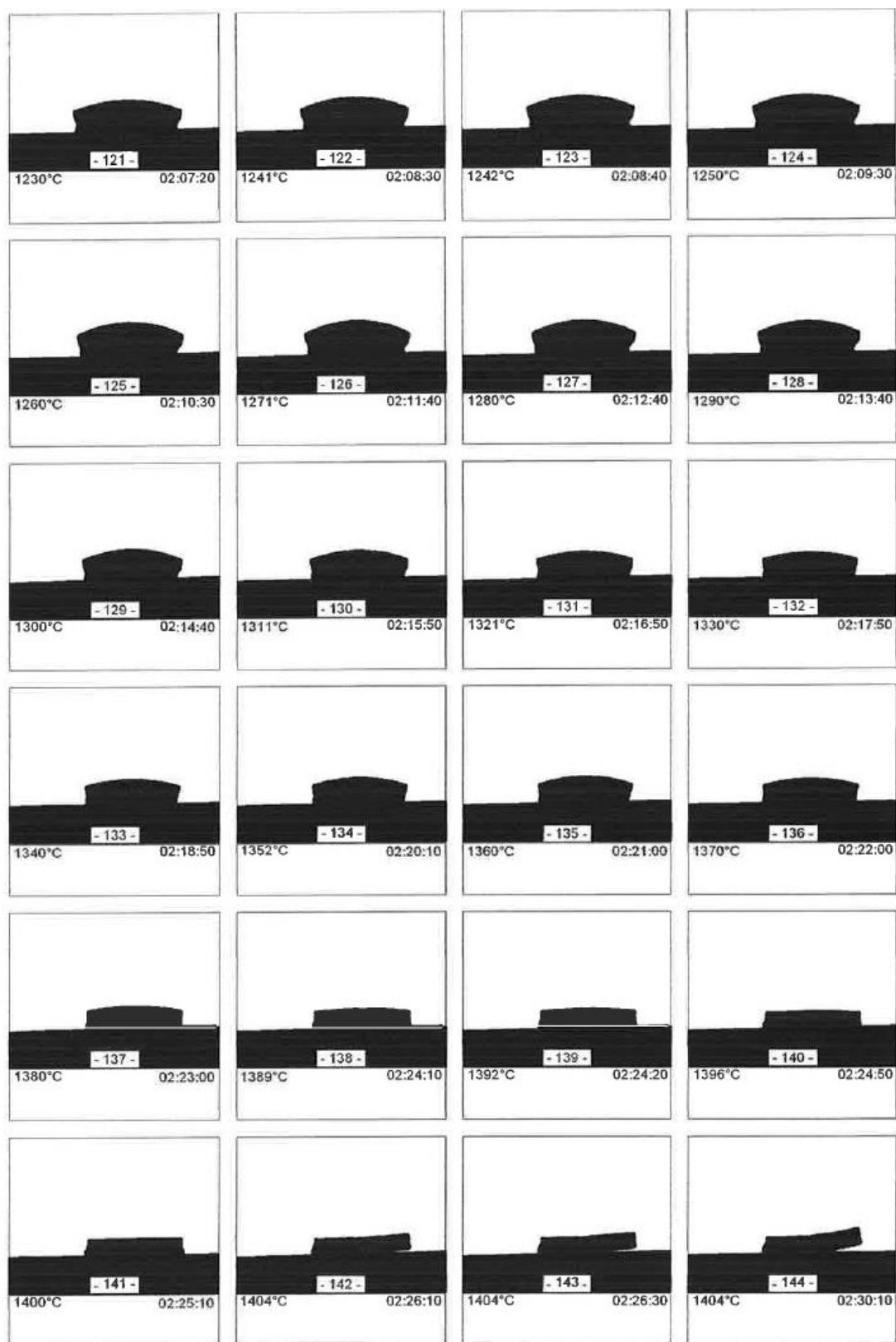
A. 35: Heating microscopy of PTC-ZrO₂ prototype (510-740°C)

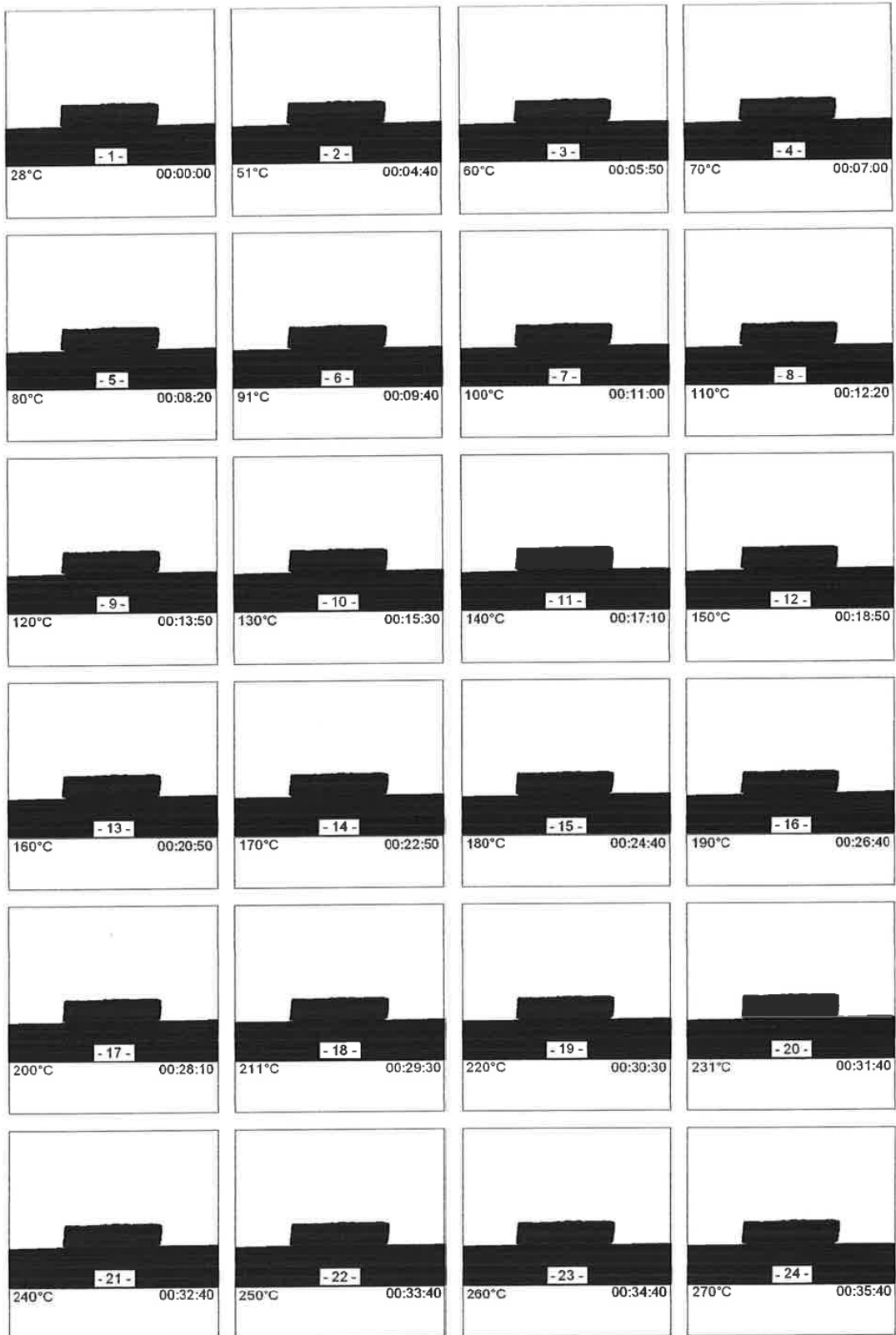


A. 36: Heating microscopy of PTC-ZrO₂ prototype (750-980°C)

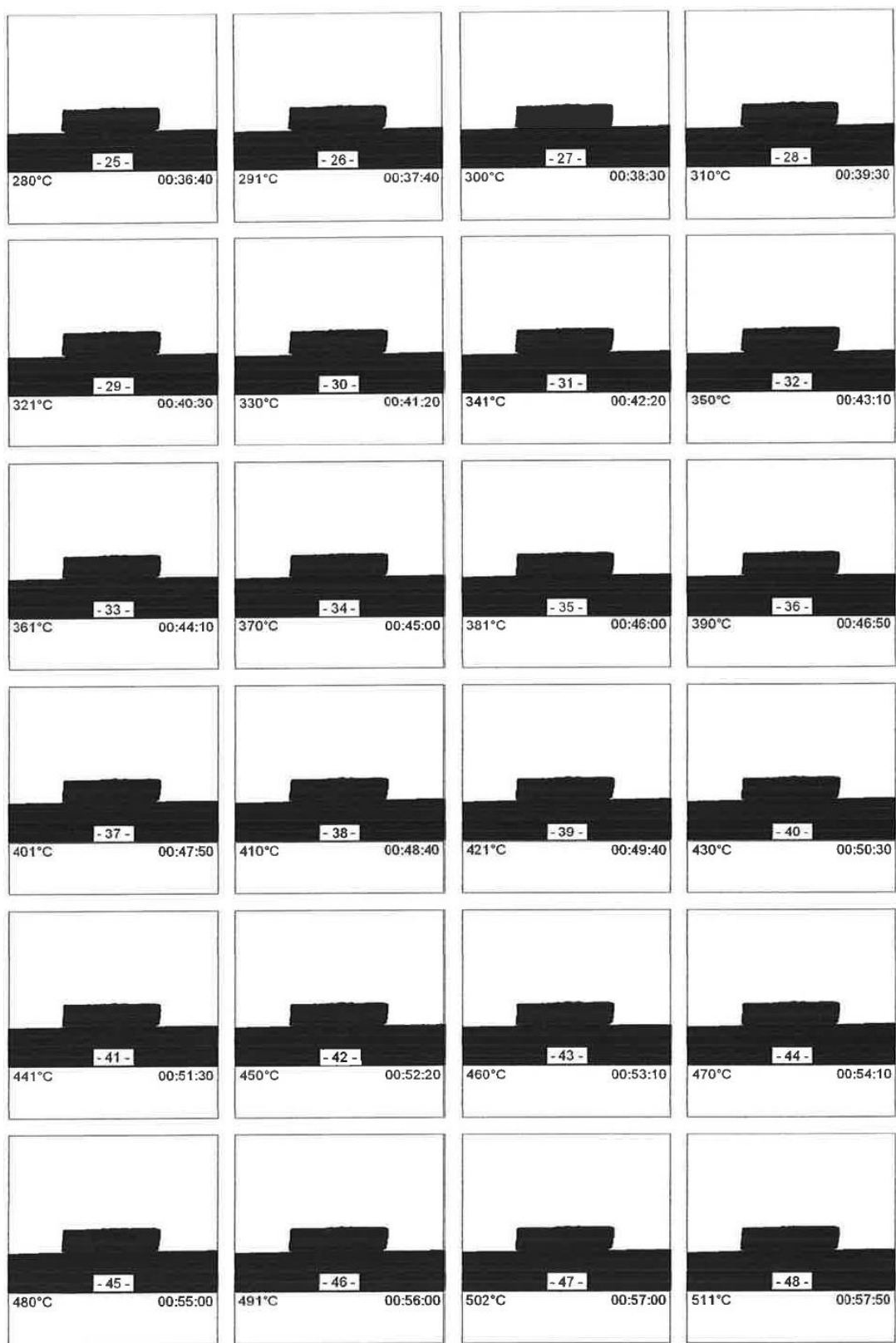


A. 37: Heating microscopy of PTC-ZrO₂ prototype (990-1220°C)

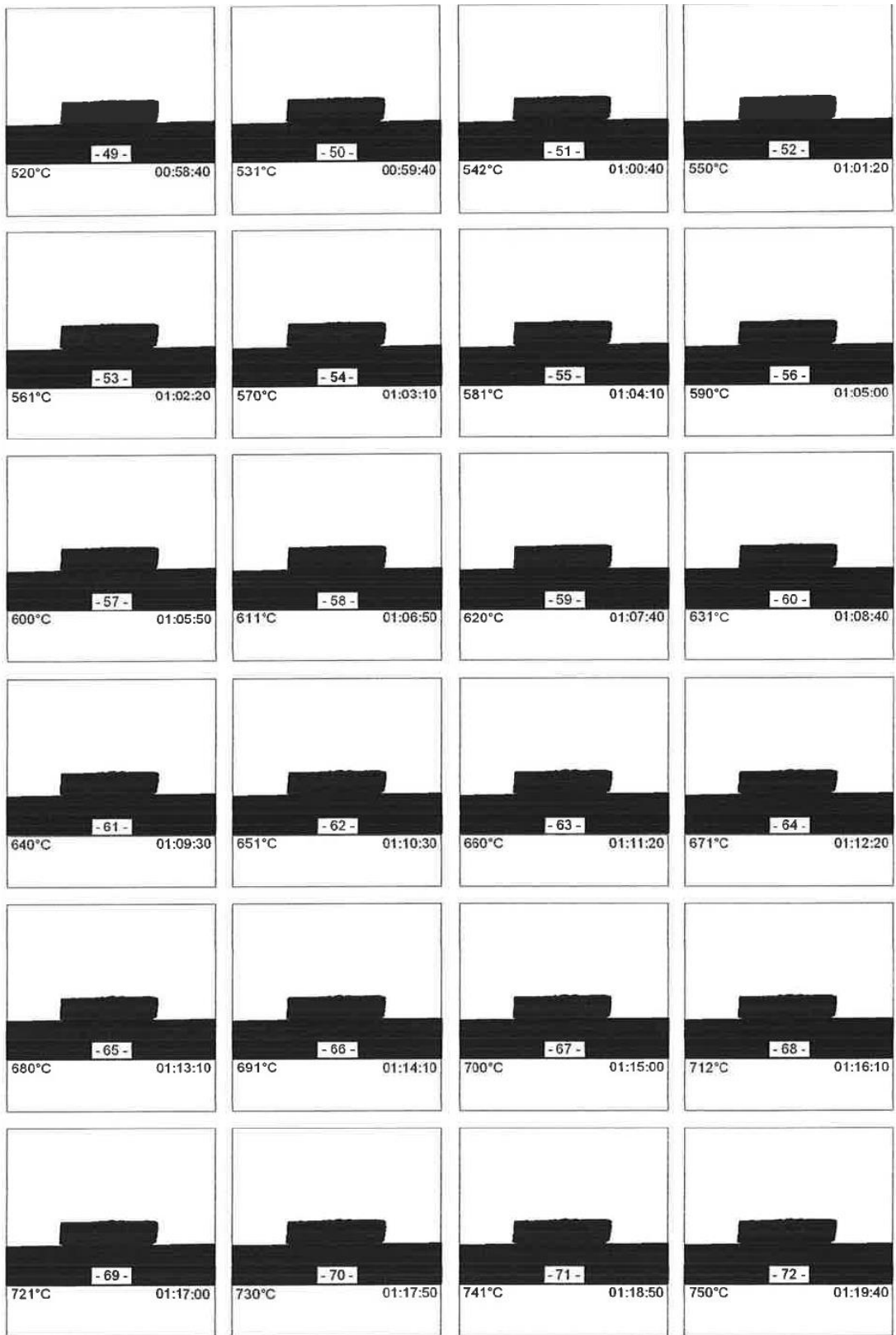
A. 38: Heating microscopy of PTC-ZrO₂ prototype (1230-1400°C)



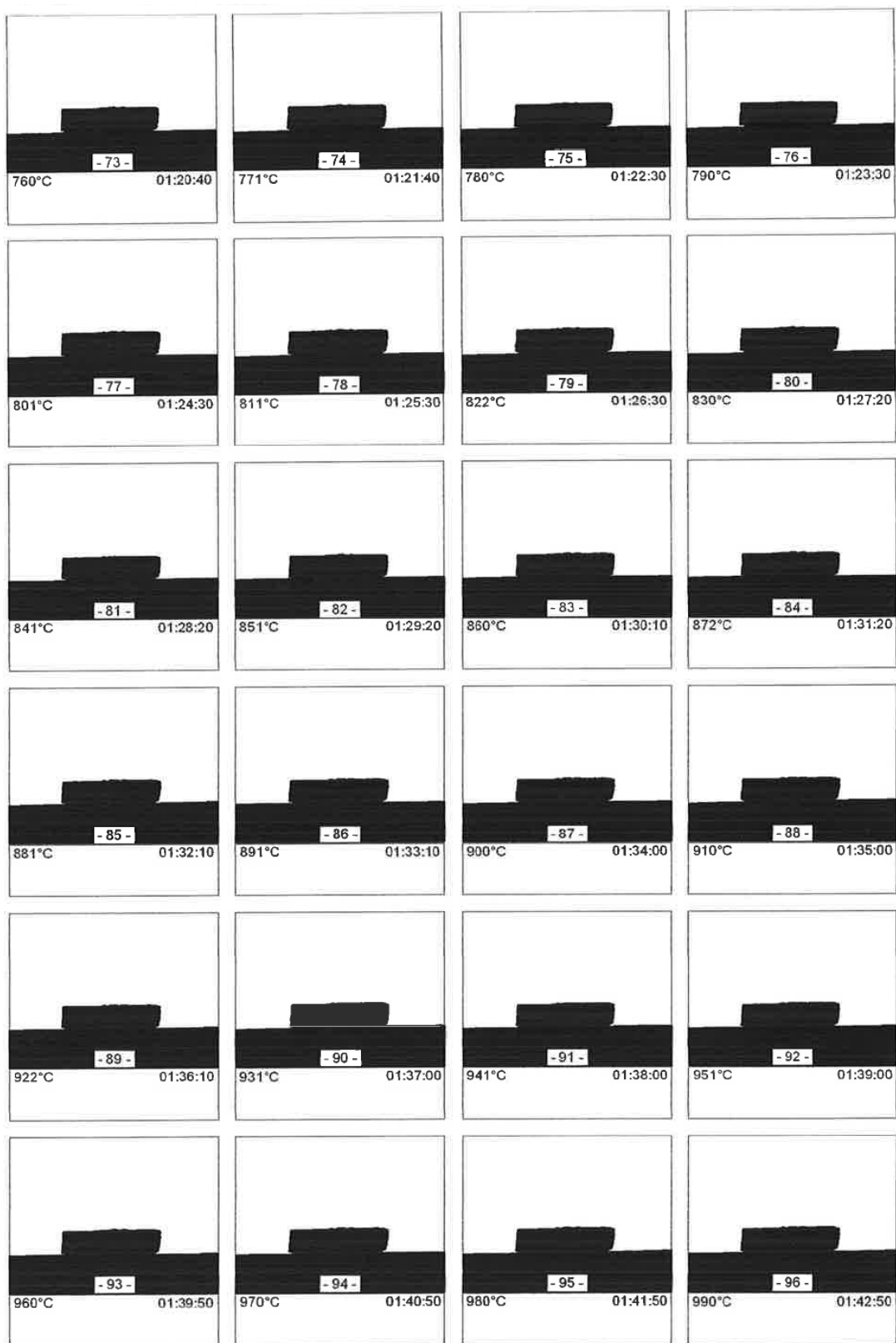
A. 39: Heating microscopy of PTC-BT-ZrO₂ prototype (25-270°C)



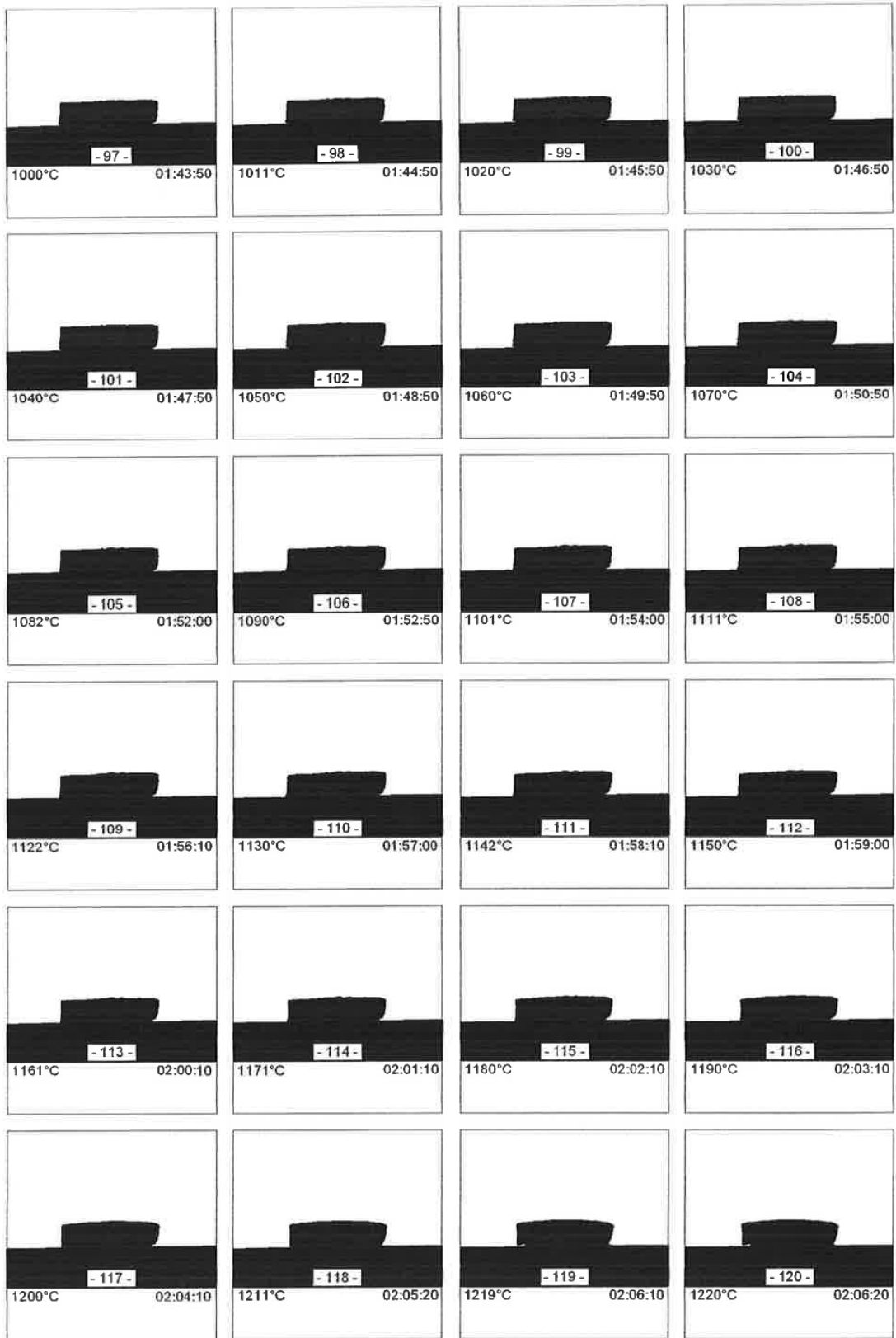
A. 40: Heating microscopy of PTC-BT-ZrO₂ prototype (280-510°C)



A. 41: Heating microscopy of PTC-BT-ZrO₂ prototype (520-750°C)

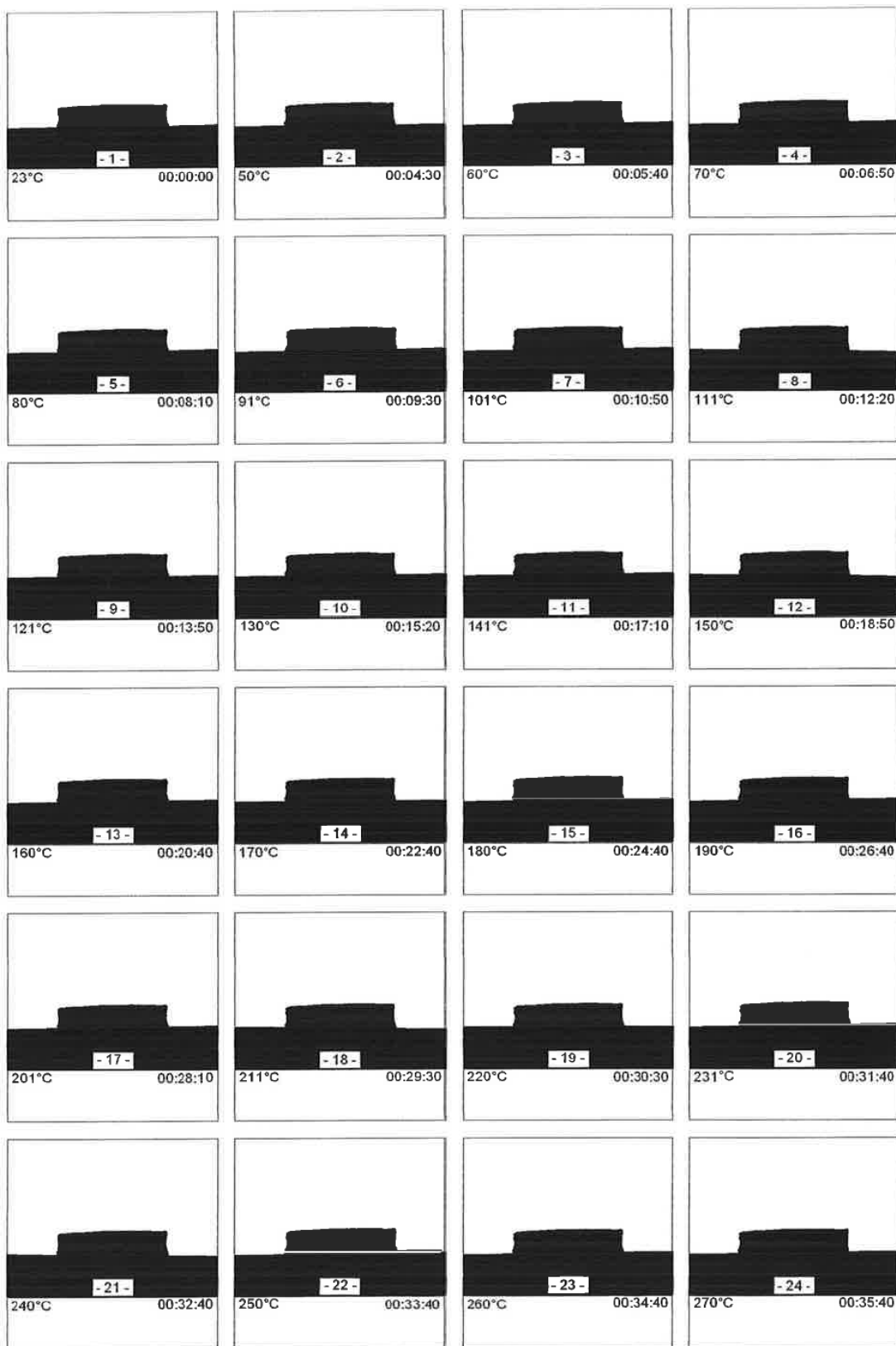


A. 42: Heating microscopy of PTC-BT-ZrO₂ prototype (760-990°C)



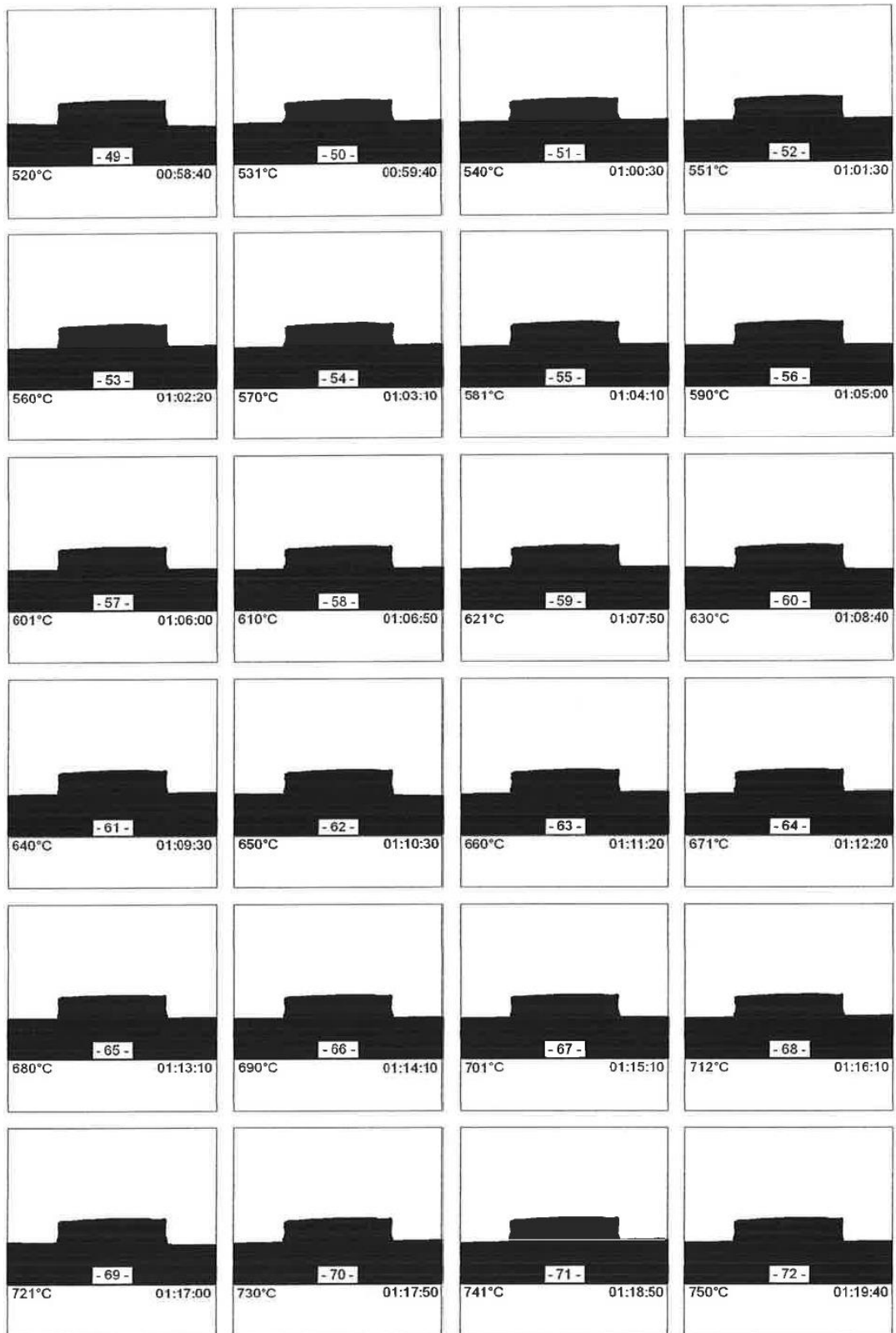
A. 43: Heating microscopy of PTC-BT-ZrO₂ prototype (1000-1220°C)

A. 44: Heating microscopy of PTC-BT-ZrO₂ prototype (1230-1400°C)



A. 45: Heating microscopy of PTC-Al₂O₃ prototype (25-270°C)

A. 46: Heating microscopy of PTC- Al_2O_3 prototype (280-510°C)



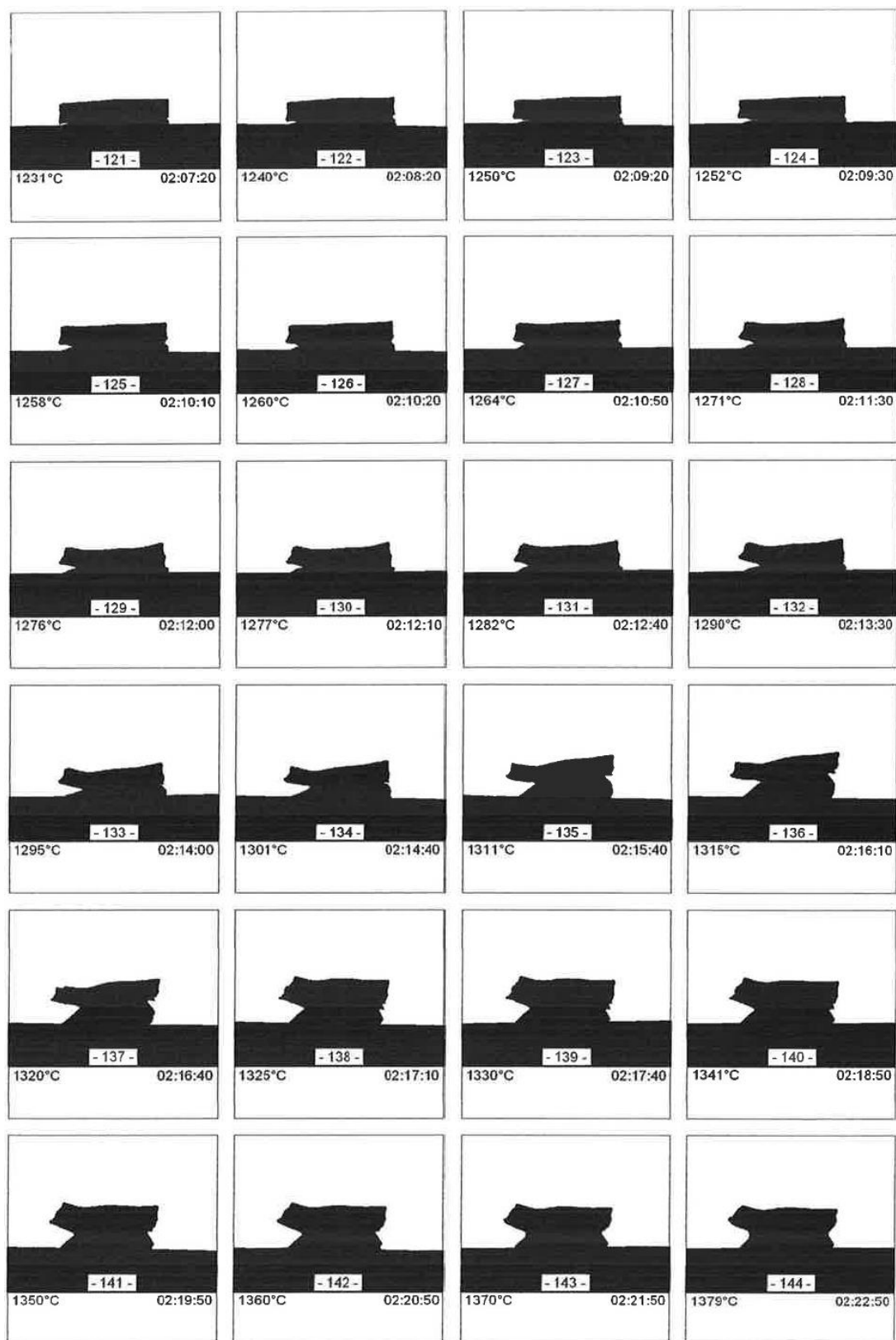
A. 47: Heating microscopy of PTC-Al₂O₃ prototype (520-750°C)

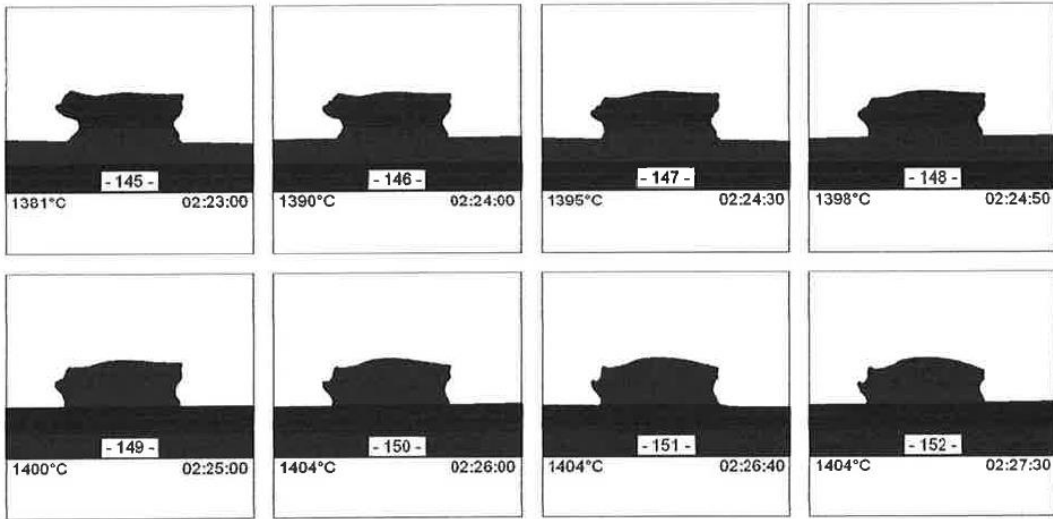


A. 48: Heating microscopy of PTC-Al₂O₃ prototype (760-990°C)



A. 49: Heating microscopy of PTC-Al₂O₃ prototype (1000-1220°C)

A. 50: Heating microscopy of PTC-Al₂O₃ prototype (1230-1380°C)



A. 51: Heating microscopy of PTC-Al₂O₃ prototype (1280-1400°C)

Picture	Temperature	radius ZrO2	angle ZrO2	radius PTC	angle PTC	length		height	change in length		change in height
						ZrO2	PTC		Δx ZrO2	Δx PTC	
Nr.	[°C]	px	°	px	°	px	px	px	%	%	%
1	35	-	-	-	-	170,7	168,7	28,4	0,00	0,00	0,00
2	50	-	-	-	-	170,7	168,7	28,4	0,02	0,00	0,00
3	60	-	-	-	-	170,7	168,7	28,4	0,02	0,00	0,00
4	70	-	-	-	-	170,7	168,7	28,4	0,02	0,00	0,00
5	81	-	-	-	-	170,7	168,7	28,4	0,02	0,00	0,00
6	90	-	-	-	-	170,7	168,7	28,4	0,02	0,00	0,00
7	100	-	-	-	-	170,7	168,7	28,4	0,02	0,00	0,00
8	111	-	-	-	-	170,7	168,7	28,4	0,02	0,00	0,00
9	120	-	-	-	-	170,7	168,7	28,4	0,02	0,00	0,00
10	130	-	-	-	-	170,7	168,7	28,4	0,02	0,00	0,00
11	141	-	-	-	-	170,7	168,7	28,4	0,02	0,00	0,00
12	150	-	-	-	-	170,8	168,9	28,5	0,08	0,12	0,35
13	160	-	-	-	-	170,8	168,9	28,5	0,08	0,12	0,35
14	170	-	-	-	-	170,8	169,0	28,5	0,08	0,18	0,35
15	180	-	-	-	-	170,8	169,0	28,5	0,08	0,18	0,35
16	190	-	-	-	-	170,8	169,1	28,5	0,08	0,24	0,35
17	201	-	-	-	-	170,8	169,1	28,5	0,08	0,24	0,35
18	212	-	-	-	-	170,8	169,1	28,5	0,08	0,24	0,35
19	221	-	-	-	-	170,9	169,1	28,6	0,13	0,24	0,70
20	230	-	-	-	-	170,9	169,3	28,6	0,13	0,36	0,70
21	240	-	-	-	-	170,9	169,3	28,6	0,13	0,36	0,70
22	251	-	-	-	-	170,9	169,5	28,7	0,13	0,47	1,06
23	260	-	-	-	-	170,9	169,6	28,7	0,13	0,53	1,06
24	272	-	-	-	-	171,0	169,6	28,7	0,19	0,53	1,06

A. 52: heating microscopy analysis of PTC-ZrO₂ prototype (35-270°C)

Picture	Temperature	radius ZrO2	angle ZrO2	radius PTC	angle PTC	length		height	change in length		change in height
						ZrO2	PTC		Δx ZrO2	Δx PTC	Δz
Nr.	[°C]	px	°	px	°	px	px	px	%	%	%
25	280	-	-	-	-	171,0	169,6	28,7	0,19	0,53	1,06
26	291	-	-	-	-	171,0	169,6	28,7	0,19	0,53	1,06
27	300	-	-	-	-	171,1	169,7	28,7	0,25	0,59	1,06
28	310	-	-	-	-	171,2	169,7	28,7	0,31	0,59	1,06
29	323	-	-	-	-	171,2	169,7	28,7	0,31	0,59	1,06
30	325	-	-	-	-	171,2	169,7	28,8	0,31	0,59	1,41
31	330	-	-	-	-	171,3	169,7	28,8	0,37	0,59	1,41
32	341	-	-	-	-	171,3	169,7	28,8	0,37	0,59	1,41
33	352	-	-	-	-	171,4	169,7	28,8	0,43	0,59	1,41
34	361	-	-	-	-	171,4	169,7	28,8	0,43	0,59	1,41
35	370	-	-	-	-	171,4	169,7	28,9	0,43	0,59	1,76
36	381	-	-	-	-	171,4	169,7	28,9	0,43	0,59	1,76
37	390	-	-	-	-	171,5	169,7	28,9	0,49	0,59	1,76
38	400	-	-	-	-	171,5	169,8	29,0	0,49	0,65	2,11
39	412	-	-	-	-	171,5	169,8	29,0	0,49	0,65	2,11
40	420	-	-	-	-	171,5	169,8	29,0	0,49	0,65	2,11
41	431	-	-	-	-	171,5	169,8	29,0	0,49	0,65	2,11
42	440	-	-	-	-	171,5	169,8	29,1	0,49	0,65	2,46
43	451	-	-	-	-	171,5	169,8	29,1	0,49	0,65	2,46
44	460	-	-	-	-	171,5	169,8	29,1	0,49	0,65	2,46
45	472	-	-	-	-	171,5	169,8	29,1	0,49	0,65	2,46
46	481	-	-	-	-	171,5	169,8	29,1	0,49	0,65	2,46
47	490	-	-	-	-	171,5	169,8	29,1	0,49	0,65	2,46
48	501	-	-	-	-	171,6	169,8	29,1	0,54	0,65	2,46
49	512	-	-	-	-	171,7	169,9	29,1	0,60	0,71	2,46
50	521	-	-	-	-	171,8	169,9	29,1	0,66	0,71	2,46
51	531	-	-	-	-	171,8	169,9	29,1	0,66	0,71	2,46
52	540	-	-	-	-	171,9	169,9	29,2	0,72	0,71	2,82
53	551	-	-	-	-	172,0	169,9	29,2	0,78	0,71	2,82
54	560	-	-	-	-	172,1	169,9	29,2	0,84	0,71	2,82
55	571	-	-	-	-	172,1	169,9	29,2	0,84	0,71	2,82
56	580	-	-	-	-	172,2	170,0	29,3	0,90	0,77	3,17
57	591	-	-	-	-	172,2	170,0	29,3	0,90	0,77	3,17
58	600	-	-	-	-	172,3	170,0	29,3	0,93	0,77	3,06
59	610	-	-	-	-	172,3	170,0	29,4	0,96	0,77	3,52
60	621	-	-	-	-	172,3	170,0	29,6	0,96	0,77	4,23
61	630	-	-	-	-	172,4	170,0	29,8	1,01	0,77	4,93
62	641	-	-	-	-	172,4	170,0	29,9	1,01	0,77	5,28
63	650	-	-	-	-	172,4	170,0	30,0	1,01	0,77	5,63
64	661	-	-	-	-	172,5	170,1	30,0	1,07	0,83	5,63
65	672	-	-	-	-	172,5	170,1	30,0	1,07	0,83	5,63
66	681	-	-	-	-	172,6	170,2	30,0	1,13	0,89	5,63
67	690	-	-	-	-	172,6	170,2	30,0	1,13	0,89	5,63

A. 53: heating microscopy analysis of PTC-ZrO₂ prototype (280-690°C)

Picture	Temperature	radius ZrO2	angle ZrO2	radius PTC	angle PTC	length		height	change in length		change in height
						ZrO2	PTC		Δx ZrO2	Δx PTC	Δz
Nr.	[°C]	px	°	px	°	px	px	px	%	%	%
68	700	-	-	-	-	172,7	170,2	30,0	1,19	0,89	5,63
69	711	-	-	-	-	172,8	170,4	30,0	1,25	1,01	5,63
70	720	-	-	-	-	172,9	170,6	30,0	1,31	1,13	5,63
71	731	-	-	-	-	173,0	170,6	30,0	1,37	1,13	5,63
72	740	-	-	-	-	173,0	170,7	30,0	1,37	1,19	5,63
73	752	-	-	-	-	173,1	170,8	30,0	1,42	1,24	5,63
74	761	-	-	-	-	173,1	170,8	30,1	1,42	1,24	5,99
75	770	-	-	-	-	173,1	170,8	30,2	1,42	1,24	6,34
76	780	-	-	-	-	173,1	170,8	30,2	1,42	1,24	6,34
77	791	-	-	-	-	173,1	170,8	30,3	1,42	1,24	6,69
78	803	-	-	-	-	173,2	170,9	30,3	1,48	1,30	6,58
79	810	-	-	-	-	173,2	170,9	30,4	1,48	1,30	7,04
80	820	-	-	-	-	173,2	170,9	30,5	1,48	1,30	7,39
81	831	-	-	-	-	173,2	170,9	30,5	1,48	1,30	7,39
82	841	-	-	-	-	173,2	170,9	30,6	1,48	1,30	7,75
83	850	-	-	-	-	173,2	170,9	30,7	1,48	1,30	7,99
84	860	-	-	-	-	173,2	171,0	30,7	1,48	1,36	8,10
85	870	-	-	-	-	173,2	171,0	30,7	1,48	1,36	8,10
86	881	-	-	-	-	173,2	171,0	30,8	1,48	1,36	8,45
87	891	-	-	-	-	173,2	171,1	30,8	1,48	1,42	8,45
88	903	-	-	-	-	173,2	171,2	30,8	1,48	1,48	8,45
89	910	-	-	-	-	173,2	171,2	30,8	1,48	1,48	8,45
90	920	-	-	-	-	173,2	171,2	30,8	1,48	1,48	8,45
91	930	-	-	-	-	173,2	171,3	30,9	1,48	1,54	8,80
92	940	-	-	-	-	173,2	171,3	30,9	1,48	1,54	8,80
93	950	-	-	-	-	173,2	171,4	30,9	1,48	1,60	8,80
94	961	-	-	-	-	173,3	171,4	31,0	1,54	1,60	9,15
95	972	-	-	-	-	173,3	171,4	31,0	1,54	1,60	9,15
96	981	-	-	-	-	173,3	171,4	31,1	1,54	1,60	9,51
97	993	-	-	-	-	173,3	171,5	31,2	1,54	1,66	9,86
98	1001	-	-	-	-	173,3	171,5	31,0	1,54	1,66	9,15
99	1011	-	-	-	-	173,2	171,7	31,0	1,48	1,78	9,15
100	1021	-	-	-	-	173,1	171,7	30,9	1,42	1,78	8,80
101	1031	-	-	-	-	172,8	171,7	30,9	1,25	1,78	8,80
102	1041	-	-	-	-	172,5	171,7	30,8	1,07	1,78	8,45
103	1050	-	-	2520,0	3,9	172,0	171,5	30,8	0,78	1,68	8,45
104	1060	-	-	2180,0	4,5	171,8	171,2	30,8	0,66	1,49	8,45
105	1070	-	-	2178,0	4,5	171,6	171,1	30,7	0,54	1,40	8,10
106	1082	-	-	2127,0	4,6	171,4	170,8	30,7	0,43	1,22	8,10
107	1090	-	-	2122,0	4,6	171,2	170,4	30,7	0,31	0,99	8,10
108	1100	1360,0	7,2	1500,0	6,5	170,9	170,2	30,7	0,14	0,87	8,10
109	1111	905,0	10,8	1392,0	7,0	170,6	170,1	30,7	-0,05	0,81	8,10
110	1122	847,0	11,5	1247,0	7,8	170,0	169,8	30,8	-0,39	0,63	8,45

A. 54: heating microscopy analysis of PTC-ZrO₂ prototype (700-1122°C)

Picture	Temperature	radius ZrO2	angle ZrO2	radius PTC	angle PTC	length		height	change in length		change in height
						ZrO2	PTC		Δx ZrO2	Δx PTC	Δz
Nr.	[°C]	px	°	px	°	px	px	px	%	%	%
111	1130	800,0	12,2	900,0	10,8	170,3	169,6	31,2	-0,19	0,56	9,86
112	1140	800,0	12,2	850,0	11,4	170,3	169,1	31,1	-0,19	0,25	9,51
113	1150	625,0	15,4	643,2	15,1	168,0	169,0	30,7	-1,57	0,15	8,10
114	1161	450,0	21,3	645,0	15,0	167,3	168,9	30,5	-1,98	0,10	7,39
115	1170	450,0	21,2	597,0	16,2	166,5	168,8	30,7	-2,44	0,06	8,10
116	1182	350,0	27,0	396,0	24,4	164,9	168,6	30,9	-3,36	-0,04	8,66
117	1190	340,0	27,5	350,0	27,6	163,2	168,6	31,1	-4,38	-0,06	9,40
118	1201	301,0	31,0	298,0	32,4	162,9	168,5	31,2	-4,58	-0,11	9,86
119	1210	230,0	40,5	260,2	37,1	162,6	168,5	31,3	-4,74	-0,13	10,21
120	1220	200,0	46,1	250,0	38,6	160,9	168,4	31,6	-5,71	-0,16	11,27
121	1230	180,0	50,0	193,7	49,8	157,1	168,4	31,8	-7,96	-0,20	11,97
122	1241	180,0	49,6	196,8	49,0	155,8	168,3	31,8	-8,70	-0,23	11,97
123	1242	170,0	52,4	200,0	48,2	155,5	168,2	31,8	-8,90	-0,27	11,97
124	1250	158,0	56,0	195,0	49,4	154,4	168,1	31,7	-9,52	-0,34	11,62
125	1260	155,0	57,0	185,0	51,7	154,2	166,9	31,6	-9,65	-1,05	11,27
126	1271	150,0	58,7	180,0	52,5	153,7	164,9	31,4	-9,96	-2,23	10,56
127	1280	145,0	60,0	175,0	53,3	151,8	162,8	30,7	-11,03	-3,50	8,13
128	1290	147,5	58,5	170,0	54,4	150,6	161,4	30,6	-11,76	-4,32	7,75
129	1300	160,0	52,9	177,0	51,3	147,7	158,5	29,8	-13,44	-6,06	5,04
130	1311	190,0	44,1	200,0	43,9	146,2	153,2	29,1	-14,31	-9,16	2,61
131	1321	230,0	35,5	225,0	38,1	142,5	149,6	28,1	-16,50	-11,31	-0,92
132	1330	245,0	33,2	250,0	33,8	142,0	147,5	27,5	-16,82	-12,58	-3,17
133	1340	266,0	30,5	240,0	35,0	141,6	146,6	27,4	-17,03	-13,10	-3,42
134	1352	202,5	40,0	213,5	39,1	141,4	145,7	27,2	-17,17	-13,64	-4,33
135	1360	230,0	35,4	240,0	34,7	142,1	145,4	27,2	-16,74	-13,84	-4,23
136	1370	290,0	28,2	290,0	28,6	142,7	144,8	27,2	-16,37	-14,19	-4,33
137	1380	350,0	23,6	400,0	20,7	144,2	144,5	25,7	-15,53	-14,34	-9,51
138	1389	501,0	16,5	690,0	12,0	144,3	144,5	25,1	-15,46	-14,34	-11,48
139	1392	600,0	13,8	745,0	11,1	144,5	144,3	24,8	-15,33	-14,45	-12,57
140	1396	-	-	1250,0	6,6	144,6	144,3	25,0	-15,28	-14,46	-11,97
141	1400	-	-	-	-	144,8	144,3	25,2	-15,16	-14,46	-11,37
142	1404	-	-	-	-	145,1	143,1	25,3	-14,96	-15,15	-10,92
143	1404	-	-	-	-	145,4	143,3	25,6	-14,81	-15,04	-9,86
144	1404	-	-	-	-	145,6	144,2	26,0	-14,69	-14,54	-8,45
145	1404	-	-	-	-	145,8	144,2	26,0	-14,57	-14,52	-8,45
146	1404	-	-	-	-	145,9	141,5	26,5	-14,51	-16,12	-6,69
147	1404	-	-	-	-	146,0	141,5	27,0	-14,45	-16,12	-4,93
148	1404	-	-	-	-	147,2	141,5	27,0	-13,75	-16,12	-4,93

A. 55: heating microscopy analysis of PTC-ZrO₂ prototype (1130-1400°C)

picture	Temperature	radius ZrO2	angle ZrO2	radius PTC	angle PTC	length		height	change in length		change in height
						ZrO2	PTC		Δx ZrO2	Δx PTC	Δz
Nr.	[°C]	px	°	px	°	px	px	px	%	%	%
1	28	-	-	-	-	139,6	146,0	33,3	0,00	0,00	0,00
2	51	-	-	-	-	139,6	146,0	33,3	0,00	0,00	0,15
3	60	-	-	-	-	139,6	146,0	33,3	0,00	0,00	0,15
4	70	-	-	-	-	139,6	146,0	33,3	0,00	0,00	0,15
5	80	-	-	-	-	139,6	146,0	33,3	0,00	0,00	0,15
6	91	-	-	-	-	139,6	146,0	33,4	0,00	0,00	0,45
7	100	-	-	-	-	139,6	146,0	33,4	0,00	0,00	0,45
8	110	-	-	-	-	139,6	146,1	33,4	0,00	0,07	0,45
9	120	-	-	-	-	139,6	146,1	33,4	0,00	0,07	0,45
10	130	-	-	-	-	139,6	146,1	33,5	0,00	0,07	0,75
11	140	-	-	-	-	139,6	146,2	33,5	0,00	0,14	0,75
12	150	-	-	-	-	139,6	146,2	33,5	0,00	0,14	0,75
13	160	-	-	-	-	139,6	146,2	33,5	0,00	0,14	0,75
14	170	-	-	-	-	139,6	146,2	33,6	0,00	0,14	1,05
15	180	-	-	-	-	139,6	146,2	33,6	0,00	0,14	1,05
16	190	-	-	-	-	139,6	146,2	33,6	0,00	0,14	1,05
17	200	-	-	-	-	139,6	146,2	33,7	0,00	0,14	1,35
18	211	-	-	-	-	139,6	146,3	33,7	0,00	0,21	1,35
19	220	-	-	-	-	139,6	146,3	33,7	0,00	0,21	1,35
20	231	-	-	-	-	139,6	146,3	33,7	0,00	0,21	1,35
21	240	-	-	-	-	139,6	146,3	33,8	0,00	0,21	1,65
22	250	-	-	-	-	139,6	146,3	33,8	0,00	0,21	1,65
23	260	-	-	-	-	139,6	146,3	33,8	0,00	0,21	1,65
24	270	-	-	-	-	139,6	146,3	33,9	0,00	0,21	1,95
25	280	-	-	-	-	139,6	146,3	33,9	0,00	0,21	1,95
26	291	-	-	-	-	139,6	146,3	34,0	0,00	0,21	2,26
27	300	-	-	-	-	139,6	146,3	34,1	0,00	0,21	2,56
28	310	-	-	-	-	139,7	146,3	34,1	0,07	0,21	2,56
29	321	-	-	-	-	139,7	146,3	34,2	0,07	0,21	2,86
30	330	-	-	-	-	139,7	146,4	34,2	0,07	0,27	2,86
31	341	-	-	-	-	139,8	146,4	34,3	0,14	0,27	3,16
32	350	-	-	-	-	139,8	146,4	34,3	0,14	0,27	3,16
33	360	-	-	-	-	139,8	146,4	34,3	0,14	0,27	3,16
34	370	-	-	-	-	139,9	146,4	34,3	0,21	0,27	3,16
35	381	-	-	-	-	139,9	146,4	34,3	0,21	0,27	3,16
36	390	-	-	-	-	139,9	146,4	34,3	0,21	0,27	3,16
37	401	-	-	-	-	139,9	146,4	34,3	0,21	0,27	3,16
38	410	-	-	-	-	139,9	146,4	34,4	0,21	0,27	3,46
39	421	-	-	-	-	139,9	146,4	34,4	0,21	0,27	3,46
40	430	-	-	-	-	139,9	146,4	34,4	0,21	0,27	3,46
41	441	-	-	-	-	140,0	146,4	34,4	0,29	0,27	3,46
42	450	-	-	-	-	140,0	146,4	34,4	0,29	0,27	3,46
43	460	-	-	-	-	140,0	146,4	34,5	0,29	0,27	3,76

A. 56:heating microscopy analysis of PTC-BT-ZrO₂ prototype (25-460°C)

picture	Temperature	radius ZrO2	angle ZrO2	radius PTC	angle PTC	length		height	change in length		change in height
						ZrO2	PTC		Δx ZrO2	Δx PTC	
Nr.	[°C]	px	°	px	°	px	px	px	%	%	%
44	470	-	-	-	-	140,1	146,4	34,5	0,36	0,27	3,76
45	480	-	-	-	-	140,1	146,4	34,5	0,36	0,27	3,76
46	491	-	-	-	-	140,1	146,4	34,5	0,36	0,27	3,76
47	502	-	-	-	-	140,1	146,4	34,5	0,36	0,27	3,76
48	511	-	-	-	-	140,1	146,5	34,5	0,36	0,34	3,76
49	520	-	-	-	-	140,1	146,5	34,5	0,36	0,34	3,76
50	531	-	-	-	-	140,2	146,5	34,5	0,43	0,34	3,76
51	542	-	-	-	-	140,2	146,5	34,5	0,43	0,34	3,76
52	550	-	-	-	-	140,2	146,5	34,5	0,43	0,34	3,76
53	561	-	-	-	-	140,3	146,7	34,6	0,50	0,48	4,06
54	570	-	-	-	-	140,3	146,7	34,6	0,50	0,48	4,06
55	581	-	-	-	-	140,3	146,7	34,6	0,50	0,48	4,06
56	590	-	-	-	-	140,4	146,7	34,6	0,57	0,48	4,06
57	600	-	-	-	-	140,4	146,7	34,6	0,57	0,48	4,06
58	611	-	-	-	-	140,4	146,7	34,6	0,57	0,48	4,06
59	620	-	-	-	-	140,5	146,7	34,7	0,64	0,48	4,36
60	631	-	-	-	-	140,5	146,7	34,7	0,64	0,48	4,36
61	640	-	-	-	-	140,6	146,8	34,7	0,72	0,55	4,36
62	651	-	-	-	-	140,7	146,8	34,7	0,79	0,55	4,36
63	660	-	-	-	-	140,7	146,8	34,7	0,79	0,55	4,36
64	671	-	-	-	-	140,7	146,9	34,7	0,79	0,62	4,36
65	680	-	-	-	-	140,8	146,9	34,7	0,86	0,62	4,36
66	691	-	-	-	-	140,8	146,9	34,7	0,86	0,62	4,42
67	700	-	-	-	-	140,9	146,9	34,8	0,93	0,62	4,51
68	712	-	-	-	-	140,9	147,0	34,8	0,93	0,68	4,66
69	721	-	-	-	-	141,0	147,0	34,8	1,00	0,68	4,66
70	730	-	-	-	-	141,0	147,0	34,8	1,00	0,68	4,66
71	741	-	-	-	-	141,1	147,1	34,8	1,07	0,75	4,66
72	750	-	-	-	-	141,1	147,1	34,8	1,07	0,75	4,66
73	760	-	-	-	-	141,2	147,1	34,9	1,15	0,75	4,96
74	771	-	-	-	-	141,2	147,2	34,9	1,15	0,82	4,96
75	780	-	-	-	-	141,3	147,2	34,9	1,22	0,82	4,96
76	790	-	-	-	-	141,3	147,2	34,9	1,22	0,82	4,96
77	801	-	-	-	-	141,4	147,3	34,9	1,29	0,89	4,96
78	811	-	-	-	-	141,4	147,3	34,9	1,29	0,89	4,96
79	822	-	-	-	-	141,5	147,3	34,9	1,36	0,89	4,96
80	830	-	-	-	-	141,6	147,3	34,9	1,43	0,89	4,96
81	841	-	-	-	-	141,6	147,4	34,9	1,43	0,96	4,96
82	851	-	-	-	-	141,7	147,4	34,9	1,50	0,96	4,96
83	860	-	-	-	-	141,7	147,4	34,9	1,50	0,96	4,96
84	872	-	-	-	-	141,8	147,4	35,0	1,58	0,96	5,26
85	881	-	-	-	-	141,8	147,5	35,0	1,58	1,03	5,26
86	891	-	-	-	-	141,9	147,5	35,0	1,65	1,03	5,26

A. 57: heating microscopy analysis of PTC-BT-ZrO₂ prototype (470-890°C)

picture	Temperature	radius ZrO2	angle ZrO2	radius PTC	angle PTC	length		height	change in length		change in height
						ZrO2	PTC		Δx ZrO2	Δx PTC	
Nr.	[°C]	px	°	px	°	px	px	px	%	%	%
87	900	-	-	-	-	141,9	147,5	35,0	1,65	1,03	5,26
88	910	-	-	-	-	141,9	147,6	35,1	1,65	1,10	5,56
89	922	-	-	-	-	141,9	147,6	35,1	1,65	1,10	5,56
90	931	-	-	-	-	141,9	147,7	35,1	1,65	1,16	5,56
91	941	-	-	-	-	141,9	147,7	35,2	1,65	1,16	5,86
92	951	-	-	-	-	141,9	147,8	35,2	1,65	1,23	5,86
93	960	-	-	-	-	141,9	147,8	35,3	1,65	1,23	6,17
94	970	-	-	-	-	141,9	147,9	35,3	1,65	1,30	6,17
95	980	-	-	-	-	141,9	147,9	35,4	1,65	1,30	6,47
96	990	-	-	-	-	141,9	147,9	35,4	1,65	1,30	6,47
97	1000	-	-	-	-	141,9	147,9	35,4	1,65	1,30	6,47
98	1011	-	-	-	-	141,8	147,9	35,4	1,58	1,30	6,47
99	1020	-	-	-	-	141,8	148,0	35,5	1,58	1,34	6,77
100	1030	-	-	-	-	141,8	148,0	35,5	1,58	1,37	6,77
101	1040	-	-	-	-	141,8	148,0	35,5	1,58	1,37	6,77
102	1050	-	-	-	-	141,8	148,0	35,6	1,58	1,37	7,07
103	1060	-	-	-	-	141,7	148,0	35,7	1,50	1,37	7,37
104	1070	-	-	-	-	141,7	148,0	35,9	1,50	1,37	7,97
105	1082	-	-	-	-	141,7	148,0	36,0	1,50	1,37	8,27
106	1090	-	-	-	-	141,6	148,0	36,1	1,43	1,37	8,57
107	1101	-	-	-	-	141,5	148,0	36,3	1,36	1,37	9,17
108	1111	-	-	-	-	141,4	148,0	36,3	1,29	1,37	9,17
109	1122	-	-	750,4	11,3	141,3	148,0	36,2	1,22	1,37	8,87
110	1130	-	-	750,2	11,3	141,1	148,0	36,1	1,07	1,34	8,57
111	1142	1491,0	5,4	750,1	11,3	140,5	147,9	36,0	0,66	1,33	8,27
112	1150	990,0	8,1	750,0	11,3	140,0	147,9	36,0	0,26	1,31	8,27
113	1161	1185,0	6,7	750,0	11,3	138,6	147,9	35,7	-0,74	1,31	7,28
114	1171	905,0	8,7	724,0	11,7	137,4	147,8	35,3	-1,56	1,26	6,26
115	1180	800,0	9,8	700,0	12,1	136,8	147,8	34,9	-1,98	1,25	4,96
116	1190	650,0	12,0	600,0	14,1	136,1	147,7	34,7	-2,48	1,13	4,36
117	1200	345,0	22,5	500,0	16,9	135,5	147,5	34,6	-2,95	1,01	4,06
118	1211	335,0	23,0	480,0	17,6	134,5	147,4	33,2	-3,67	0,99	-0,15
119	1219	335,0	22,8	425,0	19,7	133,3	146,1	32,8	-4,51	0,09	-1,35
120	1220	335,0	22,8	425,0	19,7	133,3	146,1	32,8	-4,51	0,09	-1,41
121	1230	325,0	23,4	425,0	19,6	132,7	145,4	32,6	-4,92	-0,42	-1,95
122	1241	270,0	27,7	400,0	20,5	130,5	143,1	32,2	-6,49	-1,97	-3,16
123	1251	250,0	29,2	340,0	23,8	127,4	141,2	32,0	-8,73	-3,27	-3,76
124	1261	250,0	28,9	388,0	20,8	126,1	140,9	31,8	-9,67	-3,52	-4,36
125	1270	250,0	28,6	385,0	20,8	124,8	139,8	31,2	-10,61	-4,27	-6,17
126	1281	300,0	23,3	325,0	24,1	122,0	136,7	30,0	-12,61	-6,37	-9,77
127	1291	325,0	21,4	375,0	20,5	121,4	134,2	29,2	-13,05	-8,10	-12,18
128	1300	375,0	18,1	475,0	15,9	118,5	131,8	29,0	-15,14	-9,72	-12,78
129	1310	290,0	23,3	450,0	16,4	117,9	128,8	28,8	-15,52	-11,78	-13,38

A. 58:heating microscopy analysis of PTC-BT-ZrO₂ prototype (900-1310°C)

picture	Temperature	radius ZrO2	angle ZrO2	radius PTC	angle PTC	length		height	change in length		change in height
						ZrO2	PTC		Δx ZrO2	Δx PTC	
Nr.	[°C]	px	°	px	°	px	px	px	%	%	%
130	1313	290,0	23,3	529,0	13,9	117,9	128,3	28,8	-15,52	-12,10	-13,38
131	1320	375,0	18,0	510,0	14,3	117,8	127,3	28,4	-15,61	-12,82	-14,59
132	1331	301,0	22,4	461,0	15,8	117,7	127,1	28,2	-15,70	-12,93	-15,19
133	1340	325,0	20,7	484,0	15,0	117,4	126,7	27,6	-15,89	-13,21	-16,99
134	1350	300,0	22,4	500,0	14,5	117,3	126,5	27,5	-15,98	-13,33	-17,29
135	1361	300,0	22,3	450,0	16,1	116,8	126,4	27,4	-16,36	-13,39	-17,59
136	1371	298,0	22,5	441,0	16,4	117,0	126,2	27,4	-16,17	-13,54	-17,59
137	1375	300,0	22,4	432,0	16,7	117,3	125,9	27,3	-15,98	-13,76	-17,89
138	1379	301,0	22,4	426,0	16,9	117,4	125,7	27,2	-15,89	-13,94	-18,20
139	1380	300,0	22,5	599,0	12,0	117,8	125,5	27,1	-15,61	-14,07	-18,50
140	1390	300,0	22,6	854,0	8,4	118,3	125,2	27,0	-15,23	-14,24	-18,80
141	1401	-	-	1300,0	5,5	119,0	124,8	27,0	-14,76	-14,53	-18,80
142	1405	-	-	1650,0	4,3	119,0	123,8	27,0	-14,76	-15,18	-18,80
143	1405	-	-	1645,0	4,3	119,5	123,5	27,0	-14,40	-15,44	-18,80
144	1405	-	-	1644,0	4,3	119,8	123,4	27,0	-14,18	-15,49	-18,80
145	1405	-	-	1643,0	4,3	120,0	123,3	27,0	-14,04	-15,54	-18,80
146	1405	-	-	1640,0	4,3	120,2	123,1	27,0	-13,90	-15,70	-18,80

A. 59: heating microscopy analysis of PTC-BT-ZrO₂ prototype (1310-1400°C)

picture	Temperature	radius PTC	angle PTC	PTC length	change in length
					Δx PTC
Nr.	[°C]	px	°	px	%
1	27	-	-	115,7	0,00
2	50	-	-	115,7	0,00
3	60	-	-	115,7	0,00
4	72	-	-	115,7	0,00
5	80	-	-	115,7	0,00
6	90	-	-	115,7	0,00
7	101	-	-	115,7	0,00
8	110	-	-	115,7	0,00
9	121	-	-	115,7	0,00
10	130	-	-	115,7	0,00
11	140	-	-	115,7	0,00
12	150	-	-	115,7	0,00
13	161	-	-	115,7	0,00
14	170	-	-	115,7	0,00
15	180	-	-	115,7	0,00
16	190	-	-	115,7	0,00
17	201	-	-	115,7	0,00
18	210	-	-	115,7	0,00
19	220	-	-	115,7	0,00
20	231	-	-	115,7	0,00

A. 60: heating microscopy analysis of thin PTC prototype (25-230°C)

picture	Temperature	radius PTC	angle PTC	PTC length	change in length
Nr.	[°C]	px	°	px	Δx PTC %
21	241	-	-	115,7	0,00
22	250	-	-	115,7	0,00
23	260	-	-	115,7	0,00
24	269	-	-	115,8	0,09
25	281	-	-	115,8	0,09
26	290	-	-	115,8	0,09
27	300	-	-	115,9	0,17
28	311	-	-	115,9	0,17
29	320	-	-	116,0	0,26
30	331	-	-	116,0	0,26
31	340	-	-	116,0	0,26
32	351	-	-	116,1	0,35
33	360	-	-	116,1	0,35
34	370	-	-	116,1	0,35
35	380	-	-	116,2	0,43
36	391	-	-	116,2	0,43
37	400	-	-	116,2	0,43
38	411	-	-	116,3	0,52
39	420	-	-	116,3	0,52
40	431	-	-	116,3	0,52
41	440	-	-	116,3	0,52
42	451	-	-	116,4	0,61
43	461	-	-	116,4	0,61
44	470	-	-	116,4	0,61
45	481	-	-	116,5	0,69
46	490	-	-	116,5	0,69
47	501	-	-	116,5	0,69
48	510	-	-	116,5	0,69
49	520	-	-	116,5	0,69
50	531	-	-	116,5	0,69
51	540	-	-	116,5	0,69
52	551	-	-	116,5	0,69
53	560	-	-	116,5	0,69
54	571	-	-	116,5	0,69
55	580	-	-	116,5	0,69
56	590	-	-	116,5	0,69
57	601	-	-	116,5	0,69
58	610	-	-	116,5	0,69
59	621	-	-	116,5	0,69
60	630	-	-	116,5	0,69
61	641	-	-	116,5	0,69
62	652	-	-	116,5	0,69
63	661	-	-	116,5	0,69

A. 61: heating microscopy analysis of thin PTC prototype (240-660°C)

picture	Temperature	radius PTC	angle PTC	PTC length	change in length
					Δx PTC
Nr.	[°C]	px	°	px	%
64	670	-	-	116,5	0,69
65	681	-	-	116,5	0,69
66	690	-	-	116,5	0,69
67	699	-	-	116,5	0,69
68	710	-	-	116,5	0,69
69	721	-	-	116,5	0,69
70	730	-	-	116,5	0,69
71	742	-	-	116,5	0,69
72	751	-	-	116,5	0,69
73	760	-	-	116,5	0,69
74	770	-	-	116,5	0,69
75	780	-	-	116,5	0,69
76	790	-	-	116,5	0,69
77	801	-	-	116,5	0,69
78	810	-	-	116,6	0,78
79	820	-	-	116,6	0,78
80	831	-	-	116,7	0,86
81	841	-	-	116,7	0,86
82	850	-	-	116,7	0,86
83	860	-	-	116,8	0,95
84	871	-	-	116,8	0,95
85	881	-	-	116,8	0,95
86	890	-	-	116,9	1,04
87	901	-	-	116,9	1,04
88	910	-	-	117,0	1,12
89	921	-	-	117,1	1,21
90	931	-	-	117,2	1,30
91	941	-	-	117,3	1,38
92	950	-	-	117,3	1,38
93	960	-	-	117,3	1,38
94	970	-	-	117,4	1,47
95	980	-	-	117,4	1,47
96	992	-	-	117,5	1,56
97	1000	-	-	117,5	1,56
98	1010	-	-	117,6	1,64
99	1020	-	-	117,7	1,73
100	1031	-	-	117,7	1,73
101	1041	-	-	117,8	1,82
102	1050	-	-	117,8	1,82
103	1060	-	-	117,9	1,90
104	1070	-	-	117,9	1,90
105	1080	-	-	117,9	1,90
106	1090	-	-	118,0	1,99

A. 62: heating microscopy analysis of thin PTC prototype (670-1090°C)

picture	Temperature	radius PTC	angle PTC	PTC length	change in length
Nr.	[°C]	px	°	px	Δx PTC
					%
107	1100	-	-	118,0	1,99
108	1111	-	-	117,9	1,90
109	1123	-	-	117,9	1,90
110	1131	-	-	117,8	1,82
111	1140	-	-	117,8	1,82
112	1150	-	-	117,6	1,64
113	1160	-	-	117,6	1,64
114	1170	-	-	117,4	1,47
115	1182	-	-	117,4	1,47
116	1190	-	-	117,0	1,12
117	1200	-	-	116,8	0,95
118	1210	-	-	116,6	0,78
119	1220	-	-	116,3	0,52
120	1231	-	-	116,0	0,26
121	1240	-	-	115,5	-0,17
122	1250	-	-	114,9	-0,69
123	1261	-	-	111,8	-3,37
124	1271	-	-	110,8	-4,24
125	1280	-	-	109,0	-5,79
126	1290	-	-	104,8	-9,46
127	1300	-	-	102,0	-11,84
128	1311	700,0	8,0	97,7	-15,52
129	1320	490,0	11,1	94,9	-17,95
130	1330	490,0	11,0	94,1	-18,69
131	1341	490,0	11,0	94,1	-18,69
132	1351	490,0	11,0	94,1	-18,69
133	1360	490,0	11,0	94,1	-18,69
134	1370	500,0	10,8	94,2	-18,54
135	1380	500,0	10,8	94,2	-18,54
136	1391	500,0	10,9	95,1	-17,79
137	1400	450,0	12,2	95,8	-17,18

A. 63: heating microscopy analysis of thin PTC prototype (1100-1400°C)